UNIVERSITY OF LIVERPOOL

Investigating the Role of CCN2 in a Bleomycin Model of Idiopathic Pulmonary Fibrosis

Thesis submitted in accordance with the requirements of the University of Liverpool for the degree of Doctor in Philosophy by Amy Louise Horwell

October 2018

Abstract

Idiopathic Pulmonary Fibrosis (IPF) is a chronic, progressive and ultimately lethal disease of the lung characterised by excessive synthesis and deposition of extracellular matrix (ECM). The 5-year survival rate for IPF is lower than that of breast, prostate and skin cancer, with the average mortality rate currently standing at 3 years post diagnosis. Incidence and mortality appear to be on the rise, and prevalence is expected to increase in an aging population. Recently several new drugs have been approved (Pirfenidone, Nintedanib and Pamrevlumab). However, the pathobiology of IPF still remains elusive and there is an ever more pressing need to elucidate the molecular processes behind this disease to identify potential therapeutic targets.

It is widely believed that at the cellular level, the key mediators of fibrosis are the fibroblast cell and their profibrotic phenotype, the myofibroblast. In normal homeostasis the myofibroblast is activated to synthesise new ECM during wound healing. In IPF there is believed to be a dysregulation in this process leading to persistent activation of myofibroblasts after the healing response is complete. Transforming growth factor – β (TGF-β) is known to be one of the master regulators of wound healing has been shown to be capable of activating myofibroblasts. However, research has looked downstream in the TGF – β signalling pathway to another protein - connective tissue growth factor (CCN2).

CCN2 is considered a key downstream mediator of the profibrotic effects of TGF- β and has been shown to induce a fibrotic response independently of TGF-β both *in vitro* and in animal models of IPF. A clinical trial of a monoclonal antibody to CCN2 (Pamrevlumab) has demonstrated the ability to reverse the fibrosis in various murine models of fibrosis and is showing promising efficacy in human trials. The mechanism of action of CCN2 in fibrosis is still yet to be fully understood. The aim of this thesis was to utilise the murine bleomycin model of IPF to further investigate the role of CCN2 in fibrosis.

Two new double transgenic mouse lines were generated, containing a CCN2 floxed transcript and a tamoxifen-inducible cre recombinase (CreER^{T2}). Two different CreER^{T2} were used to facilitate loss of function of CCN2 in fibroblast cells specifically (Col1α2-CreER^{T2}), or in all cells (ROSA-CreER^{T2}). A dosing regimen for initiating recombination *in vivo* was established, and the phenotype in the lungs characterised for both new mouse lines. A third double transgenic mouse line was generated to examine the expression pattern of the Col1α2-CreERT2 during adulthood and embryonic development using a dual fluorescent reporter construct (mT/mG). A protocol was established for the induction of fibrosis in these mice using bleomycin, and a novel imaging protocol using an *ex vivo* μCT scanner was developed to enable full imaging of unfixed lungs prior to genetic and histological analysis.

In summary, the studies reported in this thesis presented novel findings on the role of CCN2 in the pathogenesis of fibrosis. Two novel transgenic mouse lines were established for the genetic manipulation of CCN2 *in vivo.* These were used in conjunction with the bleomycin model, which was established for the first time at the University of Liverpool. The results from these experiments unveiled unexpected results and raised further questions as to the role CCN2 plays in homeostatic regulation of ECM production by demonstrating a potent anti-fibrotic effect of CCN2. A third transgenic mouse line was used to characterise the expression profile of a fibroblast specific CreER^{T2} developed by the Bou-Gharios lab group and found that the fibroblast specificity was prevalent in a wider population of fibroblasts than described previously.

Acknowledgements

Firstly, I would like to thank my supervisors; Professor George Bou-Gharios, Professor Robert Moots and Dr. Lisa Spencer for giving me the opportunity to undertake this PhD project. I would also like to thank the Crossley Barnes Bequest to the Institute of Ageing and Chronic Disease for funding this research. I would also like to thank all the members of the technical team, post-docs and PhD students in IACD for training me in all the techniques presented in the results of these thesis. Particular thanks must go to the original members of the Bou-Gharios lab, who have offered their support and experience from my very first day of my PhD. I would also like to thank Gemma Charlesworth for the thousands of miles and flights of stairs she has covered in supporting the µCT imaging of the lungs, it would not have been possible without you. Also Lid, you have been a top cheerleader and peach for the last 2.5 years. Without the solid gym sessions, badminton and tragic nights out there would be have been much less entertainment to break down the intensive lab sessions pulled towards the end of this PhD.

Dr. Rachel Oldershaw, without you this thesis would not have been completed. I cannot put into words how grateful I have been over the last 3 years for all the support and gossip you have provided me with. You have gone far above and beyond to drag me kicking and screaming to the finish line and I owe you my deepest gratitude for this.

The greatest thanks must go to my family and friends, who have always supported me during my PhD. To all the members of the University of Liverpool badminton team, you have made these some of the best years of my life and provided some much-needed stress relief both on the court and off. To my sisters Charlotte and Alice, our daily snapchats and phone calls have kept me sane who knew a 500+ daily snap-streak could be so easy to maintain. Our food chain memes have brought much needed laughter and brightened up the darkest of days. Mum and Faja, you have given me every support throughout my life and without your words of support, encouragement and sometimes downright rudeness, I would not be the person I am today. I love you all and hope to make you proud of who I have become.

Last but not least I must thank Aaron Magee, for feeding me, nesting with me and dealing with the whirlwind of emotions that the last 4 years have brought. You have been the best boyfriend anyone could have asked for and I hope that we can spend some quality time together now it's all over.

Abbreviations

+/-	Positive (heterozygous for a gene of interest)
°C	Degrees celcius
µCT	Micro-computed tomography
µg	Microgram
µL	Microlitre
µM	Micromolar
2D	Two-dimensional
3D	Three-dimensional
4-OHT	4-Hydroxytamoxifen
a	Alveoli
ab	Air bubble
ADAMTs	A disintegrin and metalloproteinase with thrombospondin motifs
AETI	Alveolar epithelial type 1 cells
AETII	Alveolar epithelial type 2 cells
ANOVA	Analysis of variance
ASPA	Animals (Scientific Procedures) Act 1986
BMPs	Bone morphogenic proteins
bp	Base pair
br	Bronchioles
BSA	Bovine serum albumin
BSU	Biomedical services unit
ca	Cartilage
cDNA	Complementary deoxyribonucleic acid
ch	Choroid
CO_2	Carbon dioxide
Cre	Cyclization recombination
CT	C-terminal repeat
CTGF	Connective tissue growth factor
cv	Central vein

Cyr61	Cysteine Rich Angiogenic Inducer 61
D.I.C	Dead in cage
DAB	3,3’-Diaminobenzidine
ddH_2O	double distilled water
DMEM	Dulbecco's modified eagle medium
DNA	Deoxyribonucleic acid
dNTP	Deoxyribonucleotide triphosphate
ECM	Extracellular matrix
EGF	Epidermal growth factor
EGFP	Enhanced green fluorescent protein
EMT	Epithelial mesenchymal transition
ER	Endoplasmic reticulum
ER^{T2}	Estrogen receptor type 2
EtOH	Ethanol
f	Follicles
F1	First generation breeding offspring
FITC	Fluorescein isothiocyanate
Floxed	Flanked by loxP sites
FOR/Fw	Forward
g	Grams
GDFs	Growth differentiation factors
H & E	Haematoxylin and Eosin stain
HBSS	Hanks’ balanced salt solution
He	Heart
HMDS	Hexamethydisilazane
hr	Hour
I.P.	Intraperitoneal
IGFBPs	Insulin-like growth factor binding proteins
IIP	Idiopathic interstitial pneumonias
ILD	Interstitial lung disease
IM	Interstitial macrophages

IN	Intranasal
IPF	Idiopathic pulmonary fibrosis
IT	Intratracheal
IU	International units
IV	Intravenous
kb	Kilobase
KI	Potassium Iodide
L	Litre
LN_2	Liquid nitrogen
LOX	Lysyl oxidase
loxP	Locus of crossing over {X} of P1
LPS	Lipopolysaccharide
M	Molar
M1	Pro-inflammatory macrophage
M2	Anti-inflammatory macrophage
mG	Enhanced green fluorescent protein fluorophore
mg	Milligram
$MgCl_2$	Magnesium chloride
min	Minutes
mL	Millilitre
mm	Master mix
MMPs	Matrix metalloproteinases
mRNA	Messenger ribonucleic acid
mT	tDTomato fluorophore
NaCl	Sodium chloride
$NaHCO_3$	Sodium bicarbonate
NBF	Neutral buffered formalin
ng	Nanogram
NICE	National institute for health and care excellence
Nm	Nanometre
nM	Nanomolar

NOV	Nephroblastoma overexpressed
O/B	Oil and bleomycin treatment
O2	Oxygen
OA	Oropharyngeal aspiration
PBS	Phosphate buffered saline
PBS-T	Phosphate buffered saline with tween
PC	Polyclonal
PCE	Pseudostratified columnar epithelial cells
PCR	Polymerase chain reaction
PF	Pulmonary fibrosis
pM	Picomolar
qPCR	Quantitative PCR
rER	Rough endoplasmic reticulum
REV/Rv	Reverse
ri	Ribs
RNA	Ribonucleic acid
ROS	Reactive oxyen species
RSMAD	Receptor associated SMAD
RT-qPCR	Reverse transcription qPCR
SC	Subcutaneous
Sch1	Schedule 1
SDS	Sodium dodecyl sulfate
Sf	Styrofoam
SP-A	Surfactant protein A
SP-C	Surfactant protein C
SPF	Specific pathogen free
T/B	Tamoxifen and bleomycin treatment
T/P	Tamoxifen and PBS treatment
TAE	Tris base, acetic acid and EDTA (buffer)
TGF - βR	Transforming growth factor beta receptor
TGF - β	Transforming growth factor beta

TIMPs	Tissue inhibitors of metalloproteinases
tr	Trachea
Tris-HCL	Tris hydrochloride
TSP	Thrombospondin repeat
Tx	Tamoxifen
UCSC	University of California, Santa Cruz
UK	United Kingdom
v	Blood vessel
V	Volts
VEGF	Vascular endothelial growth factor
VSMC	Vascular smooth muscle cells
VWC	Von Willebrand type C
WHO	World health organisation
WT	Wild type
X-gal	5-bromo-4-chloro-3-indolyl-β-D-galactoside
α - SMA	Alpha smooth muscle actin
ΔΔCt	delta-delta threshold cycle

List of Figures

List of Tables

Table of Contents

1. Introduction

1.1 The Respiratory System

The human respiratory system is a highly complex organ that primarily functions to facilitate respiration via ventilation and gas exchange whilst providing a level of protection against environmental pathogen exposure (Leeman, Fillmore, & Kim, 2014). Ventilation is the physical process of drawing in and exhaling air from the lungs. Gas exchange is the biochemical process whereby oxygen (O_2) diffuses out of the air, into the blood, and is subsequently used for metabolic cell respiration in the production of energy. Waste gases such as carbon dioxide (CO_2) are removed from the body and diffuse from the blood back into the air to be exhaled. Gas exchange occurs exclusively in the lungs, whereas the entire respiratory system is involved in breathing. This process must remain efficient to prevent build-up of toxic waste gases, maintain stable pH levels and provide sufficient energy to sustain life.

The organs and tissues that comprise the respiratory system are identified in Figure 1.1. Airflow is continuous from the nose and mouth to the alveoli, this is known as the respiratory tract. The respiratory tract can be divided into two sub categories; the upper respiratory tract and the lower respiratory tract. The upper respiratory tract is comprised of the nose, pharynx and larynx and is responsible for the conduction of air. This region of the respiratory system cleans, warms and humidifies the inhaled air. The lower respiratory tract comprises of the trachea, bronchi, bronchioles and alveoli, broadly described as ‘the lungs’. Gas exchange occurs exclusively in the lower respiratory tract. This introduction will focus on the structure and function of the lungs. For detailed anatomy on the other tissues and organs in the respiratory system see Albert, Spiro, & Jett, 2008 and Levitzky, (2007).

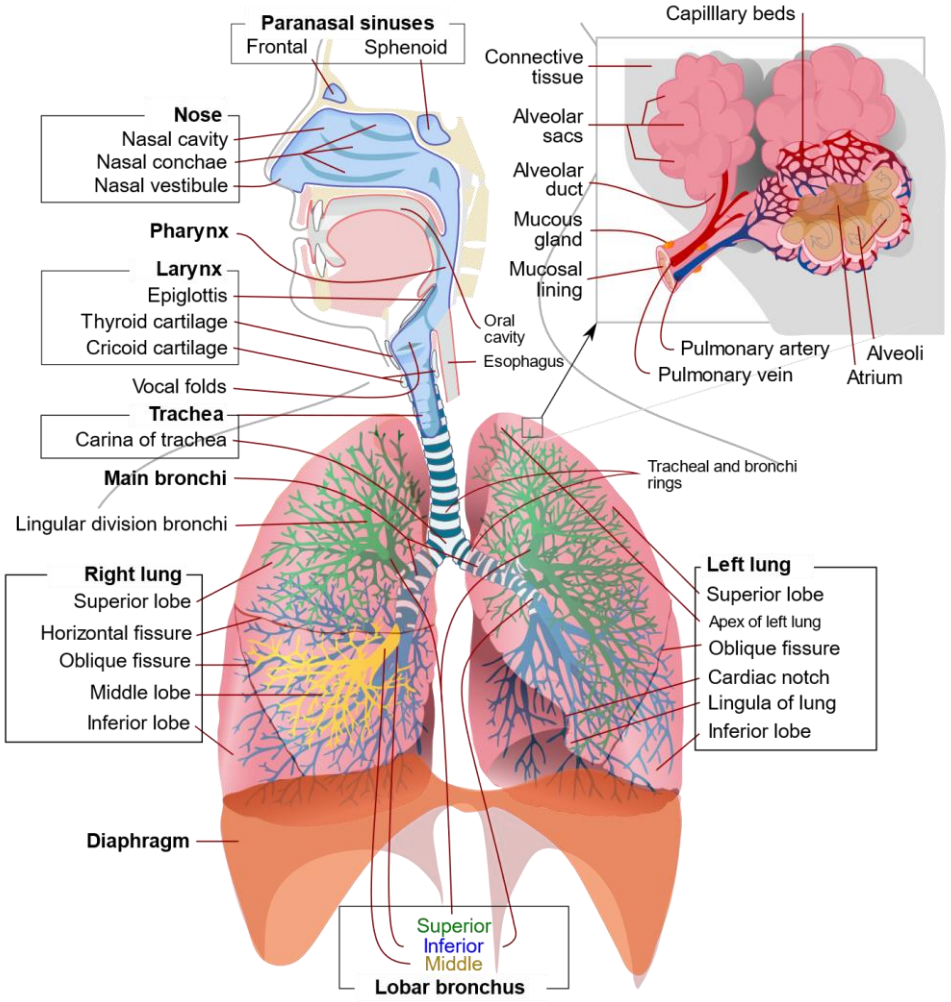

Figure 1.1. The respiratory system consists of the airways, the lungs, and the respiratory muscles that mediate the movement of air into and out of the body. Contributed by Wikimedia Commons, LadyofHats (Public Domain).

1.2 The Lungs

Three main components make up the entirety of the lung – air blood and tissue. The human lung is divided into three lobes on the right and two lobes on the left. The two primary functions of the lung are maintaining the gas exchange balance of O_2 entering the body and CO_2 leaving, and host defence against the particles and pathogens that are introduced to the body via respiration (Nomellini and Chen, 2012). The gross structure of the lung reflects this critical role of the lungs in homeostasis with blood contributing up to 50 % of the overall weight of an adult lung (Armstrong *et al.*, 1982) and a gas volume ranging from 2.5 L – 6 L at maximum expiration and inspiration respectively (Effros, 2006; Nomellini & Chen, 2012). The secondary functions of the lung lend to a much more diverse range of roles which is reflected

at the micro scale with Marciniak & Lomas, (2012) reporting over 40 different cell types present in the lung. Both these macro and micro structures are essential for understanding the homeostatic regulation of the lungs and the areas where dysregulation can occur, resulting in respiratory disease.

The major function of the lung is to facilitate gas exchange between the air and blood compartments, which takes place in the alveolar region. In the adult lung, the alveolar-capillary barrier that permits efficient gas exchange is formed by thin cytoplasmic extensions of *alveolar type I* (AETI) cells and capillary endothelial cells, separated by a common fused basement membrane.

1.2.1 Development

Human lungs first begin to develop during embryogenesis at around 7 weeks, with epithelial differentiation occurring between 16-26 weeks. Final remodelling and maturation of the lungs occurs postnatally, with new alveoli forming up to 8 years of age (Albert, Spiro and Jett, 2008). They then mature into a highly branched, specialised structure to maximise the exposure of the cardiovascular system to oxygen (Morrisey and Hogan, 2010).

1.2.2 Airways

The largest structural component of the airways is the trachea, this branches at the carina into the right and left mainstream bronchi, which subsequently divide into the lobar bronchi. This branching is asymmetric with 3 lobar bronchi forming on the right hand side of the lungs and 2 forming on the left (Weinberger, Cockrill and Mandel, 2014). The conducting airways subdivide and branch a further 15 - 20 times to form the respiratory bronchioles in the conducting section of the airway. The conducting airways transport gas and protect the rest of the lung from inhaled pathogens and particles.

Several layers of tissue contribute to the structure of the airways, each serving a specialised purpose. The intraparenchymal bronchioles are surrounded with smooth muscle, consisting of up to 20 % total tissue thickness. The elastic fibres present enable the stretch for inspiration and subsequent recoil for expiration. These elastic fibres are a required at all levels of the respiratory system and are essential components of the connective tissue in the lung, although smooth muscle is no longer present at the respiratory zone itself (Culver, 2012). The Mucosal layer consists primarily of pseudostratified columnar epithelial cells (PCE cells). Particles are trapped in the tracheobronchial secretions and migrated to the pharynx

by the ciliated epithelial cells. (Weinberger, Cockrill and Mandel, 2014). PCE cells are interspersed with goblet cells that secrete mucins into the airway lumen. Basal cells comprise of the local "stem cell" population and are capable of differentiating into the superficial mucosa cell populations (ciliated cells and secretory goblet cells) (Weinberger, Cockrill and Mandel, 2014). A secondary source of progenitor cells is the club cell (previously known as Clara cells). These are a prominent cell type in the terminal airway and have numerous functions in the lung. The first is their progenitor cell capabilities. Club cells are able to differentiate into the ciliated cells (Plopper & Hyde, 1992), secrete mucous, immune molecules and metabolise some inhaled chemicals (Peão *et al.*, 1993; Levitzky, 2007a). The final cell of note in the airways is the mast cell. These cells contain secretory granules consisting of a number of inflammatory mediators, capable of inducing bronchoconstriction, mucus production and increased permeability of the lungs (Levitzky, 2007b). These cell types are of significant importance, not only due to their homeostatic roles, but their responses to irritants and the role this plays in respiratory disease pathogenesis (Weinberger, Cockrill and Mandel, 2014).

1.2.3 Lung Parenchyma

The lung parenchyma is the location of gas exchange and consists of the alveoli, capillaries, and other interstitial tissues. There are two sequential connective tissue compartments in the lung, described by Hayek (1960). The alveolar wall (parenchymal interstitium), and the extra-alveolar connective tissue. The connective tissue, consisting of collagen, elastin and reticulin, protects the alveoli during inspiration and expiration by modulating the expansion and recoil tensions experienced by the tissues (Young, Moore & Hutchins, 1980).

1.2.4 Alveoli

Alveoli first begin to appear surrounding respiratory bronchioles, roughly 17 branching generations into the lung. The frequency of alveoli increases and following the 20^{th} generation of bronchioles the entire airway wall is comprised of alveoli, or alveolar ducts. Eventually these progress into alveolar sacs (Effros, 2006). The 300 million alveoli are around 250 µm in diameter and provide an approximate surface area of 90 m^2 for gas exchange. This number is an estimate and depends largely on the overall size of the lung. The alveolar surface area accounts for up to 99.5 % of the internal surface area of the lungs (Ochs *et al.*, 2004). Alveoli are mainly composed of a thin layer of squamous epithelial cells , and are almost completely surrounded by capillaries, up to 1,000 per alveolus (Levitzky, 2007b).

1.2.5 Type I & Type II Alveolar Epithelial cells

On the internal (air) side of the lung the alveolus is lined by two morphologically distinct types of alveolar epithelial cells: Type I (AETI) and Type II (AETII). The presence and function of these cells is highly conserved within mammalian species (Stone *et al.*, 1992). AETI cells constitute the squamous epithelium that forms the blood-air barrier (Ward and Nicholas, 1984) this network forms the gas exchange surface of the alveolus. AETII cells produce and secrete pulmonary surfactants which act to protect the lung against toxins and infectious particles that are inhaled during respiration (Mondrinos *et al.*, 2013). AETII cells also act as progenitor cells for repair for both AETI & AETII cells following injury to the alveolar epithelium (Fehrenbach, 2001), and express receptors for several growth factors, enzymes and matrix proteins (Allen *et al.*, 2001; Bejvl *et al.*, 2013).

Recently AETI cells have also been shown to have potential immunomodulatory functions (Wong, Chapin and Johnson, 2012; Yamamoto *et al.*, 2012). The previous consensus from studies in animal models of lung injury, hypothesised that damage to the alveolar epithelium is repaired by proliferation and transdifferentiation of AETII cells to AETI cells. AETI cells were considered to be terminally differentiated cells with no proliferative capabilities (Rock *et al.*, 2011; Barkauskas *et al.*, 2013). However, recent in vitro studies have demonstrated that cultured AETI cells have a high proliferative potential (Gonzalez, Allen and Dobbs, 2009; Wang and Hubmayr, 2011). This potential proliferative capacity and phenotypic plasticity of the TI cell in vitro indicate the potential for AETI cells participation in lung repair after injury in *vivo*.

AETII cells are also important in the initial innate immune response to pathogens. They secrete a variety of cytokines to activate macrophages, recruit monocytes, and trigger the adaptive immune system (J. Wang et al., 2011). AETII cells are considered important in various lung diseases (Kasper & Haroske, 1996) as they can repair the alveolar epithelium. Although during severe and chronic injury it is probable that the repair process is not solely carried out by these cells (Bhattacharya & Matthay, 2013). In interstitial lung disease, TII cell hyperplasia is a common pathologic feature.

1.2.6 Macrophages

Macrophages, first identified in the 19th century by Russian bacteriologist, Elie Metchnikoff (Gordon, 2008), are present in almost all tissues of the body, and are amongst the most

abundant immune cell in the respiratory tract. They are the cellular effectors of the innate immune system and play crucial roles in the development, metabolism, and maintenance of homeostasis. Macrophages are essential for maintaining a local tolerance to the pathogens and antigens inhaled during respiration (Kopf, Schneider and Nobs, 2014; Ballinger and Christman, 2016; Byrne, Maher and Lloyd, 2016). As well as removing pathogens via phagocytosis, macrophages are responsible for the production of a number of cellular mediators which act to initiate or suppress immune responses (Levitzky, 2007b). The tissue localisation of the macrophage largely determines its phenotype and mechanism of action (Minutti *et al.*, 2017).

Several populations of pulmonary macrophages have been identified of which interstitial and alveolar macrophage populations are the most prominent, located in the lung interstitium and alveoli respectively (Guilliams *et al.*, 2013). Other subpopulations of macrophages have been identified in lung pleural spaces, in the vasculature, and in the airways. These subpopulations are poorly characterised due to difficulties in their isolation (Laskin, Malaviya and Laskin, 2015).

Two major subpopulations of macrophages are described, proinflammatory (M1) macrophages and anti-inflammatory / wound repair (M2) macrophages (Martinez *et al.*, 2008; Laskin *et al.*, 2011). M1 macrophages release proinflammatory cytokines to initiate the Th1 immune response and are microbicidal in nature (Laskin *et al.*, 2011; Murray and Wynn, 2011; Wynn, Chawla and Pollard, 2013). M2 macrophages are primarily involved in wound repair and downregulating inflammation through the release of anti-inflammatory cytokines, and by phagocytizing apoptotic neutrophils. M2 macrophages also synthesize mediators such as TGF-β, VEGF and EGF that act on wound repair and tissue remodelling (Wynn, Chawla and Pollard, 2013; Laskin, Malaviya and Laskin, 2015). Macrophage activation is a dynamic process and the microenvironment in the lung is subject to constant changes. Macrophages have been shown not to be terminally differentiated into the M1/2 phenotype and have been shown to be capable of participating in both the pro- and anti-inflammatory response (Levitzky, 2007b; Mosser & Edwards, 2008) in order to respond effectively to these changes.

Alveolar macrophages first populate the lung during embryogenesis and are maintained for many months. The turnover rate is approximately 40 % per year, with minimal replenishment from hematopoietic precursors (Maus *et al.*, 2006; Yona *et al.*, 2013). Resident and monocyte derived alveolar macrophages have been shown to persist for up to a year following acute lung injury and act to resolve inflammation by clearing cellular debris, recruiting M2

macrophages, and aiding in remodelling of the lung parenchyma (Janssen *et al.*, 2011; Misharin *et al.*, 2017).

1.3 Pulmonary interstitium

1.3.1 Macrophages continued

The pulmonary interstitium includes the alveolar epithelium, basement membrane, perivascular and perilymphatic tissues and the pulmonary capillary endothelium. It is divided into the axial, parenchymal and peripheral zones, surrounding the bronchioles, parenchyma and pleura respectively (Society, 2010).

Interstitial macrophages are located within the parenchymal zone of the interstitium (Crapo *et al.*, 1983) where they account for approximately 40 % of pulmonary macrophages and 2 % total cell population of the lung (Lehnert, Valdez and Holland, 1985; Crowell *et al.*, 1992; Sebring and Lehnert, 1992). Though difficult to isolate and generally overlooked, current research into IM's suggest a more prominent role in regulating the negative feedback of inflammatory responses (Liegeois *et al.*, 2018). The response to bacterial products such as lipopolysaccharide (LPS) and CpG-DNA, by producing IL-10 (Harlotte *et al.*, 2002; Roy *et al.*, 2003) has been linked to the hygiene hypothesis (Strachan, 1989; von Mutius, 2007) and the increase in prevalence of respiratory diseases in society today.

First proposed in humans by Strachan, (1989) the "Hygiene Hypothesis" is a theory that suggests that if a juvenile immune system is not challenged sufficiently during development it fails to mature correctly and may not react appropriately when encountering pathogens or environmental triggers, (such as viruses, bacteria, pollen and animal dander) later in life. An increase in instance of immune-related health problems such as asthma atopic dermatitis, and hay fever have been reported in recent years, correlating with a declining incidence of most infectious diseases (Wills-karp, Santeliz and Karp, 2001; Bach, 2017). Although the phenomenon gained interest in humans in the late 1980's, the origin of this hypothesis can be traced to earlier experiments with animals, predominantly rodents maintained in SPF facilities (Abrams, Bauer and Sprinz, 1963; Wostmann *et al.*, 1970; Clarke *et al.*, 2013; Luczynski *et al.*, 2016). Exposure of low doses of an infectious agent lead to rapid rates of infection and increased death rates in SPF adolescent and young adult animals when compared to normally raised counterparts. A slow or attenuated immune response was identified in these animals.

1.3.2 Fibroblasts and Myofibroblasts

Fibroblasts are found in every tissue of the body, are of mesenchymal origin and, depending on their location, display multiple morphologies (Baum and Duffy, 2011). Fibroblasts are typically spindle-shaped cells found in the interstitial spaces of organs. During development of the lung, fibroblasts coordinate organogenesis and budding of the lung from the foregut. Fibroblasts are metabolically active cells, capable of synthesizing, secreting, and degrading extracellular matrix (ECM) components (Murray et al., 2009). In adulthood they are the primary source of ECM proteins and are key cells in homeostasis and maintenance of the ECM (Effros, 2006).

The myofibroblast is a differentiated form of the fibroblast characterised by the presence of microfilament bundles (stress fibres) and expression of α – smooth muscle actin (α – SMA). They are the predominant cell type in the tissue surrounding contractive wounds and are responsible for wound closure (Tomasek et al., 2002). Mechanical stress and TGF – β1 are both key regulators of myofibroblast differentiation, whereby TGF-β can stimulate differentiation by both the SMAD activation pathway (Van De Water, Varney and Tomasek, 2013) and via non-canonical pathways (Tomasek et al., 2005).

Dysregulation of myofibroblast activation leads to excessive synthesis and deposition of the collagen I and collagen III - rich matrix seen in fibrotic pathology such as idiopathic pulmonary fibrosis (IPF) (Leask, Denton and Abraham, 2004). Myofibroblasts are mechanically responsive cells and excess deposition of ECM alters the forces experienced in the surrounding tissue leading to persistence of myofibroblasts characteristic of fibrotic diseases such as fibrosis (Van De Water, Varney and Tomasek, 2013).

1.4 Comparative Anatomy of Human and Mouse Lungs

Mice are the most commonly used vertebrate animal in research with approximately 80% of human disease studies involving mice (Bryda, 2013). Rodents are ideal candidates for research models as they are small, inexpensive and easy to handle. The ability to map genomes led to the discovery that 99% of human genes have an equivalent in mice, which has resulted in mice being the preferred model for genetic manipulation studies to

determine the roles genes play in homeostasis and disease (The Jackson Laboratory, 2018; MRC, 2001).

Although there is genetic similarity between species, there are considerabe differences in structure from the human lung, outlined in Figure 1.2 and Table 1.1. The total lung capacity of the mouse is about 1 mL compared to 6,000 ml of a human (Irvin and Bates, 2003). Similar to human anatomy, the mouse lung consists of 5 lobes, arranged in a different distribution (Figure 1.2). The lung parenchyma of the mouse occupies a smaller proportion of the total lung than humans (mouse: 18%, human: 12% lung volume) (Irvin and Bates, 2003). The blood-gas barrier and structural components of the parenchyma are considerably smaller than that of the human (Table 1.1), which might have important implications for both gas exchange and parenchymal lung mechanics and must be considered when modelling human disease. To date, mice have been extensively used for modelling human respiratory disease. The availability of immunological reagents and the convenience of genetic manipulation (transgenic and gene knockout mice) makes the mouse model the most commonly employed (Han *et al.*, 2018). This will be discussed further in Chapter 3.

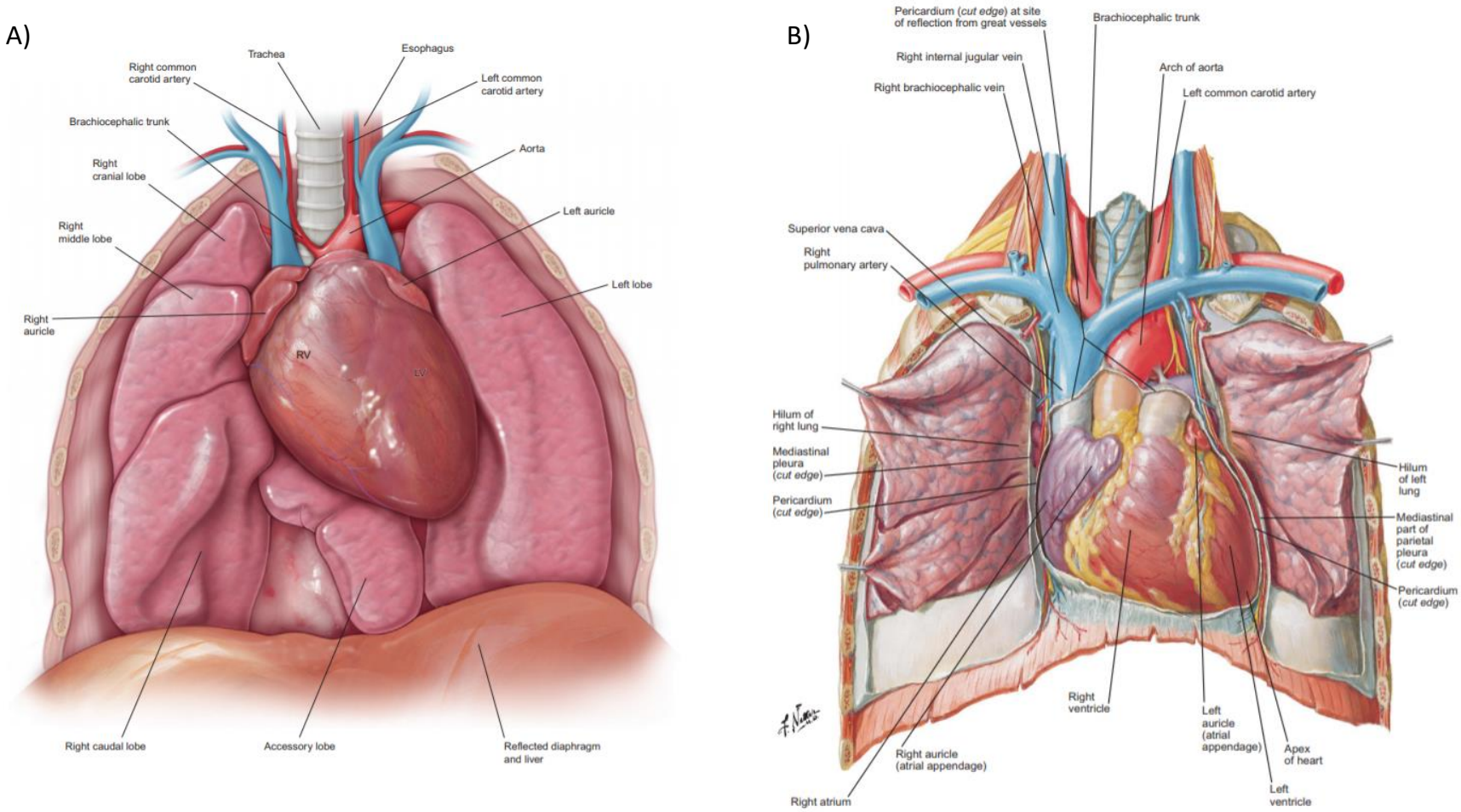

Figure 1.2. Regional anatomy of mouse and human lungs. A) Mouse lungs, B) Human lungs taken from (Suarez, Dintzis and Frevert, 2012).

Table 1.1. Comparative anatomy of mouse and human lungs. Adapted from Fox *et al.*, 2006; Suarez, Dintzis and Frevert, 2012

	Feature	Mouse	Human
Gross	*Lung lobes*	*4 right, 1 left*	*3 right, 2 left*
	Airway Generations	*13 - 17*	*17 - 21*
	Airway branching pattern	*Monopodial*	*Dichotomous*
	Diameter of main bronchus (mm)	*1*	*Oct-15*
	Respiratory rate (breaths per minute)	*80 - 230*	*12 - 16*
	Tidal volume (mL)	*1*	*6,000*
Tissue	*Diameter of terminal bronchiole (mm)*	*0.01*	*0.6*
	Alveoli (µm)	*39 - 80*	*200 - 400*
	Blood-gas barrier thickness (µm)	*0.32*	*0.62*
Airway cellular composition	*Lung Parenchyma*		
	Epithelial thickness (µm)	*8 - 17*	*40 - 50*
	Ciliated cells (%)	*28 - 36*	*37*
	Clara cells (%)	*59 - 61*	
	Mucous goblet cells (%)	*<1*	*10*
	Serous cells (%)	*<1*	*3*
	Basal cells (%)	*<1*	*32*
	Other (%)	*2 - 14*	*18*

1.5 Pulmonary Fibrosis

Pulmonary fibrosis (PF) is a severe, chronic and progressive disease state that is the final common pathway for many parenchymal diseases of the lung. It is characterised by chronic and excessive ECM deposition leading to distortion of the normal lung architecture, ultimately leading to respiratory failure.

PF is an umbrella term for a group of over 200 rare interstitial lung diseases (ILDs) sharing similar pathology and clinical symptoms. These diseases are characterised by damage to the lung parenchyma as a result of fibrosis and inflammation (Raghu, Nicholson and Lynch, 2008). Although sharing common characteristics, each disease presents with variable prognosis, treatment and outcome. Some ILDs have known aetiologies such as systemic disorders of the ECM (rheumatoid arthritis, systemic sclerosis), domestic and occupational exposures to asbestos, dust and other inhaled irritants, genetic inheritance (neurofibromatosis) or can occur as a result of drug treatments (bleomycin in chemotherapy) (Society, 2002). The remaining pathologies of unknown aetiology are classified under the umbrella term idiopathic interstitial pneumonias (IIPs).

Identifying and classifying these diseases has proven problematic. Since 1969 various classification systems have been proposed to distinguish the ILD's into distinct categories. In

2002 a new classification system was agreed upon by consensus of the European Respiratory Society and the American Thoracic Society (Society, 2002), this was revised further in 2013 (Travis *et al.*, 2013) resulting in the current classification guidelines currently in use in clinic today (Figure 1.2). Following this classification, it is now possible to identify these diseases in the clinic based on their symptomatic presentation, histological biopsy characteristics and radiological patterning. Statistical evaluation on the prevalence and mortality associated with ILD has subsequently been possible and used to understand the burden and cost associated with ILD both in the UK and across Europe. Recent initiatives and publications in the UK such as the National Institute for Health and Care Excellence (NICE) care guidelines (NICE, 2013) have since aimed to implement a standard of care across the UK which was further supported by efforts to standardise patient identification (Thickett *et al.*, 2014) in order to address the increasing incidence of lung disease.

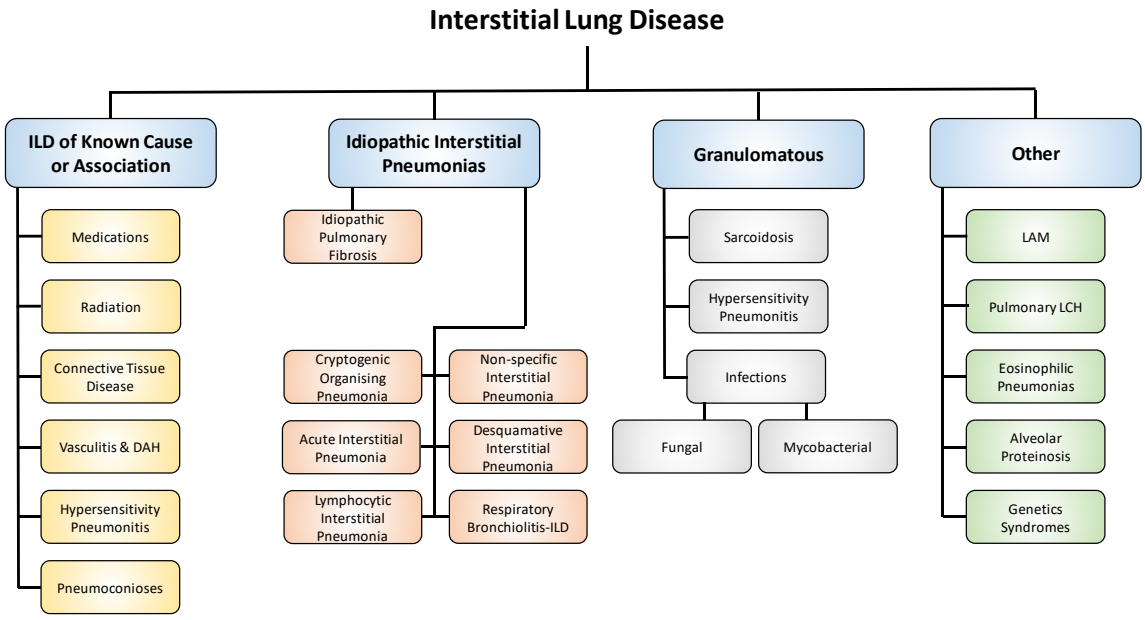

Figure 1.3. Current classification guidelines for diagnosis of IPF adapted from (Society, 2002).

1.5.1 Idiopathic Pulmonary Fibrosis

IPF is a chronic, progressive and ultimately lethal disease of the lung with no known cause (Raghu *et al.*, 2011). Following the consensus in ILD classification, IPF has been identified as the most commonly occurring IIP, accounting for up to 64 % of cases (Kim, 2006). Subsequent analysis of incidence and survival of IPF patients by Strongman, Kausar, & Maher (2018)

describes a trend of increasing incidence in IPF cases in the UK, whilst prognosis remains incredibly poor with an average life expectancy of 3 - 4 years following diagnosis. This is in line with previous analyses on the prevalence of IPF, (Coultas et al., 1994; Gribbin et al., 2006; Navaratnam et al., 2011) and the subsequent mortality (Johnston et al., 1990; Hubbard et al., 1996). Based on recent projections Navarro and Driscoll, (2017) describe that an average of 5,000 deaths per year are seen in patients with IPF.

IPF is rare in people below the age of 45, with the average age of onset being around 70. There has been no observed pattern in the geographical distribution of cases, and no racial or ethnic predisposition has been reported (Coultas et al., 1994). The clinical course of IPF is highly variable with some patients remaining stable for longer periods of time, whilst others experience acute exacerbations leading to rapid progressive respiratory failure and eventual death (Herzog et al., 2014). Traditional anti-inflammatory therapies, which are the main line of therapy used in the treatment of all IIDs show no effect in IPF (Society, 2002) and until recently the only treatment options for IPF patients were to target the symptoms. However, 2013 saw the approval of new antifibrotic therapies Pirfenidone (NICE, 2013; King *et al.*, 2014), followed by Nintedanib in 2015 (Richeldi *et al.*, 2014). Current trials are also underway for a targeted monoclonal antibody therapy, FG-3019 / Pamrevlumab (Raghu *et al.*, 2012, 2016; Lipson *et al.*, 2017). Current reports indicate that these drugs have shown an ability to slow disease progression in some patients. However, there is still no curative treatment option for IPF and the pathophysiology of this disease remains poorly understood (Hui Hoo and B Whyte, 2012).

1.5.2 Pathogenesis of IPF

As suggested by its name, the aetiology of IPF is unknown. However studies using tissues from patients and from animal models have revealed some insight into some of the factors contributing to the development of this disease (Moore and Hogaboam, 2008; Lindahl *et al.*, 2013; Williamson, Sadofsky and Hart, 2015). A recurring finding and current hypothesis is that fibrosis arises as a result of dysregulation in wound healing. This is suspected to be a response to repetitive alveolar injury in genetically susceptible individuals (Liu, Nepali and Liou, 2017). In 5 % of cases of pulmonary fibrosis, individuals have one or more affected first-degree relatives (Garcia-Sancho et al., 2011). Genetic factors (Zhou and Wang, 2016) and exposure to drugs such as bleomycin (Reinert *et al.*, 2013), amiodarone (Wolkove and Baltzan, 2009), and methotrexate (Jakubovic *et al.*, 2013) have all been shown to cause IPF, although the typical progression of IPF resulting from these is slower than that of IPF in

general. One of the more recent hypotheses on the pathogenesis of IPF is that AETII cell dysfunction causes the fibrotic response as a result of protein misfolding and ER stress, which ultimately leads to secretion of TGF-β and other profibrogenic factors (Haschek & Witschi, 1979; Selman, King, & Pardo, 2001). Epithelial mesenchymal transition (EMT) has previously been considered to be an important part of the fibrotic response, however recent lineage tracing studies indicate this is unlikely to be the case (Rock et al., 2011). Mutations of surfactant proteins A and C (SP-A and SP-C) are thought to cause some types of familial pulmonary fibrosis, and this is thought to be due to protein misfolding and ER stress (Korfei et al., 2008; Lawson et al., 2011; Maitra, Wang, Gerard, Mendelson, & Garcia, 2010; Tanjore, Blackwell, & Lawson, 2012; Zhong et al., 2011).

A number of reviews have discussed the current theories on the initiation and progression of IPF in greater detail (Selman, King and Pardo, 2001; Wolters, Collard and Jones, 2014; Berngard and Afshar, 2016; Richeldi, Collard and Jones, 2017; Wolters et al., 2018). However, none of these has been widely accepted and further research into IPF is desperately required.

1.6 Extracellular matrix and the Fibrotic lung

1.6.1 Collagen

The collagen superfamily in vertebrates comprises of over 50 collagens and collagen-like proteins (Hulmes, 2008). In mammals, collagens are the most abundant protein, accounting for up to 30 % total protein mass. 28 collagen proteins have been identified in humans, and classified into smaller subfamilies (Kadler *et al.*, 2007; Ricard-Blum, 2011). These are listed in Table 1.1.

Collagens are trimeric ECM molecules, consisting of three polypeptide chains ranging between 662 – 3152 amino acids in length (Gordon and Hahn, 2010). These α - chains are composed of a characteristic repeating peptide triplet sequence of Gly-X-Y, where X is commonly proline and Y is hydroxyproline (Miller, 1985). The presence of glycine causes these chains to form the triple helical domains commonly referred to as collagenous domains or triple helix motif (Gordon and Hahn, 2010). These α - chains can combine into homotrimers such as collagen III or heterotrimers containing up to three different α - chains e.g. collagen I consisting of two α1 chains and one α2 chain. Kirk *et. al.* (1984) determined that the predominant collagens of the lung are types I and III, accounting for a total of 90 %

of total lung collagen, therefore for the purposes of this thesis these two collagen types will be discussed further.

Table 1.2. Collagen sub-families (Hulmes, 2008).

Sub - Family	**Members**
Fibrillar Collagens	Types I, II, III, V, XI, XXIV and XXVII
Fibril associated and related collagens	Types IX, XII, XIV, XVI, XIX, XX,XXI and XXII
Beaded filament forming collagens	Type VI
Basement membrane and associated collagens	Type IV, VII, XV and XVIII
Short chain collagens and related proteins	Types VIII and X; C1q; hibernation-related proteins HP-20, HP-25 and HP-27; emilins 1 and 2; adiponectin; CTRPs 1-7: inner ear (saccular) collagen
Transmembrane collagens and collagen-like proteins	Types XIII, XVII, XXIII and XXV/CLAC-P; ectodysplasins; macrophage scavenger receptors I-III; MARCO; SRCL; gliomedin; CL-P1
Collectins and ficolins	Mannan binding protein; surfactant proteins A and D; conglutinin; CL-43; CL-46; CL-L1; CL-P1; L-, M- and H-ficolins
Other collagens and collagen-like proteins	Emu1; collagen XXVI/Emu2; collagen XXVIII; acetylcholinesterase tail subunit

1.6.2 Fibrillar Collagen

Fibrillar collagens have been described in almost all animals and are the components of striated fibrils (Exposito *et al.*, 2010). Collagens I and III are both classified as fibril-forming interstitial collagens. Both are predominantly found in tissues with elastic properties such as skin, lung and vasculature (Hulmes, 2008). Fibrillar collagen provides tensile strength which is of particular importance in organs such as the lungs, which experience constant

stretch/relax stress. Collagens I and III are distributed throughout the pulmonary interstitium to provide the structural support required by the alveolar-capillary network (Seyer, Kang and Rodnan, 1981). Although epithelial cells, endothelial cells, and smooth muscles are capable of producing these collagens, fibroblasts (previously discussed) are thought to be the main source of Collagen I and III in the lung.

1.5.3 Collagen Synthesis

Collagen biosynthesis is a complex, multi-step process that requires both intracellular and extracellular processing to form a 'mature' collagen protein. This process is outlined in Figure 1.3. The collagen genes are transcribed to mRNA which is ribosome-bound. This is translated into procollagen α - chains in the rough endoplasmic reticulum (rER). Of the subsequent posttranslational modifications, hydroxylation of proline and lysine residues is of notable importance. The formation of 4-hydroxyproline and hydroxy-lysine is essential for ensuring the triple helices remain stable through the formation of intramolecular hydrogen bonds (Gelse, Poschl and Aigner, 2003).

Further post-translational modifications are required before the procollagen molecules can be transported to the Golgi complex and secreted into the extracellular space. These include trimerization, chain folding, and formation of disulphide bonds. The final stage in processing of the procollagen molecules requires the cleavage of the C- and N-propeptide groups and formation of covalent cross-links. A number of enzymes and proteases control these processes including the ADAMTs and the lyase oxidase (LOX) family and are essential for the formation of collagens I and III (Herchenhan *et al.*, 2015). LOX enzymes act to convert the lysine or hydroxy-lysine residues in the C- and N- terminal regions of the procollagen chains to peptidyl aldehydes. These residues are then able to react with several other molecules to form the covalent cross-links that are required for stable collagen fibril formation (Hulmes, 2008).

A fibrillar procollagen α - chain contains one of the aforementioned collagenous domains made of approximately 338 Gly-X-Y triplets (Ramshaw, Shah and Brodsky, 1998). This triple helical region is flanked by the N- and the C-pro-peptides. Figure shows the processing of a procollagen molecule to a mature collagen protein. The glycine and peptide bonds are frequently contained within or alongside the helical structure, rendering collagen highly resistant to proteolysis.

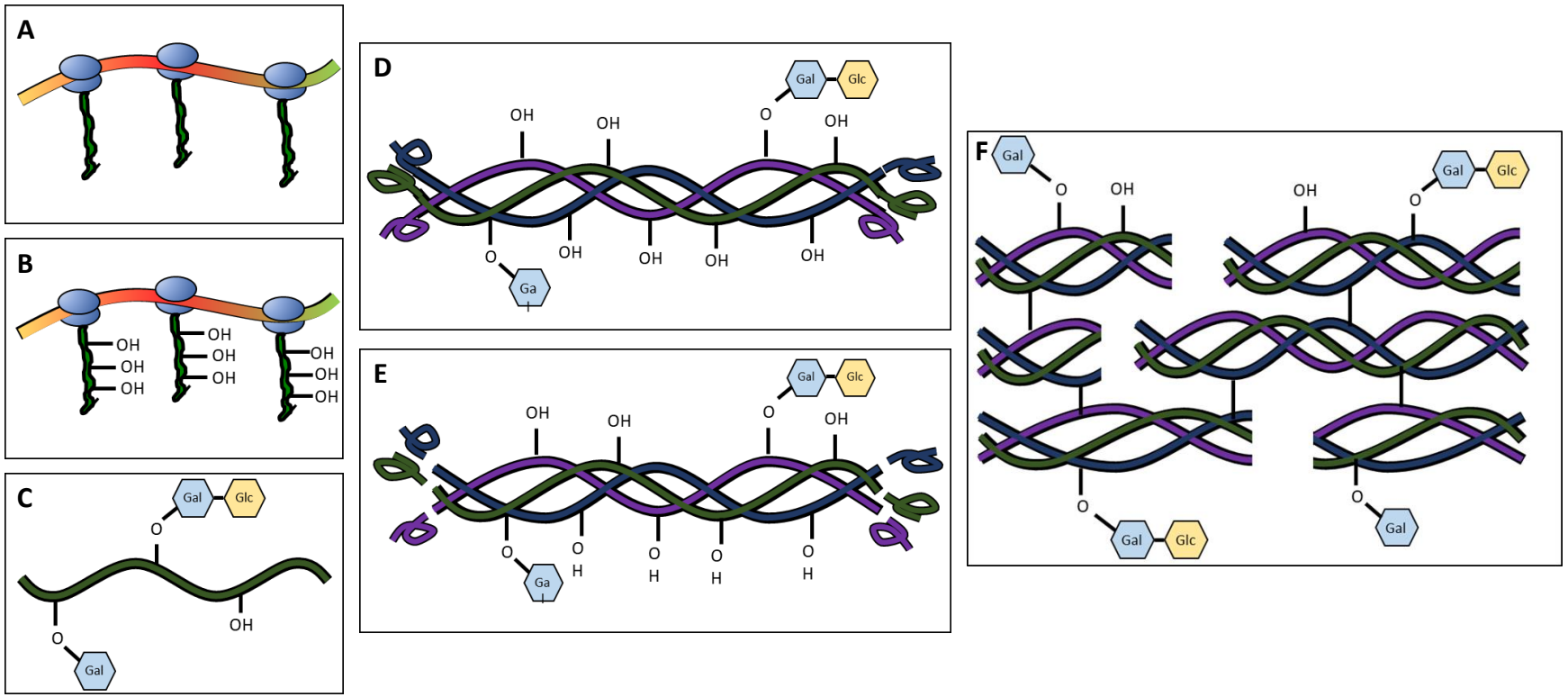

Figure 1.4. Mechanism of collagen I synthesis. Adapted from (https://step1.medbullets.com/biochemistry/102078/collagen). A) In the fibroblast nucleus; ribosomes translate pre-pro-collagen α – chain sequence. B) Hydroxylation of Proline and Lysine residues. C) Pro-collagen, translocation from the nucleus to the cytoplasm occurs, ER sugars are added (hexagons). D) Formation of triple helix and folding of globular domains, secretion from cell. E) In extracellular space; Removal of N and C terminal domains. F) Deamination of lysine residues, formation of crosslinks to form Collagen fibres.

1.6.4 Collagen deposition in a normal and fibrotic lung

Contradictory to the original hypothesis that collagen was inert, it has since been conclusively proven that a dynamic state of synthesis and degradation of collagen exists within the lung. Up to 10 % of the total collagen in an adult mammal lung is synthesised and degraded over a single 24-hour period (McAnulty and Laurent, 1987), with in *vivo* and in *vitro* studies finding that up to 30 % of this degradation occurs intracellularly within minutes of synthesis (Bienkowski, Baum and Crystal, 1978; McAnulty and Laurent, 1987). These studies were the first indicator that the fibroblast cell may not be a quiescent cell population, only active during a disease state, but rather constitutively active, producing and degrading collagen both intra- and extracellularly.

In a disease state this synthesis/degradation equilibrium is disturbed, resulting in excessive synthesis and disorganised deposition of collagen. Phenotypically, this results in an abnormal and progressive thickening of the alveolar interstitium, which ultimately destroys the architecture and functionality of the alveoli for gas exchange (Martin-Mosquero *et al.*, 2006). As previously mentioned, the two most abundant collagens in the lungs are collagens I and III in a ratio of approximately 2:1 (Seyer, Kang and Rodnan, 1981). Several studies investigating fibrosis found different ratios of both collagens, yet failed to conclusively determine whether an altered ratio of collagen I to III was sufficient to cause the disease state, or a product of the processing and sample type examined i.e. post mortem vs. biopsy (Bateman *et al.*, 1983; Kirk *et al.*, 1984). The current consensus is that excessive production of collagen is the important physiological change that leads to the establishment and progression of fibrosis rather than the change in ratios.

Animal models of pulmonary fibrosis, such as the bleomycin model have demonstrated increases in pro-fibrotic markers such as TGF-β1 and fibronectin, as well as the procollagen genes Col1α1, Col1α2 and Col3α1 (Amtje Moeller *et al.*, 2008), which are comparable to biomarkers found in human studies (Giménez et al., 2017.; Guiot, Moermans, Henket, Corhay, & Louis, 2017; Zhang, Kaminski, & Simmons, 2012). These correlate with the increase in collagen production. Conversely, alternative studies have identified a decrease in the degradation of collagen by examining the expression of matrix metalloproteinases (MMPs) and tissue inhibitors of metalloproteinases (TIMPs) in patients presenting with IPF (Selman *et al.*, 1986; Dancer, Wood and Thickett, 2011; Leeming *et al.*, 2012). Increases in TIMPs that are greater than the associated MMPs lead to a state of persistent matrix deposition.

Therefore, current literature is inconclusive as to whether a state of increased synthesis, decreased degradation or a combination effect leads to the development of fibrosis in IPF.

Excess collagen is deposited in fibrotic foci, these are used as one of the key diagnostic elements when examining histological samples from lung biopsy. The presence and prevalence of these foci are linked to disease progression, with an increase in incidence indicating a decreased likelihood of survival (King *et al.*, 2001). The rate of collagen deposition by fibroblasts is therefore one of the primary predictors of disease progression. The mechanisms regulating this deposition are therefore attractive therapeutic targets.

1.7 TGF - β function and signalling

For evolution of complex, multicellular organisms to continue, a tightly regulated system for the communication and control of individual cells is required. Basic physiological processes such as cell proliferation, differentiation, metabolism and apoptosis are regulated by an intricate signalling system comprised of cytokines, growth factors and polypeptide hormones (Biernacka, Dobaczewski and Frangogiannis, 2011). Of these factors TGF – β is particularly important.

TGF - β isoforms form a superfamily of growth factors together with bone morphogenetic proteins (BMPs) and growth differentiation factors (GDFs) (Györfi, Matei and Distler, 2018). TGF - β proteins are multi-functional growth factors that are secreted and stored in the ECM as a latent complex. This enables spatial and temporal regulation during homeostasis (Massagué, 2012). TGF - β is considered a master regulator of tissue regeneration and repair, as such dysregulation of TGF – β leads to pathologies such as fibrosis (Denton and Abraham, 2001; Ihn, 2002; Leask, 2004).

The pro-fibrotic effects of TGF - β have been shown to be mediated through the downstream effector; CCN2. Upregulation of CCN2 is mediated by the canonical SMAD signalling pathway (Figure 1.5). TGF - β induces the expression of CCN2 via a functional Smad3 binding site in

the CCN2 promoter, which in turn stimulates myofibroblast differentiation and collagen synthesis (Duncan et al., 1999).

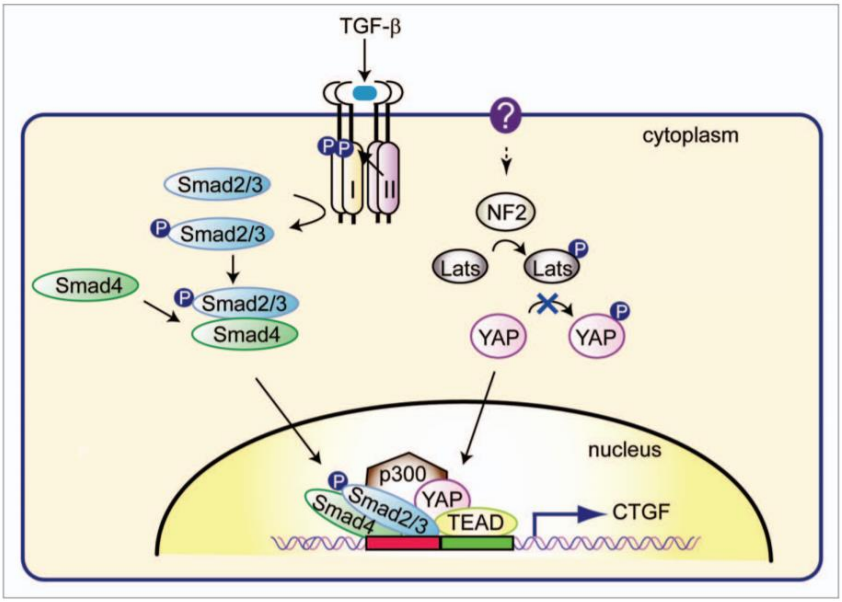

Figure 1.5. Schematic model of CTGF promoter activation through TGFβ/Smad signalling. Upon TGFβ stimulation, Smad2/3 and Smad4 associate, move to the nucleus, make a complex with YAP/TEAD, and recruit p300 to the promoter to activate CTGF expression (Nakanishi *et al.*, 2012).

1.8 CCN Family

The CCN gene family, whose name is derived from the early nomenclature of the first three proteins to be identified (Cyr61, CTGF and NOV) consists of six members. Previous nomenclature and original literature citing their discovery each of these family members can be found in Table (Malik, Liszewska and Jaworski, 2015). In 2003 Brigstock *et al.* proposed a unification of the CCN protein nomenclature in order to reduce confusion and challenges in tracking research involving this protein family.

Table 1.3. CCN family proteins and their previous nomenclature.

CCN Family Name	Previous Nomenclature
CCN1	CYR61, CTGF-2, IGFB10, IGFB-rP4 (Lau and Nathans, 1987)
CCN2	CTGF, IGFBP8, IGFBP-rP2, HBGF-0.8, ecogenin, FISP12 (Bradham *et al.*, 1991)
CCN3	NOV, NOVH, IGFBP9, IGFBP-rP3 (Joliot *et al.*, 1992)
CCN4	WISP-1, Elm-1 (Hashimoto *et al.*, 1998)
CCN5	WISP-2, CTGF-L, CTGF-3, HICP, Cop-1 (Zhang *et al.*, 1998)
CCN6	WISP-3 (Pennica *et al.*, 1998)

The CCN family are cysteine-rich matricellular proteins that are relatively small; approximately 35 – 40 kDa. The members of this protein family share similar mechanisms of action due to their shared primary structure. This comprises of 38 cysteine residues conserved throughout the peptide which form four distinct, multifunctional binding domains preceded by a secretory amino peptide. The exception being CCN5, which lacks the fourth structural domain and contains only 28 conserved cysteine residues, shown in Figure 1.6 (Brigstock, 1999; Jun and Lau, 2011). CCN proteins share a common intron/exon pattern. Each containing five exons, where the first exon corresponds to the signal sequence, and the remaining four corresponding to one of the protein domains (Holbourn, Acharya and Perbal, 2008a).

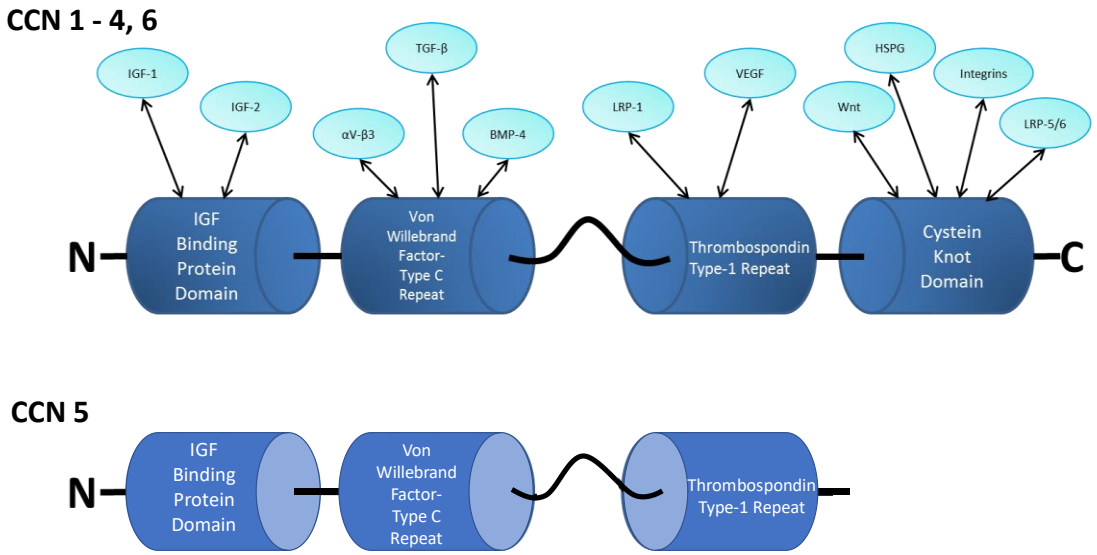

Figure 1.6. Domain structures and binding ligands of the CCN family of proteins.

The first domain shares 32 % homology to insulin-like growth factor binding proteins (IGFBPs) and is therefore termed the IGFBP-binding domain. The second domain encodes a von Willebrand type C (VWC) repeat, mediating interactions with integrins and growth factors such as BMPs and TGF - β. The third domain is a type-1 thrombospondin (TSP) repeat, known to mediate the ability of TSP to bind to ECM proteins, MMPs, and integrins. The final C-terminal (CT) motif contains a cysteine knot (Leu, Lam and Lau, 2002; Gao and Brigstock, 2004; Hall-Glenn and Lyons, 2011).

CCN proteins have been found to share similarities in their molecular mechanisms of action and the cellular processes that they regulate. These include but are not limited to cell adhesion, migration, proliferation, survival, and differentiation. Current research suggests that these activities are tissue and cell dependent with the same CCN family member displaying antagonistic effects depending on their location. There are many reviews available which explore this family of proteins and their actions in greater depth (Holbourn, Acharya, & Perbal, 2008; Jun & Lau, 2011; Leask & Abraham, 2006; Malik et al., 2015; Perbal & Takigawa, 2005; Perbal, 2013; Wu et al., 2016; Yeger & Perbal, 2007).

Our research has investigated the actions of the second member of this family – CCN2, previously known as CTGF. We will examine the physiological roles this protein plays in further detail.

1.8.1 CCN2

CCN2 is the second member of the CCN protein family. Early analysis of CCN2 function *in vivo* focused primarily on its role as a mediator of ECM synthesis in multiple fibrotic diseases. However, CCN2 and the remaining CCN family members have also been found to play key roles during development, as well as modulating cell adhesion, proliferation, survival, migration, and ECM production across a diverse range of cell types during adulthood.

During embryogenesis, CCN2 is highly expressed in mesenchymal cells and acts to mediate renal, cardiovascular and skeletal development (Liu *et al.*, 2011; Ramazani *et al.*, 2018). Expression of CCN2 was found to be critical for development when a global knockout model of CCN2 noted premature mortality of pups, caused by respiratory failure owing to rib malformation (Ivkovic *et al.*, 2003). Expression of CCN2 is limited during adulthood unless a disease state is present (Liu *et al.*, 2011).

Regulation of CCN2 occurs both at the transcriptional and post -translational level and is controlled by a variety of factors (Ramazani *et al.*, 2018). At the transcriptional level, CCN2 expression is induced by stimuli such as growth factors, cytokines, hormones, mechanical stress, outlined in Figure 1.7 (Kubota and Takigawa, 2015). These stimuli can act directly, or by recruiting transcription factors (Jun and Lau, 2011). TGF - β was one of the first cell-signalling molecules to be implicated as a regulator of CCN2 and many of the TGF - β responses involve CCN2 to varying degrees (Leask and Abraham, 2006; Shi-wen *et al.*, 2006; Arnott *et al.*, 2007; Ponticos *et al.*, 2009; Holmes *et al.*, 2001; Leask *et al.*, 2003; Geisinger *et al.*, 2012).

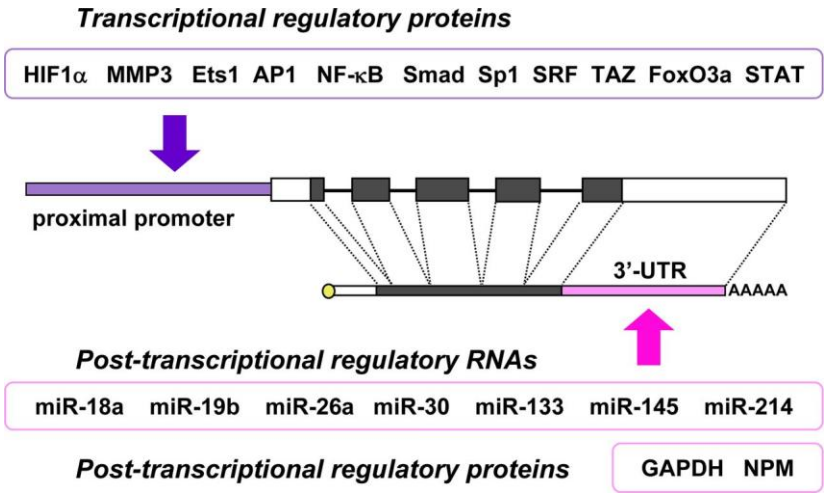

Figure 1.7. Transcriptional and post-transcriptional regulation of the CCN2 gene. The structures of the CCN2 gene and its mRNA are illustrated at the centre. Transcription factors and post-transcriptional regulatory molecules that are known to directly regulate CCN2 expression are summarized.

Aberrant expression of CCN2 has been associated with several fibrotic diseases such as systemic sclerosis, and lung, kidney and liver fibrosis; reviewed by (Ramazani *et al.*, 2018), in addition to being associated with osteoarthritis and cancer (Planque and Perbal, 2003; Omoto et al., 2004; Leask, 2009). In animal models of IPF CCN2 has been shown to be increased in fibroblasts (Lasky et al., 1998; Liu et al., 2011; Yang et al., 2014; Ashley et al., 2017). CCN2- deficient animals have fewer myofibroblasts and decreased ECM disposition, indicating that CCN2 is necessary for induction of fibrosis in these animals (Liu et al 2011). Based on this evidence CCN2 is likely a good and viable target for pharmaceutical intervention in IPF further research *in vivo* is required to elucidate the specific role CCN2 plays in the pathogenesis of this disease.

1.9 Hypothesis Statement

I hypothesise that the loss of function of CCN2 prior to induction of bleomycin will provide a beneficial effect and will impair the cells ability to produce extracellular matrix. I hypothesise that this effect will be more profound when CCN2 functionality is removed in a ubiquitous manner, compared to a fibroblast specific loss of function.

1.10 Aims

1.1 Generation of Transgenic animals

Four single transgenic mouse colonies will be established at the University of Liverpool, each containing one of the following: a CCN2 floxed gene, a dual fluorescent reporter construct, a fibroblast specific tamoxifen inducible Cre recombinase or a ubiquitously expressing tamoxifen inducible Cre recombinase. These animals will be bred to generate novel double transgenic mouse lines to examine the effects of CCN2 loss of function in a bleomycin model of IPF.

1.2 Generation of double transgenic animals

Two double transgenic mouse lines will be established for the inducible loss of function of CCN2. Mice homozygous for the CCN2 floxed gene will be bred with mice containing either the fibroblast specific tamoxifen inducible Cre recombinase or the ubiquitously expressing tamoxifen inducible Cre recombinase. Offspring from these breeding pairs will be interbred to generate colonies homozygous for the CCN2 floxed gene and positive for one of the Cre recombinase genes.

1.3 Characterisation of expression of fibroblast specific Cre in double transgenic animals

A dual fluorescent reporter mouse line will be bred with the fibroblast specific tamoxifen inducible Cre recombinase line to generate a double transgenic colony homozygous for the reporter construct and positive for the fibroblast specific Cre recombinase. Tamoxifen will be administered at different stages of development and adulthood to investigate the localisation pattern of activity of the fibroblast specific Cre recombinase.

2. Testing the Bleomycin model of Fibrosis

3. Testing the loss of function CCN2 models

2. Materials and Methods

2.1 Declaration of Ethics

All procedures performed during this research project were carried out in accordance with the UK Home Office guidelines and regulations under the Animals (Scientific Procedures) Act 1986 (ASPA). This work was carried out under the project licences granted to Professor George Bou-Gharios PPL70/9060, and a personal licence (PIL. I0BCA5D31) granted to Amy Horwell for the completion of experiments, Schedule 1 (Sch1) humane killing of mice and the collection and use of the resultant tissue for analysis.

2.2 Mouse Husbandry

All mice were housed and maintained within the University of Liverpool's Biomedical services unit (BSU) in accordance with Home Office UK guidelines. Mice were maintained in a specific pathogen free (SPF) environment, under a 12-hour light/dark cycle, and granted access to food and drinking water ad libitum.

2.3 Mouse Colony establishment and maintenance

2.3.1 Inducible fluorescent reporter line (Col1α2-R26TmG)

Founder breeding pairs were established by breeding female mice containing the reporter construct B6CB; 129-(Cg)-Gt (ROSA) 26Sortm4 (ACTB-tdTomato,-EGFP) Luo/Liv (Muzumdar *et al.*, 2007), purchased from Jackson Laboratories, 007676, with male mice containing the Col1α2 driven CreER^{T2} B6CB-Tg (Col1a2-17=1.5kbenh-350mp-CreErt2)3.18/Liv, generated by the Bou-Gharios lab (Bou-Gharios *et al.*, 1996; De Val *et al.*, 2002; Li *et al.*, 2017). The resulting offspring were genotyped for both mTmG and Cre transgenes as heterozygous, double transgenic (mTmG +/-, Cre +/-).

Further crossing of littermate male and female mice was used to establish and maintain a colony of double transgenic mice (mTmG +/+, Cre +/-) on a mixed background; B6CB;129-Tg(Col1a2-17=1.5kbenh-350mp-CreErt2)3.18-(Cg)-Gt(ROSA)26Sortm4(ACTB-tdTomato,-EGFP)Luo/Liv (strain identifier – Col1α2-mTmG) at the University of Liverpool, UK.

2.3.2 Inducible knock out of CCN2 in Fibroblasts (Col1α2-CCN2fl)

Founder breeding pairs were established from transgenic mice containing the CCN2 floxed transgene B6; 129S-CTGFtm1.Alea**,** (provided by Dr Andrew leask, (Ponticos *et al.*, 2009; Liu *et al.*, 2011)) bred with mice carrying the transgene for a Col1α2 driven CreER^{T2} B6CB-Tg (Col1a2-17=1.5kbenh-350mp-CreErt2) 3.18/Liv, generated by the Bou-Gharios Lab (Bou-Gharios *et al.*, 1996; De Val *et al.*, 2002; Li *et al.*, 2017). The resulting offspring were genotyped and heterozygote CCN2 floxed +/-, Cre +/- animals were interbred to yield and maintain a colony of double transgenic mice (CCN2 floxed +/+, Cre +/-) on a B6CBA background; B6CB; 129S-Tg (Col1a2-17=1.5kbenh-350mp-CreErt2)3.18-CTGFtm1.Alea/Liv (strain identifier – Col1α2-CCN2fl) at the University of Liverpool, UK.

2.3.3 Inducible Ubiquitous knockout of CCN2 (ROSA-CCN2fl)

A founder breeding pair was generated by breeding a male mouse containing the CCN2 floxed transgene B6;129S-CTGFtm1.Alea (Ponticos *et al.*, 2009; Liu *et al.*, 2011), with a female mouse containing a ubiquitously expressed ROSA26CreER^{T2} B6CB;129-Gt(ROSA)26Sortm1(cre/ERT)Nat/Liv bought from the Jaxson lab, Stock No: 008463 (B6.129-*Gt(ROSA)26Sor$^{tm1(cre/ERT2)Tyj}$*/J), (Badea, Wang and Nathans, 2003)s. The resulting offspring were genotyped and heterozygous, double transgenic (CCN2 floxed +/-, Cre +/-) animals were interbred to yield and maintain a colony of double transgenic mice (CCN2 floxed +/+, Cre +/) on a mixed background; B6CB; 129S-CTGFtm1.LeaskGt (ROSA) 26Sortm1 (Cre/ERT) Nat/Liv (strain identifier – ROSA-CCN2fl) at the University of Liverpool, UK.

2.4 Mouse Colony Genotyping

2.4.1 Proteinase K based DNA Extraction

Genomic DNA extracted from ear punch biopsies was used to identify each animal. Notches were obtained from all experimental animals. DNA from all strains was extracted using the following protocol.

Proteinase K from *Tritirachium album* (Sigma Aldrich) was prepared to a final concentration of 10 mg/mL in 50 % glycerol. 10 µL proteinase K was added to 100 µL lysis buffer and incubated at 55 °C overnight in a water bath.

Samples were then vortexed and the tissue dissolved. If tissue remained solid / failed to dissolve a further 10 µL proteinase K was added and the sample incubated further (up to 1 hour) at 55 °C. Samples were then centrifuged at 14,000 xg for 7 minutes. The supernatant was transferred to a clean, labelled 1.5 mL eppendorf and the remaining tissue was discarded. An equal volume of isopropanol (Sigma Aldrich) was added to the supernatant and the tube inverted several times. Samples were centrifuged at 14,000 xg for 3 minutes and the supernatant removed. A clear pellet of DNA remained in the bottom of the eppendorf. A final 30 s centrifugation step was carried out at 14,000 xg and any remaining supernatant was pipetted off. The DNA was then left to air dry at room temperature for a maximum of 10 minutes. DNA was reconstituted in 50 µL ddH_2O for one hour at room temperature, or at 4 °C overnight. DNA concentration was then determined using a NanoDrop 200 prior to PCR analysis. A 260/230 value ≥ 0.6 was acceptable for genotyping PCR.

2.4.2 Solutions

2.4.2.1 Lysis Buffer

Reagent	**Volume**
50mM Tris-HCL (pH8)	4.5 mL of 2 M stock solution
0.1M NaCl	7 mL of 3 M stock solution
1% SDS	8 mL of 10 % stock solution
20mM EDTA	7.2 mL of 500 mM stock solution
ddH_2O	144.3 mL
Autoclave solution and store at room temperature	

2.4.2.2 Proteinase K stock

10 mg/mL in 50 % Glycerol stored at -20 °C

2.4.3 Polymerase Chain Reaction (PCR)

For a single gene PCR reaction (CCN2 Floxed, mTmG), 100 ng DNA was added to a 25 µL PCR reaction mix containing 0.2 µL GoTaq® G2 Flexi DNA Polymerase, 5 µL 5X Green GoTaq® Flexi Buffer, 2 µL 25 mM $MgCl_2$ (all reagents supplied with GoTaq® G2 Flexi DNA Polymerase, Promega) with the addition of 0.5 µL 10 mM dNTPs (Bioline) and 0.5 µL 10 pM specific primers (Table 2.1., Eurofins Genomics). ddH_2O was added to make a final reaction volume of 25 µL.

For a duplex PCR reaction (Cre / LacZ plus Internal), 100 ng DNA was added to a 25 µL PCR reaction mix containing 0.2 µL GoTaq® G2 Flexi DNA Polymerase, 5 µL 5X Green GoTaq® Flexi Buffer, 3 µL 25 mM $MgCl_2$ (all reagents supplied with GoTaq® G2 Flexi DNA Polymerase, Promega) with the addition of 1 µL 10 mM dNTPs (Bioline) and 0.5 µL 10 pM specific primers (Table 2.1., Eurofins Genomics). ddH_2O was added to make a final reaction volume of 25 µL.

PCR conditions for all reactions were: initial denaturation for 5 minutes at 94 °C, followed by 35 cycles of denaturation at 94 °C for 30 seconds, annealing at primer specific temperatures (Table 2.1., for primer specific annealing temperatures) for 45 seconds, elongation at 72 °C for 1 minute, then a final elongation at 72 °C for 5 minutes. Once finished the reaction was maintained at 4 °C until electrophoresis.

2.4.4 Agarose Gel Electrophoresis

Agarose gels of 1-2 % were prepared by melting agarose (Sigma Aldrich) in 1 % TAE in a microwave, 4 µL of SYBRSafe (Invitrogen) was added to 200 µL gel. Gels of 1 % were used for DNA fragments below 500 bp, 2 % was used for fragments larger than 500 bp. In order to estimate DNA fragment size, one well was loaded with 5 µL of 2-Log DNA Ladder (NEB). 15 µL of PCR reaction mix was added to each well. Samples were electrophoresed for ≥ 50 minutes at 120 V on a 2 % agarose gel. Expected band sizes for each gene are described in Table 2.1. Resultant gels were visualised using a Biorad transluminator and ImageLab software.

Table 2.1. Primer sequences used for genotyping of transgenic animals

Gene	Primer I.D.	.	Primer Sequence (5' -> 3')	Annealing Temperature (°C)	Amplicon Size
Cre	*Cre010 (HELpr010)*	*FOR*	GCATTACCGGTCGATGCAACGAGTGATGAG	68	389 bp
	Cre011 (HELpr011)	*REV*	GAGTGAACGAACCTGGTCGAAATCAGTGCG		
Col1α2 enhancer + Cre	*Col1α2 enh Fw*	*FOR*	AGAGTTCTGCCCACTCCCTT	60	479 bp
	Col1α2 enh Rv	*REV*	GCCTCCAAAAACGTCTCCAC		
Internal	*Internal012 (HELpR012)*	*FOR*	TGGACAGGACTGGACCTCTGCTTTCCTAGA	68	194 bp
	Internal013 (HELpR013)	*REV*	TAGAGCTTTGCCACATCACAGGTCATTCAG		
LacZ	*LacZ008 (HELpR008)*	*FOR*	GTTGCAGTGCACGGCAGATACACTTGCTGA	68	389 bp
	LacZ009 (HELpr009)	*REV*	GCCACTGGTGTGGGCCATAATTCAATTCGC		
CTGF	*CTGF Flx*	*FOR*	AATACCAATGCACTTGCCTGGATGG	65	Floxed = 1003 bp Wild Type = 878 bp
	CTGF Flx	*REV*	GAAACAGCAATTACTACAACGGGAGTGG		(recombined 587 bp)
mTmG	*oIMR7318*	*FOR*	CTC TGC TGC CTC CTG GCT TCT	61	mTmG = 128 bp Wild type = 212 bp
	oIMR7319	*REV*	CGA GGC GGA TCA CAA GCA ATA		
	oIMR7320	*REV*	TCA ATG GGC GGG GGT CGT T		

2.5 Mouse Treatments

All animals used in gain and loss of function experimental cohorts were ≥ 6 weeks of age before any treatments were administered. For lineage tracing experiments, tamoxifen treatments were administered at different stages during embryonic development and postnatally. Where the same animal was administered multiple treatments; i.e. tamoxifen followed by bleomycin injury, one-week recovery was given after completion of the first treatment before administering the second.

2.5.1 Tamoxifen

For a final concentration of 10 mg/mL, 50 mg Tamoxifen (Sigma Aldrich), was added to 4.5 mL corn oil (Sigma Aldrich) and 500 µL 100 % Molecular grade Ethanol (Sigma Aldrich). This was sonicated for a total of 5 minutes until tamoxifen crystals dissolved.

2.5.1.1 Tamoxifen – Col1α2-CCN2fl

A dose of 0.025 mg/g was administered intraperitoneally (I.P.) to each animal on experimental days 1, 3, and 5. All animals were weighed prior to dosing and the volume adjusted accordingly based on whole grams of weight. For example, following this protocol a 20g mouse would receive an I.P. dose of 200 µL containing 2 mg of tamoxifen.

2.5.1.2 Tamoxifen – ROSA-CCN2fl

A dose of 0.0125 mg/g was administered via I.P. injection to each animal on experimental days 1, 3, and 5. All animals were weighed prior to dosing and the volume adjusted accordingly based on whole grams of weight. For example, following this protocol a 20g mouse would receive an I.P. dose of 200 µL containing 1 mg of tamoxifen. A reduced dose of tamoxifen was required for transgenic animals inducing the ubiquitous CCN2 loss of function. Poor recovery and early termination of animals was required when 0.025mg/g was dosed during preliminary studies. We postulate that this is a result of the role of CCN2 in the repair pathway although this was not investigated as part of this PhD.

2.5.1.3 Tamoxifen – Col1α2-R26TmG

Embryonic Development - A single I.P. dose of 3 mg tamoxifen (300 µL tamoxifen at 10 mg/mL concentration) was administered intraperitoneally in a total volume of 300 µL alongside a 3 mg dose of Progesterone (Sigma Aldrich) to the pregnant female at Embryonic Days 13.5 and 15.5.

Adulthood - Mice of 6-7 weeks of age were administered an I.P. dose of 0.0125 mg/g on experimental days 1, 3, and 5. They were then allowed to recover and maintained as previously described for 7 days, 14 days and 3 months. For example, following this protocol a 20g mouse would receive an I.P. dose of 200 µL containing 2 mg of tamoxifen. A further group were administered bleomycin (described in 2.5.2) and left for 14 Days prior to tissue collection.

2.5.2 Bleomycin

A stock solution of bleomycin at 0.15 mg/mL was prepared in sterile PBS. A single dose of 0.375 ng/g was delivered via oropharyngeal aspiration (OA) e.g. a 20g mouse was administered a volume of 50 µL for a total dose of 0.0075 mg bleomycin. Animals were anaesthetised using isoflurane. An elastic band wrapped around an icebox was used as a suspension system to open the airways and expose the back of the throat. Animals were suspended via their incisors and forceps used to hold the tongue outside the mouth during administration as previously described by (Lakatos *et al.*, 2006). Animals were weighed daily in the 3 days immediately following bleomycin administration, and bi-weekly for the duration of the experimental time frame.

2.6 Micro-computed tomography (µCT) Analysis

2.6.1 Unfixed scans

Animals were Sch1 using an overdose of Pentoject (pentobarbital). Lungs and trachea were exposed and a monoject #202 blunt 20-gauge x 1.5” blunt needle was inserted into the trachea. Cotton thread was used to seal the airway around the needle and lungs were manually inflated prior to removal from the ribcage. Isolated lungs were suspended in 3 % potassium Iodide (KI) and stabilised between two Styrofoam guides. A Bruker Skyscan 1272 ex-*vivo* µCT system was used to scan lungs at a resolution of 20 µm, using a 0.25 mm

aluminium filter and 0.3 ° rotation step. Images were reconstructed using Skyscan NRecon software using the following settings:

Table 2.2 Reconstruction settings for µCT scan analysis.

Smoothing	2
Misalignment Compensation	-2
Ring artifacts reduction	12
Beam Hardening correction	38%
Log values	0.0 - 0.03

An average X-Ray attenuation value for each scan was determined using a macro developed by Professor Rob Van 'T Hof, using CtAN software (see Appendix).

2.6.2 Fixed and dehydrated scans

Lungs were isolated as described in section 2.6.1, and fixed in 10 % neutral buffered formalin (NBF) overnight at 4 °C. They were then dehydrated through the following series of ethanol concentrations: 70 %, 80 %, 90 %, 100 %, 100 %. Lungs were suspended in 6x the total tissue volume of each solution for 1.5 hours. They were then suspended in hexamethyldisilazane (HMDS) (Sigma Aldrich, 440191) for 1.5 hours, before drying in a fume hood for 2 hours. Lungs were then scanned using the Bruker Skyscan 1272 ex-*vivo* µCT system, at a resolution of 13 µm, using a 0.25 mm aluminium filter and 0.3 ° rotation step.

2.7 RNA Analysis

2.7.1 Tissue homogenisation

Tissues were snap frozen in liquid nitrogen (LN_2) and stored at -80 °C until RNA extraction was carried out. 70 % Ethanol (EtOH) and RNase Zap (Invitrogen™ AM9780) were used to clean the working area and mortar and pestle which were subsequently cooled using LN_2. The tissue samples were added to the mortar and manually homogenised into a powder. The powder was collected into a clean, labelled, DNase and RNase free tube. 1 mL TRIzol® (Invitrogen™, 15596026) was added and the sample shaken vigorously. Samples were incubated at room temperature for 5 minutes then centrifuged for 3 minutes at 8,000 xg at

4 °C. The supernatant was transferred to a second clean, DNase and RNase free tube and 200 µL chloroform was added. The tube was sealed tightly and vigorously shaken, then incubated at room temperature for 5 minutes. The sample was then centrifuged at 16,000 xg for 15 minutes at 4 °C. The clear aqueous phase was pipetted off and split between two fresh RNase and DNase free 1.5 mL centrifuge tubes.

2.7.2 RNA Extraction using Qiagen RNeasy mini kit

A 1:1 ratio of 70 % EtOH was added to the sample and pipetted to mix before being transferred to a Qiagen RNeasy mini kit spin column inside a 2 mL collection tube. RNA isolation was carried out according to the following Qiagen RNeasy kit instructions. Samples were centrifuged at room temperature, at 8,000 xg for 15 seconds. The run-through in the collection tube was discarded and this step repeated if sample volume exceeded 700 µL until the total volume was run through the column. 700 µL of RW1 buffer was added to the column and the sample was centrifuged at 8,000 xg for 15 seconds at room temperature, flow through was discarded. 500 µL Buffer RPE was added to the column and the sample was centrifuged at 8,000 xg for 15 seconds at room temperature, flow through was discarded. A second volume of 500 µL was added to the column and the sample was centrifuged at 8,000 xg for 2 minutes at room temperature. The spin column was then placed into a new 2 mL collection tube and the old collection tube and flow-through was discarded. The samples were then centrifuged for 1 minute at full speed (16,000 xg) and the spin column transferred to a new 1.5 mL collection tube. RNA was eluted in a total volume of 50 µL RNase free water. An initial volume of 30 µL RNase free water was added directly to the spin column membrane and left to incubate for 3 minutes before centrifuging at 16,000 xg for 3 minutes. A second volume of 20 µL RNase free water was added directly to the membrane and left to incubate for 2 minutes. Samples were then centrifuged for 2 minutes at 16,000 xg. RNA concentration and purity was determined using a NanoDrop 200. Samples were immediately used for cDNA synthesis or stored at -80 °C.

2.7.3 RNA Extraction using Isopropanol

A single volume of 500 µL isopropanol was added per 1 mL TRIzol® used for initial tissue disruption. The sample was mixed vigorously and incubated at room temperature for 15 minutes then subsequently centrifuged for 10 minutes at 12,000 xg at 4°C. The supernatant was removed and discarded to leave a clear pellet of RNA. 1 mL of 70 % EtOH was added to the pellet and centrifuged for 1 minute at 12,000 xg. The EtOH was removed and the pellet

air dried for no longer than 10 minutes. 50 µL of RNase free water was added to the pellet and gently pipetted to re-suspend the RNA. RNA concentration and purity was determined using a NanoDrop 200. A minimum 260/230 ratio of 1.90 and 260/230 ratio of 2.0 was required for RNA samples to be used for transcript analysis. Samples were immediately used for cDNA synthesis or stored at -80°C.

2.7.4 cDNA Synthesis

The High-Capacity cDNA reverse transcription kit (Applied Biosystems) was used for cDNA synthesis. A total concentration of 2 µg RNA was added to a 20 µL reaction consisting of 2 µL 10x RT Buffer, 2 µL 10x RT Random Primers, 0.8 µL 25x dNTP mix (100 mM) and 1 µL MultiScribe® Reverse Transcriptase (50 U/µL). RNase free water was added to a final volume of 20 µL.

2.7.5 Real Time PCR

Quantitative PCR (qPCR) was carried out using the SensiMIX™ SYBR® Hi-ROX kit (Bioline) for genes listed in Table 2.3. A reaction volume of 20 µL consisting of 0.01 µg cDNA (2 µL cDNA stock diluted 1:20), 10 µL SYBR Green, 0.6 µL forward and reverse primer and 6.8 µL ddH_2O was used and plated in triplicate. Samples were analysed using a Corbett Rotor Gene RG-6000 using cycling parameters: Initial hold for 10 minutes at 95 °C followed by 40 cycles of 95 °C for 10s, 60 °C for 15s, 72 °C for 20s and acquire on the green channel. A melt curve was generated at the end of every run to confirm a single amplification product was present. Rotor-Gene 6000 series software version 1.7 was used to analyse the results. The housekeeping gene 18s was used for all experiments and ΔΔCt values were calculated and normalised to this gene.

2.7.6 Primer Validation

Prior to use for qPCR, calibration curves for all primers were generated and compared to 18s. Melt curve analysis and end stage PCR was also performed to ensure that single products were obtained at the expected product size. See appendix for details.

Table 2.3. Primers and sequences used for RT-qPCR analysis.

Gene	Primer I.D.	.	Primer Sequence (5' -> 3')	Temperature (°C)	Amplicon Size
18s	*18s Tas*	*FOR*	GGAAAGCAGACATCGACCTCA	60	130bp
	18s Tas	*REV*	AGTTCTCCAGCCCTCTTGGT		
CCN2	*CCN2*	*FOR*	CACAGAGTGGAGCGCCTGTTC	60	165bp
	CCN2	*REV*	GATGCACTTTTTGCCCTTCTTAATG		
Collagen I	*Col1α2*	*FOR*	GCAACAGTCGCTTCACCTACA	60	138bp
	Col1α2	*REV*	CAATGTCCAAGGGAGCCACAT		
Fibronectin	*Fibronectin ED-A*	*FOR*	GATGATATGGAGAGCCAGCCC	60	101bp
	Fibronectin ED-A	*REV*	GCAGTAAAGCTGGTGGGTGT		
Collagen III	*COL3a1*	*FOR*	CTGTAACATGGAAACTGGGGAAA	60	144 bp
	COL3a1	*REV*	CCATAGCTGAACTGAAAACCACC		

2.8 Histological Analysis

2.8.1 Cryogenic histology

The following protocol was adapted from (Ono *et al.*, 2014). The tissues of interest, such as embryos of different developmental stages, lung and other internal organs were dissected and fixed overnight in 4 % paraformaldehyde at 4 °C. Samples were then washed twice in PBS and transferred to 30 % Sucrose/PBS and incubated overnight at 4 °C. Finally samples were transferred to 30 % sucrose / PBS:OCT (1:1) and incubated overnight at 4 °C. Tissues were then embedded in OCT embedding media (TissueTek, Sakura) using cork discs and moulds (Electron Microscopy Solutions). The samples were left to solidify on a sheet of dry ice and immediately transferred to storage at -80 °C until required. A Leica CM1850 cryostat was used to section the tissues at 5 – 7 µm. Sections were collected on Superfrost™ Plus microscope slides (ThermoScientific) and imaged using a Zeiss Axio Observer apotome microscope and Axio Cam MR R3 camera. When not in use slides were stored at -80 °C and protected from light exposure to reduce colour bleaching. For fluorescent imaging a wavelength of 610 nm was used to image the tdTomato and 519 nm for EGFP. Images were viewed using ZEN Blue microscopy software.

2.8.2 Paraffin Wax histology

2.8.2.1 Tissue Processing

Adult soft tissues were isolated from animals Sch1 by overdose of anaesthetic (pentobarbital), and immediately suspended in 6x total tissue volume of 10 % NBF. Tissues were fixed overnight at 4 °C in 6x total tissue volume of NBF prior to processing and embedding in paraffin wax blocks as per the following protocol:

Table 2.4. Processing protocol using a Leica EM TP6 tissue processor for paraffin wax embedding of adult mouse soft tissue.

Reagent	Immersion Time under vacuum (Minutes)	Temperature	Drain time (seconds)
70 % Ethanol	30	Ambient	80
90 % Ethanol	30	Ambient	80
100 % Ethanol	10	Ambient	80
100 % Ethanol	10	Ambient	80
100 % Ethanol	10	Ambient	80
100 % Ethanol	15	Ambient	80
Xylene	10	Ambient	120
Xylene	20	Ambient	120
Xylene	30	40 °C	120
Wax	240	60 °C	140

2.8.2.2 Tissue Sectioning

5 µm sections were cut using the Micron HM355S microtome with cool-cut and tissue transfer system (Thermo Scientific) and collected on Superfrost™ Plus microscope slides (ThermoScientific). Slides were stored at room temperature prior to use for staining and analysis.

2.8.2.3 Sample Staining

Slides were de-waxed using the following protocol (Table 2.5). Once dewaxed, slides were stored in water until staining.

Table 2.5. Parameters for dewaxing of paraffin embedded sections.

Reagent	Immersion Time (Minutes)
Xylene	2
Xylene	2
100 % Ethanol	2
100 % Ethanol	2
H_2O	Until Use

2.8.2.4 Haematoxylin Eosin Stain (H&E stain)

The following staining protocol was used for Haematoxylin and Eosin staining of paraffin embedded sections.

Table 2.6. Staining schedule for Haematoxylin and Eosin staining of 5µm sections of paraffin embedded mouse lung.

Reagent	**Immersion Time (Minutes)**
Haematoxylin	5
H_2O	1
Acid Alcohol	0.25
H_2O	5
Eosin	3
H_2O	0.25
70% Ethanol	0.5
90% Ethanol	0.5
100% Ethanol	0.5
Xylene	2
Xylene	2
CV1 - Coverslip	Auto

Stained slides were imaged using a Zeiss LSM 800 confocal microscope.

2.8.2.5 Goldners Trichrome Stain

All stains and reagents were prepared freshly prior to use and the following staining schedule used.

2.8.2.5.1 Solutions

2.8.2.5.1.1 Weigarts Haematoxylin

A working solution of Weigarts Haematoxylin was made by mixing equal parts of solution A with solution B.

2.8.2.5.2 Solution A

10 g Hematoxylin crist. C.I.75290 was added to 1 L 95 % EtOH.

2.8.2.5.3 Solution B

12 g Ferric Chloride was added to 40 mL water and 10 mL Hydrochloric Acid. ddH_2O was added to make a total volume of 1 L.

2.8.2.5.4 Acid Fuchsin- Ponceau

A working solution of acid fuchsin was made by adding 6 mL solution A and 2 mL solution B to 9 mL 2 % Acetic acid and 73 mL ddH_2O.

2.8.2.5.5 Solution A

1 g Ponceau 2R was added to 100 mL ddH_2O.

2.8.2.5.6 Solution B

1g Acid Fuchsin was added to 100 mL ddH_2O.

2.8.2.5.7 Phosphhotungstic-acid- Orange G

3 g phosphotungstic acid and 2 g Orange G was added to 100 mL distilled water.

2.8.2.5.8 Light Green

1 g Light green was added to 1 mL Acetic acid and 500 mL ddH_2O.

Table 2.7. Staining schedule for Goldner's Trichrome staining of 5 µm sections of paraffin embedded mouse lung.

Reagent	**Immersion Time (Minutes)**
Weigert's Haematoxylin	10
H_2O	10
Acid Fuschin	15
1% Acetic Acid	2
PTA Orange	5
1% Acetic Acid	0.5
Fast Green	10
1% Acetic Acid	3
70% Ethanol	2
90% Ethanol	2
100% Ethanol	3
Xylene	5
Xylene	5
CV1 - Coverslip	Auto

Stained slides were imaged using a Zeiss LSM 800 confocal microscope.

2.9 Immunohistochemistry

This protocol and stained slides were provided by Mr. Lorenzo Ramos-Mucci at the University of Liverpool. Paraffin embedded lungs were sectioned, and the slides provided to Mr. Ramos-Mucci who carried out the antibody staining procedure detailed below. Stained slides were then imaged using a Zeiss LSM 800 confocal microscope. This protocol was adapted from DAB (Vector Labs, SK-4100), Avidin/Biotin blocking kit (Vector Labs, SP-2001), and Vectastain (Vector Labs, PK-6100).

Slides were dewaxed following the protocol described in Table 2.5. A ring was drawn around each lung section using a Pap pen. For this staining protocol no antigen retrieval was required. Slides were washed twice at 5 min intervals in PBS-T prior to incubation in 3 % H_2O_2 for 15 min at 37 °C. A second series of washes in PBS-T at 5 min intervals was followed by an Avidin/Biotin blocking kit: Avidin 15 min, Biotin 15 min. Blocking steps were carried out at room temperature. Slides were then washed for 5 minutes in PBS and blocked with -10 % goat serum in PBS - BSA (0.1% BSA) for 1 hour at room temperature. Following two further 5-minute wash steps in PBS, primary antibody (Anti-CTGF Antibody (Abcam, ab6992)), PC, Rabbit) was added at 1/1000 dilution in PBS and incubated overnight at 4 °C. The following day slides were washed in PBS 3 times for 10 minutes before adding the secondary antibody (anti-rabbit diluted 1/200 in PBS) for 1 hour and incubating at room temperature. While slides were washed in PBS at 3 10-minute intervals, the Vectastain (1 mL PBS, 10 µL A, 10 µL B), was combined and stored in dark for 30 min prior to use. Slides were incubated in Vectastain for 30 minutes at room temperature. After two 5-minute washes with PBS, DAB (2.5 mL H_2O, 1 drop buffer, 2 drops DAB, 1 drop H_2O_2) was added and slides were left for 1 minute until colour developed. Slides were then washed with ddH_2O, dehydrated using the ethanol concentration's and timings outlined in Table 2.6.

2.10 Cell Culture

The following protocol for the isolation of lung fibroblasts was developed by Mr. Michele Scotto di Masse at the University of Liverpool.

A 1x solution of Hanks' Balanced Salt Solution (HBSS) was prepared using the following reagents:

Reagent	**Volume required for 1x HBSS solution (mL)**
Hanks' Balanced Salt Solution 10x (Sigma Aldrich, H1641)	100
Sodium bicarbonate solution (7.5%), sterile-filtered, $NaHCO_3$ (Sigma Aldrich, S8761)	4.7
Hepes Buffer (Sigma Aldrich, H0887)	10
Penicillin-Streptomycin (10,000 U/mL), (ThermoFisher Scientific, 15140122)	10
ddH_2O	875.3

A working solution of 1 mg/mL collagenase/HBSS solution was made by diluting 1 mL of 100 mg solution of Collagenase Hystolyticum (Sigma Aldrich, C26474) in 9 mL HBSS. Mice were Sch1 by cervical dislocation and the lungs immediately isolated and suspended in ice cold PBS for transfer to a tissue culture hood. Using a sterile scalpel blade, lungs were transferred to a sterile petri dish and chopped until the tissue resembled a pulp. Chopped tissue was transferred to a sterile T25 flask. The petri dish was rinsed with the collagenase/HBSS solution and added to the lung pulp in the T25 flask. Tissue was incubated in a shaking water bath at 37 °C for 60 minutes, or until the tissue started forming sticky fibres. To break up clumps, the homogenate was pipetted against the inside of the flask using a 10 mL stripette, the homogenate was then filtered into a sterile 50 mL falcon tube using a 0.44 µm filter. The sample was then centrifuged at 330 xg for 5 minutes. The supernatant was discarded, and the tissue pellet washed with 20 mL 1x HBSS. HBSS was removed from the pellet and discarded. The remaining tissue sample was centrifuged at 330 xg for 5 minutes. Any residual supernatant was discarded. The tissue pellet was resuspended in 5 mL warm DMEM, high glucose (supplemented with 10 % FBS, 5 mL L-Glutamine (200 mM) and 100 I.U/ penicillin and 100µg/mL streptomycin (Thermofisher, 10500064, 25030081, 15140-122)). Cells were incubated in a tissue culture incubator for 4-5 days at 37 °C, 5 % CO_2. Cultures were maintained in fully supplemented DMEM.

2.10.1 4-Hydroxytamoxifen (4-OHT) treatment of cells

To make a 10 mM stock of (Z)-4-Hydroxytamoxifen (4-OHT) (Sigma Aldrich, H7904-5MG), 1.25 mL of 100% ethanol (Sigma Aldrich, 51976) was added to the 5 mg vial of 4-OHT. The stock solution was pipetted into 12 µL aliquots and stored at -20 °C until use. The 10 nM stock solution was serially diluted as follows to produce a 100 nM working solution for 4-OHT treatment of cells. 5 µL of stock solution was added to 495 µL of DMEM, high glucose (Thermofisher scientific, 11965092) to make a 100 µM solution. 20 µL of the 100 µM solution was added to 1980 µL DMEM, high glucose to make a 1 µM solution. 200 µL of the solution was added to 1800 µL DMEM, high glucose (supplemented with 10 % FBS and 100 I.U/ penicillin and 100µg/mL streptomycin) to make a 100 nM working solution. 2 mL of 100 nM solution were added to 6-well plates. Cells were incubated for 12 hr in 5 % CO_2 at 37 °C.

3. Establishing the Bleomycin Model of Idiopathic Pulmonary Fibrosis

3.1 Animal models of disease

Animal models are an essential tool for investigating the pathology and mechanisms of human disease. Although limited by their inability to encapsulate the full range of features present in human disease, they remain a useful means for examining key physiological traits and as a screening platform for candidate pharmaceutical molecules. The pathogenesis of IPF still remains controversial and elusive, with attempts to understand the scientific basis of the disease and identification of novel therapeutic targets relying predominantly on animal models.

3.1.1 Animal models of IPF

Spontaneous development of fibrosis has been observed in species such as cats, dogs and horses (Webb and Armstrong, 2002; Cohn *et al.*, 2004; Williams *et al.*, 2007). These cases are informative for comparative medicine however they are impractical for laboratory investigation. Therefore, research over the last few decades has predominantly focussed on development of murine models of IPF. Most frequently used are: radiation damage (Paun *et al.*, 2010; Haston, 2012) and instillation of a variety of molecules to the lung, including: silica (Barbarin *et al.*, 2005; Lakatos *et al.*, 2006; Roggli *et al.*, 2010), Fluorescein isothiocyanate (FITC) (Roberts *et al.*, 1995; Davis, Leslie and Hemenway, 1998; Moore *et al.*, 2005), asbestos (Padilla-Carlin *et al.*, 2011; Cyphert *et al.*, 2012; Rasmussen and Pfau, 2012) and bleomycin (Ponticos *et al.*, 2009; Egger *et al.*, 2013; Scotton *et al.*, 2013; Gilhodes *et al.*, 2017). Of these models, bleomycin is perhaps the most widely used, and was the animal model employed to characterise the drugs currently available for treatment of IPF; Nintedanib and Pirfenidone (Schaefer *et al.*, 2011; Wollin *et al.*, 2014).

3.1.2 Bleomycin model of IPF

Bleomycin is a chemotherapeutic antibiotic isolated from the bacterium *Streptomyces verticillus* (Umezawa *et al.*, 1967; Adamson, 1976). Fibrosis was noted as a major adverse effect when bleomycin was used for the treatment of human cancer. Subsequent animal trials characterised its ability to induce fibrosis in a number of species such as dogs (Fleischman *et al.*, 1971), mice (Adamson and Bowden, 1974) and rats (Thrall *et al.*, 1979). Different susceptibilities to bleomycin have been observed in the murine models, with CBA

and C57Bl/6 being the preferred strains of choice (Schrier, Kunkel and Phan, 1983; Phan and Kunkel, 1992).

The therapeutic potency of bleomycin is attributed to its ability to induce single and double-strand DNA breaks, which interrupts the progression of the cell cycle (Williamson, Sadofsky and Hart, 2015). This process has been described in detail in a number of publications (Lopez-Larraza, De Luca and Bianchi, 1990; Sidik and Smerdon2, 1990; Smith, Bauer and Povirk, 1994; Chen *et al.*, 2008) however the reason fibrosis occurs as a result of this process is still undetermined. It is hypothesised that an overproduction of reactive oxygen species (ROS) instigates an inflammatory response causing pulmonary toxicity, activation of fibroblasts and subsequent fibrosis due to a lack of the enzyme bleomycin hydrolase (Chaudhary, Schnapp and Park, 2006).

Over recent decades several methods of instillation of bleomycin to the lungs have been trialled and the resulting fibrotic pathologies compared. These include subcutaneous (SC), intravenous (IV), intranasal (IN), intratracheal (IT) and oropharyngeal aspiration (OA) routes of administration (Lindenschmidt *et al.*, 1986; Braun *et al.*, 1996; Egger *et al.*, 2013; Williamson, Sadofsky and Hart, 2015).

For this research project, the OA method of administration was used as described by (Lakatos *et al.*, 2006). Animals were anaesthetised using isoflurane, suspended by their incisors and forceps used to hold the tongue outside the mouth during administration. This process is shown in Figure 3. and described in more detail in methods section 2.2.2. As the animal regains consciousness from anaesthesia, a reflex inhalation occurs because of the restriction of the nose by the forceps, resulting in delivery of the bleomycin suspension to the lungs.

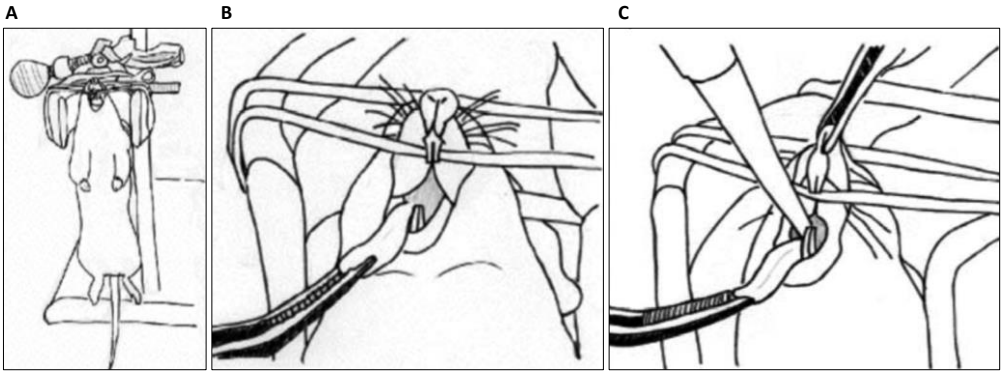

Figure 3.1. Method of oropharyngeal aspiration of bleomycin in mice. Image taken from (Lakatos *et al.*, 2006). *A, Anesthetized mouse is suspended by the cranial incisors on a thin rubber band. B, The tongue of the animal is held outside the mouth using forceps. C, The nose is pinched shut using forceps. The bleomycin suspension is pipetted into the back of the throat. A reflex inhalation occurs as the animal regains consciousness, delivering the bleomycin to the lungs.*

3.2 Chapter Aims

The aims of this chapter were as follows:

1) Establish and characterise a model for bleomycin-induced IPF.

The first objective was to reproduce the results previously described for the induction of a bleomycin induced fibrosis by the Bou-Gharios lab group. The second objective addressed the characterisation of this model. Lung tissue from this experiment was assessed using qPCR and histology to confirm the induction of fibrosis.

2) Develop a dosing regimen for the administration of bleomycin.

To address future requirements of inducible transgene activation using tamoxifen, a combined dosing regimen of tamoxifen followed by bleomycin was assessed for tolerance and adverse effects in the animals. Alternative doses of bleomycin were assessed for their ability to induce fibrosis up to 28 days following administration.

3) Develop a method for the assessment of fibrosis in lung following administration of bleomycin.

Bleomycin is known to induce variable responses between subjects. Therefore, there was a requirement for a method of analysis to be developed that enabled visualisation of the whole lung whereby samples of lung tissue could be subsequently used for histological and qPCR analysis. A second requirement for a quantitative assessment to be made from these whole analyses led to the development of an automated macro to assess the total x-ray attenuation value of the lungs.

3.3 Establishing the baseline response to bleomycin administration

In order to establish the baseline response to bleomycin treatment in non-transgenic / wild type (WT) animals, an initial experiment was performed testing the bleomycin model of IPF using mixed background (B6CBA F1) male mice. Three combined treatment groups were examined:

1) Oil then bleomycin, (O/B)

2) Tamoxifen then PBS, (T/B)

3) Tamoxifen then bleomycin, (T/B)

Treatments were administered to animals as described in methods section 2.5.1.

The transgenic animal models utilise a tamoxifen dependent CreER^{T2}, therefore tamoxifen treatment was combined with bleomycin to account for any adverse effects that the combined therapy might induce. Oil was used as a vehicle for the tamoxifen and PBS as a vehicle for the bleomycin. Previous research by the Bou-Gharios lab group had established in-house protocols using a concentration of 0.025 mg bleomycin, with individual animals receiving a 50 µL dose in saline (Ponticos *et al.*, 2009) and the same protocol was used in this experiment.

Thirty-six mice were assigned to one of three treatment groups (4 animals per treatment, 3 treatments) and timepoints (3 timepoints). Lungs were collected at days 7, 14 and 28 post bleomycin administration Tamoxifen / oil was administered following the dosing schedule outlined in the methods section 2.5.1. Bleomycin was subsequently administered using the oropharyngeal aspiration method outlined in Figure 3.1.

Animals were treated as described in methods sections 2.5.1.1 and 2.5.2.As timepoints of 7, 14 and 21 days post bleomycin were reported by Ponticos et al., (2009), and survival up to 84 days has previously been reported for this model (Scotton *et al.*, 2013), adverse effects were not anticipated.

One animal was culled due to ill health following I.P. injection of oil (treatment group 7 days O/B). This was considered unrelated to the treatment as all remaining animals receiving oil or tamoxifen displayed no adverse response. Adverse events occurred around day 10 with one animal being found dead in cage (D.I.C) and two more animals appeared moribund, with piloerection and hunching and were therefore culled. Assessment of the mice during the

24 hr period prior had not raised any concerns over ill health. All three animals belonged to the O/B treatment group. Three of the four remaining animals receiving the same treatment (O/B) survived to the final timepoint of 28 days. Around day 16 four more animals exhibited signs of ill health and were culled. Two were treated with T/P and two with T/B. As with the previously culled animals, no signs of ill health were noted in the 24-hr period prior to culling.

During the study an overall mortality rate of 25 % was observed with 15% attributed to the O/B treatment group and 5% from both the T/P and T/B treatment groups. Animals that experienced weight loss exceeding 20 % of their start weight and/or exhibited signs of illness (hunching, piloerection), and were culled via cervical dislocation at earlier time points to negate a breach of Home Office licence conditions. Lungs were collected from the culled animals and the left lobe isolated for histological analysis. The remaining lobes were snap frozen and analysed by qPCR for the expression of collagen I, using the *COL11α2* gene as a readout.

The sections taken for histology enabled visualisation of the extent of fibrosis that had formed at each time point (Figure 3.2, (A – I)). At 7 days the O/B treatment group showed early fibrotic foci formation particularly surrounding the blood vessels and bronchioles (A, black arrows). The tamoxifen and PBS treatment exhibited a more widespread thickening of the epithelial lining of the alveoli (Figure 3.2 B, black arrows) predominantly in the area immediately surrounding the bronchioles. The tamoxifen and bleomycin treatment showed widespread and established tissue deposits throughout the section (Figure 3.2 C, black arrows). The lungs collected from O/T and T/P treated mice (Figure 3.2, A - B) still retained some regions of normal lung morphology, for example the individual alveoli could still be identified, and blood vessels were easily distinguishable from the surrounding tissue. In T/B treated mice the main anatomical feature that could be identified was the bronchioles. Most of the structural integrity of the alveoli in these animals was lost or unrecognisable. By 14 days all animals displayed increased levels of immune infiltrates, as was apparent by the increase in haematoxylin stained nuclei (Figure 3.2, D – I), however this staining was present in all sections and was particularly obvious in tissue surrounding the airways. O/B treated animals (Figure 3.2, D) demonstrated thickening of the alveolar epithelium which was comparable to that seen in T/P treated lungs at 7 Days (Figure 3.2, B), whereas T/P (Figure 3.2, E) and T/B (Figure 3.2, F) treated lungs showed increased similarity in morphology to T/B at 7 Days (Figure 3.2, C). The tissue deposition was more widespread, and the alveoli were more difficult to identify. At 28 days, all groups showed a decrease in fibrosis, with a reduction in infiltrate presence when compared to the same treatment at 14 days. O/B

treated lungs demonstrated comparable levels of fibrosis to the same treatment at 7 days (Figure 3.2, A & G).

In lung sections from both T/P and T/B groups, there was an increased instance of alveoli that retained somewhat normal morphology when compared to the 14-day treatment counterparts.

The qPCR analysis on the remaining lobes of the lungs examined the levels of *COL1α2* gene as a readout of collagen I synthesis. Sample cycle threshold (Ct) values were normalised to untreated animals of the same background and are expressed as a fold change using the ΔΔCt method. Significance was determined using a one-way ANOVA, and Tukey's post hoc test. At 7 days the T/P treatment was the only group to show a significant increase in *COL1α2* transcript (Figure 3.2, J) with a mean ΔΔCt of 3.46 (s.e.=0.9). The mean ΔΔCt values for O/B and T/B treated lungs was 0.98 (s.e.=0.24) and 1.03 (s.e.=0.17) respectively. At 14 days the O/B and T/P ΔΔCt values weren't significantly different for the O/B and T/P groups, mean 1.21 (s.e.=0), 1.06 (s.e.=0.07) respectively (Figure 3.2, K). Whereas the T/B treatment averaged a ΔΔCt of 2.41 (s.e.=1.03). Finally, at 28 days the T/P group failed to reach significance; 1.39 (s.e.=0.61) whereas both the O/B and T/B groups showed increased transcription of the *COL1α2* gene with mean ΔΔCt values of 2.11 (s.e.=0.42) and 1.75 (s.e.=0.14) (Figure 3.2, L). At each time point. a different treatment group displayed the largest increase in expression fold change; 7 days was the T/P group, followed by T/B at 14 days and O/B at 28 days.

The variation in these results highlighted the importance of assessing the extent of fibrosis in the entire lung. For this experiment, individual lobes were only able to be analysed for either histology or qPCR. It was not possible to confirm whether the histological data was representative of the entire lung and by extension it cannot be determined whether the qPCR results were accurate for the remaining lobes. Oropharyngeal aspiration of bleomycin is a notoriously variable model, with the potential to see a different effect on each lobe within the lung. It was therefore decided to adopt a method that would enable the assessment of the extent of fibrosis in the whole lung, prior to further analysis.

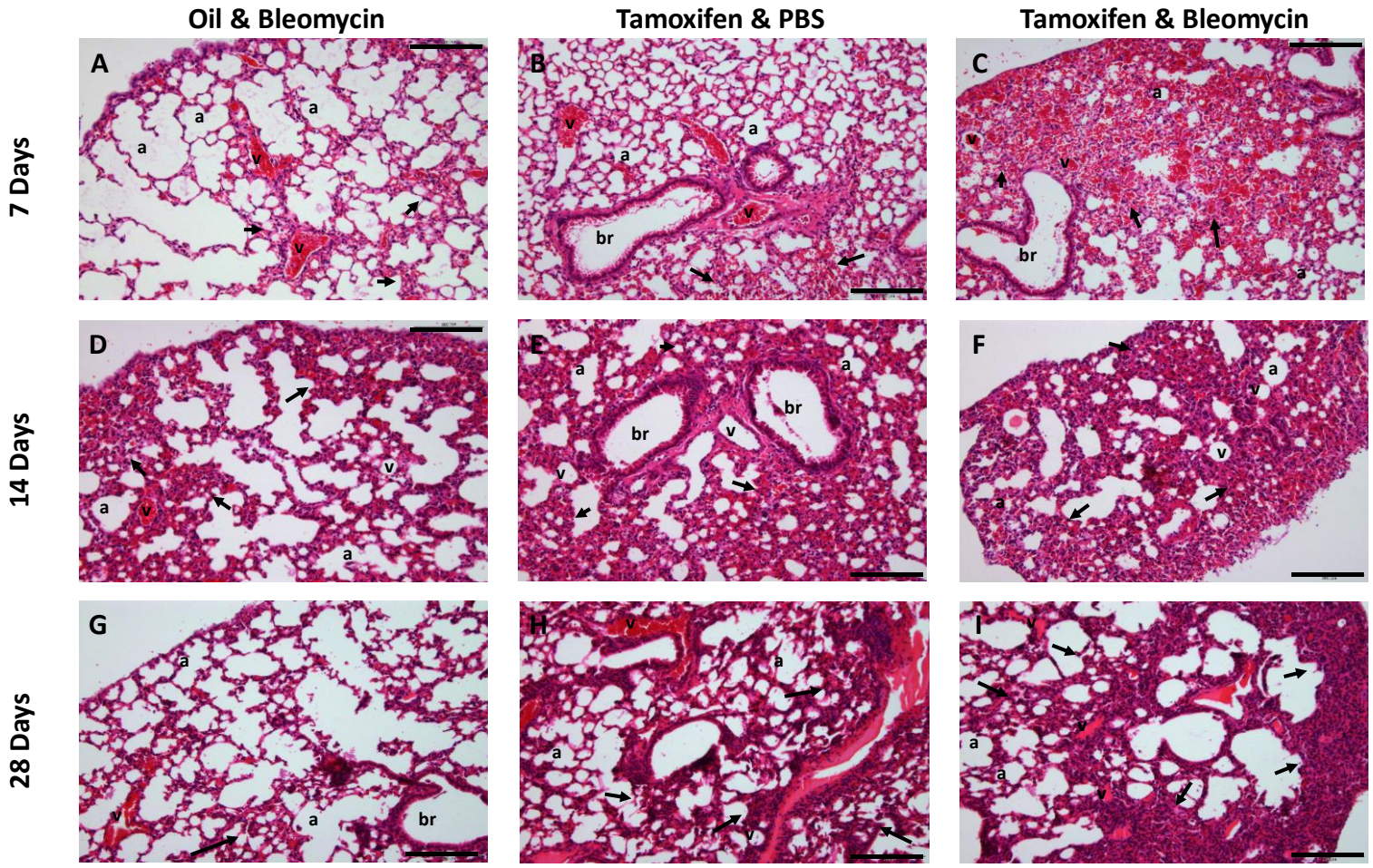
Oil & Bleomycin
Tamoxifen & PBS
Tamoxifen & Bleomycin
7 Days
14 Days
28 Days
A
B
C
D
E
F
G
H
I
a
v
br

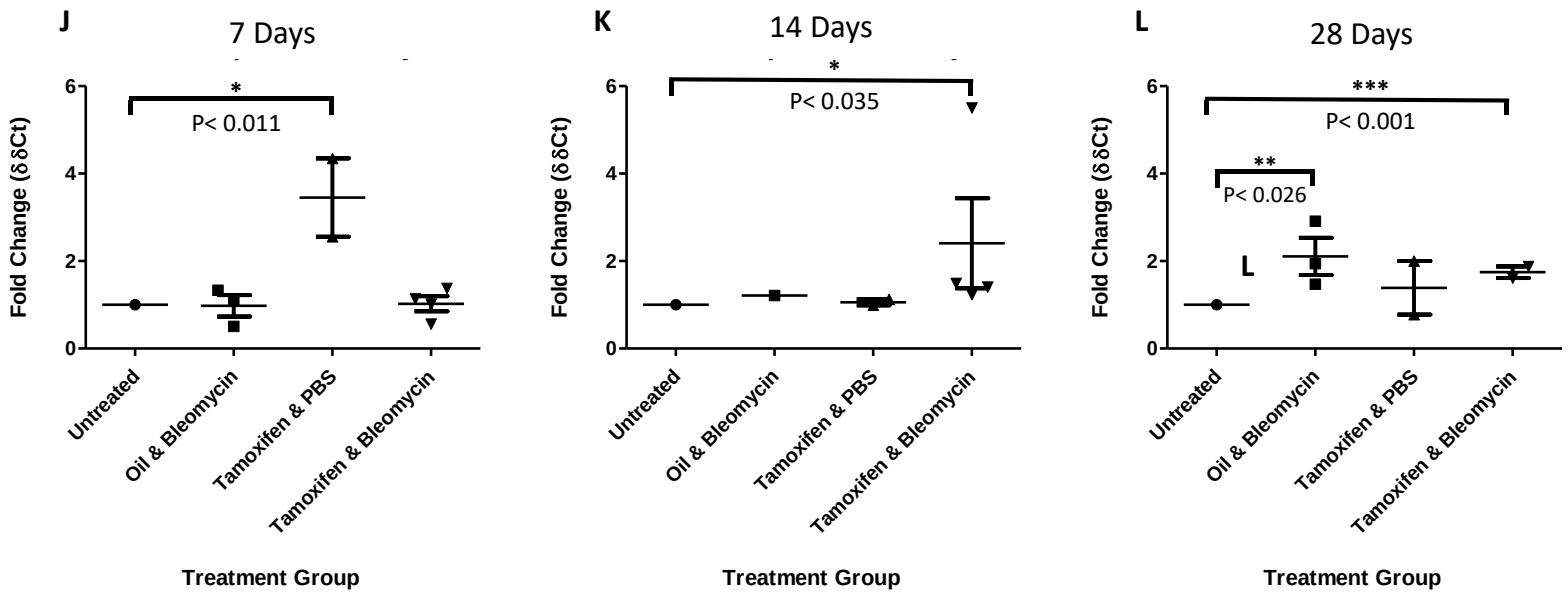

Figure 3.2. Histological evaluation and qPCR analysis of lung samples taken from B6CBA WT mice. Lungs were collected at 7 (J), 14 (K) and 28 (L) Days following treatment with tamoxifen and bleomycin or vehicle treatment. Images A – I are representative histology sections collected at designated time points from each treatment group. Lung lobes were processed for wax histology and stained with H&E. Anatomical features are identified as follows: a- alveoli, br-bronchioles, v-blood vessels. Black arrows indicate regions of fibrosis. Scale bars represent 200 µm. Graphs J – L represent qPCR analysis for the Col1α2 gene. ΔΔCt fold change results are plotted, significance was determined using a one-way ANOVA, and Tukey's post hoc test.

3.4 Micro computed tomography (μCt) analysis of the lungs

3.4.1 Chemical dehydration and scanning of the lung

Following a discussion with Professor Rob Van 'T Hof at the University of Liverpool, it was decided to utilise the Bruker Skyscan 1272 *ex-vivo* μCT scanner and a protocol developed at Edinburgh University to examine the lungs of the mice. Whole lungs were isolated from healthy adult mice, dehydrated and scanned at 13 μm resolution, following the protocol outlined in methods section 2.6.2. Example images from the resulting scans are shown in Figure 3.3.

The first whole lung scan was performed using a healthy control animal to ensure that anatomical features would be identifiable in a lung with no morphological defects. Individual 2D images from the same region in the 3D reconstruction can be seen from the X, Y and Z planes (red, green and blue boxes respectively; Figure 3.3, A). Tissue is identified by differential shades of grey, depending on its x-ray attenuation capabilities, i.e. denser tissue is represented in a darker shade of grey. The coloured lines indicate the location of the 2D scan images in relation to their position in the 3D reconstruction. Images in DataViewer software are displayed as shown in Figure 3.3, A & C. A more detailed image can be viewed at full resolution by looking at individual planes as shown in Figure 3.3, B & D. All scans can be viewed as part of the 3D reconstruction as in Figure 3.3 or can be accessed individually.

Using the 3-plane view of the control scan we were able to identify key anatomical features of the lung including the trachea, bronchioles, and heart (Figure 3.3, A). At a higher resolution (Figure 3.3, B) we were then able to identify smaller features such as the blood vessels and the alveoli, where the grey outlines within the gross structure of the lung is staining of the epithelial lining of the alveoli by hexamethyldisilazane (HMDS).

The next step was to determine if regions of fibrosis could be identified using the same protocol. A single dose of bleomycin was administered to a WT (B6CBA F1) mouse, as per the previous protocol and the lungs collected 14 days later for processing and scanning. As with the control lung, it was possible to identify the same key anatomical features of the lung using the 3-plane view (Figure 3.3, C). Dense regions were also identified which we hypothesised to be fibrotic scar tissue deposits (indicated by the black arrows). At a higher resolution (Figure 3.3, D) the structure of the alveoli could be identified in regions of normal tissue morphology but not in fibrotic regions.

The limitation of the scanning protocol was that RNA was unable to be extracted from the samples after the processing and scanning was complete. The aims of the project were to examine the effects of CCN2 removal on the bleomycin model of IPF both at the phenotypic and genetic level. Therefore, a method of scanning the lungs was required that resulted in a comparable level of morphological detail achieved by these scans, without the requirement for chemical dehydration.

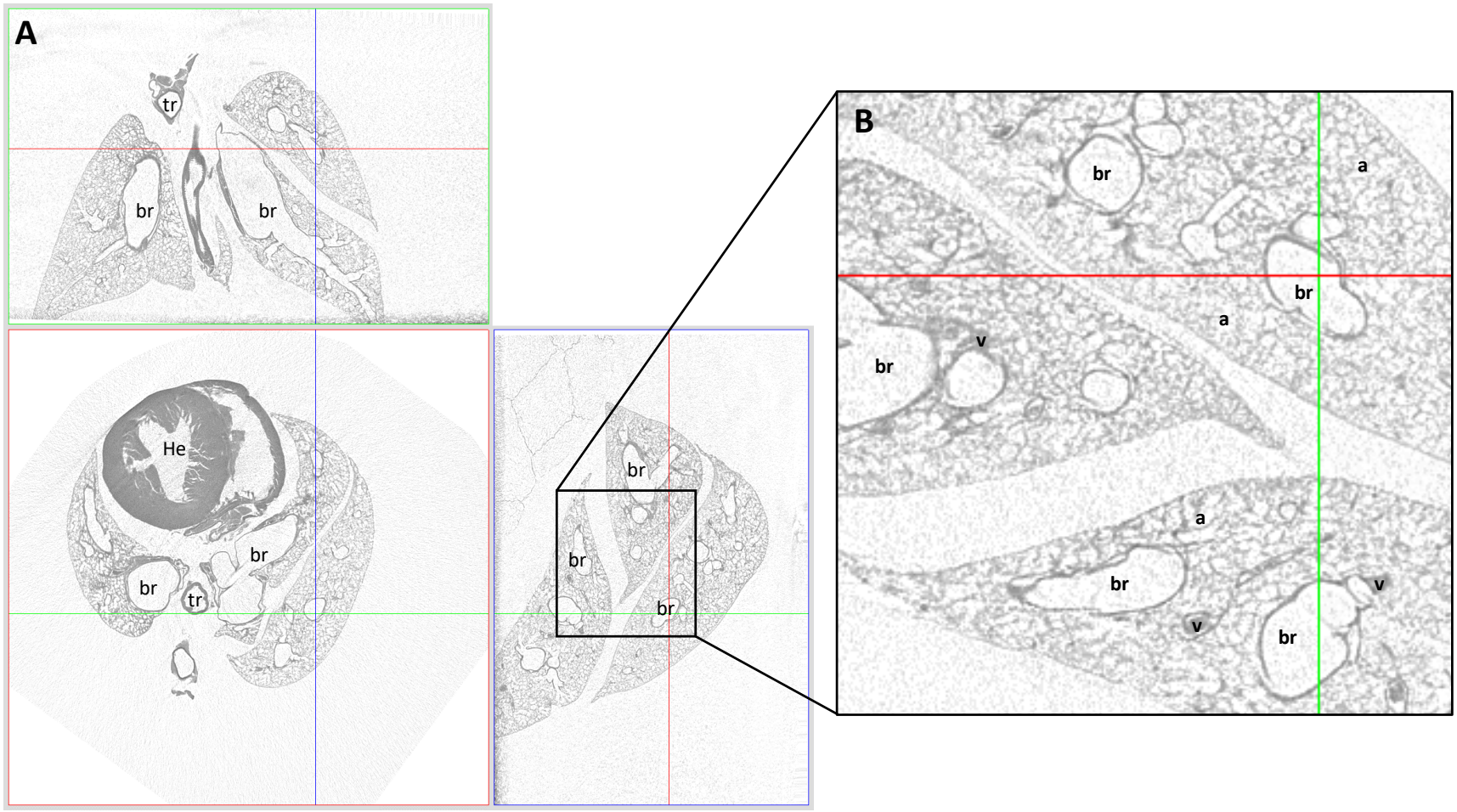
A
tr
br
br
He
br
br
tr
br
br
br
B
br
a
br
a
v
br
a
br
v
v
br

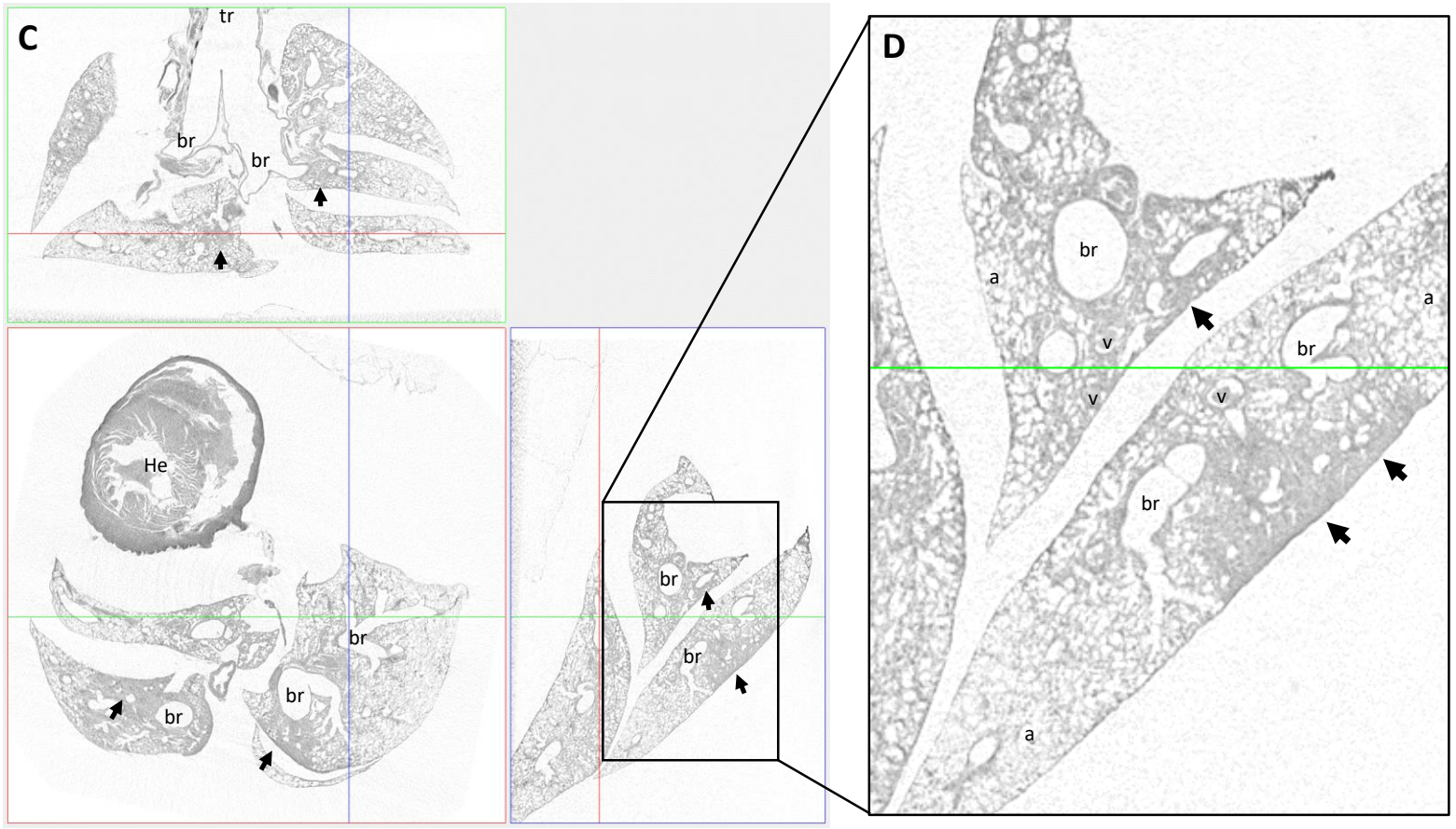

Figure 3.3. µCT scans of chemically dehydrated mouse lungs. Representative X, Y and Z plane images (red box, green box and blue box respectively) from a control mouse (A & B) and from a bleomycin treated mouse collected at 14 days following a single 0.025 mg dose in 50 µL PBS (C & D). Coloured lines indicate the location of the 2D scan images in relation to their position in the 3D reconstruction. Lungs were scanned using a SkyScan 1272 µCT system at a resolution of 13 µm (0.25 mm aluminium filter, 0.3 ° rotation step). Images were reconstructed using Skyscan Nrecon software and visualised using DataViewer. Images shown are single representative sections from individual mice. A & C show the example view when analysing the scans in DataViewer software. B & D represent full size resulution of each scan image. Anatomical features are identified by the following: tr- trachea, br- bronchioles, He- heart, v- blood vessels, a- alveoli and black arrows indicate fibrotic regions.

3.4.2 Inflated and suspended scanning of unfixed lungs

A protocol was developed, which utilised the contrast in x-ray attenuation capabilities of a liquid compared with air. Lungs were manually inflated, isolated and suspended in PBS for the duration of the μCT scan. A lower resolution of 20 μm was used to reduce the total time required for the scan to approximately 13 minutes, and this allowed for isolation of a lobe for histology and snap freezing of the remaining lung tissue in liquid nitrogen for RNA isolation and gene expression analysis.

Representative 2D images from a single scan performed using a healthy control mouse are shown in Figure 3.4. The same images, Figure 3.4, A – C, in the X, Y and Z planes (red, green and blue boxes respectively) are repeated in D – F with an added outline to clarify the location of the lung in the PBS. The coloured lines indicate the location of the 2D scan images in relation to their position in the 3D reconstruction. Performing this experiment highlighted several issues. The first was the lungs floated to the top of the bijou. The depth of the scanner is limited, making it difficult to capture the whole lung inside the field of view for analysis. It also meant that the bijou needed to be completely filled to maintain an equal contrast field surrounding the lung. Thirdly the x-ray attenuation capability of the tissue was not substantially different to the PBS. A relatively obvious difference in the greyscale value of the air compared to the other constituents (light grey/white regions) is seen in Figure 3.4 However, the tissue and PBS resulted in very similar greyscale values, which would be difficult to distinguish between in future analysis of the scans when assessing the extent of tissue fibrosis (Figure 3.4, A – C).

From these scans only the gross structures of the trachea, bronchioles and heart were able to be identified. Finer details such as the alveoli and blood vessels seen in Figure 3.2, were unable to be identified. This may in part be due to the level of inflation in the lung, a better inflation would have increased the contrast between the air, tissue and surrounding PBS. However, it was concluded that the density of the PBS did not produce sufficient contrast to the tissue and alternative solutions in which to suspend the lungs were sought. It was also decided to explore alternative methods of suspending and immobilising the lungs at the centre of the tube to prevent them floating to the top of the bijou, as well as reducing movement artefacts and subsequent loss of detail during the scans.

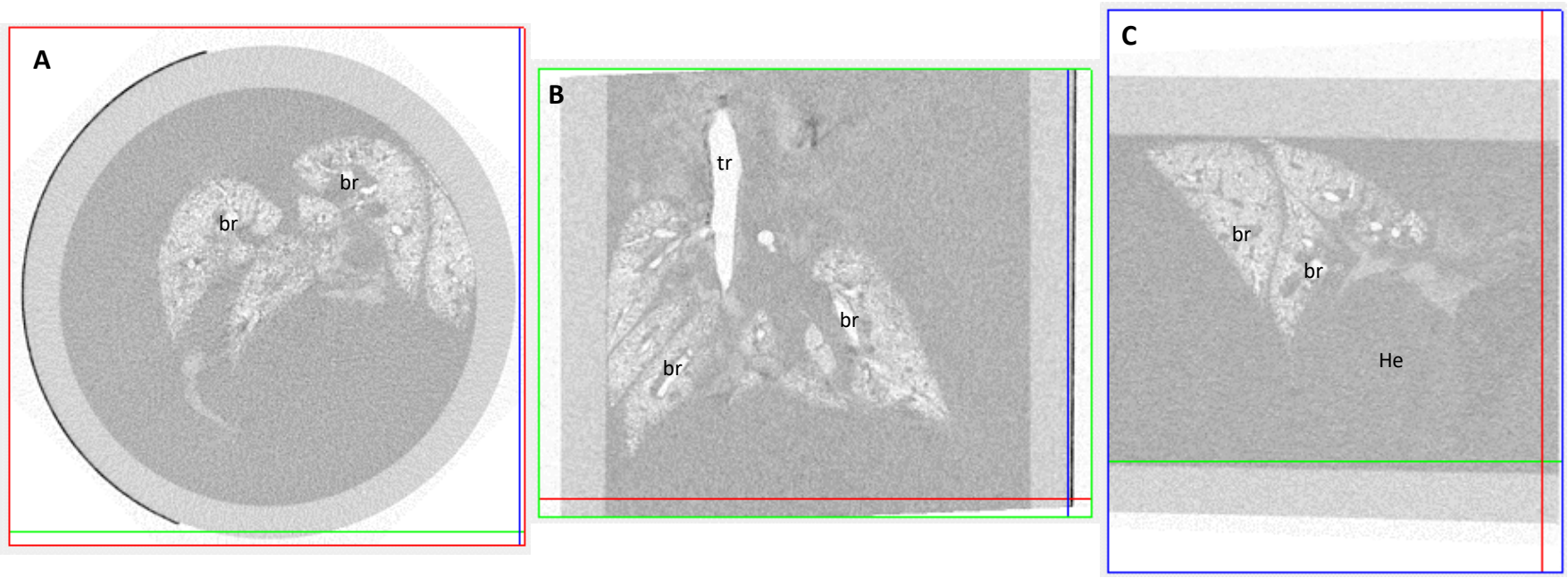
A
br
br
B
tr
br
br
C
br
br
He

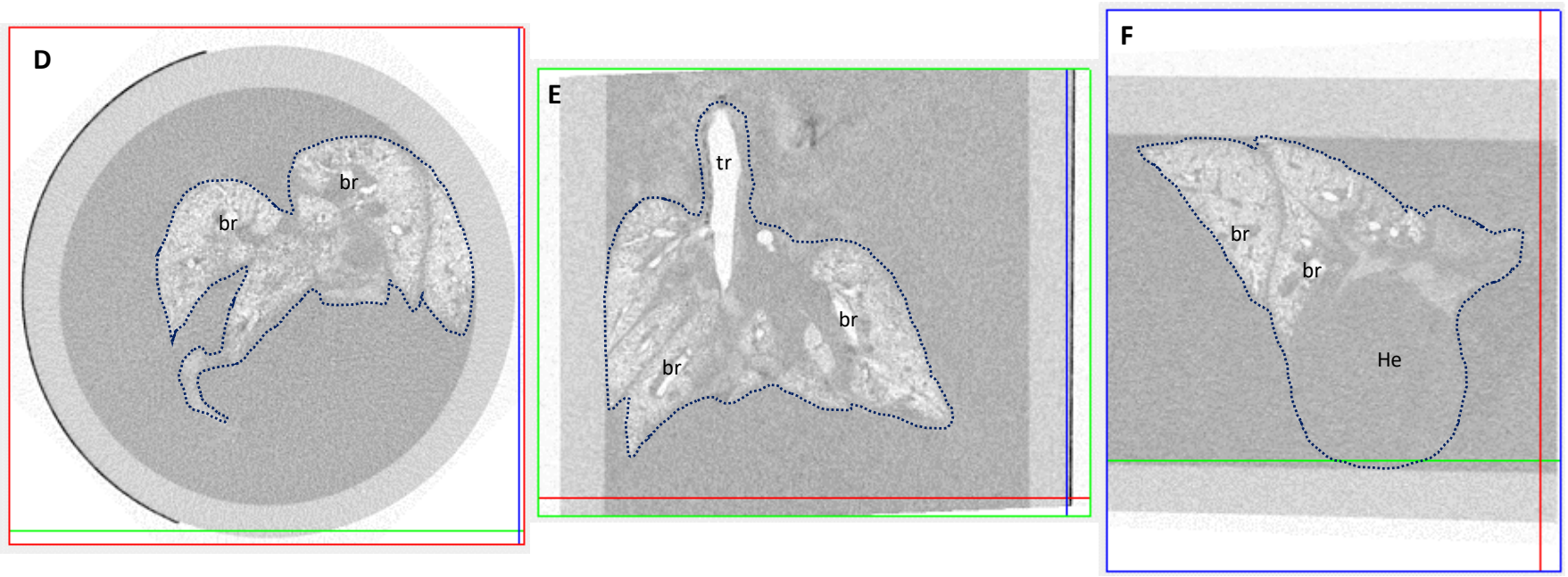

Figure 3.4. µCT scan images of unfixed, inflated mouse lungs suspended in PBS. Representative X, Y and Z plane images (red box, green box and blue box respectively) are shown. Lungs were isolated from a healthy adult control animal immediately after Sch1 by anaesthetic overdose and manually inflated prior to extraction. Isolated lungs were then suspended in PBS for µCT scanning. Lungs were scanned using a SkyScan 1272 µCT system at a resolution of 20 µm (0.25 mm aluminium filter, 0.3 ° rotation step). Images were reconstructed using Skyscan Nrecon software and visualised using DataViewer. Images shown are single representative sections from a single mouse. Anatomical features are identified by the following: tr- trachea, br- bronchioles, He- heart. A – C are the images as seen, D – F emphasise the outline of the lung and heart, identified by the dotted line.

3.4.3 Investigating the effects of adding different concentrations of KI to the PBS suspension for µCT scanning of unfixed lungs

To increase the x-ray attenuation capability and subsequently increase the greyscale value of the suspension agent, candidate molecules to add to the PBS that would have a minimal effect on the lung tissue were investigated. The first candidate molecule was potassium iodide (KI). KI has been used in medicine and as a dietary supplement since the 1820's and has been identified by the WHO as one of the safest medicines available (Oriel, 1994; WHO, 2015). It is highly soluble in water, which suited the purpose of the experiment as a contrast agent. The effect of adding different concentrations of KI to PBS was investigated. We tested concentrations of 1, 3, 5, 7 and 10 % (wt / vol) (0.06 M, 0.18 M, 0.30 M, 0.42 M and 0.60 M respectively) KI and suspended the lungs between Styrofoam cubes to immobilise them to the centre of the bijou.

Adding 1 % (wt / vol) KI, failed to demonstrate any significant difference in greyscale value (Figure 3.5, A), when compared to the scans in PBS (Figure 3.4). However, the improvement in inflation and immobilisation of the lungs did show a marked improvement in the quality of the scan. At 3 %, even with the decrease in inflation of the lung, there was a clearer distinction in the contrast between the lung tissue and the contrast agent, particularly with identification of the heart (He, Figure 3.5, B). This was also seen in the 5 % (wt / vol) KI scan (Figure 3.5, C) as the outline of the lung was still clearly visible, even with the movement distortion of the image. There was no further change in greyscale value when the concentration of KI was increased to 7 and 10 % (wt /vol) KI (Figure 3.5, D & E). When compared to the results using 5 % (wt /vol) KI (Figure 3.5, C) there was no further improvement in contrast when increased concentrations of KI were used.

Based on these results we decided that future scans of unfixed lungs would use a concentration of 3 – 5 % (wt /vol) KI suspended in PBS and suspended between Styrofoam blocks.

3.4.4 Scanning of inflated, unfixed lungs using 3 – 5 % KI contrast agent

Using these parameters, the lungs of two healthy adult mice were scanned; one male and one female, with a view to adopting this method of scanning for future experiments using the transgenic animal strains. Representative images in the X and Y viewing planes from lungs isolated from a female (Figure 3.6, A – H) and a male (Figure 3.6, I – P) healthy,

untreated adult mouse are shown in Figure 3.6. Images were collated from different regions of the 3D scan and anatomical features are identified using the previously described notation.

In these scans, the lung could easily be identified within the contrast agent (light grey / white), and there was a distinct difference in the greyscale value of the tissue within the lung when compared to the surrounding KI. The inflation of the lung and resolution of the scan was sufficient to enable us to identify normal alveolar structure from these scans to a level of detail comparable to Figure 3.2.

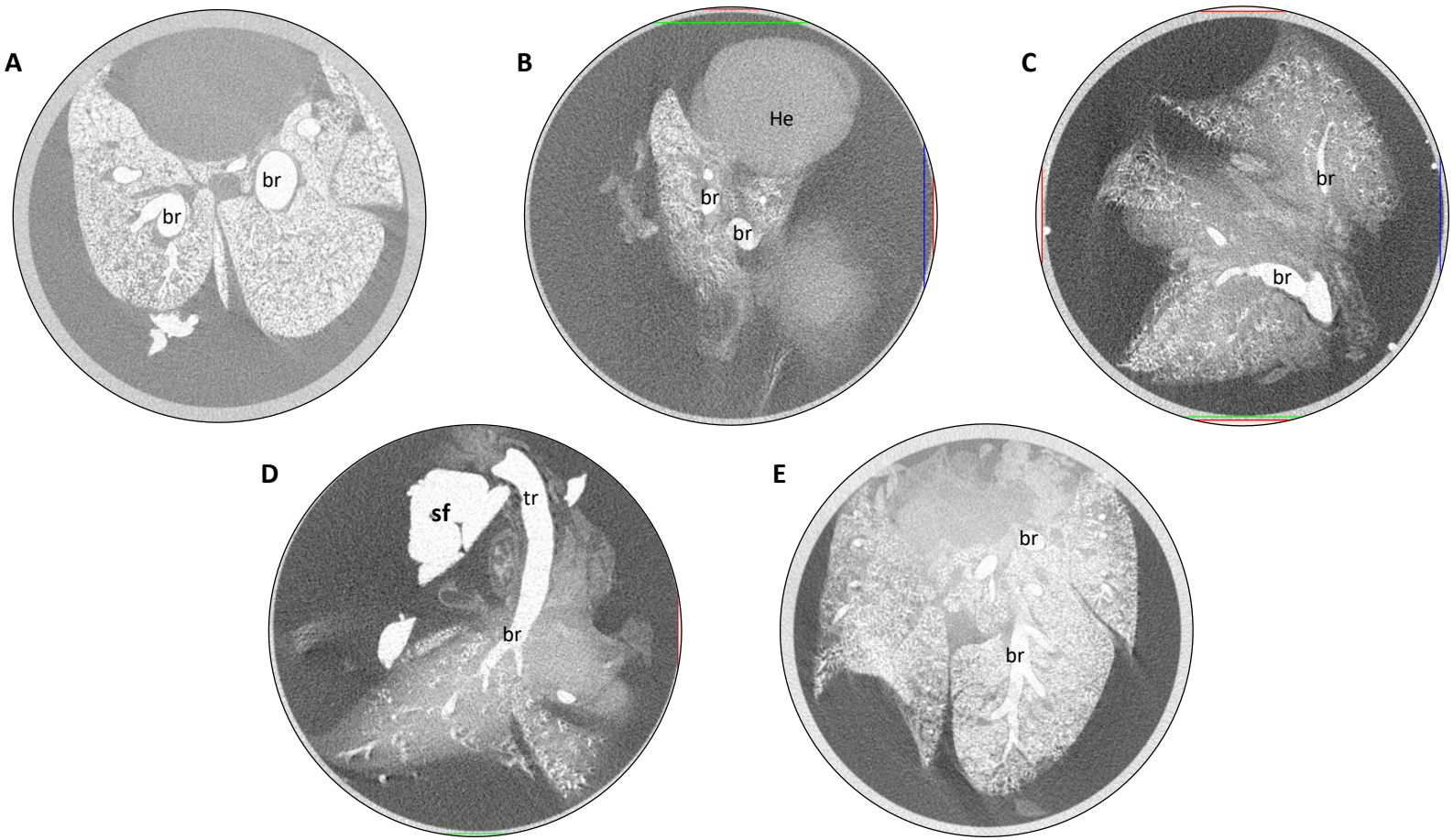

Figure 3.5. µCT scans of unfixed, inflated mouse lungs suspended in different concentrations of KI contrast agent. Single images are shown for 1, 3, 5, 7 and 10 % (wt / vol) KI contrast agent (A – E respectively). Lungs were isolated from a healthy adult control animal immediately after Sch1 by anaesthetic overdose and manually inflated prior to extraction. Isolated lungs were then suspended between pieces of Styrofoam (sf) for µCT scanning. Lungs were scanned using a SkyScan 1272 µCT system at a resolution of 20 µm (0.25 mm aluminium filter, 0.3 ° rotation step). Images were reconstructed using Skyscan Nrecon software and visualised using DataViewer. Anatomical features are identified by the following: tr- trachea, br- bronchioles, He- heart.

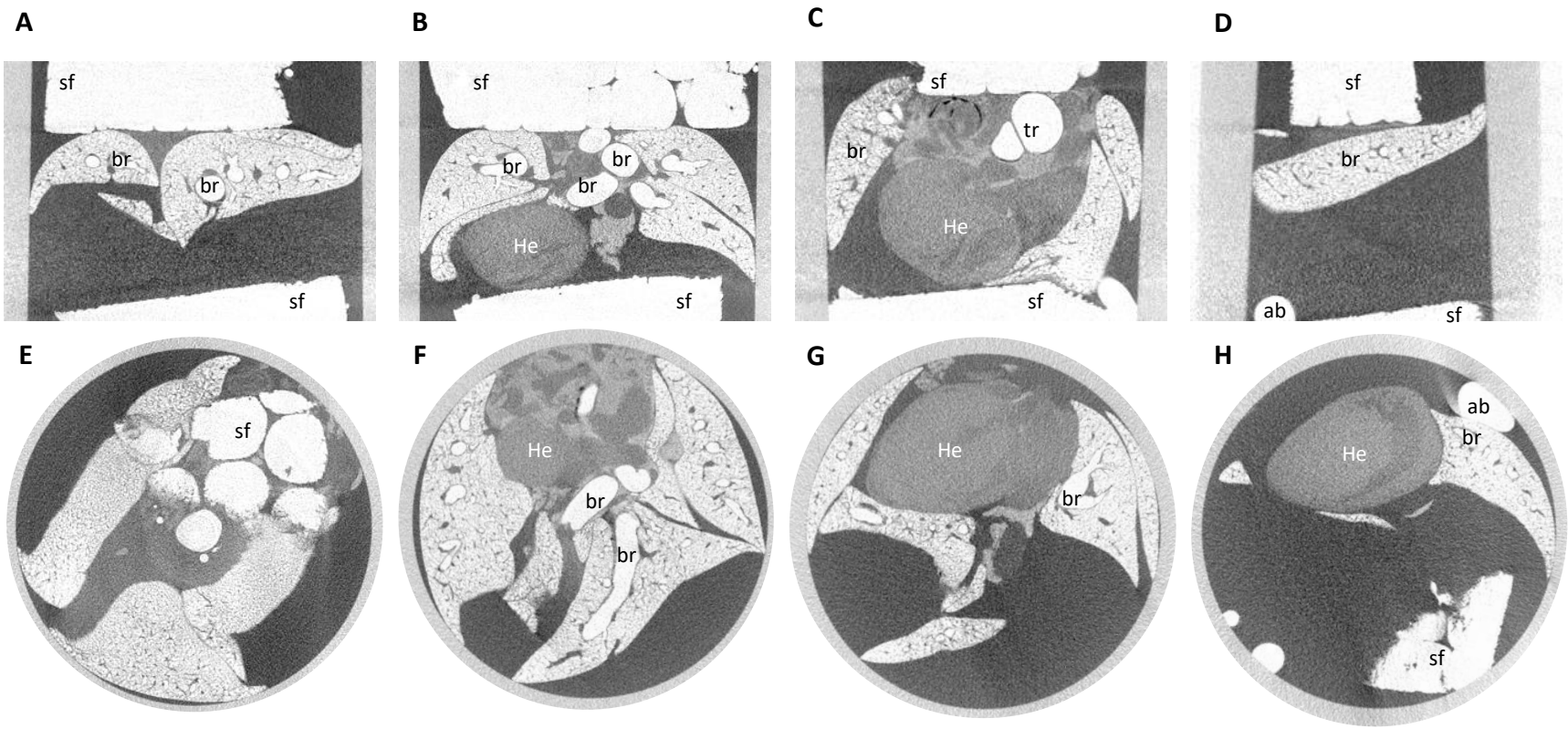
A
sf
br
br
sf
B
sf
br
br
br
He
sf
C
sf
tr
br
He
sf
D
sf
br
ab
sf
E
sf
F
He
br
br
G
He
br
H
ab
br
He
sf

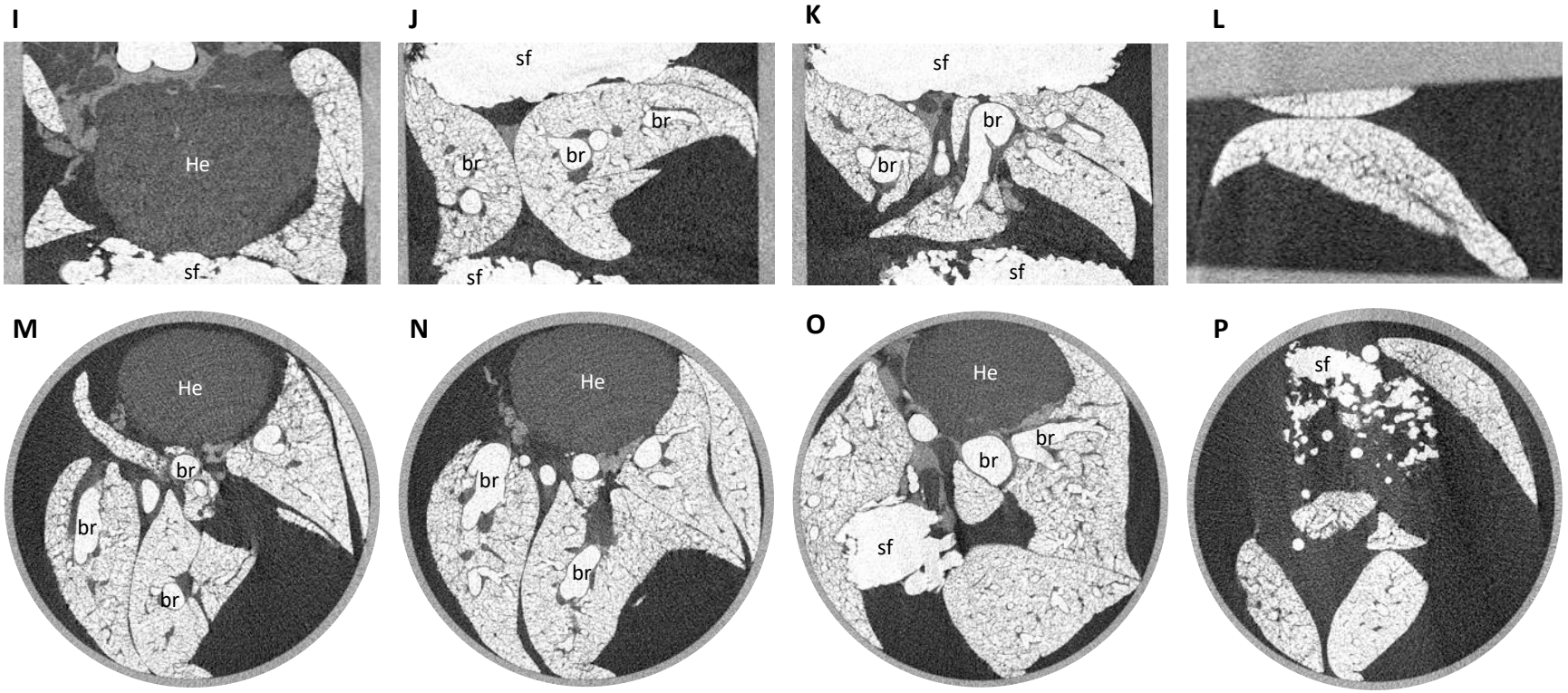

Figure 3.6. µCT scans of unfixed, inflated mouse lungs isolated from healthy control animals and suspended in 3 – 5 % (wt / vol) KI contrast agent. A series of images from a single scan are shown in the X (E - H, M - P) and Y (A - D, I - L) plane of view using DataViewer software. Lungs were isolated from a healthy adult control Female (A - H) and Male (I - P) mouse immediately after Sch1 by anaesthetic overdose and manually inflated prior to extraction. Isolated lungs were then suspended between pieces of Styrofoam (sf) for µCT scanning. Lungs were scanned using a SkyScan 1272 µCT system at a resolution of 20 µm (0.25 mm aluminium filter, 0.3 ° rotation step). Images were reconstructed using Skyscan Nrecon software and visualised using DataViewer. Anatomical features are identified by the following: tr- trachea, br- bronchioles, He- heart.

3.5 Establishing a reproducible model of fibrosis

Following the mortality rate and instance of adverse events during the WT study, the treatment schedules described for bleomycin models of IPF in recent literature were reassessed. The aim was to identify a bleomycin dose, which would result in sufficient fibrosis to be visualised using the µCT scanning technique but induce a less severe response in the animals. The results of this literature search are presented in Table 3.1.

When comparing the dose of 0.25 mg per mouse used in the initial experiment (section 2.5.2) with the published literature it was confirmed that a concentration comparable to other research groups had been used. However, it was decided to undertake a dose response experiment using lower concentrations of bleomycin. The following concentrations of bleomycin in PBS were prepared: 0.025 mg/mL, 0.5 mg/mL, 0.1 mg/mL and 0.2 mg/mL trialled and delivered at a volume of 2.5 µL per whole gram of weight. The resulting doses of bleomycin received by each group were: 0.0625 ng/g, 0.125 ng/g, 0.25 ng/g and 0.5 ng/g. Lungs were examined for signs of fibrosis at 28 days post bleomycin administration using the µCT scanning protocol established and described in section 2.6. Three WT mice were assigned to each concentration of bleomycin, representative scans of each group are shown in Figure 3.7. At 28 days mice treated with 0.0625 ng/g and 0.125 ng/g showed no signs of fibrosis (Figure 3.7, A & E, B & F). Animals dosed with 0.25 ng/g showed some signs of fibrosis with a thickened alveolar lining indicated by red arrows (Figure 3.7, C & G), whereas animals receiving 0.5 mg/g showed extensive fibrosis throughout the lung (red arrows, Figure 3.7, D & H). All animals survived for the duration of the experiment and no adverse reactions were observed.

For the experiments researching the fibrotic effects in transgenic animals, investigation of three timepoints; 7, 14 and 28 days were planned. Therefore, based on these dose-response results it was decided to trial a dose of 0.375 ng/g of bleomycin. It was hypothesised that a slightly higher concentration than 0.25 ng/g would result in a fibrotic phenotype more extensive than that seen in Figure 3., C & G, but less than 0.5 ng/g (Figure 3.7, D & H) without the severe response in the animals and risk losing the later timepoints due to illness. Three mice were treated as previously described in methods section 2.5.2, with a single dose of 0.375 ng/g bleomycin in PBS and the lungs were collected for analysis at 14 days.

The µCT scans exhibited a good extent of fibrosis present in the lung by 14 days in each of the subject animals (Figure 3.8, red arrows). A good distribution of the fibrosis throughout

the lung was able to be identified. The pairs of scan images in Figure 3.8, (A - C) represent individual animals, with each scan representing a different depth of the lung. All pairs of images show regions of fibrosis (red arrows), indicating that the fibrosis had extended throughout the lung and not just remained in the superficial regions surrounding the main airways. As with the scans in the previous dose-response experiment, we were able to distinguish not only the lung from the KI contrast agent, but the key anatomical features of the lungs including the trachea, heart and bronchioles.

Table 3.1. Literature search results for bleomycin treatment of mice and associated parameters for consideration during treatment.

Animal Age	Sec	Bleomycin Dose	Volume Administered & vehicle	Number of Administrations	Sample time points	Reported Mortality	Reference
7 - 9 weeks	Male	0.1 - 0.25 - 0.5 mg/kg	40 µl saline	6 x once daily	7, 14, 21, 28	40 % at 0.5 mg/kg – 20 % weight loss	(Egger *et al.*, 2013)
8 - 10 weeks	Male	0.05 mg/mouse (50 IU / mouse)	50 µl saline	1	3, 7, 10, 14, 21, 28, 84, 168	-	(Scotton *et al.*, 2013)
8 - 10 weeks	Male	1 - 2 mg/kg	50 µl saline	1	7, 10, 14	50 % saline, 33.3 % bleomycin	(Scotton *et al.*, 2009)
	Male	1.25-2.5 mg/kg	50 µl saline	1	7, 14, 21	-	(Tsukui *et al.*, 2013)
6 - 7 weeks	Male	0.055 mg	50 µl saline	1	3, 7, 14	-	(Moshai *et al.*, 2014)
6 - 7 weeks	Male	0.055 mg	50 µl saline	1	3, 7, 14	-	(Bantsimba-Malanda *et al.*, 2010)
-	-	0.08 mg (0.08 units)	intratracheal injection	1		-	(Tanjore *et al.*, 2009)
-	-	0.04, 0.06, 0.08 units	intratracheal injection	1	7, 14, 21, 28	-	(Lawson *et al.*, 2005)
6 - 7 weeks	Male	5 & 10 mg/kg	50 µl saline intratracheal injection	1	21	at 10 mg/kg 20 % mice survived to day 17	(Y. Wang *et al.*, 2015)
7 - 8 weeks	Male	5 mg/kg	PBS	1	3, 7, 14, 28	-	(Dong *et al.*, 2015)
10 weeks	Male	3 mg/kg (3 units/kg)	50 µl saline	1	3, 8, 15, 21	-	(Guo *et al.*, 2015)
8 weeks	Male	1.5 mg/kg	50 µl saline	1	7,21 days	-	(Lan *et al.*, 2015)
20 weeks	Male	80 mg/kg	200 µl saline tail vein	1	14, 21, 28 days	-	(Ni *et al.*, 2015)
20 - 22 g	-	2 mg/kg	-	1	28 days	65 % dead by 28 days	(X. Wang *et al.*, 2015)
8 - 10 weeks	Female	2.5 mg / body weight	saline continuously via pump	7 days continuously	7, 14, 28 days	-	(Yatomi *et al.*, 2015)
5-9 weeks	Female	0.12 units	50 µl saline	1	7, 14, 21 days	-	(Ponticos *et al.*, 2009)
8 weeks	Female	1.25 mg/kg (1.25 units/kg)	-	1	21 days	-	(Kurundkar *et al.*, 2016)

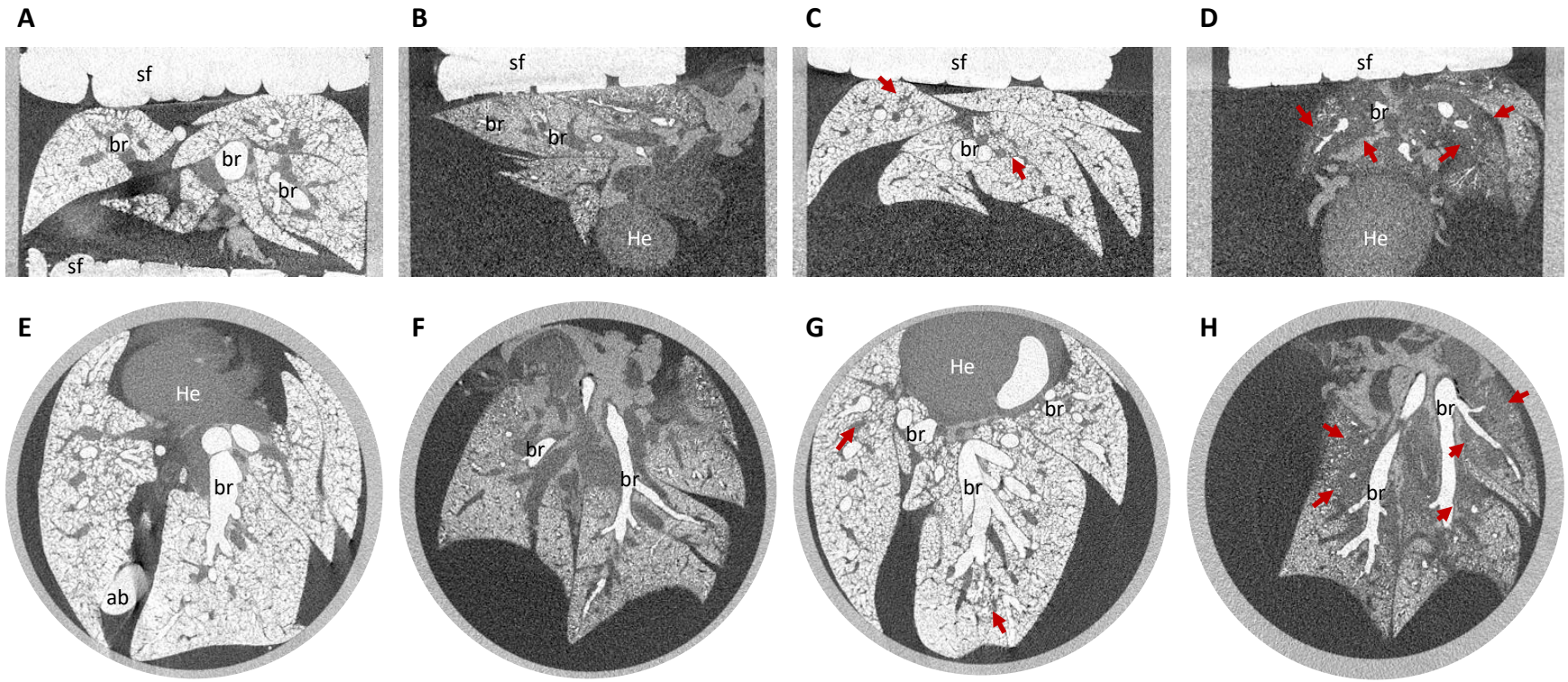

Figure 3.7. X and Y plane views of µCT scans of inflated mouse lungs treated with different concentrations of bleomycin and collected 28 days post administration. Lungs were isolated immediately after Sch1 by anaesthetic overdose and manually inflated prior to extraction. Isolated lungs were then suspended in 5 % KI, between pieces of Styrofoam (sf) for µCT scanning. Lungs were scanned using a SkyScan 1272 µCT system at a resolution of 20 µm (0.25 mm aluminium filter, 0.3 ° rotation step). Images were reconstructed using Skyscan Nrecon software and visualised using DataViewer. Anatomical features are identified by the following: br- bronchioles, He- heart. Air bubbles in the scan are denoted by ab. Red arrows indicate fibrotic regions within the lungs. Pairs of images were taken from animals treated with the associated concentration of bleomycin: A & E: 0.0625 ng/g, B&F: 0.125 ng/g, C & G: 0.25 ng/g, D & H: 0.5 ng/g. Images A - D are taken in the Y-field of view, E - H are taken in the X-field of view.

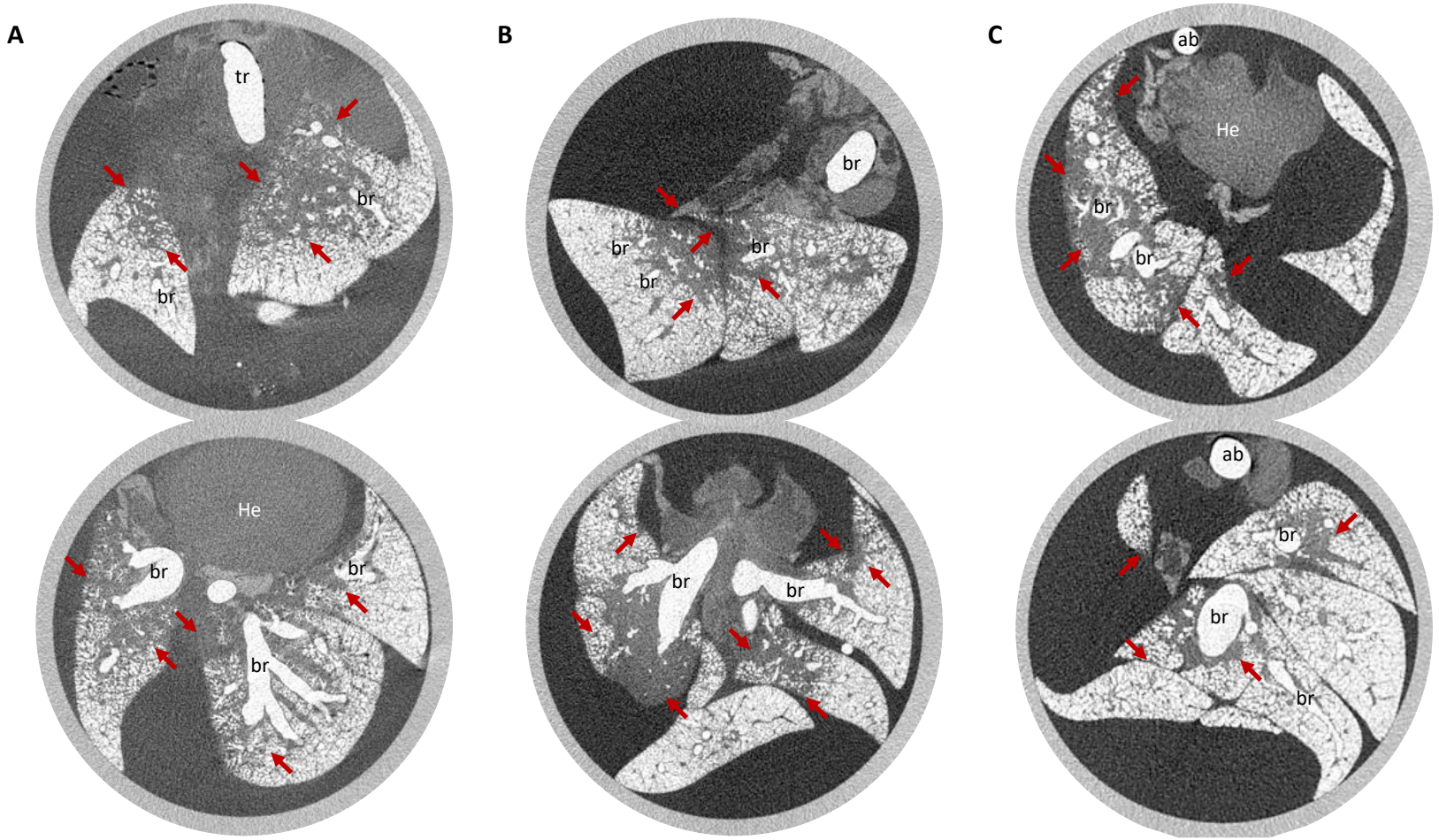

Figure 3.8. µCT scans of unfixed, inflated mouse lungs isolated at 14 days from mice treated with 0.375 ng/g bleomycin in PBS. Lungs were isolated immediately after Sch1 by anaesthetic overdose and manually inflated prior to extraction and suspension in 5 % KI. Lungs were scanned using a SkyScan 1272 µCT system at a resolution of 20 µm (0.25 mm aluminium filter, 0.3 ° rotation step). Images were reconstructed using Skyscan Nrecon software and visualised using DataViewer. Anatomical features are identified by the following: tr- trachea, br- bronchioles, He- heart. Air bubbles in the scan are denoted by ab. Red arrows indicate fibrotic regions within the lungs. Pairs of images were taken from the same animal. A - C each represent a different mouse.

3.6 Macro analysis of the µCT scan

Whilst the µCT images provided qualitative data into the extent of fibrosis in the lungs, the interpretation of the extent of fibrosis in one lung compared to another was dependent on the researcher examining the scans. There was a need to assign an independent, quantitative value to the scanned lungs to increase the reliability in the data when interpreting the effects of CCN2 removal in the transgenic animals. Professor Van 'T Hof developed a macro using the CtAN software that was able to analyse the greyscale (x-ray attenuation) values of each pixel within the designated region of the scan and assign an overall average greyscale value to the dataset (see appendices).

The macro was designed to assign a greyscale value between 0 – 255 to every pixel, where air is white or 0 and black is 255. The frequency of each of these values was then totalled to give an overall average x-ray attenuation (greyscale) value. Numbers of pixels assigned each grey value were presented as histograms (Figure 3.9), where the percentage frequency of each greyscale value is plotted against the assigned grey value. In control lungs (Figure 3.9, A & B) the average grey value assigned to female and male lungs was 64.6 and 65.6 respectively. The distribution is skewed to the left with an initial peak readout at 0, and a second around 60 - 70. In bleomycin treated lungs a shift to the right in both female and male animals (Figure 3.9, C & D) was seen, indicating an increase in pixels with a greater x-ray attenuation value, with mean average grey values of 120 and 83 (Figure 3.9, C & D respectively). The peak readout at 0 remained present in both bleomycin treated lungs, however the grey values in bleomycin treated lungs were more evenly distributed across the higher grey values (Figure 3.9, C & D) when compared to the bell curve pattern seen with a clear peak in the control lungs (Figure 3.9, A & B).

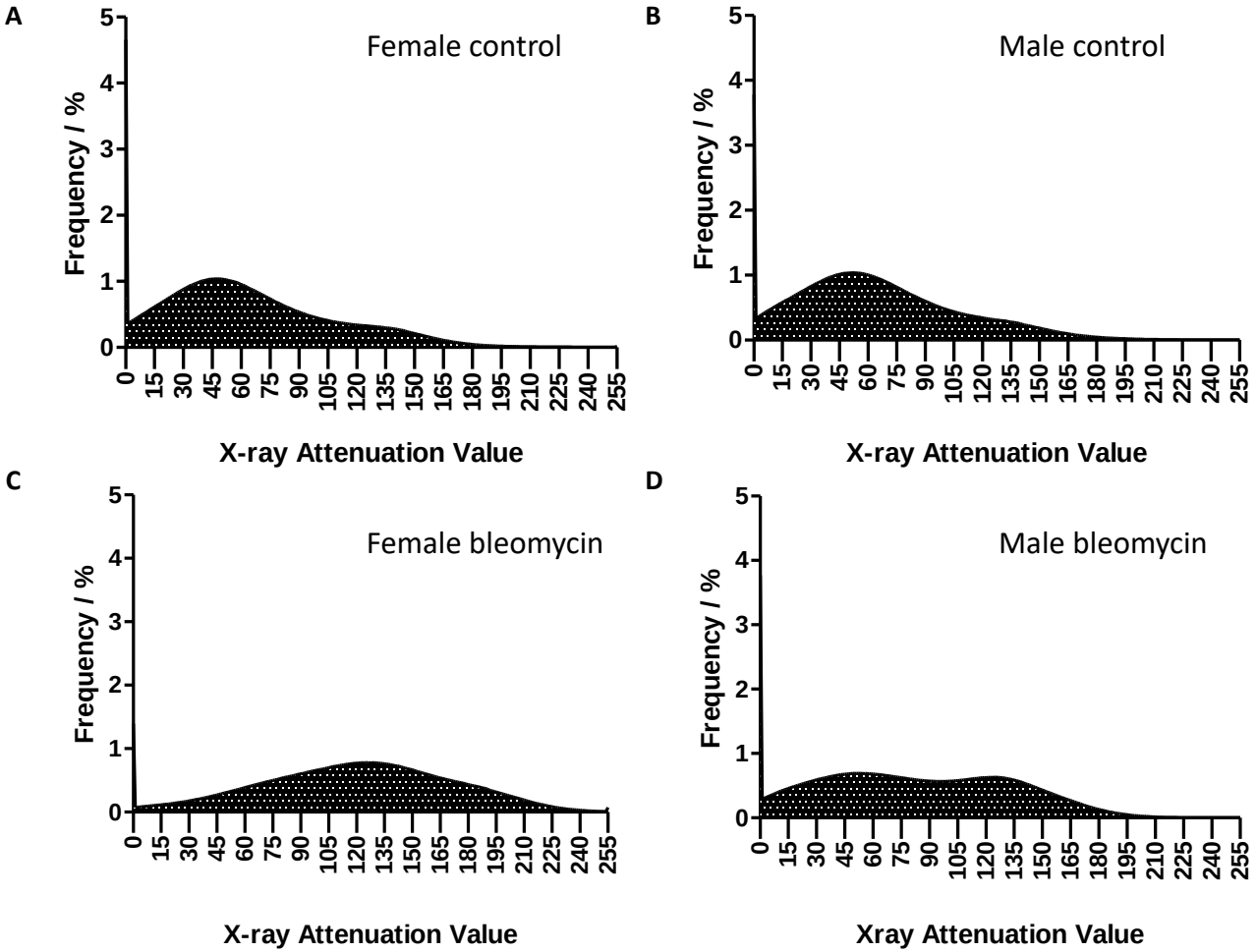

Figure 3.9. Percentage frequency histograms of pixel density calculated using an x-ray attenuation value macro in CtAN software. Histograms were generated using the readouts from female (A & C) and male (B & D) lungs isolated from untreated animals (A & B) and lungs isolated at 14 days from animals treated with 0.375 ng/g bleomycin (C & D). Lungs were scanned using a SkyScan 1272 µCT system at a resolution of 20 µm (0.25 mm aluminium filter, 0.3 ° rotation step). Images were reconstructed using Skyscan Nrecon software and analysed using CtAN software.

3.7 Histological analysis of lungs

To confirm the dense regions in the lung identified in the µCT scans were in fact fibrosis a lobe from experimental lungs was isolated and processed for histology following the protocol described in methods section 2.8. Sections of 5 µm were stained with H & E, or Goldner's trichrome stains. Protocols can be found in methods section 2.8.

H & E stain was used to identify anatomical features of the lung including the bronchioles, alveoli and blood vessels as well as fibrotic regions of tissue (black arrows). A stitched image taken at 10 x magnification was used to visually assess the level of fibrosis present in the whole lung section (Figure 3.10, A & B), where scale bars represent 1 mm. For closer analysis of the morphology of the lung, individual images were taken at 10x magnification (Figure 3.10, C - F), scale bars represent 500 µm.

In untreated control lungs the single cell epithelial lining of the alveoli can be seen clearly at 10x magnification (Figure 3.10, C & D). Blood vessels can be seen associated with the bronchioles, as well as being dispersed throughout the alveoli (Figure 3.10, C & D). The morphology demonstrated in Figure 3.10 is consistent with the reported literature for healthy murine lungs. In lungs treated with bleomycin (Figure 3.10; B, E & F) dense regions of tissue fibrosis are indicated by black arrows. Examination of the whole stitch image (Figure 3.10 B) showed these fibrotic regions to be generally localised to the immediate area surrounding the bronchioles. Closer examination of individual sections (Figure 3.10, E & F) showed increased nuclear staining of the immune infiltrates that are characteristic of the bleomycin model of fibrosis. In regions of fibrosis fewer alveoli are visible with a marked thickening of the epithelial lining. Blood vessels remain dispersed in a comparable fashion to control lungs and are present within regions of fibrosis and associated with bronchioles (Figure 3.10, E).

Goldner's trichrome stain was used to identify collagen deposits from muscular tissues. Cell nuclei appear black, cytoplasm - red and collagen - green. A stitched image taken at 10 x magnification was used to visually assess the presence of collagen across in the whole lung section (Figure 3.11, A & B), where scale bars represent 1 mm. For closer analysis of the morphology of the lung, individual images were taken at 10x magnification (Figure 3.11, C - F), scale bars represent 500 µm. Anatomical features of the lung are identified in the figure as: bronchioles, alveoli and blood vessels, fibrotic regions of tissue are indicated by black arrows.

Collagen is a major constituent of the pulmonary interstitium and major structures including the bronchioles, blood vessels alveoli and bronchioles. Therefore, green staining of these structures was anticipated and seen in both control and bleomycin treated lungs (Figure 3.11, A - F). Red staining inside bronchioles demonstrates the presence of the epithelial cells lining these structures. A reduction of this staining was seen in the bronchioles of bleomycin treated animals when examined at a higher magnification (Figure 3.11, E & F) when compared to images taken at the same magnification from healthy control animals (Figure 3.11, C & D). An increase in nuclear staining was seen in the fibrotic region of bleomycin treated lungs (Figure 3.11, E). This is characteristic of the immune infiltrates identified in the bleomycin model of fibrosis, which are not present in the lungs of control animals (Figure 3.11, C & D), or in regions where fibrosis is not present in bleomycin treated lungs (Figure 3.11, F). The structure of the alveoli is not identifiable in (Figure 3.11, E) the comprehensive green staining of the tissue indicates widespread deposits of collagen, with the only determinable features being bronchioles and blood vessels.

Assessment of µCT scans with these subsequent histological analyses confirmed that dense regions apparent on µCT scans (Figure 3.8) were synonymous with tissue deposits when stained with H & E (Figure 3.10) and that these deposits consisted of collagen (Figure 3.11). Histological analysis allowed for analysis of the structural changes occurring at the alveolar level, which was not possible to ascertain when analysing the µCT scan. Larger structures such as bronchioles could be identified by both analyses and therefore be used to identify the same region from a µCT scan on a slide.

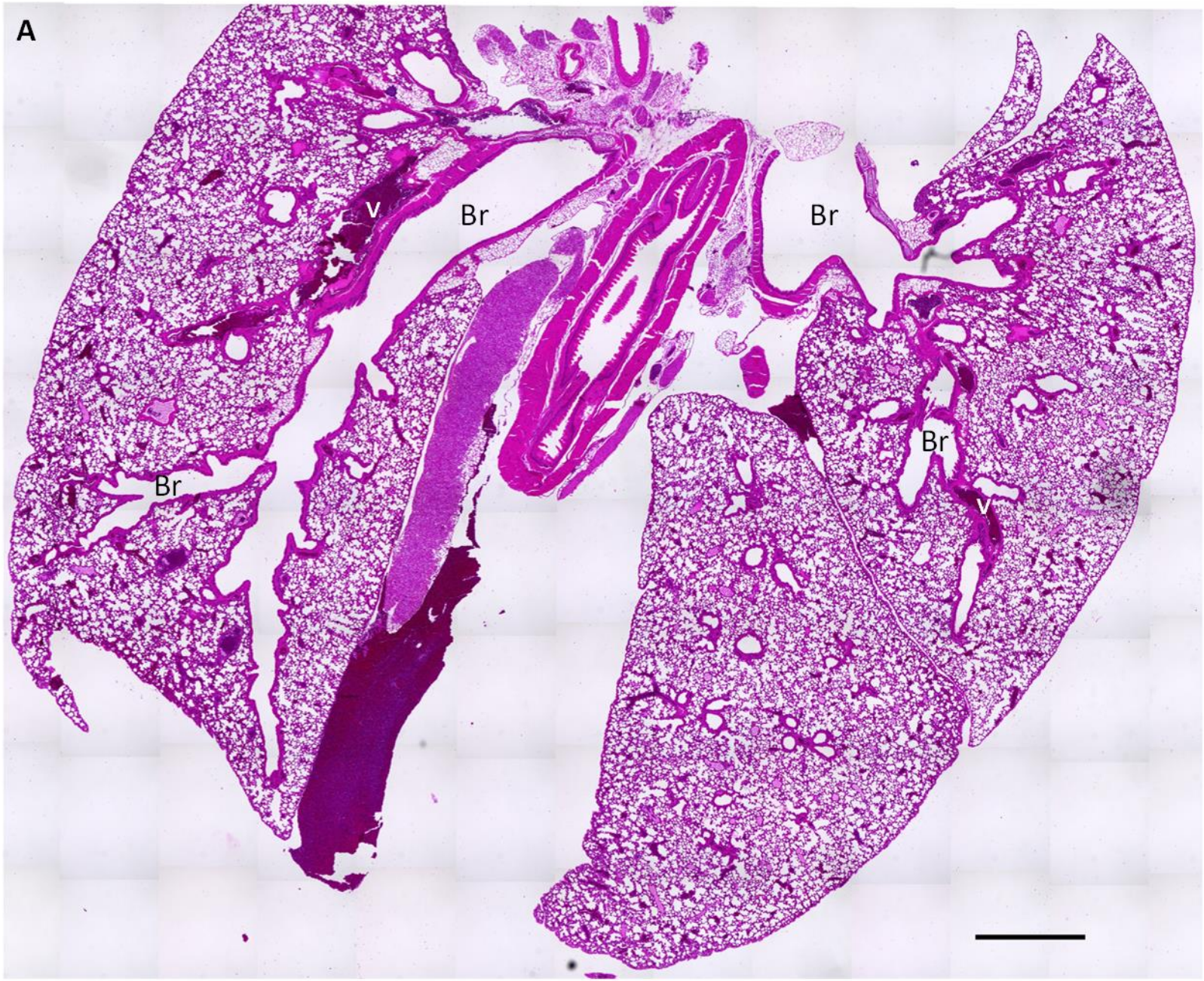
A
V
Br
Br
Br
Br
V

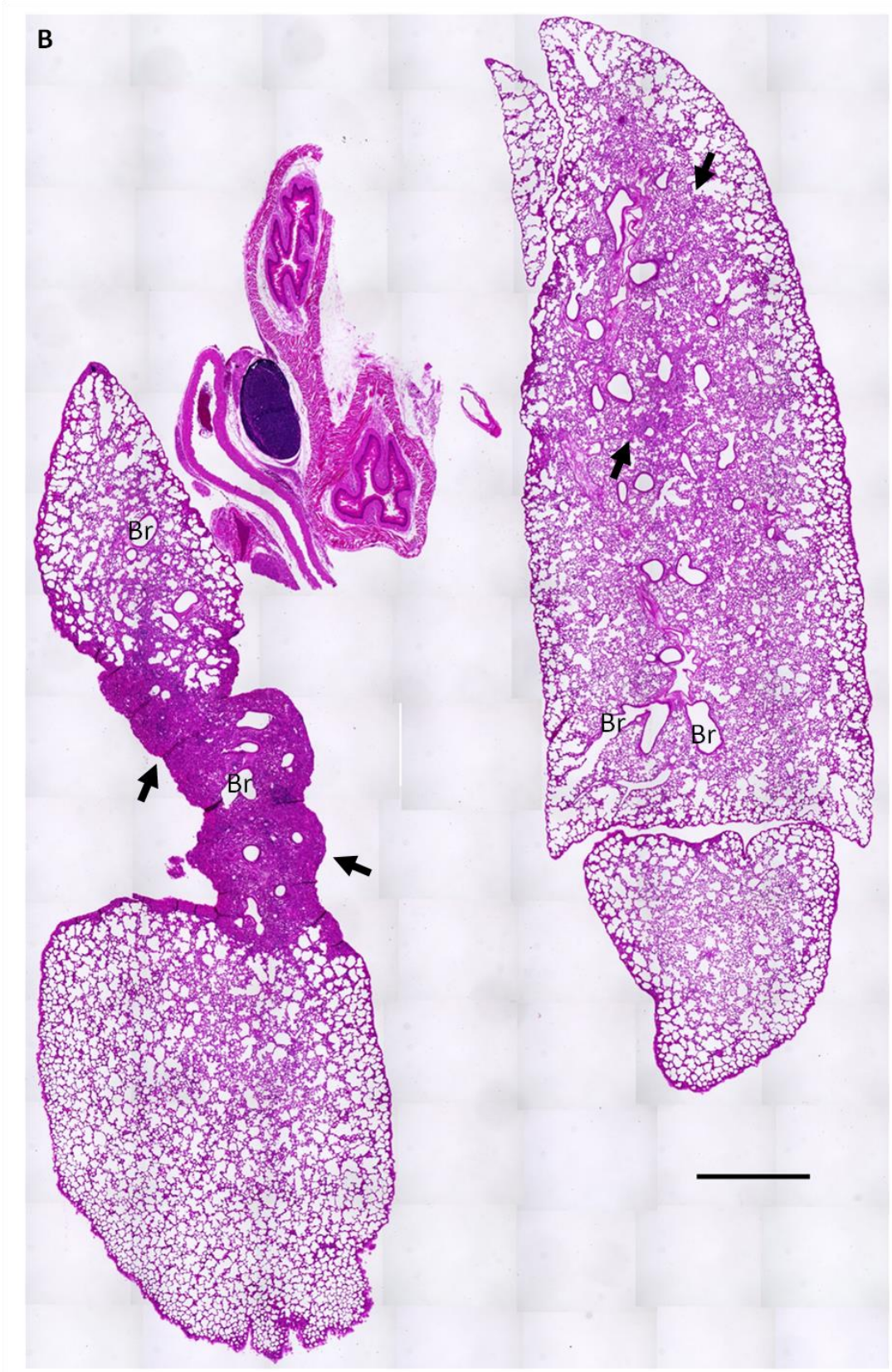
B
Br
Br
Br
Br

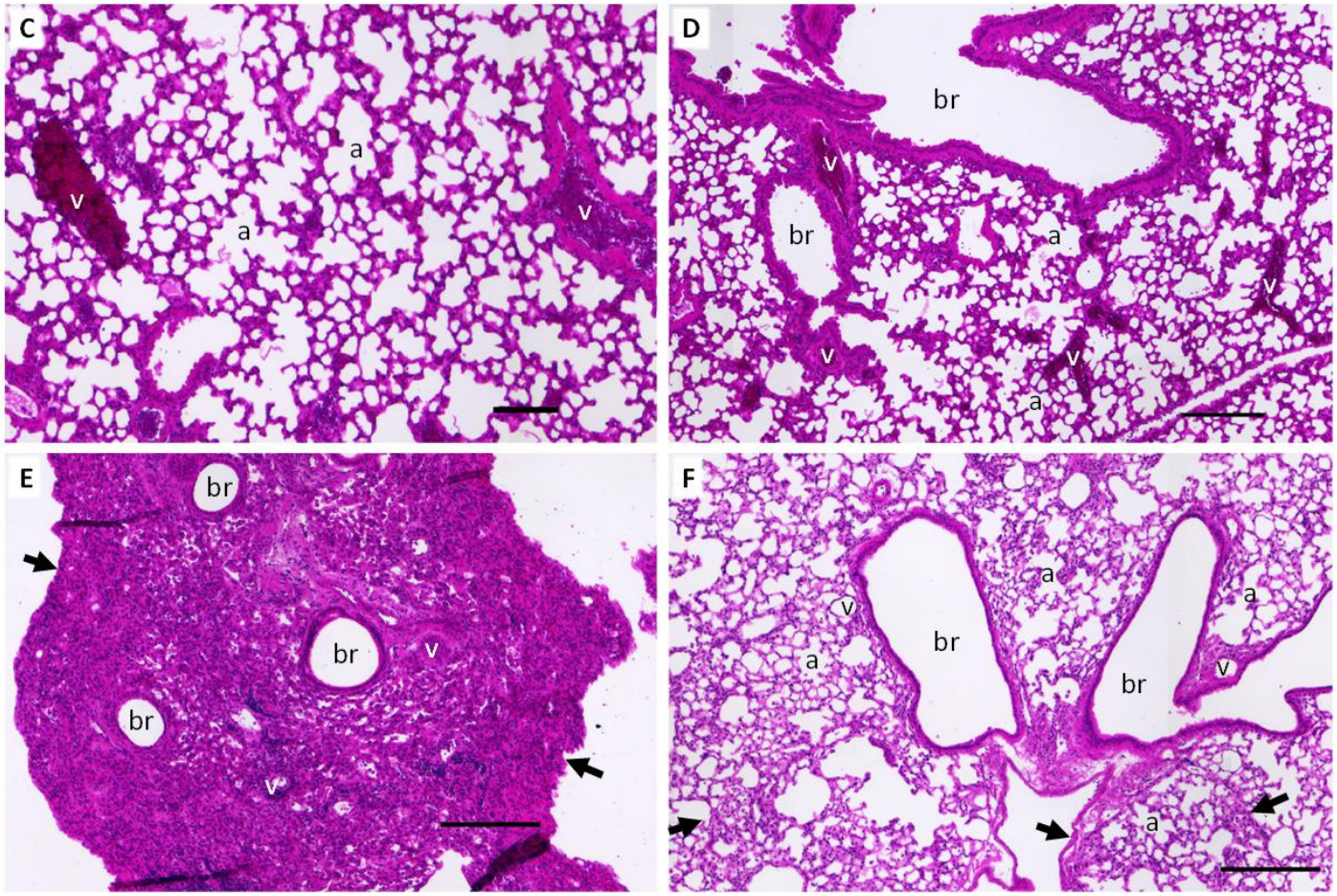

Figure 3.10. Histological evaluation of lung samples after µCT scan using H & E stain. Lungs were isolated immediately after Sch1 by anaesthetic overdose and manually inflated for scanning, using a SkyScan 1272 µCT system at a resolution of 20 µm (0.25 mm aluminium filter, 0.3 ° rotation step). Lungs were processed for wax histology and stained with H & E. Anatomical features are identified as follows: a- alveoli, br- bronchioles, v- blood vessels. Black arrows indicate regions of fibrosis. A, Whole lung stitch of control lungs taken at 10x magnification. B, Whole lung stitch of bleomycin treated lungs taken at 10x magnification. Scale bars represent 1 mm. C & D, Single images at 10x magnification of control lungs. E & F, Single images at 10x magnification images of bleomycin treated lungs. Scale bars represent 500 µm.

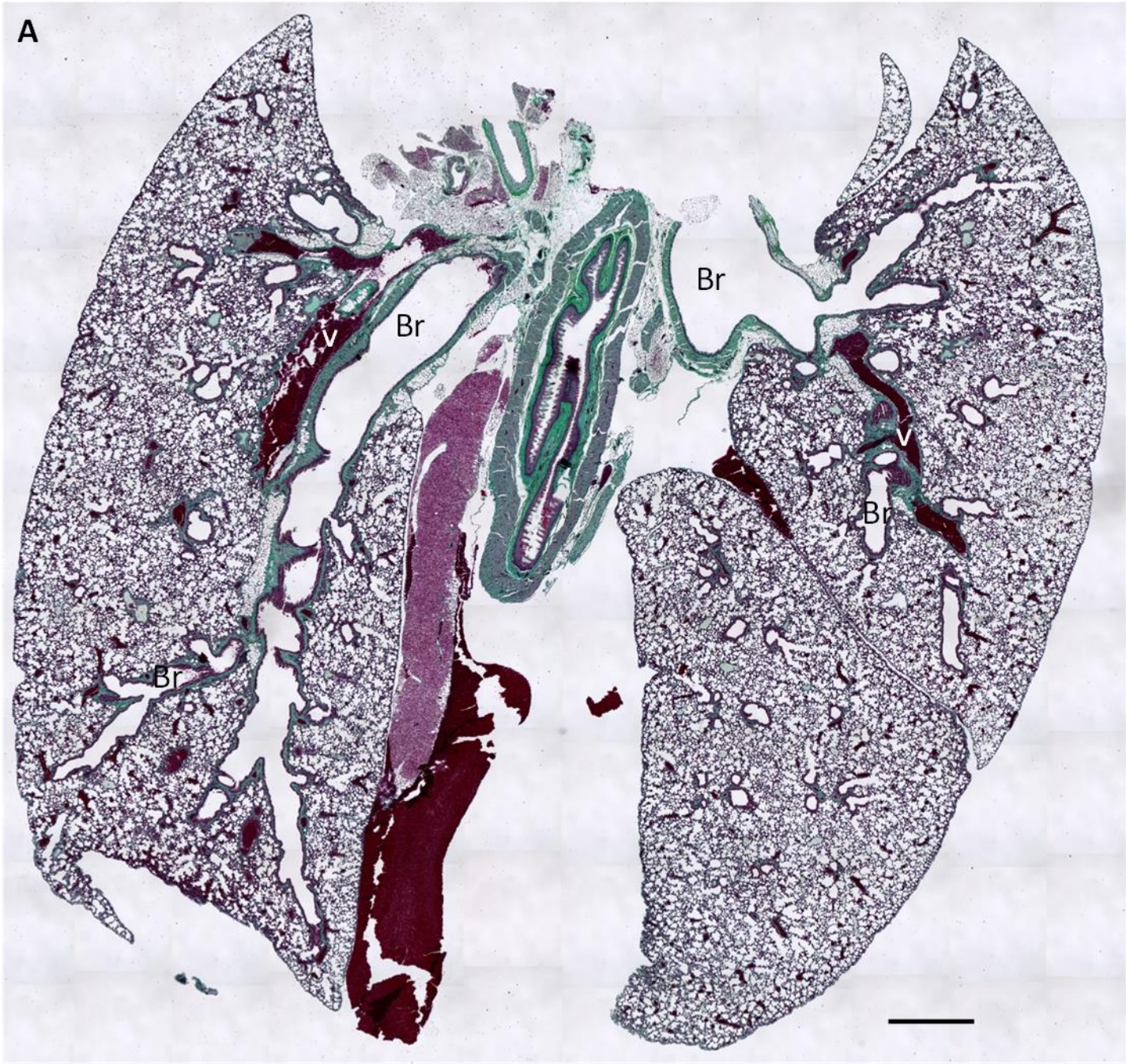
A
Br
Br
V
Br
V
Br

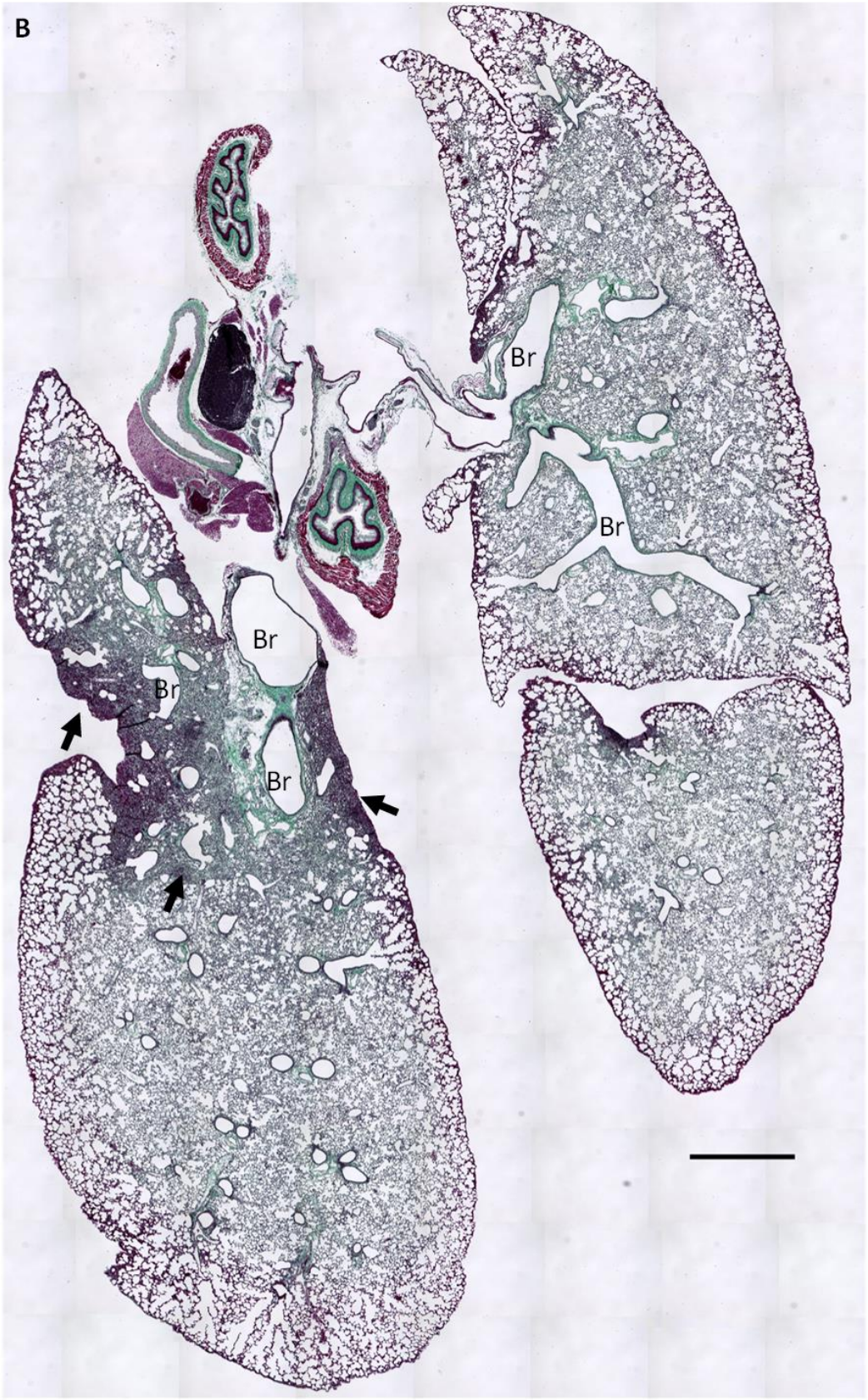
B
Br
Br
Br
Br
Br

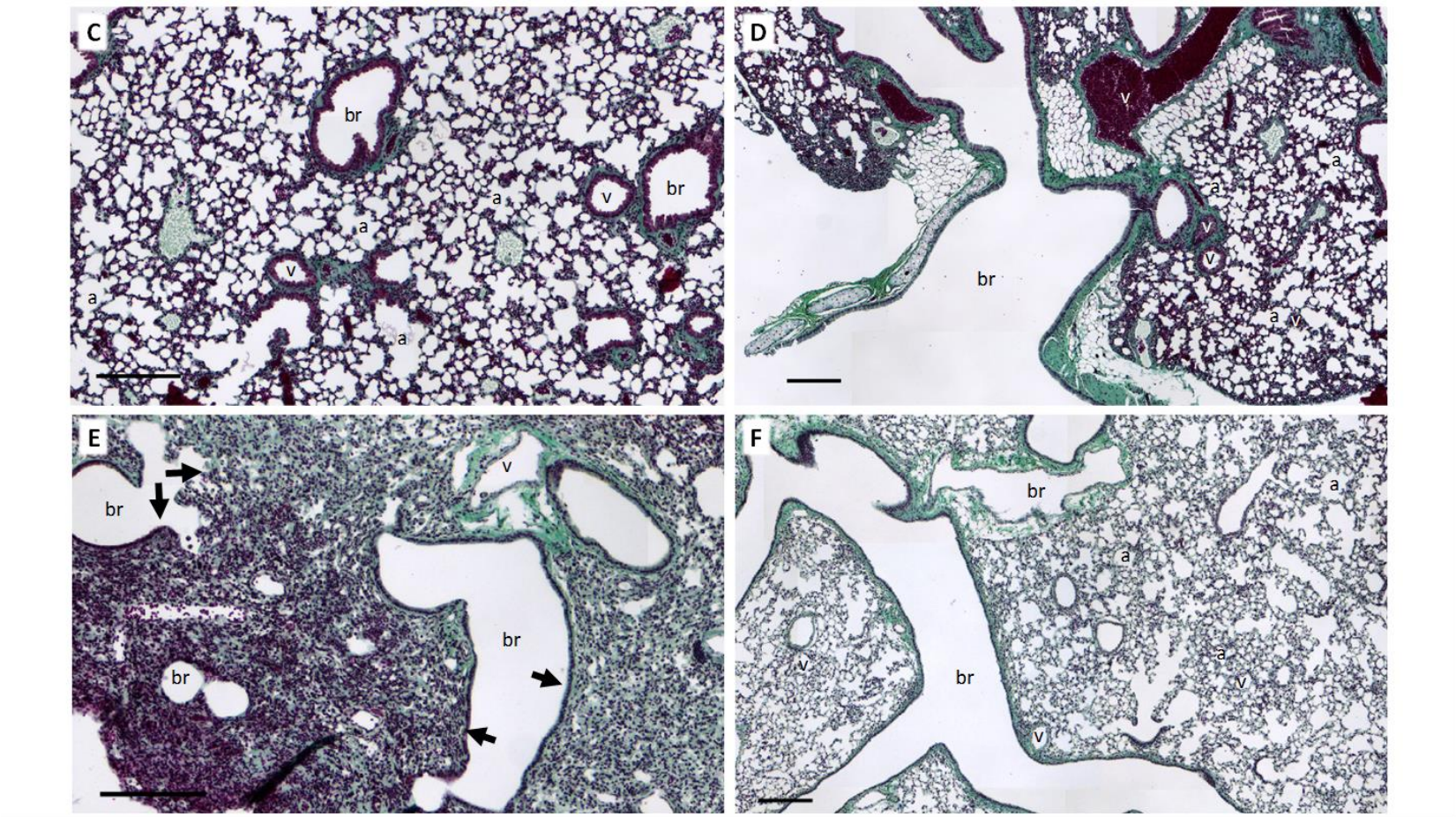

Figure 3.11. Histological evaluation of lung samples after µCT scan using Goldner's trichrome. Lungs were isolated immediately after Sch1 by anaesthetic overdose and manually inflated for scanning, using a SkyScan 1272 µCT system at a resolution of 20 µm (0.25 mm aluminium filter, 0.3 ° rotation step). Lungs were processed for wax histology and stained with Goldner's trichrome. Anatomical features are identified as follows: a- alveoli, br- bronchioles, v- blood vessels. Black arrows indicate regions of fibrosis. A, Whole lung stitch of control lungs taken at 10x magnification. B, Whole lung stitch of bleomycin treated lungs taken at 10x magnification. Scale bars represent 1 mm. C & D, Single images at 10x magnification of control lungs. E & F, Single images at 10x magnification images of bleomycin treated lungs. Scale bars represent 500 µm.

3.8 Discussion

This chapter presents the first original data on the establishment of a murine model of IPF at the University of Liverpool, using oropharyngeal aspiration of bleomycin. A novel protocol for *ex-vivo* μCT scanning and method of analysis is described for unfixed whole mouse lungs. The bleomycin model is widely described in literature and lab groups globally report in-house protocols for establishing a reproducible fibrosis with which to test candidate molecules or interventions in the wider context of pulmonary fibrosis (Ponticos *et al.*, 2009; Egger *et al.*, 2013; Scotton *et al.*, 2013; Gilhodes *et al.*, 2017). This research was unsuccessful in an attempt to reproduce a previously established protocol (Ponticos *et al.*, 2009). An unanticipated severity of responses meant animals were culled prior to reaching designated experimental timepoints and the overall mortality rate of the study was not acceptable under local severity limits and Home Office licence conditions. An alternative protocol was developed using a lower dose of bleomycin. This was well tolerated by the mice and the data in this chapter confirms that this dosing regime was reproducible and produced an established fibrosis.

3.8.1 Establishing a baseline response to bleomycin

The first study in this chapter used thirty-six mixed background (B6CBA F1) male mice aged 7 weeks to establish the baseline response to bleomycin when administered via OA 7 days after a series of I.P. injections of tamoxifen. Research described in chapters 4 and 5 of this thesis utilised a tamoxifen dependent CreER^{T2}, therefore it was necessary to determine the response to the combined therapy to account for potential adverse effects that might arise and would otherwise be masked if bleomycin was administered as a single treatment.

As timepoints of 7, 14 and 21 days post bleomycin were reported by Ponticos et al., (2009), and survival up to 84 days has previously been reported for this model (Scotton *et al.*, 2013), adverse effects were not anticipated.

One animal was culled due to ill health following I.P. injection of oil (treatment group 7 days O/B). This was considered unrelated to the treatment as all remaining animals receiving oil or tamoxifen displayed no adverse response. Adverse events occurred around day 10 with one animal being found dead in cage (D.I.C) and two more animals appeared moribund, with piloerection and hunching and were therefore culled. This was surprising as assessment of the mice during the 24-hr period prior had not raised any concerns over ill health. All three

animals belonged to the O/B treatment group. Three of the four remaining animals receiving the same treatment (O/B) survived to the final timepoint of 28 days. Around day 16 four more animals exhibited signs of ill health and were culled. Two were treated with T/P and two with T/B. As with the previously culled animals, no signs of ill health were noted in the 24-hr period prior to culling. An increased mortality at earlier time points was associated with the oil vehicle treatment. Although there was no obvious explanation as to why, when animals receiving tamoxifen suspended in the same vehicle did not demonstrate comparable mortality. Recent research into the effects of corn oil and sustained tamoxifen treatment for inducible transgenic models have reported conflicting evidence into the adverse effects seen. Liu et al., (2018) report effects on fat and glucose metabolism, where animals display fat associated weight loss that is independent of activity and food intake, starting at 5 days following the initial administration of corn oil and persisting for up to 12 weeks. Whereas Hubbard, Chen, & Boyd, (2017) observed no effect on body weight when comparing pharmaceutical-grade corn oil with non-pharmaceutical grade corn oil and PBS. This experiment used a tamoxifen concentration half that described by Liu et al., (2018), and administered 40 % less volume. Furthermore, the onset of weight loss appeared in a far shorter time frame and to a much greater degree than reported therefore it is to unlikely that the adverse effects seen in this study are unlikely to result from alterations to metabolism.

Interestingly, the extent of fibrosis in the O/B treatment is the most morphologically similar to the progression described in the literature (Izbicki *et al.*, 2002) when based on the histological pathology. Typical development of fibrosis shows activation of the immune system around day 3 following bleomycin instillation, followed by formation of early fibrotic foci around day 7, and established regions of fibrosis by day 14. Resolution of this fibrosis usually begins around day 21 and by day 28 a marked reduction in fibrosis can be seen when compared to 14 days. The histology results for corresponding timepoints for O/B treatment correlates to these predictions. For T/P treated lungs it was not expected that any fibrosis would develop as PBS is typically administered as a vehicle for bleomycin and tamoxifen administration alone should not induce a fibrosis. However fibrotic foci could be clearly seen in the lungs of these mice at 14 and 28 days. The pathology seen in these sections also correlates closely to that described by Izbicki et *al.*, (2002). Lungs isolated from T/B treated animals displayed an unusually high extent of fibrosis, present as early as 7 days and no obvious signs of resolution by day 28. These findings were considered the most concerning

(and interesting) as they displayed a grossly exacerbated response to the combined treatment, with fibrosis developing at a decidedly accelerated rate.

Expression patterns of transcription of the *COL1α2* gene were expected to correlate with the appearance of fibrosis on the histology sections, with peak increases in expression anticipated at 14 days. However, none of the analyses carried out on the samples taken corresponded to this. Transcript abundance of *COL1α2* appeared relatively unaffected by the combined treatments with the exception of 28 days, where O/B and T/B treatments showed a significant increase in mRNA levels. At 14 days T/B treatment showed significant increase in mRNA levels, however closer examination of the data identified a single animal with a 5.5-fold increase in transcription which increased the mean fold change disproportionately to achieve a significant result. The significant increase in T/P treatment is unusual on two accounts, the first being that PBS is a vehicle and should not induce a fibrotic response. Secondly, as previously mentioned, peak transcription is usually seen at 14 days, whereas for these results a mean fold change of 3 is greater than that seen across the entire study.

Initial considerations were that housing of animals in an SPF unit may have had an unanticipated effect on the immune system. As the initial inflammation response to bleomycin is believed to be the catalyst for the formation of fibrosis in this model, it would follow that animals with juvenile immune systems may exhibit a disproportionate immune response to DNA damage by bleomycin. Recent literature supports this idea, with a number of recent publications exploring the concept that SPF housing conditions result in a reduction of immune cell population numbers and diversity, as well as decreased diversity in the genetic profile of these cells (Masopust, Sivula and Jameson, 2017). Beura et *al.*, (2016) report that the immune systems of SPF mice compared to that of their wild type counterparts is analogous to comparing the immune system of a human neonate to that of an adult. Consequently, Stelekati & Wherry, (2012) describe the same phenomenon in humans that lack exposure to pathogens also lack diversity in their immune cell populations. They speculate as to the effects this has on the recognition of pathogens, innate immune responses, priming and differentiation of adaptive effector responses, as well generation and maintenance of immunological memory.

Based on this evidence it was considered highly likely that the exacerbated response was, in part, due to an over-stimulation of a juvenile immune system and it is likely that this is the reason a fibrotic response to PBS administration was observed. Retrospective consideration

into this study led to the conclusion that analyses of immune markers would have provided a valuable insight as to whether this was in fact the case.

The conclusions provided by this study were limited by the requirement to isolate individual lobes from the lung for analysis by either histology or qPCR, essentially at random. It was not possible to confirm whether either the histological data or qPCR was representative of the entire lung when analysed separately. Oropharyngeal aspiration of bleomycin is a notoriously variable model, with the potential to see a differential effect on each lobe within the lung (Antje Moeller *et al.*, 2008; Scotton and Chambers, 2010; Robbe *et al.*, 2015). This study therefore highlighted the requirement to adopt a method that would enable the assessment of the extent of fibrosis in the whole lung, prior to further analysis. As well as indicating that the dosing regimen with concern to bleomycin treatment would need to be reinvestigated to ensure reproducibility of the response and survival of the animals.

3.8.2 Imaging the whole lung

To address the third aim, to develop a method for the assessment of fibrosis in lung following administration of bleomycin, a solution to the aforementioned issue of examining the whole lung needed to be identified. Following a discussion with Professor Rob Van 'T Hof at the University of Liverpool regarding this limitation, it was decided that the Bruker Skyscan 1272 *ex-vivo* µCT scanner located at the University of Liverpool would be a suitable option for assessing the extent and localisation of fibrosis across the lungs.

Micro-computed tomography (µCT) imaging has seen an exponential rise in popularity over recent decades, in line with improvements in the resolution of images obtained and the diversity of samples that can be evaluated (Schambach *et al.*, 2010). Although more commonly used for imaging of bones (Muller *et al.*, 1998; Bauer and Link, 2009), more recent literature describes the use of *ex-vivo* µCT for finer anatomical components such as blood vessels (Downey *et al.*, 2012). Utilisation of this process achieved the aim of visualising the fibrotic extent of the whole lung, however the limitation of processing for µCT scanning was the inclusion of a chemical fixation step with 10 % NBF. The detrimental effects of fixation on DNA and RNA have been described on numerous occasions, with the consensus that it is not possible to recover reliable samples of RNA from tissues that have undergone fixation (Finke *et al.*, 1993; Tyrrell, Elias and Longley, 1995; Masuda *et al.*, 1999; Srinivasan, Sedmak and Jewell, 2002). As the intention of this research was to examine the genetic profile of transgenic animals, this posed a major limitation in the study design and protocol. Scotton et

al., (2013) approached a similar issue by using an experimental design where sample groups were split with 50 % animals' lungs subjected to µCT imaging and the remaining 50 % were snap frozen for qPCR analysis. This approach was considered; however, this would have doubled the number of animals required for each study group as a minimum, and still fail to account for the intra-animal variability of bleomycin administration. Therefore, attention was focussed on modifying the current method of µCT scans to remove the requirement for fixation and dehydration.

A protocol was developed, which utilised the contrast in x-ray attenuation capabilities of a liquid compared with air. Different levels of x-ray attenuation (ability to block x-ray waves) present as differential shades of grey where dense tissue appears black and air appears white on resultant scan images. Scanning of bones includes a liquid phase surrounding the tissue to prevent drying, such as PBS (Sharir, Ramniceanu and Brumfeld, 2011). It was decided that PBS would be a suitable medium with which to suspend unfixed lungs. X-ray attenuation of the liquid phase compared to the gaseous phase was postulated to be provide sufficient contrast. However it was evident from the scans that although the contrast between air and PBS was sufficient, the difference in x-ray attenuation of the lung tissue compared to that of PBS was negligible. Movement artefacts also reduced the quality of the scans as lungs were not compact within the bijou. Analysis of these scans identified only the gross structures of the trachea, bronchioles and heart. This was in part accounted for by the inept manner of lung inflation and compounded by a lack of immobilisation of the lung. The larger issue remained of achieving sufficient contrast between the suspension agent and the lung sample.

To address this issue KI was added to the PBS. The efficacy and safety profile of this molecule (Oriel, 1994; WHO, 2015) led to the assumption that its presence would not affect the physiology of the lung whilst its solubility did not significantly alter the preparation time for scanning. Of the concentrations tested, 3 – 5 % (wt / vol) KI suspension provided sufficient contrast to distinguish tissue. Addition of Styrofoam cubes above and below the lung was sufficient to immobilise it and reduce movement artefacts to a degree where scan resolution was comparable to fixed tissue. As such the aim of developing a protocol for the visualisation of lungs was met and the issue of establishing a reproducible model of fibrosis was re-addressed.

A literature search and re-examination of the bleomycin specification sheet revealed that the international units (IU) of our dosage (0.25 mg/mouse) was 2.23 IU, compared with 0.12 IU described by Ponticos et *al.*, (2009). This is an oversight in the reporting of bleomycin

treatment doses, as units of activity (IU) are batch dependent, and therefore difficult to determine from reported dosing concentrations in 'mg/kg'. A dose / response experiment identified that a single OA administered dose of 0.375 ng/g bleomycin (0.035 IU) was sufficient to produce fibrosis that was reproducible, and identifiable using the protocol established for µCT scanning.

Whilst the µCT images provided a qualitative means of assessment of the lungs, the interpretation of the extent of fibrosis in one lung compared to another was dependent on the researcher examining the scans. The requirement remained to assign an independent quantitative value to the scanned lungs, to increase the reliability in our data when interpreting the effects of CCN2 removal in our transgenic animals (data presented in chapter 4). Professor Van 'T Hof has previously developed software for similar requirements in assessing bone morphology (Van 'T Hof *et al.*, 2017), therefore assistance was sought to develop a macro capable of analysing the tissue content present in the lung scans. Specifics of this process are highlighted in the appendices. In short; a greyscale value between 0 – 255 was assigned to every pixel, where air is white or 0 and black is 255. The frequency of each of these values was then totalled to give an overall average x-ray attenuation value. Numbers of pixels assigned each grey value were presented as histograms. The x-ray attenuation profile was not affected by gender, with mean x-ray attenuation values of 64.5 and 65.6 attributed to females and males respectively. Both the distribution of values and mean attenuation value was notably different in animals treated with bleomycin. Therefore, it was concluded that analysis of scans using this macro was a sufficient quantitative measure of fibrosis.

Further analysis of lungs using this method determined that the scan quality significantly impacted the resultant greyscale value determined using this macro. Analysis of scans obtained from transgenic and bleomycin treated lungs found that a poor-quality scan of a control lung would read-out with a similar distribution and mean to a fibrotic lung. Therefore, the decision was made to exclude the macro analysis from the subsequent data chapters of this thesis.

The outstanding requirement for this protocol was to conclusively determine that the dense regions postulated to be fibrosis in the µCT scans was in fact a tissue deposit and not a scan artefact. This was straightforward to explore by histological examination of the lungs. We assessed the lungs using a general H & E tissue stain, and a trichrome stain (Goldner's trichrome). Firstly H & E staining confirmed that the dense area corresponded to the

presence of tissue with clear cytoplasmic staining seen across. Trichrome staining further confirmed that this tissue was predominantly composed of collagen which was expected for the bleomycin model of IPF.

3.8.3 Summary

The overall aim of this research was to investigate the role of CCN2 in a murine model of IPF. Here we described the process for establishing the bleomycin model of IPF at the University of Liverpool. The results discussed describe the challenges faced when attempting to develop an animal model of disease that is inherently variable by its mechanism of action, and the solutions that were adopted to overcome them. The primary outcome was the development of a protocol that produced a consistent and established fibrosis in mixed background mice (B6CBA F1). This was confirmed with histological analysis by staining with both a general tissue stain (H & E) and a collagen specific stain (Goldner's trichrome). The secondary outcome of these experiments was the development of a novel method of scanning lungs using a Bruker SkyScan 1272 ex-*vivo* µCT scanner. This method was optimised for unfixed, manually inflated lungs, whereby samples could be subsequently analysed for both qPCR and histology from the same animal. The third and outcome was the development of a quantitative method of assessment of fibrosis utilising the data acquired from the µCT scans. This was an important addition to improve the reliability of the data when interpreting the effects of CCN2 removal in our transgenic animals.

4. Generating the Double Transgenic Animals for Loss of Function of CCN2 in a Fibroblast-Specific and Ubiquitous Manner

4.1 Genetically modified animals as models for disease

The laboratory mouse is an ideal model organism for studying the pathobiology of human disease, owing to their physiological similarity to humans, the ease of genetic manipulation and their accelerated gestation and life span compared to humans (Gierut, Jacks and Haigis, 2014). These traits enable the study of disease across their entire life span (approximately 2 years), a feat impossible in studies of chronic human disease. Genetic manipulation has enabled researchers to generate specific loss of function mutations in genes, and subsequent study of the resultant phenotypes in *vivo* from as early as 1989 (Capecchi, 1989). Discovery of site-specific recombinase systems that could be controlled in a spatio-temporal manner in 1994 (Gierut et al., 2014; Nagy, 2000; Nagy, Mar, & Watts, 2009) enabled the study of gene functions in a tissue specific manner, and evaluation of the phenotypes arising from genes who's systemic inactivation causes embryonic lethality or profound developmental defects, such as the protein of interest in this research; CCN2 (Lambi *et al.*, 2012).

4.1.1 Cre / Lox recombinase system

Of the site-specific recombinase systems, the most commonly used in current research is the Cre / Lox system. Cre (cyclization recombination) is a 38-kDa, site-specific DNA tyrosine recombinase derived from P1 bacteriophage. Cre catalyses DNA recombination between two *loxP* sites (locus of crossing over {X} of P1) which are 34-bp palindromic recognition sequences (Buchholz *et al.*, 1996). The utilisation of this system requires the insertion of the *lox*P sites at the chromosomal location of interest (subsequently described as a 'floxed' gene), and expression of the Cre gene by the mouse (Babinet, 2000). $CreER^{T2}$ is a modified, tamoxifen-inducible Cre and is currently one of the most successful used in inducible genetic systems (Metzger *et al.*, 1995; Schwenk *et al.*, 1998; Zhong *et al.*, 2015). A mutated estrogen receptor is fused to Cre as a transgene (Cre-ER), which is activated via binding of 4 - OHT, (Zhong *et al.*, 2015). The mechanism of activation of $CreER^{T2}$ is outlined in Figure 4.1.

Over 11,000 mouse Cre lines are described on the Jackson Laboratories Mouse Genome Informatics website (Jackson Laboratories, www.informatics.jax.org, accessed October 2018). Time-dependent and tissue-specific $CreER^{T2}$ have been reported in numerous tissues, including cartilage, endothelium, epithelium and lung.

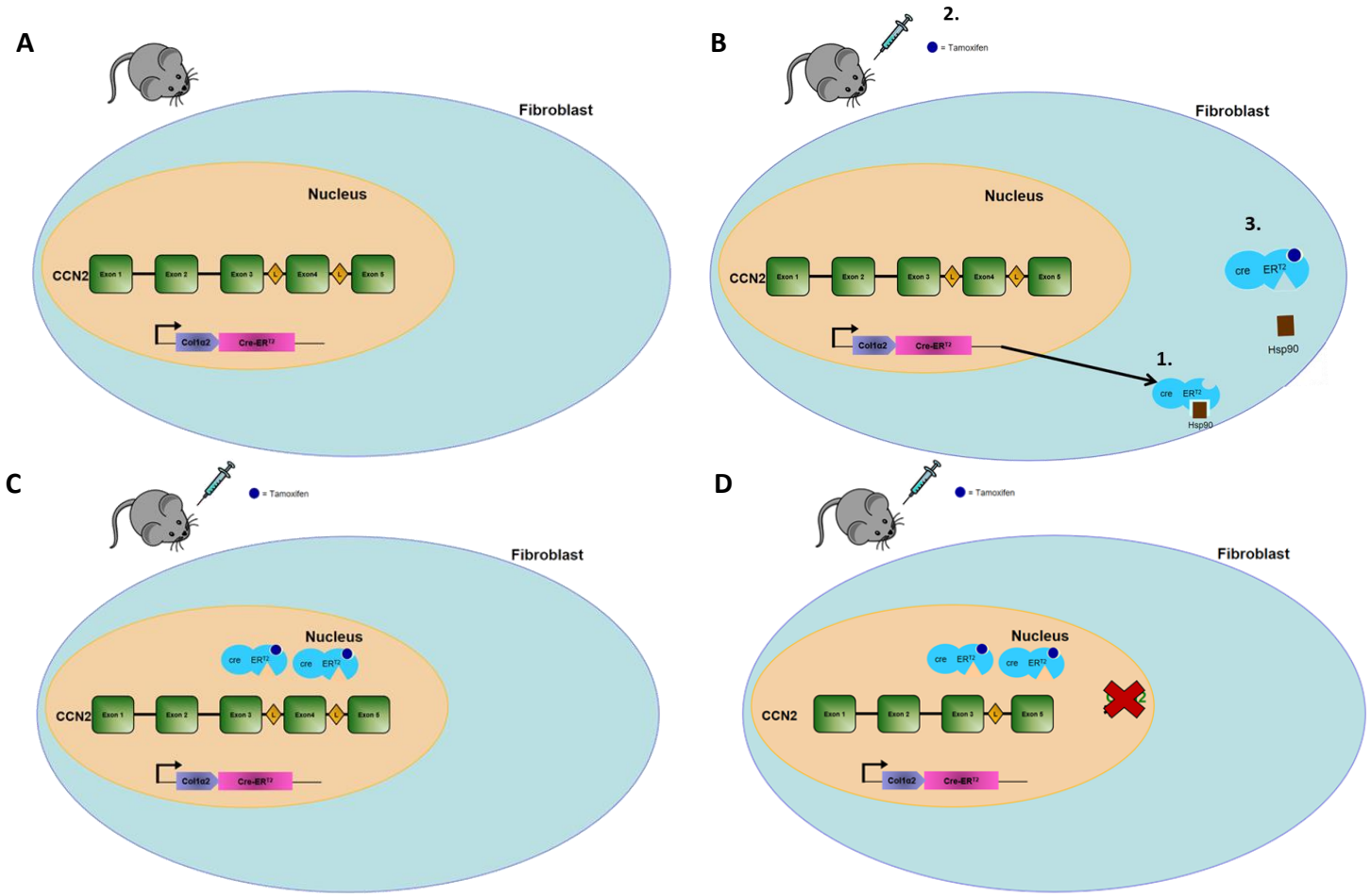

Figure 4.1. Mechanism of action of the tamoxifen dependent CreER^{T2}. A, Double transgenic animals are born without a phenotype and possess a floxed gene of interest (L-loxP site) and a tamoxifen-dependent CreER^{T2} (in this example Cre expression is driven by a fibroblast specific enhancer). B, when the Cre is synthesised the ER^{T2} modification directs its localisation to the cell cytoplasm where it remains membrane bound (1), when tamoxifen is administered (2.) the 4-OHT metabolite binds to the modified estrogen receptor causing a mutation, releasing the Cre from the membrane. C, Cre translocates to the nucleus, where it recognises the loxP sites (L). D, Recombination of the region within the loxP sites occurs, for this figure the result is excision of the flanked region resulting in loss of function of the CCN2 gene.

(Zhu *et al.*, 2008; Feil, Valtcheva and Feil, 2009; Gui *et al.*, 2012). These are used in conjunction with floxed genes of interest for gain and loss of function experiments. Activation of the CreER^{T2} can be initiated by I.P. injection of tamoxifen to pregnant females, postnatal pups, or adult mice. Dosing route and timing is primarily dependent on the animal age and target tissue (Gierut, Jacks and Haigis, 2014).

4.1.2 Characterisation of inducible CreER^{T2} lines

Characterisation of the expression profile of inducible CreER^{T2} lines was originally accomplished using a Cre reporter transgene, in which marker gene (e.g. LacZ) expression is dependent on Cre-mediated recombination (De Val *et al.*, 2002; Muzumdar *et al.*, 2007). Double reporter transgenes were a modification of this system and act via labelling cells that have undergone Cre-mediated recombination with one marker and non-recombined cells with another (Novak *et al.*, 2000). One of the recent advances in this technology was described by Muzumdar *et al.*, (2007) who developed a double fluorescent Cre reporter mouse, (mT/mG) that expresses membrane-targeted tdTomato (mT) prior to Cre excision and membrane-targeted EGFP (mG) following (Cre excision, Figure 4.2). This reporter line overcomes some of the key limitations when determining the reliability of expression patterns of new Cre lines. For example, the penetration of a substrate (e.g. X-gal in LacZ reporters) through tissue samples both *in vivo* and *ex vivo* may be insufficient to identify activity and result in mischaracterisation of the expression profile. Leading to unanticipated adverse events when the Cre is used in gene manipulation.

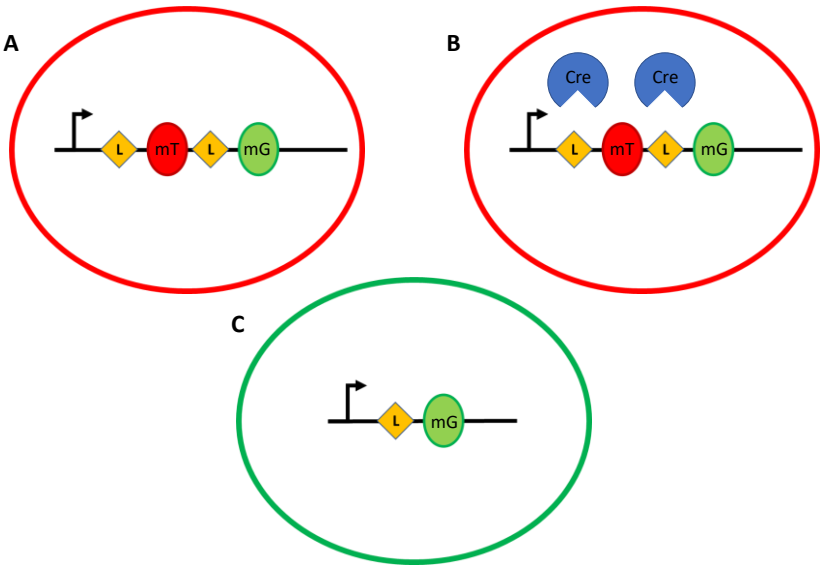

Figure 4.2. Representative diagram of the mT/mG construct described by (Muzumdar *et al.*, 2007). *A, The mT/mG reporter construct consists of a ubiquitously expressed promoter driving expression of membrane-targeted tandem dimer Tomato (mT) that is flanked by loxP sites (L). tdTomato expression is ubiquitous and localised to the cell membrane. After Cre-mediated recombination (B), the mT sequence is excised allowing the promoter to drive expression of membrane-targeted enhanced green fluorescent protein (mG, C). Arrows denote the direction of transcription.*

4.2 Chapter Aims

The aims of this chapter were as follows:

1) Establish and characterise a double transgenic mouse colony containing a floxed CCN2 transgene and a Ubiquitously expressed tamoxifen-inducible CreER^{T2} (ROSA26CreER^{T2} CreER^{T2}).

The first objective was to develop a genotyping strategy for single and double transgenic mice to identify individuals containing the transgenes. The second objective was to select and maintain littermate pairings from the F1 breeding colony and subsequent offspring generations, to establish a mouse colony that was homologous for the CCN2 floxed gene, and positive for the ROSACreER^{T2}. The final objective was to assess the response to tamoxifen administration and confirm the loss of function of the CCN2 gene.

2) Establish and characterise a double transgenic mouse colony containing a floxed CCN2 transgene and a fibroblast specific tamoxifen-inducible CreER^{T2} (Col1α2-CreER^{T2}).

The first objective was to develop a genotyping strategy for single and double transgenic mice to identify individuals containing the transgenes. The second objective was to select and maintain littermate pairings from the F1 breeding colony and subsequent offspring generations, to establish a mouse colony that was homologous for the CCN2 floxed gene, and positive for the *COL1α2*-CreER^{T2}. The final objective was to assess the response to tamoxifen administration and confirm loss of function of the CCN2 gene.

3) Characterise the expression pattern of the *Col1α2*-CreER^{T2} using the B6CB; 129-(Cg)-Gt (ROSA) 26Sortm4 (ACTB-tdTomato,-EGFP) dual fluorescent reporter line.

The first objective in characterising this line was to confirm that the expression pattern during development was comparable to the LacZ staining reported by Bou-Gharios *et al.*, (1996) and Ponticos *et al.*, (2004) The second objective was to confirm the expression pattern at 7 days after tamoxifen administration. This timepoint would be used in subsequent research with the loss of function transgenic animals. The final objective was to identify the location of *COL1α2*-CreER^{T2} at 14 days after pulmonary injury with bleomycin. This treatment and timepoint would be used in subsequent research with loss of function transgenic animals and the bleomycin induced model of pulmonary fibrosis.

4.3 Establishing colonies double transgenic animals

4.3.1 Ubiquitous loss of function of CCN2 (ROSA-CCN2fl)

Founder female mice expressing the ROSA26CreER^{T2} B6CB;129-Gt(ROSA)26Sortm1(cre/ERT)Nat/Liv transgene were purchased from the Jaxson lab, Stock No: 008463 (B6.129-*Gt(ROSA)26Sor*$^{tm1(cre/ERT2)Tyj}$/J) (Figure 4.3, B), referred to as (ROSACreER^{T2}). These were bred with male animals containing the CCN2 floxed gene, B6; 129S-CTGFtm1.Alea (Figure 4.3, A). These mice were a generous gift from Dr. Andrew Leask. The generation of this floxed CCN2 transgene is described in Liu, Shi-Wen, Abraham, & Leask, (2011). F1 offspring were genotyped for the presence of CCN2 and CreER^{T2}, the methodology is described in methods section 2.4. Mice that were heterozygous for both transgenes were bred back onto founder parent animals to generate F2 offspring, typical genotyping results from F2 and subsequent generations are shown in Figure 4.4. The genotyping strategy for CCN2 was able to identify animals both heterozygous and homozygous for the CCN2 floxed gene (Figure 4.4, A, +/- heterozygous, +/+ homozygous) owing to the presence of a WT allele present in the genome. A primer pair was used that specific for sequence recognition sites outside the region of DNA recombination. The CreER^{T2} gene is not found endogenously in the mouse genome therefore it was possible to identify positive (+/-) or negative (WT) animals (Figure 4.4, B). A housekeeping gene (18s) was used to confirm presence of DNA to prevent false negatives (Figure 4.4, B) in ROSA26CreER^{T2} genotyping. Double transgenic animals that were genotyped as homozygous for CCN2 floxed and positive for ROSA26CreER^{T2} were selected and bred to maintain a colony of animals for use in CCN2 loss of function experiments. The in-house identifier for these mice was ROSA-CCN2fl, this nomenclature will be used for the remainder of these results.

4.3.2 Fibroblast specific loss of function of CCN2

Founder breeding pairs were established from transgenic mice containing the CCN2 floxed transgene (described above) that were bred with mice carrying the transgene for a Col1α2-CreER^{T2}, B6CB-Tg (Col1a2-17=1.5kbenh-350mp-CreErt2) 3.18/Liv, generated by the Bou-Gharios Lab. F1 offspring were genotyped for the presence of CCN2 and CreER^{T2}, the process is described in methods section 2.4. Mice that were heterozygous for both transgenes were bred back on founder parent animals to generate F2 offspring, typical genotyping results from F2 and subsequent generations is shown in Figure 4.4. The genotyping strategy for CCN2 floxed and CreER^{T2} was the same as described in the previous section. A further genotyping strategy was developed to confirm the presence of the *COL1α2* enhancer driving the CreER^{T2} (Figure 4.4, C). A primer pair was identified with the forward strand binding within the enhancer sequence, and the reverse strand binding within the CreER^{T2} gene. Double transgenic animals that were genotyped as homozygous for CCN2 floxed and positive for Col1α2-CreER^{T2} were selected and bred to maintain a colony of animals for use in CCN2 loss of function experiments. The in-house identifier for these mice was Col1α2-CCN2fl, this nomenclature will be used for the remainder of these results.

A

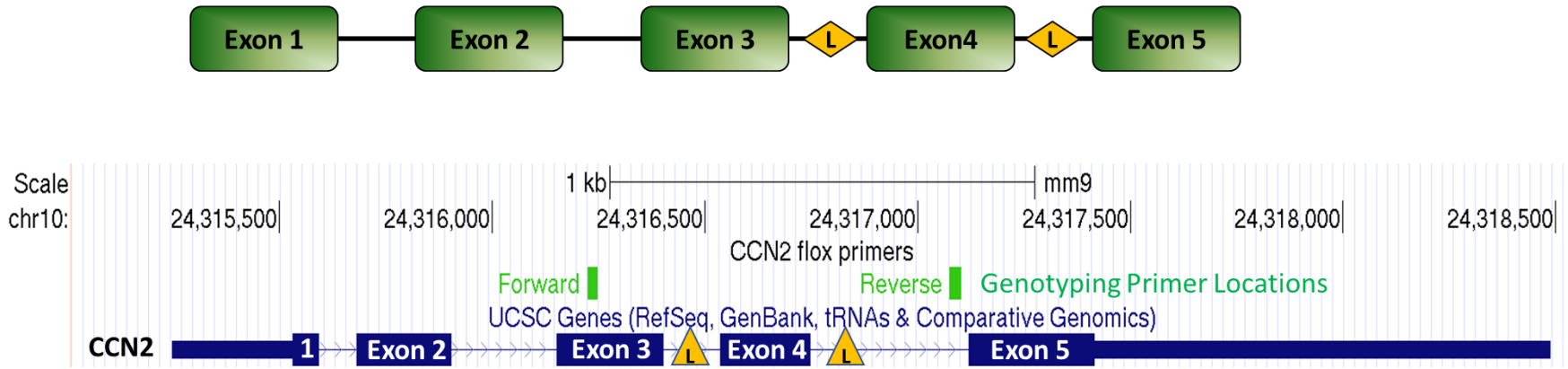
Exon 1
Exon 2
Exon 3
L
Exon4
L
Exon 5
Scale
chr10:
1 kb
mm9
24,315,500
24,316,000
24,316,500
24,317,000
24,317,500
24,318,000
24,318,500
CCN2 flox primers
Forward
Reverse
Genotyping Primer Locations
UCSC Genes (RefSeq, GenBank, tRNAs & Comparative Genomics)
CCN2
1
Exon 2
Exon 3
L
Exon 4
L
Exon 5

B

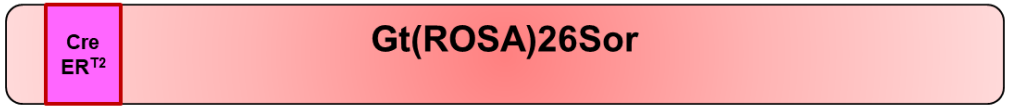
Cre
ER^{T2}
Gt(ROSA)26Sor

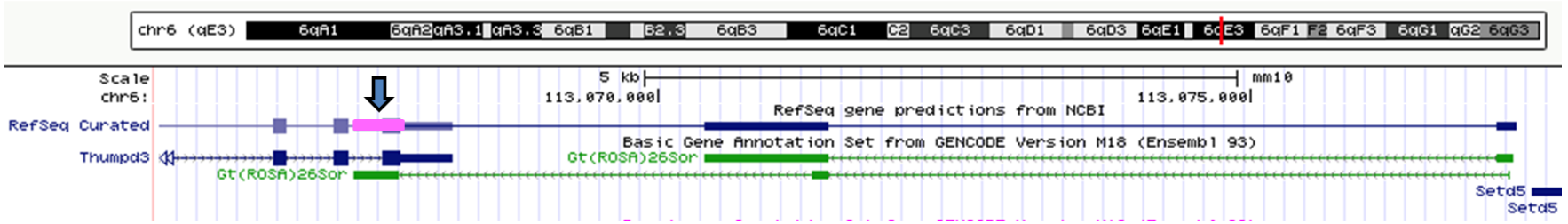
chr6 (qE3)
Scale
chr6:
5 kb
mm10
113,070,000
113,075,000
RefSeq gene predictions from NCBI
RefSeq Curated
Basic Gene Annotation Set from GENCODE Version M18 (Ensembl 93)
Thumpd3
Gt(ROSA)26Sor
Gt(ROSA)26Sor
Setd5
Setd5

C

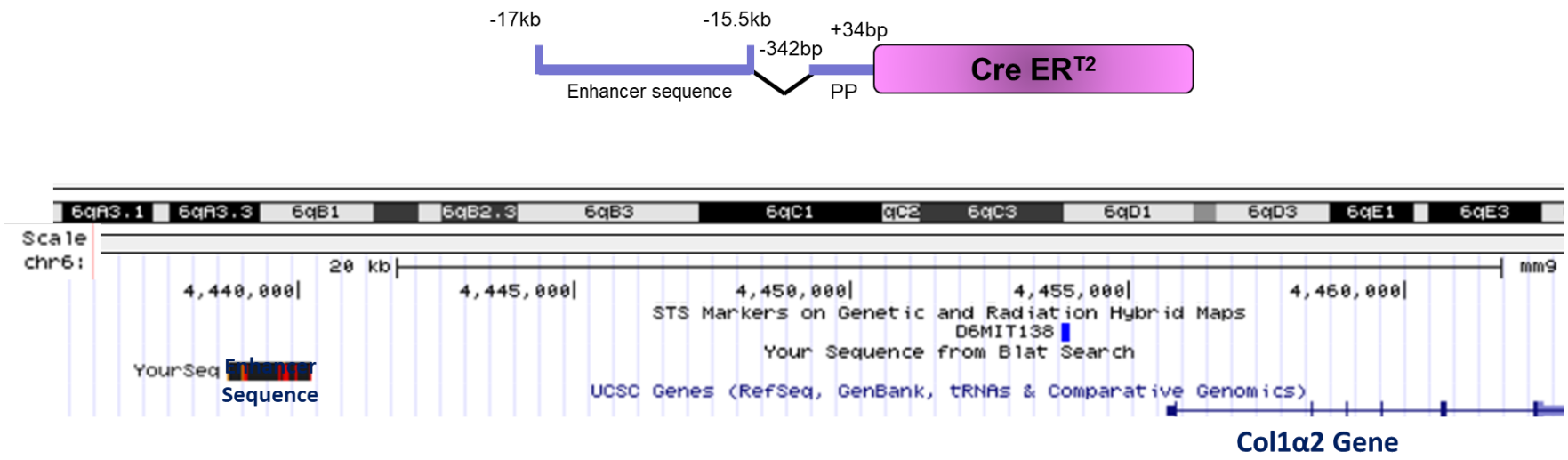

Figure 4.3. Location of genetic modifications using UCSC genome browser. A, CCN2 gene showing the localisation of loxP sites (L) for generation of CCN2 floxed transgene. B, Location of knock in of CreER^{T2} (pink & arrow) into intron 1 of Gt(ROSA)26Sor. C, Location of enhancer sequence driving fibroblast specific expression of CreER^{T2}.

A

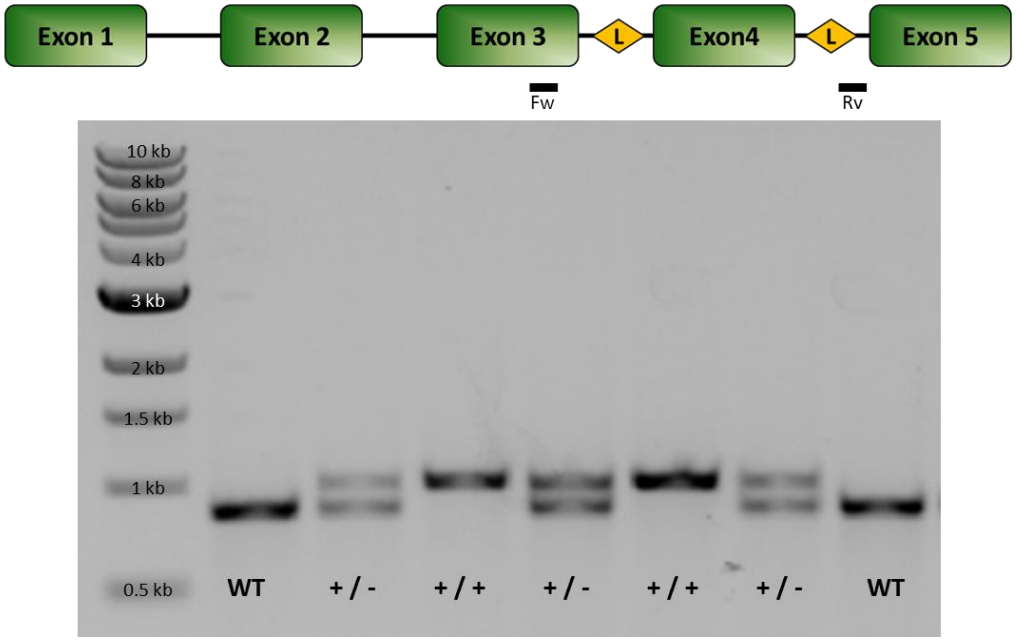
Exon 1
Exon 2
Exon 3
L
Exon4
L
Exon 5
Fw
Rv
10 kb
8 kb
6 kb
4 kb
3 kb
2 kb
1.5 kb
1 kb
0.5 kb
WT
+ / -
+ / +
+ / -
+ / +
+ / -
WT

B

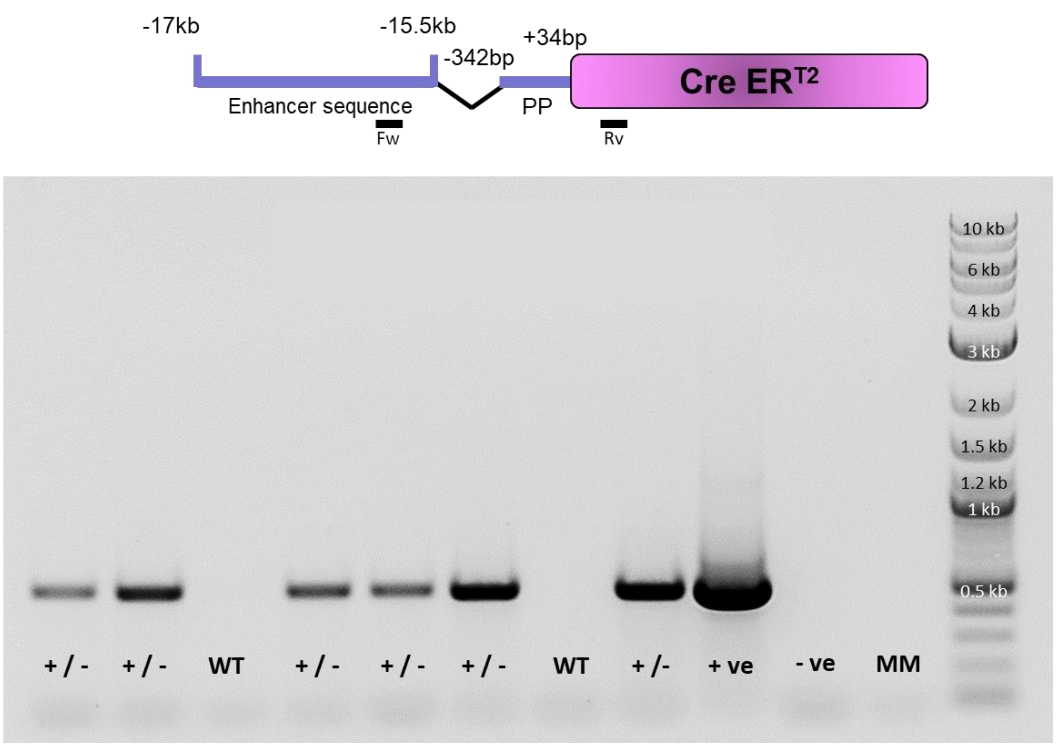
-17kb
-15.5kb
+34bp
-342bp
Cre ER^{T2}
Enhancer sequence
PP
Fw
Rv
10 kb
6 kb
4 kb
3 kb
2 kb
1.5 kb
1.2 kb
1 kb
0.5 kb
+ / -
+ / -
WT
+ / -
+ / -
+ / -
WT
+ /-
+ ve
- ve
MM

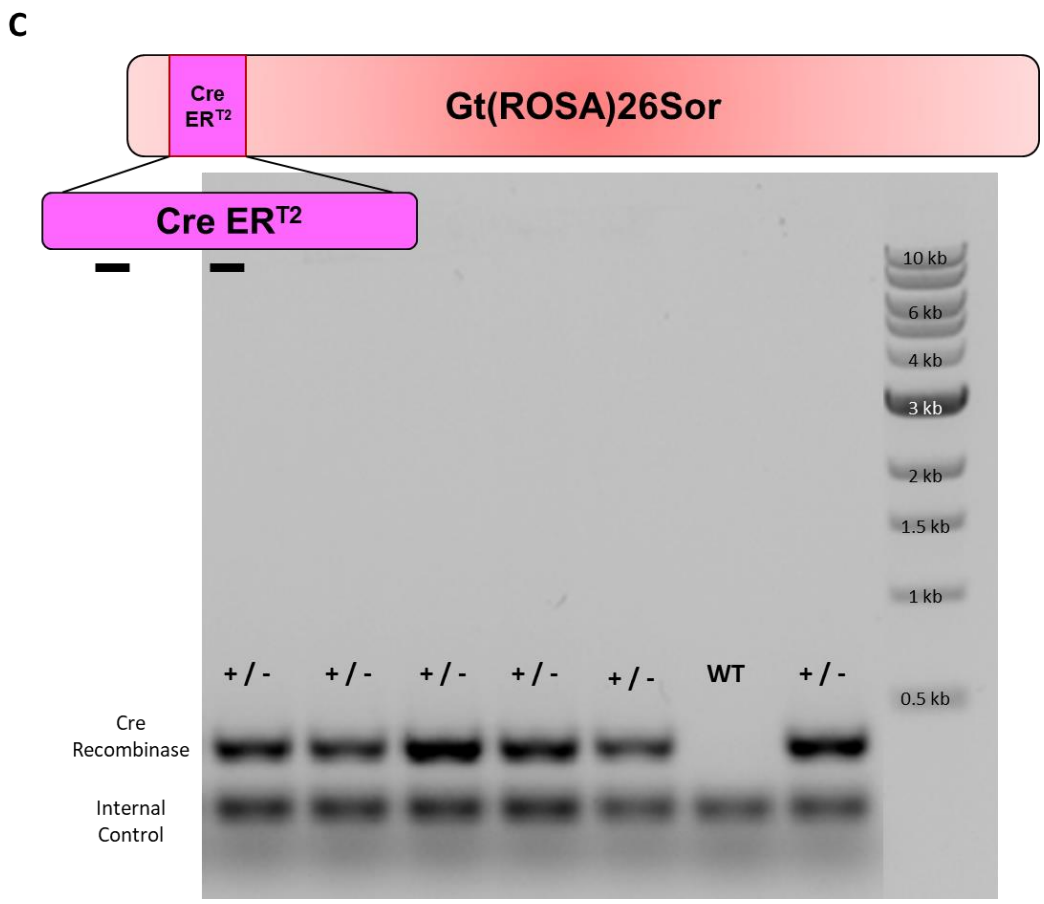

Figure 4.4. DNA genotyping gel results from ear punch biopsy of transgenic mice. Primer locations are identified on the representative images of the gene of interest by black lines with Fw and Rv indicating the location of the forward and reverse sequence respectively A, Genotyping results for CCN2 flox. WT denotes unmodified CCN2 allele, +/- indicates heterozygous expression and +/+ indicates homologous expression of CCN2 floxed transgene. B, genotyping strategy for the presence of CreER^{T2} used for both ubiquitous and fibroblast specific CCN2 knock out lines. WT indicates non-transgenic animals, +/- indicates CreERT2 transgene is present. C, Col1α2 enhancer specific genotyping strategy, WT indicates non-transgenic animals, +/- indicates the presence of the Col1α2- CreER^{T2}. Control wells containing Col1α2- CreER^{T2} plasmid (+ve), Acan- CreER^{T2} (-ve) and master mix (mm) were included as PCR controls. For A & B a 1 kb DNA ladder was loaded for reference (NEB, N3232L). For C, a 2-log ladder was loaded for reference (NEB, N0469S).

4.4 Characterising the lung morphology of double transgenic mouse colonies

Double transgenic animals from the ROSA-CCN2fl mouse colony and the Col1α2-CCN2fl colony were Sch1 at 6 weeks of age and processed for paraffin histology (methods section 2.8). It was necessary to determine that no morphological defects occurred due to the of the presence of the transgenes. Lung samples were stained with H & E and examined for key anatomical features defined as bronchioles, blood vessels and alveoli. No defects or morphological differences were observed (Figure 4.5).

It was determined that double transgenic animals displayed no difference in phenotype to that described for non-transgenic animals of the same background (mixed-C57B/6 x CBA). The next series of experiments aimed to confirm recombination of the CCN2 floxed gene occurred following administration of tamoxifen.

4.4.1 Response to tamoxifen in-vitro

Fibroblast cells were isolated and cultured from double transgenic animals from both the ROSA-CCN2fl and Col1α2-CCN2fl lines (described in methods 2.10). On day 7 of culture, media containing 100 nM of active tamoxifen metabolite 4-OHT was added to the cells. Cultures were left for 12 hours to allow recombination of the CCN2 floxed gene. Cells were imaged prior and post tamoxifen administration (Figure 4.6). Extensive cell death was observed in cultures from both ROSA-CCN2fl (Figure 4.6, A - D) and Col1α2-CCN2fl lines (Figure 4.6, E - G) 12 hours after tamoxifen administration. This response was seen across multiple culture and treatment experiments.

As it was not possible to identify recombination *in vitro* the next experiments focussed on identifying recombination *in vivo*.

4.4.1.1 DNA recombination assay

Offspring from the ROSA-CCN2fl and Col1α2-CCN2fl lines aged ≥ 6 weeks, that were not required for colony maintenance were administered three I.P. injections of 0.025 mg/g tamoxifen, (described in methods section 2.5.1). Animals were Sch1 at 7, 14 and 28 days after the final I.P. injection and DNA was isolated from a tail snip. A representative DNA genotyping gel result for the CCN2 floxed gene in animals from the ROSA-CCN2fl line, Sch1 at 7 days, is shown in Figure 4.7. Notation is as follows; WT = animals homologous for the unmodified CCN2 allele, +/- = animals heterozygous for the CCN2 floxed allele (1 copy of CCN2 floxed, 1

copy unmodified CCN2) and +/+ - animals are homozygous for the CCN2 floxed allele. CreER^{T2} negative animals (Figure 4.7, A-D) showed no recombination of the CCN2 allele, neither did WT CCN2 animals that contained CreER^{T2} (Figure 4.7, H). Heterozygous samples (Figure 4.7, F, J & K) showed recombination of the CCN2 floxed allele, but not the CCN2 WT allele. Homozygous samples (Figure 4.7, E & I) showed complete recombination of both alleles.

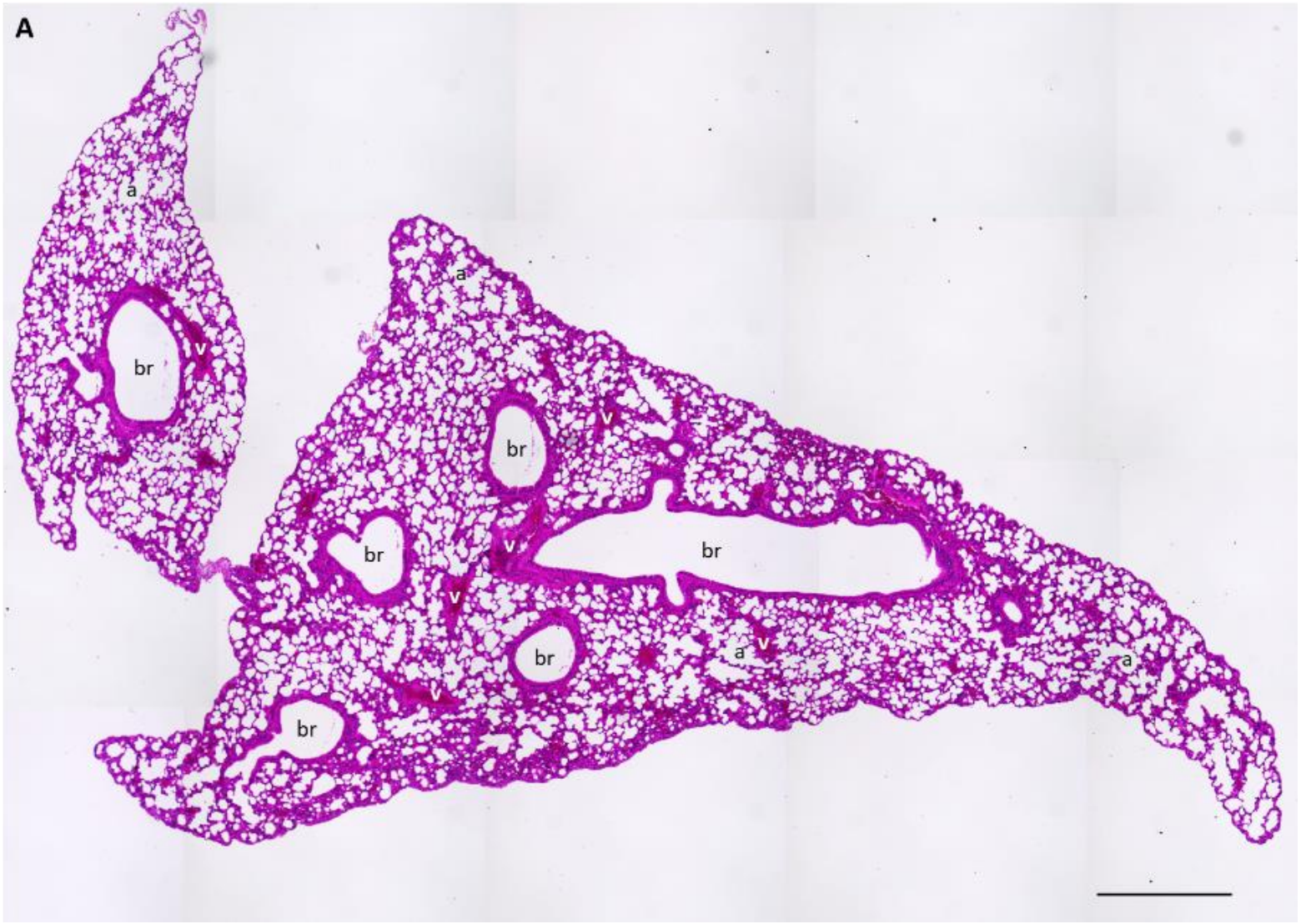
A
a
br
v
a
br
v
br
br
v
v
br
a
v
a
br

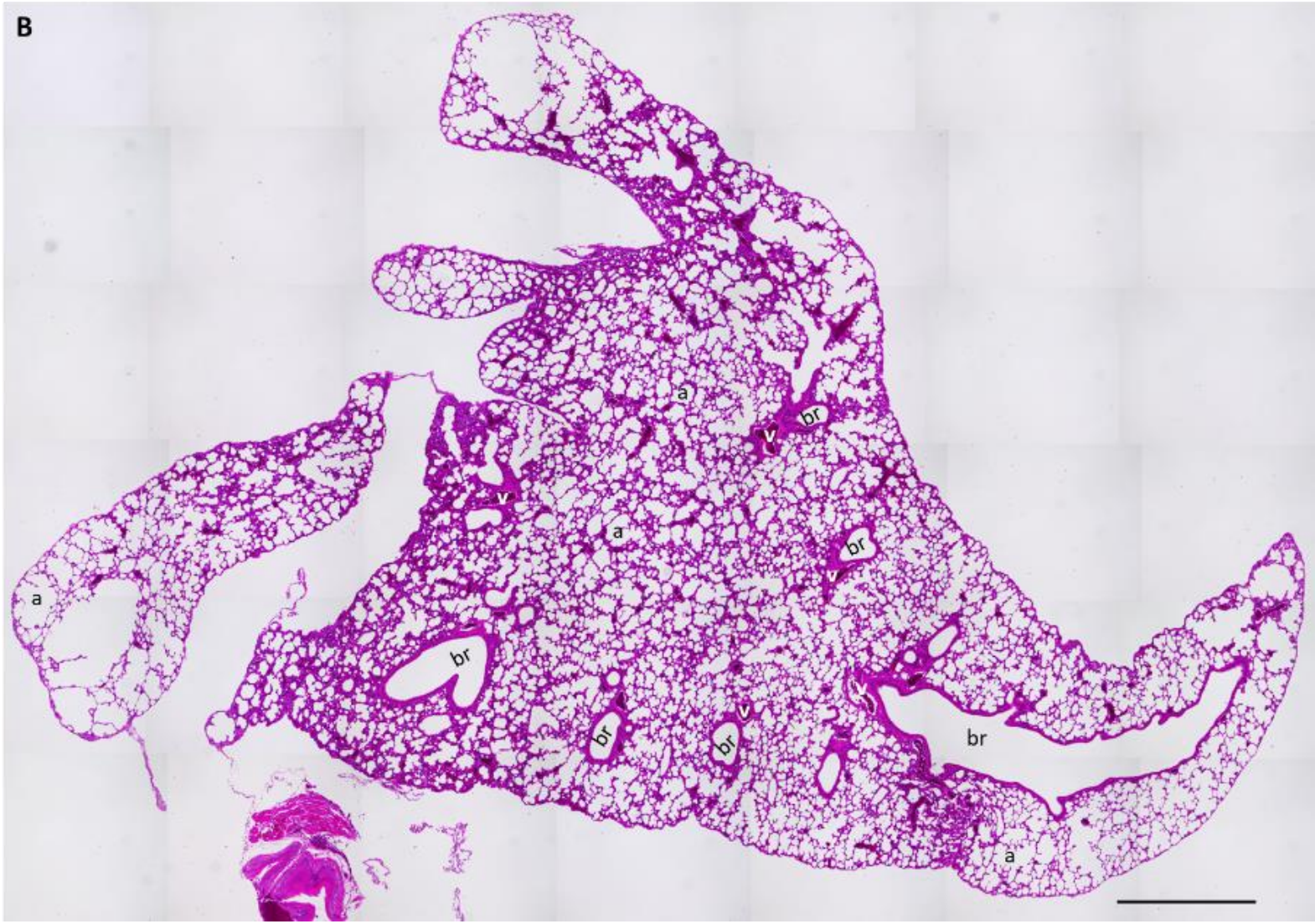
B
a
br
v
a
v
br
a
v
br
br
br
v
v
br
a

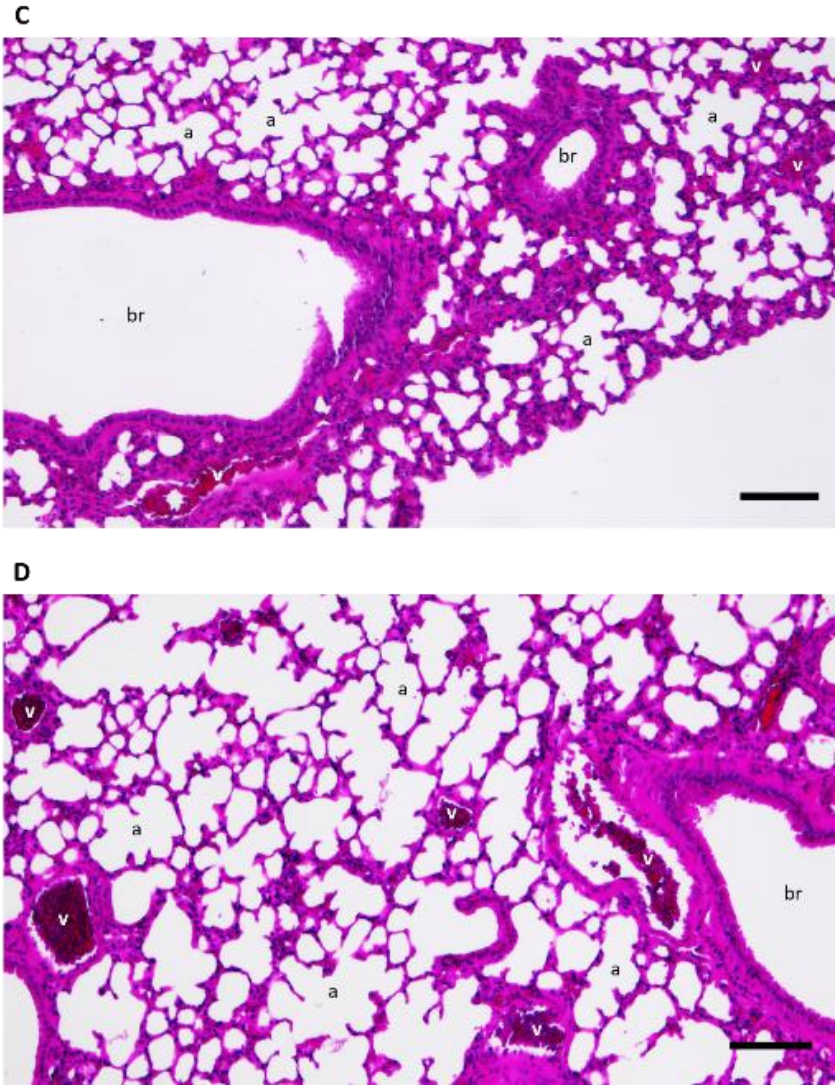

Figure 4.5. H & E stained paraffin embedded lung samples from double transgenic mice. Individual lobes were isolated after Sch1 by anaesthetic overdose, processed for wax histology and stained with H & E. Anatomical features are identified as follows: a- alveoli, br- bronchioles, v- blood vessels. A, Stitched image of lung lobe isolated from double transgenic animal homozygous for CCN2 floxed, and positive for Col1α2-CreERT2. B, Stitched image of lung lobe isolated from double transgenic animal homozygous for CCN2 floxed, and positive for ROSA-CreERT2. C & D, individual images taken from A & B respectively. All images were taken at 10x magnification. Scale bars in A & B represent 1 mm. Scale bars in C & D represent 200 µm.

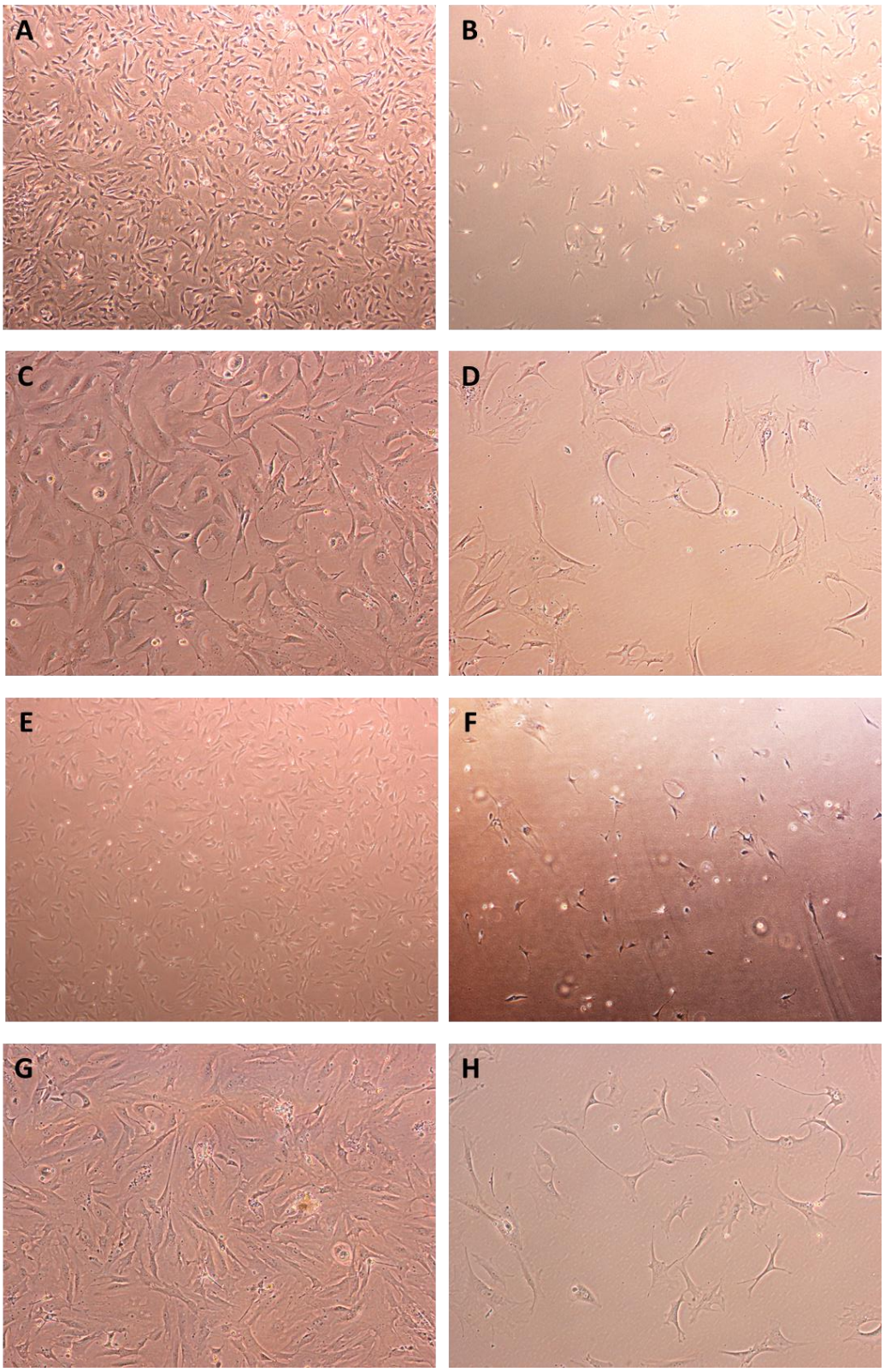

Figure 4.6. Primary fibroblast cultures isolated from double transgenic mice. Fibroblasts were isolated from double transgenic animals, homozygous for CCN2 floxed, and positive for Col1α2-CreERT2 (A - D) or ROSA- CreERT2 (E - H). A & E, 10x magnification of cells prior to Tx administration. C & G, show the same cells prior to Tx administration at 20x magnification. B & F, 10x magnification of cells 12 hr after Tx administration. D & H, show the same cell cultures 12 hr after Tx administration at 20x magnification.

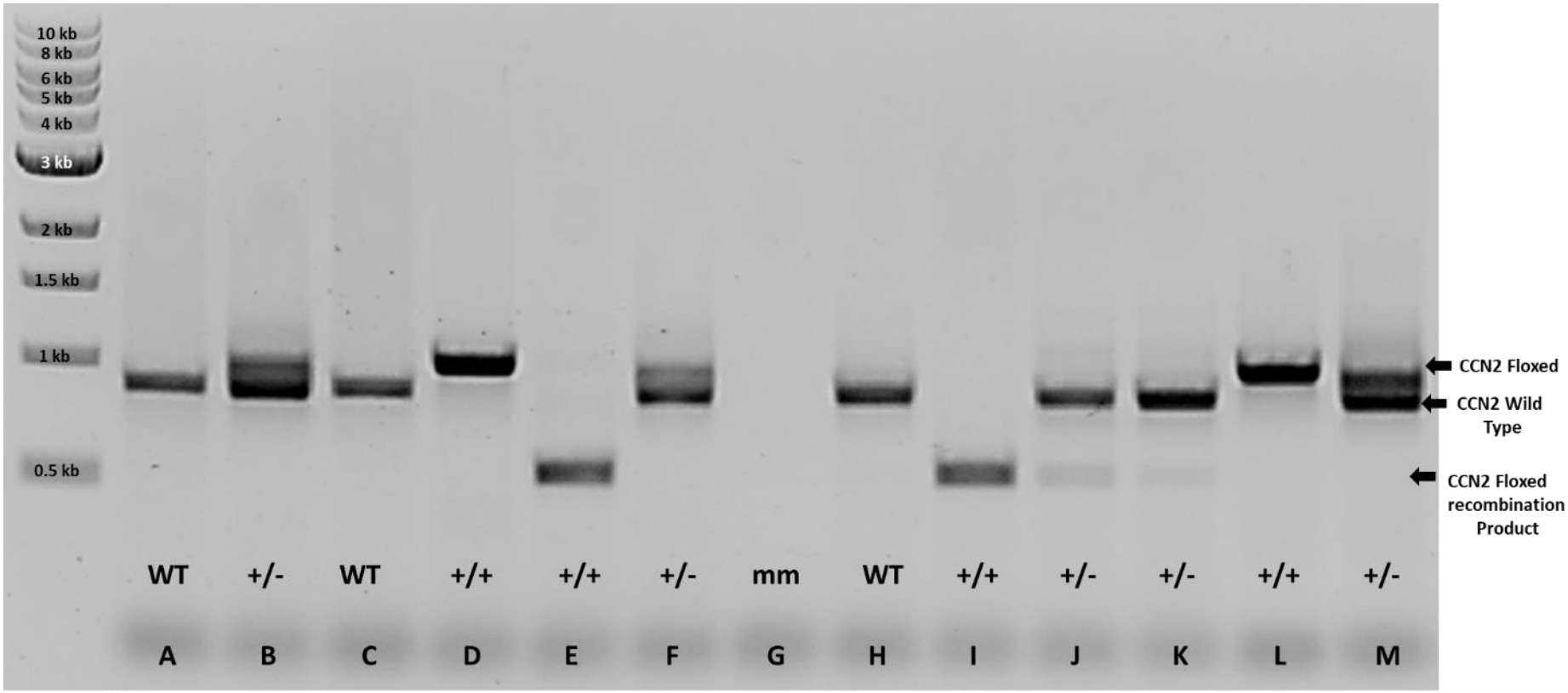

Figure 4.7. DNA gel result from in-vivo recombination assay. Tail snips were taken from mice 7 days after final dose of tamoxifen was administered. DNA was isolated and the CCN2 floxed gene was analysed for recombination. Wild type (WT) mice contain two copies of the non-floxed CCN2 gene, +/- indicates a heterozygote transgenic mouse, and +/+ indicates a homozygous transgenic mouse. A sample of master mix (mm) containing ddH_2O in place of DNA was used to confirm purity of the master mix solution. Animals A - D are Negative for $CreER^{T2}$ and samples L & M are untreated control samples. A 1 kb DNA ladder (NEB, N3232L) was loaded as a reference.

4.4.2 RT-qPCR analysis of CCN2 expression

Lung samples were isolated and snap frozen for qPCR analysis of CCN2 gene expression. Animals from the ROSA-CCN2fl and Col1α2-CCN2fl lines were homologous for the CCN2 floxed gene and positive for their specific $CreER^{T2}$. Tamoxifen was administered as described in methods section 2.5.1. Animals were Sch1 using overdose of Pentobarbital at 7, 14 and 28 days after the final I.P. injection and the lungs snap frozen in liquid nitrogen. RNA was extracted following the protocol in methods section 2.7.3 and analysed by ΔΔCt for CCN2 transcript levels (Figure 4.8).

4.4.2.1 Fibroblast specific knock out of CCN2

Figure 4.8, A – C presents the ΔΔCt results for the fibroblast specific knock out of CCN2 (Col1α2-CCN2fl colony). When gender was not accounted for, a significant ($p > 0.0001$) 2.5-fold increase in CCN2 transcript abundance was observed at 7 days (Figure 4.8, A), followed by reductions in CCN2 transcript abundance by 0.4 and 0.6-fold at 14 and 28 days respectively (Figure 4.8, B & C). Analysis of gender specific responses demonstrated different patterns of response between males and females. Males (Figure 4.8, B) demonstrated a decreasing trend of levels of CCN2 transcript abundance, with a 0.15-fold reduction in transcript level at day 7, a 0.40-fold decrease at day 14 and a 0.60 decrease by day 28. Females (Figure 4.8, C) demonstrated an initial peak in transcript abundance, with a 3-fold increase at day 7, followed by a 0.40-fold decrease by day 14, in line with the results seen in male animals (Figure 4.8, B).

4.4.2.2 Ubiquitous knock out of CCN2

Figure 4.8, D – F presents the ΔΔCt results for the ubiquitous knock out of CCN2 (ROSA-CCN2fl colony). No transcript was identified in the sample at day 14 (Figure 4.8, D). No difference was seen between genders (Figure 4.8, E & F).

4.4.3 Immunohistochemical analysis of CCN2 expression

To confirm the alterations in CCN2 transcription translated to a reduction in protein expression, the next experiment used antibody staining of paraffin embedded lung lobes isolated from the tamoxifen treated animals 14 days after the last dose of tamoxifen was received. Sections of lungs isolated from Col1α2-CCN2fl and ROSA-CCN2fl lines were compared to an untreated control lung for localisation and prevalence of CCN2 (Figure 4.9).

All samples were prepared and stained by Mr. Lorenzo Ramos-Mucci, following the protocol in methods section 2.9. Images of stained slides were taken using a Zeiss LSM 800 confocal microscope at 10x magnification.

In control lung, antibody staining of CCN2 was observed in the bronchioles, and in cells surrounding the alveoli, identified by black arrows (Figure 4.9, A, D & G). A reduction of staining in the bronchioles was seen in lungs isolated from mice where CCN2 was targeted in a fibroblast specific manner (Figure 4.9, B, E & H). Staining in cells surrounding alveoli was seen with a similar expression to control. In lungs isolated from mice where CCN2 was targeted ubiquitously, no staining of CCN2 was observed (Figure 4.9, C, F & I).

From these results it was concluded that I.P. injection of tamoxifen was sufficient to induce recombination of the CCN2 floxed gene *in vivo*. The recombination was shown to reduce CCN2 expression both at the transcriptional level and the protein level. The efficiency of this reduction was dependent on the $CreER^{T2}$ specificity. Whereby reduced expression levels of CCN2 were demonstrated in a fibroblast specific recombination, and complete ablation of CCN2 expression in ubiquitous recombination.

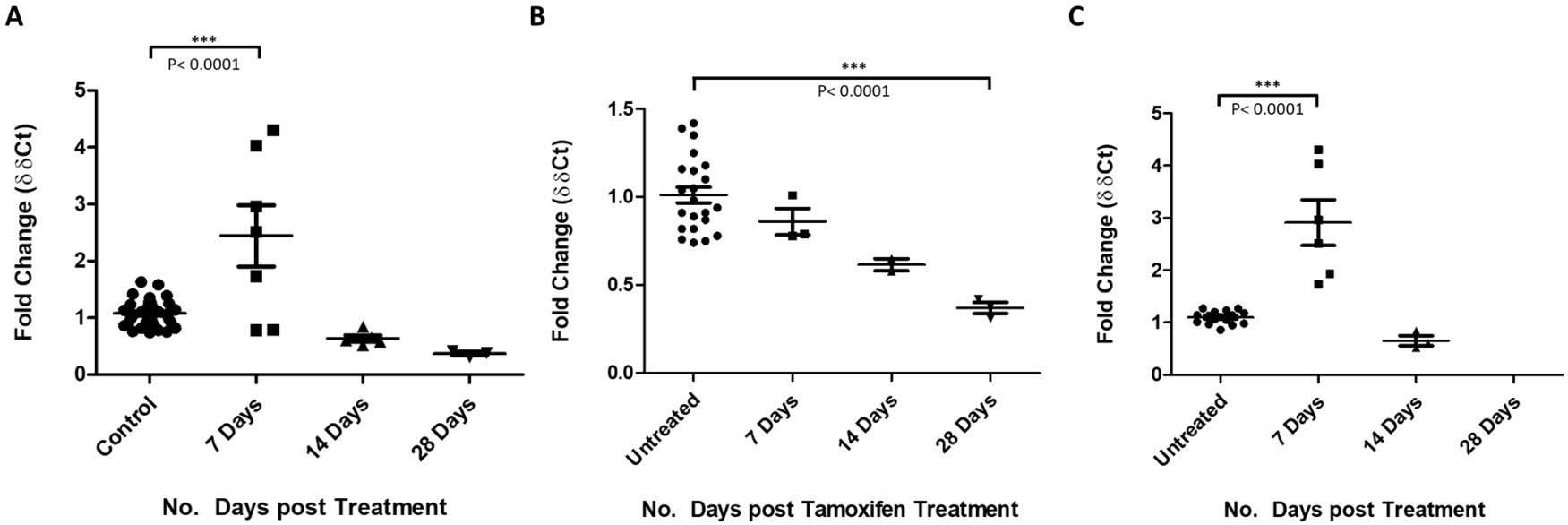
A
***
P< 0.0001
Fold Change (δδCt)
5
4
3
2
1
0
Control
7 Days
14 Days
28 Days
No. Days post Treatment
B
***
P< 0.0001
Fold Change (δδCt)
1.5
1.0
0.5
0.0
Untreated
7 Days
14 Days
28 Days
No. Days post Tamoxifen Treatment
C
***
P< 0.0001
Fold Change (δδCt)
5
4
3
2
1
0
Untreated
7 Days
14 Days
28 Days
No. Days post Treatment

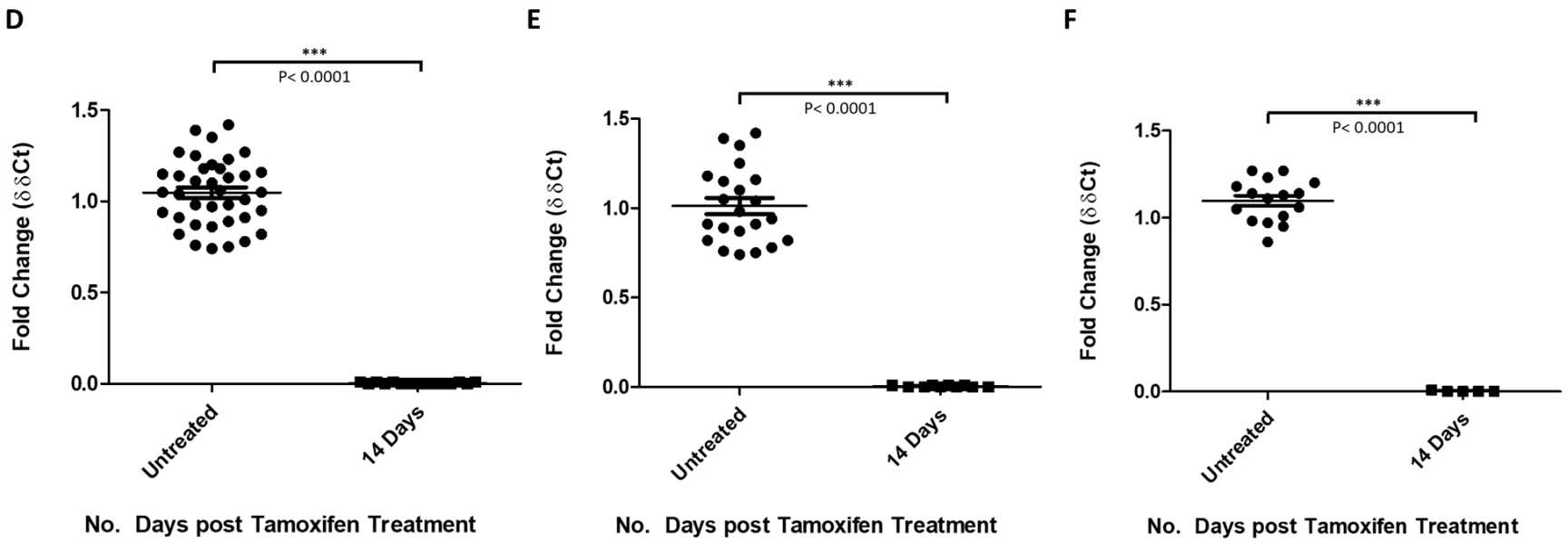

Figure 4.8. RT-qPCR analysis of CCN2 gene. ΔΔCt analysis of CCN2 mRNA compared to 18s housekeeping gene. Samples were analysed from double transgenic animals homozygous for CCN2 floxed gene and positive for fibroblast specific Col1α2-CreER^{T2} (A - C) or ubiquitously expressed ROSA26CreER^{T2} (D - F), following tamoxifen treatment. RNA was extracted from whole lungs from male and female animals culled at 14 days after final tamoxifen injection. Transcript abundance was normalised to untreated, double transgenic littermates. Statistical significance was determined using a one-way ANOVA, and Tukey's post hoc test. Significance and associated p-values are indicated by (*). A & D, ΔΔCt analysis of CCN2 mRNA carried out for all mice. B & E, ΔΔCt analysis of CCN2 mRNA in male mice only. C & F, ΔΔCt analysis of CCN2 mRNA in female mice only.

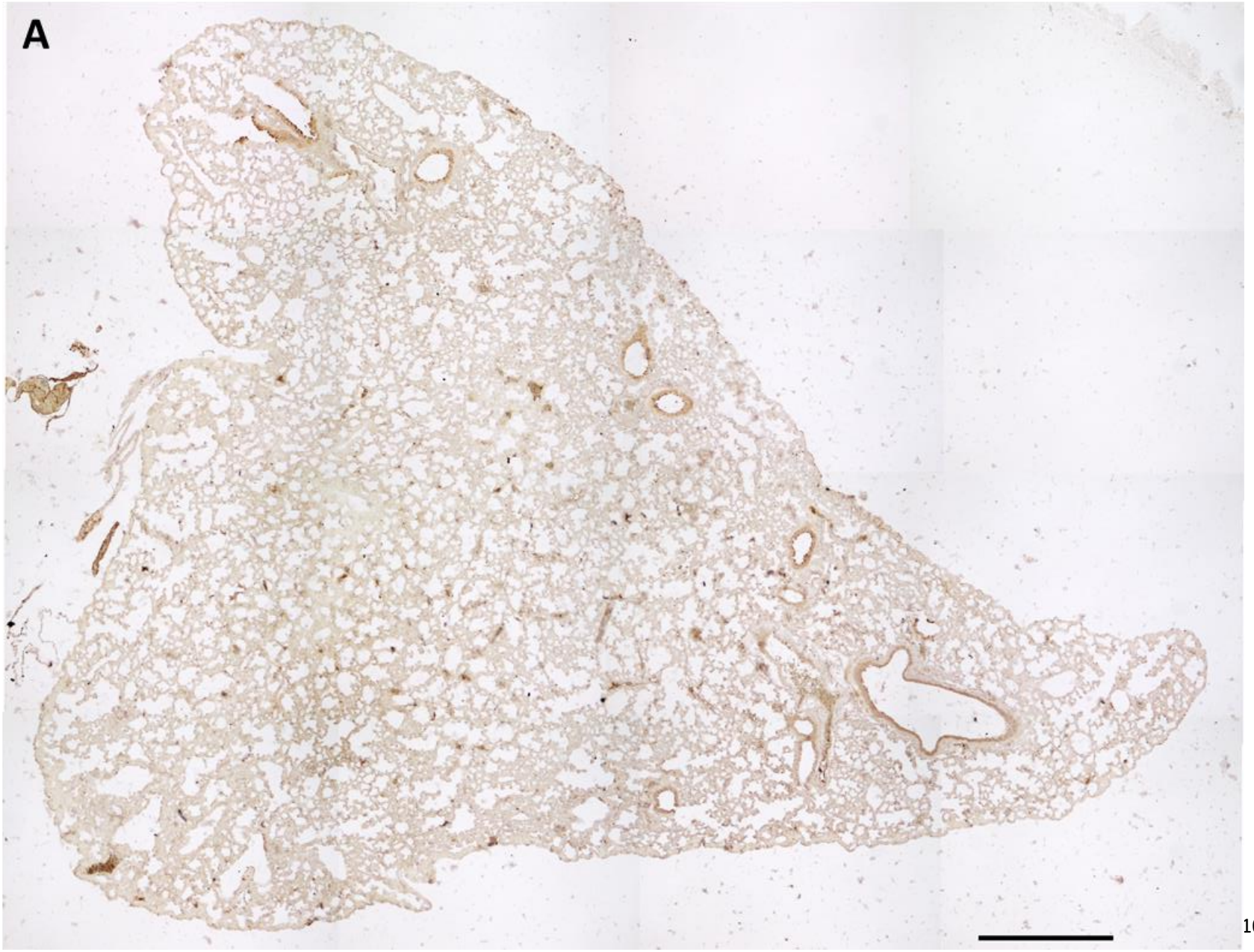
A

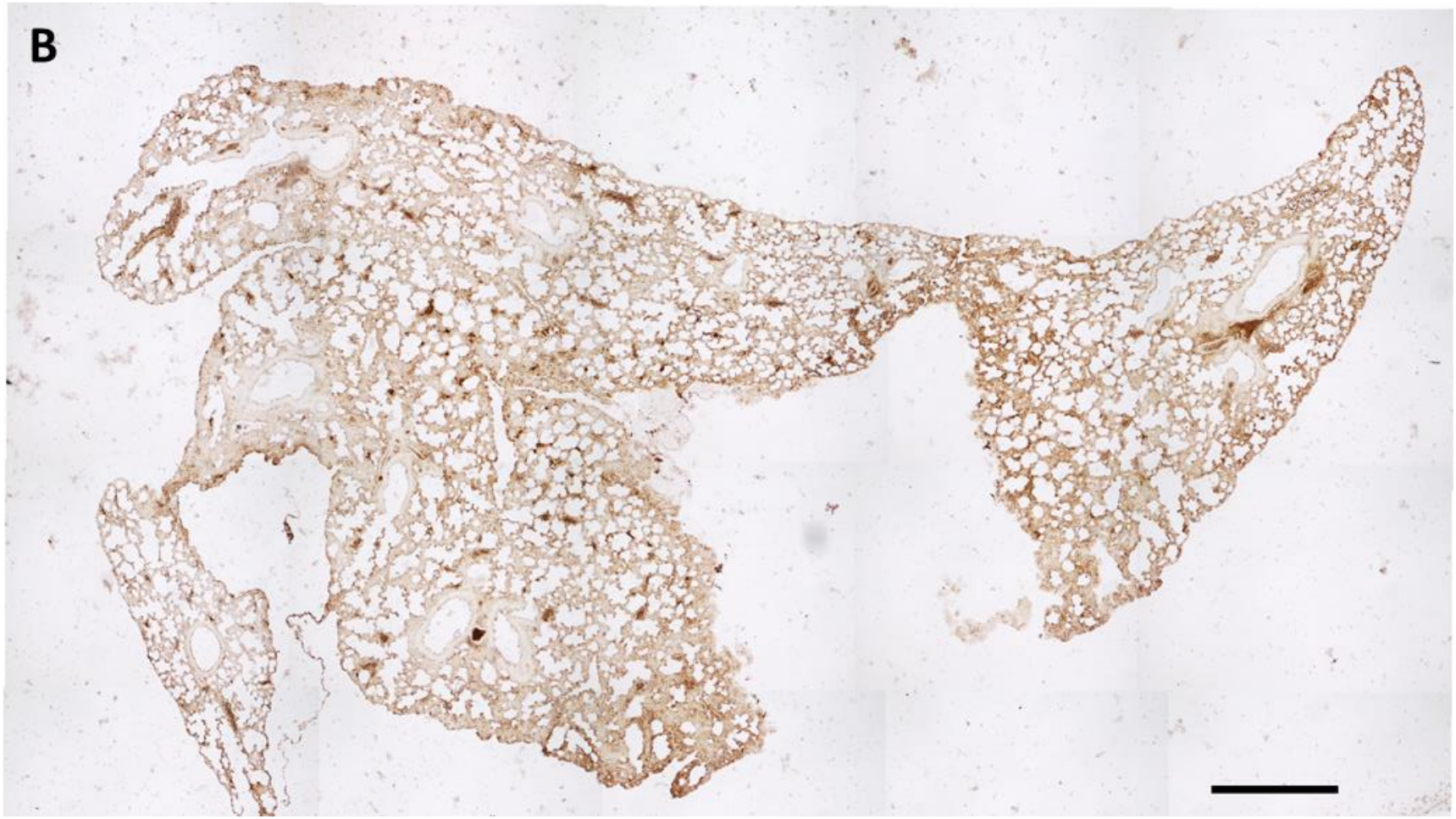
B

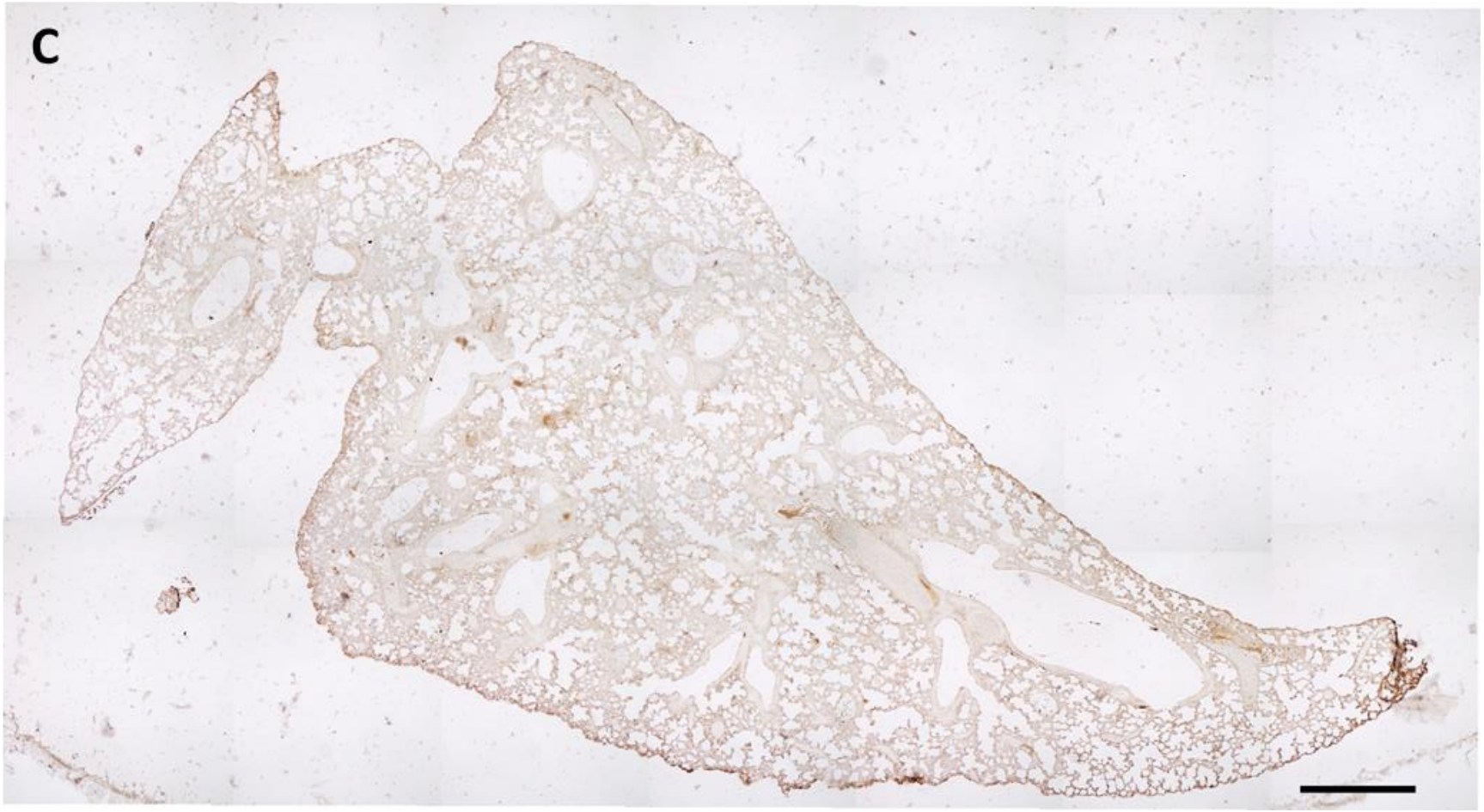
C

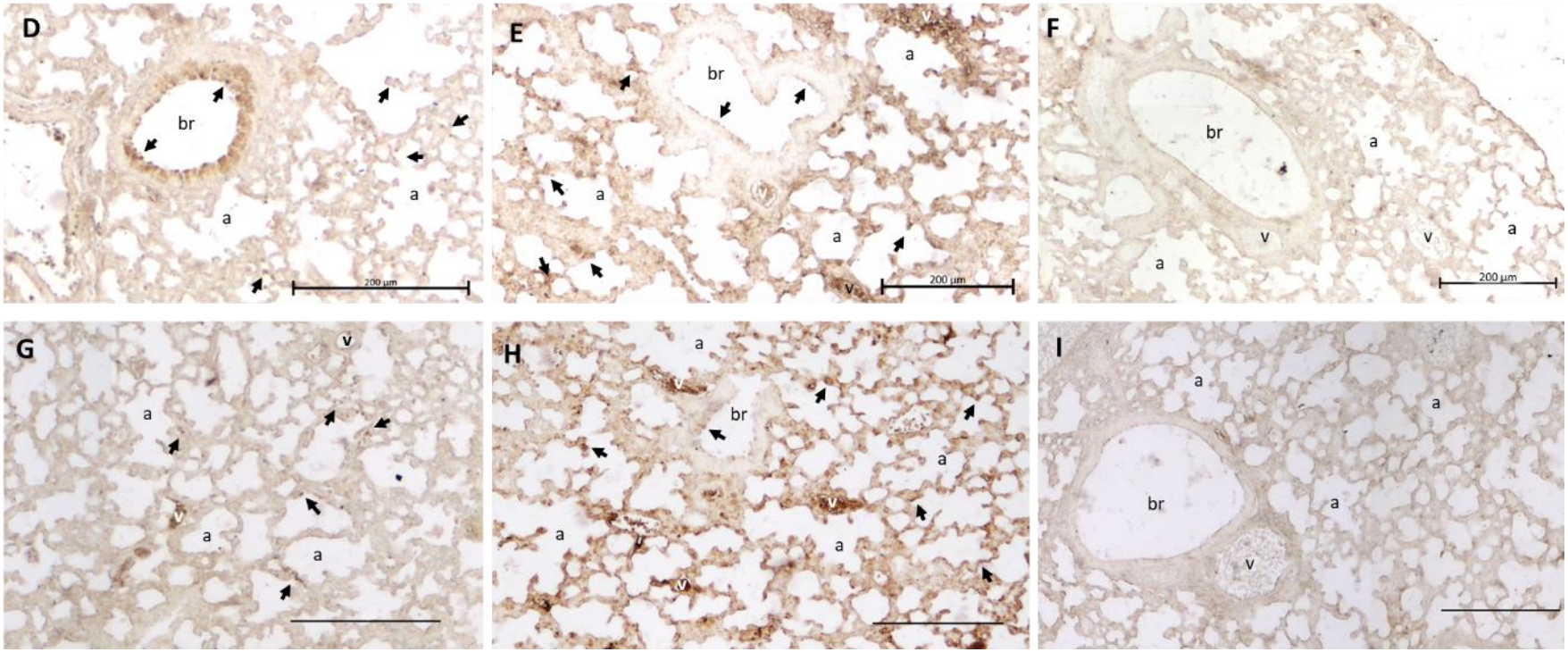

Figure 4.9. Antibody staining for CCN2 in lungs using Anti-CCN2 Antibody (ab6992). Lungs were isolated from double transgenic animals, homozygous for CCN2 floxed, and positive for Col1α2-CreERT2 (B, E & H) or ROSA- CreERT2 (C, F & I) 14 days after completion of tamoxifen dosing. Lungs from untreated mice were included for normal expression profile of CCN2 (A, D & G). Anatomical features are identified as follows: a- alveoli, br- bronchioles, v- blood vessels. Regions of antibody staining are indicated by black arrows. Scale bars represent 200 µm

4.5 Characterising the expression pattern of the Col1α2-CreER^{T2}

Having established that tamoxifen dosing *in vivo* was sufficient to drive gene recombination, the next stage of the research focused on characterising the expression pattern of the Col1α2-CreER^{T2}. Research in this section was submitted as part of published manuscript.

"Characterisation of Mesenchymal-Fibroblast Cells using the *Col1α2* Promoter/Enhancer"

Li, I. M. H., Horwell, A. L., Chu, G., de Crombrugghe, B., & Bou-Gharios, G. (2017). In Methods in Molecular Biology (Vol. 1627, pp. 139–161). https://doi.org/10.1007/978-1-4939-7113-8_10

4.5.1 Establishing a colony of inducible, fluorescent dual-reporter, double transgenic mice

Female mice containing the reporter construct B6CB; 129-(Cg)-Gt (ROSA) 26Sortm4 (ACTB-tdTomato,-EGFP) Luo/Liv, (mTmG) described by Muzumdar et al., (2007), were purchased from Jackson Laboratories (007676). These were bred with male mice containing the Col1α2 driven CreER^{T2} B6CB-Tg (Col1a2-17=1.5kbenh-350mp-CreErt2)3.18/Liv. F1 offspring were genotyped for mTmG construct following the protocol in methods 2.4 and Col1α2-CreER^{T2} as described previously in this chapter. Heterozygous, double transgenic offspring were bred onto founder parents and subsequent crossing of littermate mice was used to establish and maintain a colony of double transgenic mice homozygous for the mTmG reporter gene, and positive for Col1α2-CreER^{T2}.

These animals were used for lineage tracing experiments to determine the expression pattern of the Col1α2-CreER^{T2} during development and during adulthood.

4.5.2 Col1α2-CreER^{T2} expression during embryonic development

A single I.P. injection of 3 mg tamoxifen was administered to pregnant female mice on embryonic day 11.5 or 13.5. Females were culled 2 days after tamoxifen administration by cervical dislocation and embryos at days E13.5 and E15.5 were collected and processed for cryogenic histology (described in methods 2.8.1). Control embryos were also collected at embryonic days E13.5 and E15.5 from females that had not been injected with tamoxifen.

Sections were imaged using a Zeiss Axio Observer apotome microscope and Axio Cam MR R3 camera. A wavelength of 610 nm was used for imaging of tdTomato and 519 nm for EGFP. Images were viewed using ZEN Blue microscopy software.

Representative images are shown in Figure 4.10, taken from control embryos collected at developmental days E13.5 (Figure 4.10, A & B), and E15.5 (Figure 4.10, C & D). Fluorescent imaging of both developmental stages (Figure 4.10, A, E13.5 & C, E15.5) showed expression of tdTomato only. Sections were examined at a higher magnification to ensure no EGFP signal was present. Representative images taken at 20x magnification from control embryo at E15.5 are shown in Figure 4.11. No EGFP signal was identified in control embryos at either timepoint. After fluorescent imaging was complete slides were stained with H & E and imaged using a Zeiss LSM 800 confocal microscope. H & E staining confirmed tdTomato expression was synonymous with the presence of tissue (Figure 4.10, B & D).

Figure 4.12 shows a series of representative sections taken from a whole embryo, which was administered with tamoxifen at developmental day E11.5 and collected at E13.5. Figure 4.13 shows a series of representative sections taken from a whole embryo that was administered tamoxifen at developmental day E13.5 and collected at E15.5. Examination of fluorescent images confirmed activation of the $CreER^{T2}$ as EGFP signal was observed at both developmental stages (Figure 4.12, (A-E) & Figure 4.13 (A-E)). After fluorescent imaging was completed, slides were stained with H&E and imaged using a Zeiss LSM 800 confocal microscope. H&E staining confirmed tdTomato expression was synonymous with the presence of tissue (Figure 4.12, (E - H) & Figure 4.13, (E-H)).

To characterise the expression pattern at the cellular level, sections from embryos at both E13.5 and 15.5 were imaged at 20x magnification. Representative images from lung, liver and ribs are shown in Figure 4.14. At E13.5, EGFP signal was identified in the lung (Figure 4.14, A) in cartilage tissue surrounding the trachea and the cells immediately surrounding the bronchioles. Examination of EGFP signal in the lung at E15.5 (Figure 4.14, D) revealed signal localised to individual cells surrounding blood vessels and in individual cells located around the epithelial lining of the alveoli. In the liver at both E13.5 and E15.5 tdTomato signal was identified in cells surrounding the central vein and the surrounding vascular network branching from this. EGFP signal was localised to cells within the hepatocyte population (Figure 4.14, B & E). EGFP expression was identified in some chondrocytes present in the ribs for both E13.5 and E15.5 (Figure 4.14).

4.5.3 Col1α2-CreER^{T2} expression in adult mice

Three I.P. injections of 0.025 mg/g tamoxifen were administered to mice aged ≥6 weeks following the protocol outlined in methods section 2.5.1. Col1α2-CreER^{T2} expression was examined 7 days after the final tamoxifen injection and 3 months after tamoxifen expression. Animals were Sch1 by cervical dislocation and tissues were processed for cryogenic histology (described in methods 2.8.1). Littermate animals that were not administered tamoxifen were Sch1 at the same time as the tamoxifen treated counterparts and tissues processed for cryogenic histology for baseline control expression of the mT/mG reporter construct.

Figure 4.15 shows representative fluorescence images taken from skin and lung samples, 7 days after tamoxifen administration (A, B, D & E) compared to skin and lung taken from untreated littermate control animals (C & E). Untreated lung and skin (Figure 4.15, C & E) demonstrated expression of tdTomato only. Expression of EGFP in skin was localised to the dermis region (Figure 4.15, A & B), hair follicle and epithelium retained tdTomato expression. In lung (Figure 4.15, D & E), EGFP expression was localised to individual cells surrounding the vessels and alveoli.

Examination of fluorescence in tissues 3 months after the final injection of tamoxifen showed EGFP expression was present in skin, kidney, liver, heart, spleen, lung and eye (Figure 4.16, A, C - H). Expression patterns in skin and lung (Figure 4.16, A & G) were identical to those observed at 7 days (Figure 4.16, A & B, D & E).

4.5.4 Col1α2-CreER^{T2} expression in lungs of adult mice treated with bleomycin

Three I.P. injections of 0.025 mg/g tamoxifen were administered to mice aged ≥6 weeks following the protocol outlined in methods section 2.5.1. 7 days after the final tamoxifen injection, mice were administered a single dose of 0.375 ng/g OA bleomycin. Col1α2-CreER^{T2} expression was examined in the lung 14 days after insult with bleomycin. A littermate control was treated with tamoxifen but not bleomycin for tissue and expression comparison. Animals were Sch1 by overdose of pentobarbital and lungs were processed for cryogenic histology (described in methods 2.8.1). Lungs not treated with bleomycin (Figure 4.17, A & B) demonstrated EGFP expression in cells within the bronchioles, surrounding the vessels, with in single cells surrounding the alveoli also showing EGFP expression. In bleomycin treated lungs (Figure 4.17, C - F), increased regions of tdTomato expressing tissue were seen, revealing a loss of usual morphology. Regions of EGFP signalling could be identified within

the tdTomato signal (Figure 4.17, C & D). Individual EGFP expressing cells were visualised surrounding vessels and lining alveoli in Figure 4.17, (E & F).

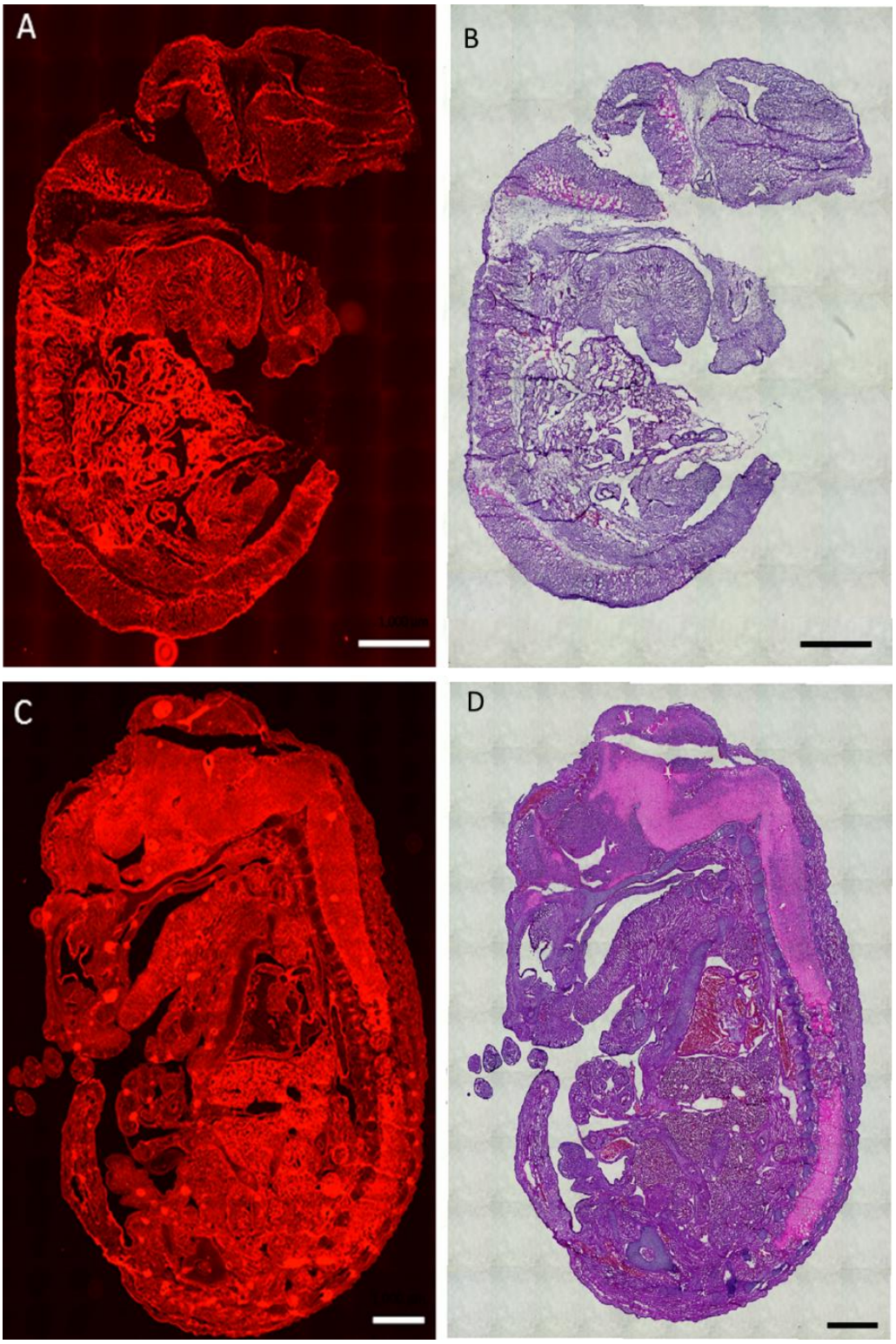

Figure 4.10. Fluorescence and H & E stained sections from double transgenic mice containing the mT/mG reporter construct (Muzumdar *et al.*, 2007) *and Col1α2-CreER^{T2} gene. Embryos were collected at embryonic days E13.5 (A & B) and E15.5 (C & D). Fluorescence images (A & C) were imaged using a Zeiss Axio Observer apotome microscope and Axio Cam MR R3 camera. FITC (519 nm) and mCherry (610 nm) fluorescence channels were used to identify tdTomato and EGFP expression. B & D, H & E staining of the same section. No tamoxifen was administered to the mice, therefore no cre activity (EGFP expression) is seen. Images were taken at 10x magnification. Scale bars represent 1 mm.*

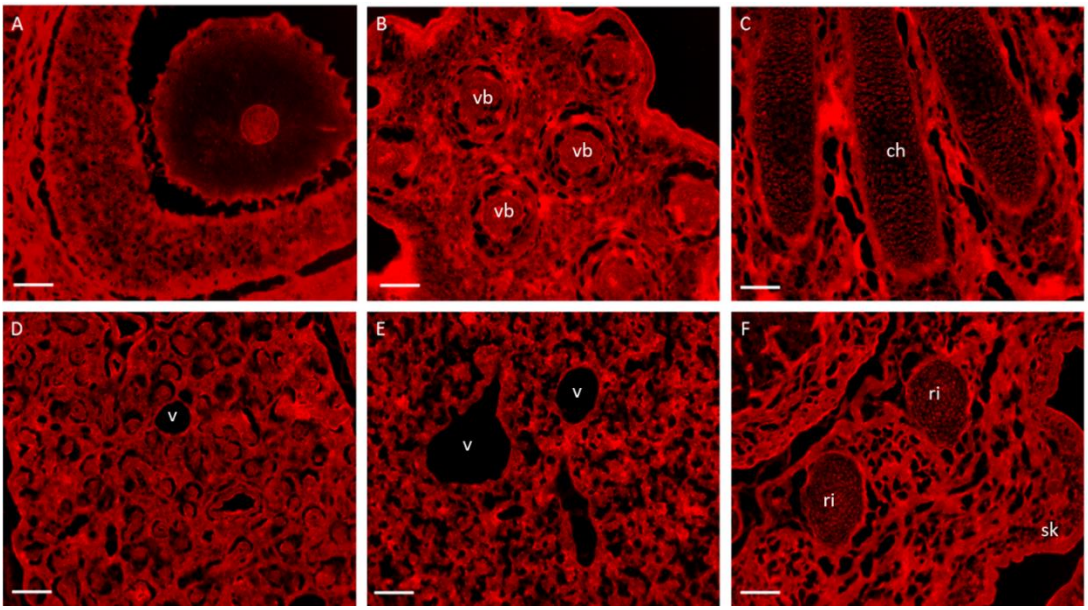

Figure 4.11. Fluorescence images of control E15.5 double transgenic mice. Fluorescence images of eye (A), snout (B), hind paw (C), kidney (D), liver (E) and back (F) were taken at 20x magnification from untreated double transgenic mice containing the mT/mG reporter construct (Muzumdar *et al.*, 2007) *and Col1α2-CreER^{T2} gene , at embryonic developmental stage E15.5. No tamoxifen was administered to the mice, therefore no cre activity (EGFP expression) is seen. Tissues were imaged using a Zeiss Axio Observer apotome microscope and Axio Cam MR R3 camera. FITC (519 nm) and mCherry (610 nm) fluorescence channels were used to identify tdTomato and EGFP expression. Anatomical features are noted as: vb- vibrissae, ch- chondrocytes, v- blood vessels, ri- ribs, sk- skin. Scale bars represent 200 µm.*

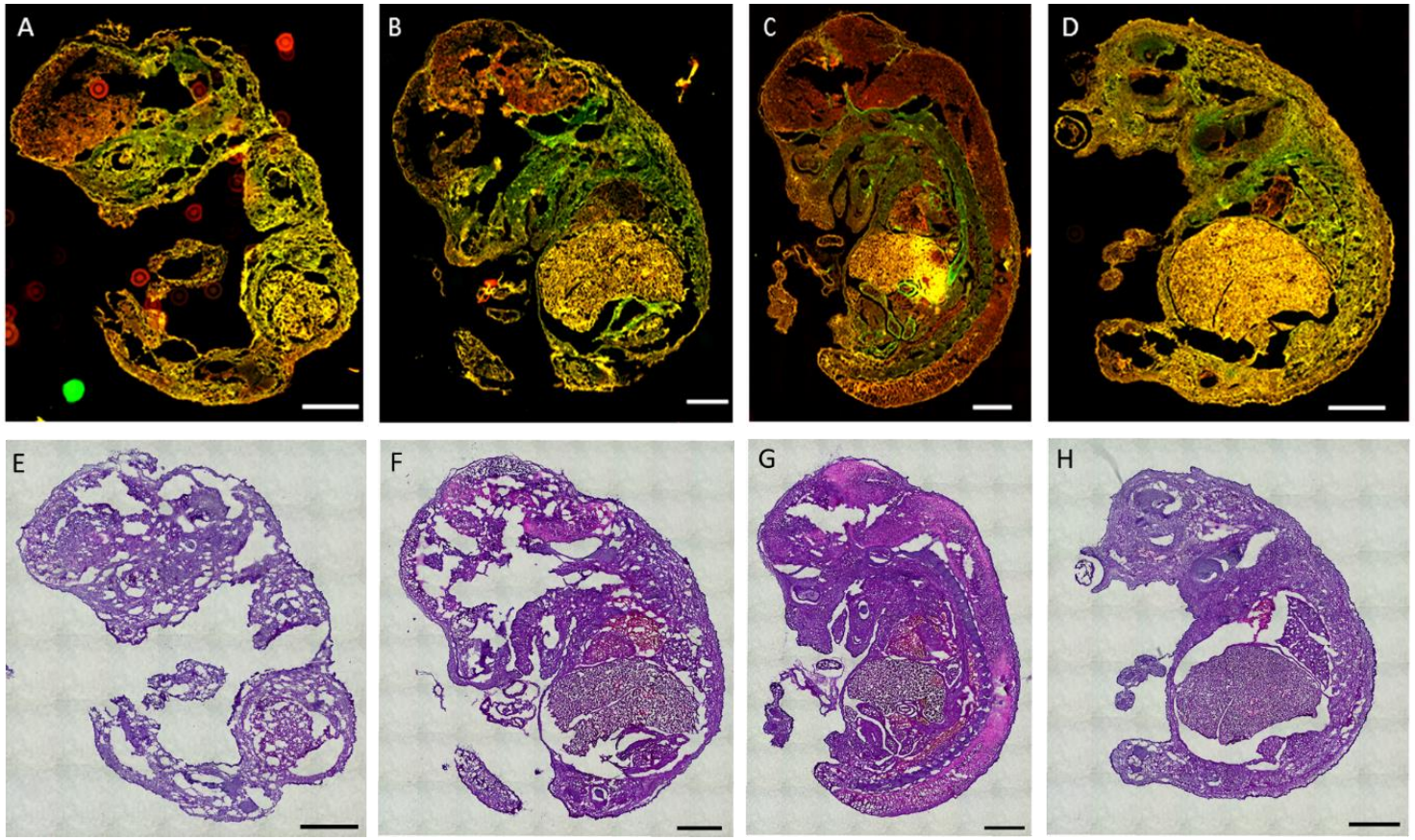

Figure 4.12. Fluorescence and H & E stained sections from double transgenic mice containing the mT/mG reporter construct (Muzumdar *et al.*, 2007) *and Col1α2-CreER^{T2} gene. Embryos were collected at embryonic days E13.5 following tamoxifen injection at E11.5. Fluorescence images (A - D) were imaged using a Zeiss Axio Observer apotome microscope and Axio Cam MR R3 camera. FITC (519 nm) and mCherry (610 nm) fluorescence channels were used to identify tdTomato and EGFP expression. E - H, H & E staining of the same section. Col1α2-CreER^{T2} activity is indicated by EGFP signal. Images were taken at 10x magnification. Scale bars represent 1 mm.*

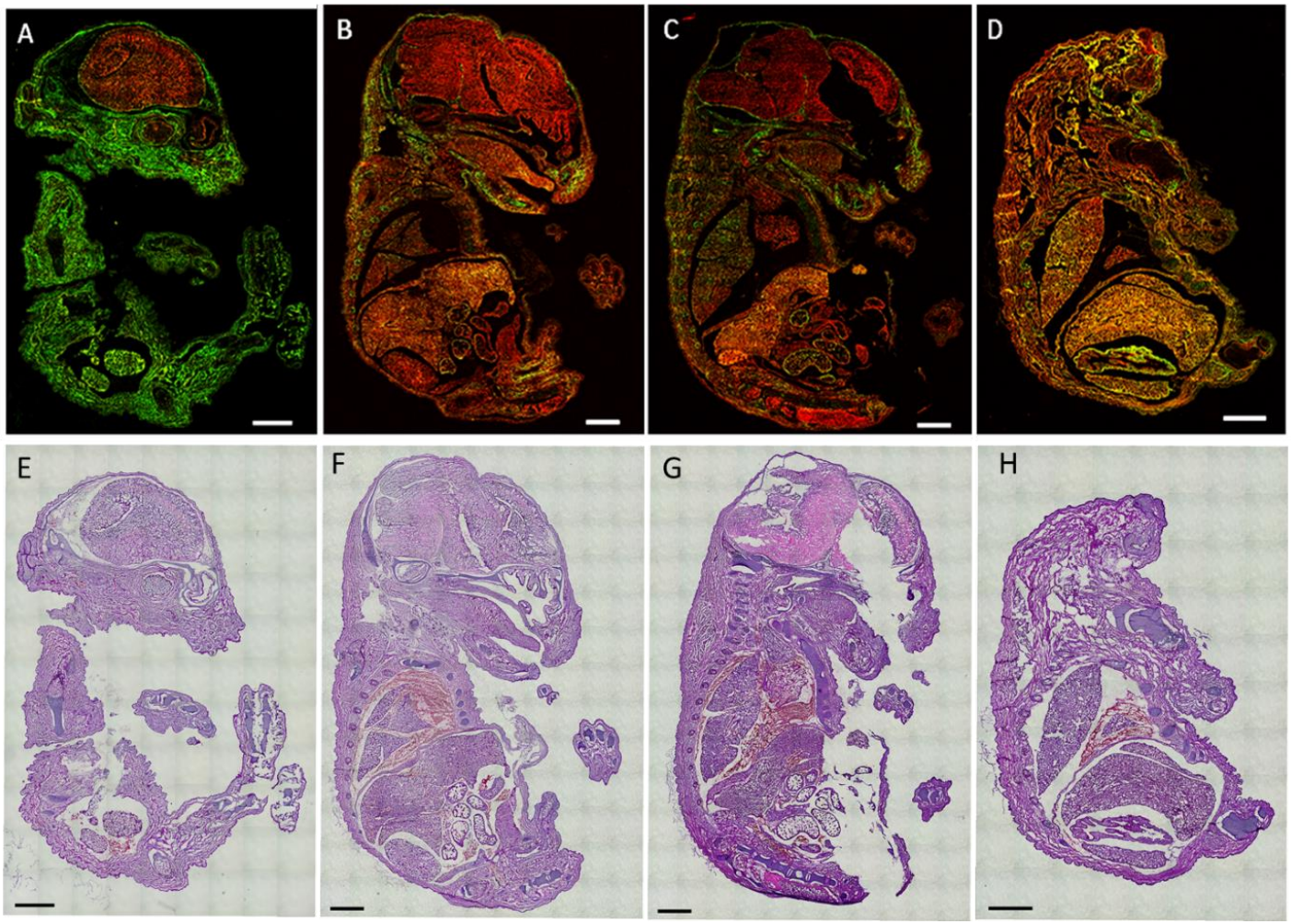

Figure 4.13. Fluorescence and H & E stained sections from double transgenic mice containing the mT/mG reporter construct (Muzumdar *et al.*, 2007) *and Col1α2-CreER^{T2} gene. Embryos were collected at embryonic days E15.5 following tamoxifen injection at E13.5. Fluorescence images (A - D) were imaged using a Zeiss Axio Observer apotome microscope and Axio Cam MR R3 camera. FITC (519 nm) and mCherry (610 nm) fluorescence channels were used to identify tdTomato and EGFP expression. E - H, H & E staining of the same section. Col1α2-CreER^{T2} activity is indicated by EGFP signal. Images were taken at 10x magnification. Scale bars represent 1 mm.*

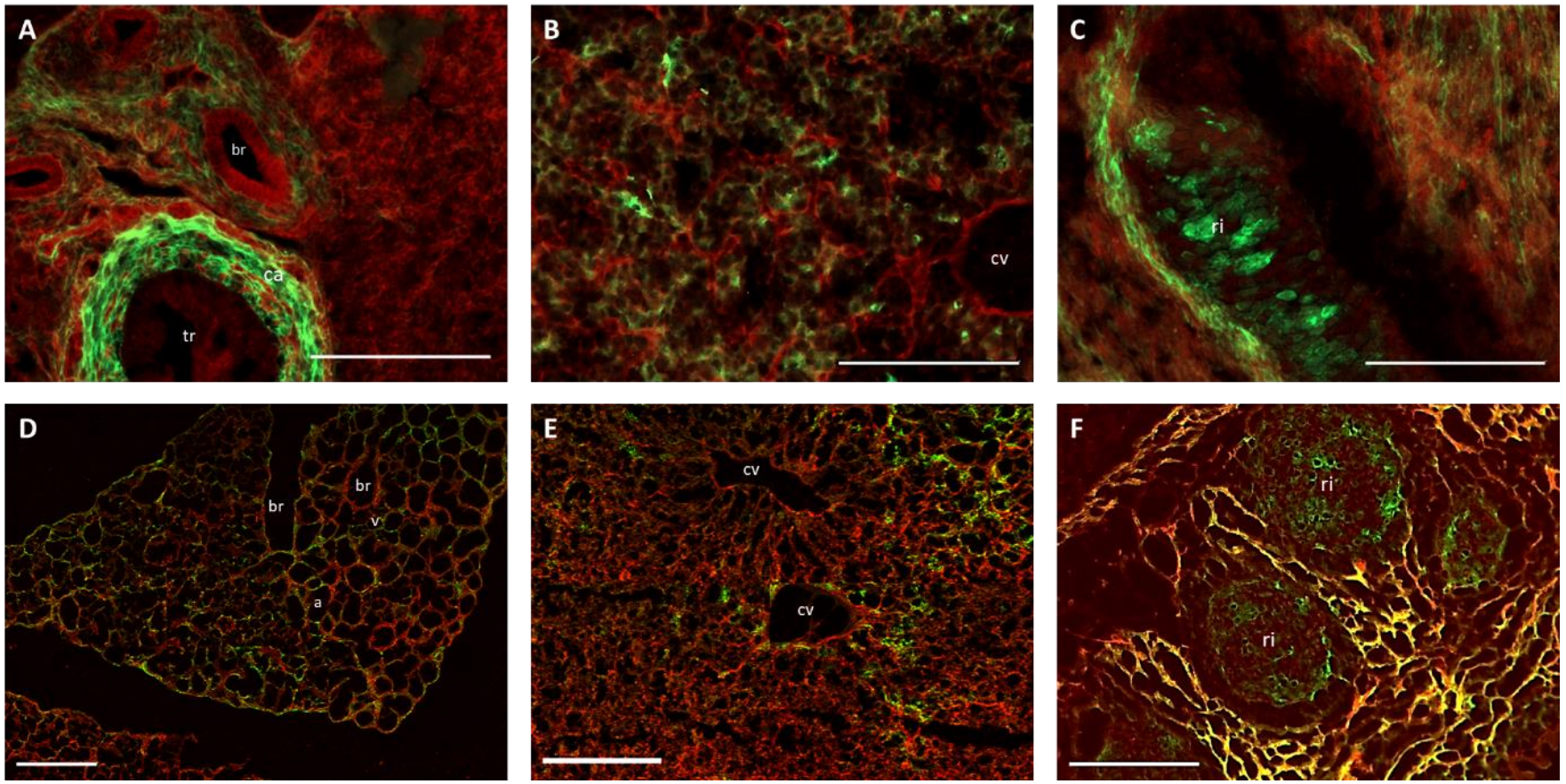

Figure 4.14. Fluorescence images of tamoxifen treated double transgenic mice at E13.5 and E15.5. Fluorescence Images of lung (A & D), liver (B & E), and ribs (C & F) were taken at 10x magnification from tamoxifen-treated double transgenic mice containing the mT/mG reporter construct (Muzumdar *et al.*, 2007) *and Col1α2-CreER^{T2} gene , at embryonic developmental stage E13.5 (A - C) and E15.5 (D - F). Col1α2-CreER^{T2} activity is indicated by EGFP signal. Tissues were imaged using a Zeiss Axio Observer apotome microscope and Axio Cam MR R3 camera. FITC (519 nm) and mCherry (610 nm) fluorescence channels were used to identify tdTomato and EGFP expression. Anatomical features are noted as: tr- trachea, br- bronchioles, ca- cartilage, a- alveoli, v- blood vessels, cv- central vein, ri-ribs. Scale bars represent 200 µm.*

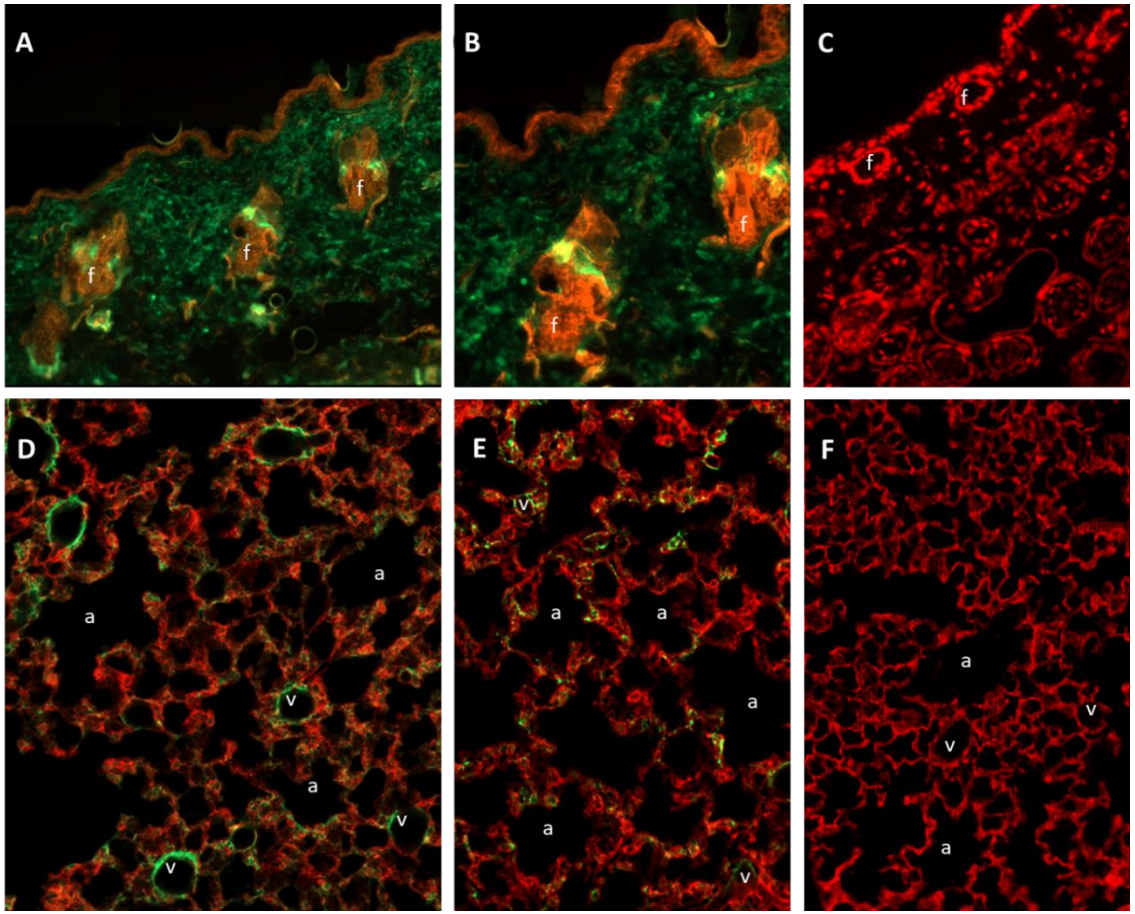

Figure 4.15. Fluorescence images of tamoxifen treated double transgenic adult mice, 7 days after tamoxifen treatment. Skin (A - C) and lung (D - F) were isolated from double transgenic mice containing the mT/mG reporter construct (Muzumdar *et al.*, 2007) *and Col1α2-CreER^{T2} gene. Tissues were collected 7 days after tamoxifen treatment (A & B, D & E) or from untreated littermate control animals (C & F). Tissues were imaged at 10x magnification (A, D & F) and 20x magnification (B, C & E). Col1α2-CreER^{T2} activity is indicated by EGFP signal. Tissues were imaged using a Zeiss Axio Observer apotome microscope and Axio Cam MR R3 camera. FITC (519 nm) and mCherry (610 nm) fluorescence channels were used to identify tdTomato and EGFP expression. Anatomical features are noted as: a- alveoli, v- blood vessels, f- hair follicles.*

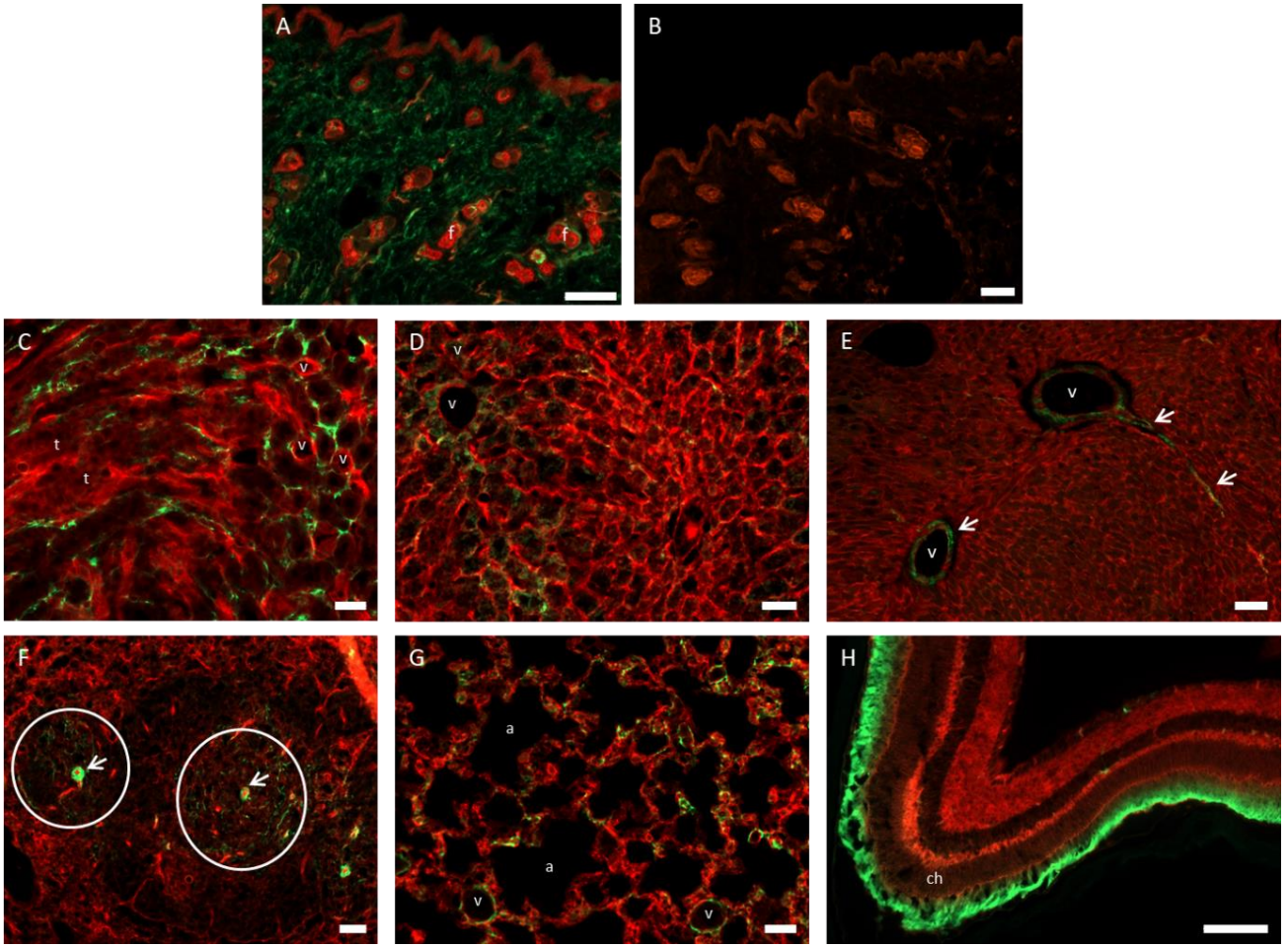

Figure 4.16. Fluorescence images of tamoxifen treated double transgenic adult mice, 3 months after tamoxifen treatment (Li *et al.*, 2017). *Tamoxifen was administered by I.P. injection at ≥6 weeks of age to double transgenic mice containing the mT/mG reporter construct* (Muzumdar *et al.*, 2007) *and Col1α2-CreER^{T2} gene. Tissues were collected at 12 weeks. Col1α2-CreER^{T2} activity is indicated by EGFP signal. A) skin, C), kidney, D) liver, E) heart, F) spleen, G) Lung, H) eye. B) untreated control skin. Anatomical features are identified by: f- follicles, t- tubules, v- blood vessels, a- alveoli, ch-choroid, splenic nodules round circles (F). Tissues were imaged at 10x magnification using a Zeiss Axio Observer apotome microscope and Axio Cam MR R3 camera. FITC (519nm) and mCherry (610nm) fluorescence channels were used to identify tdTomato and EGFP expression. Scale bar represents 32 µm*

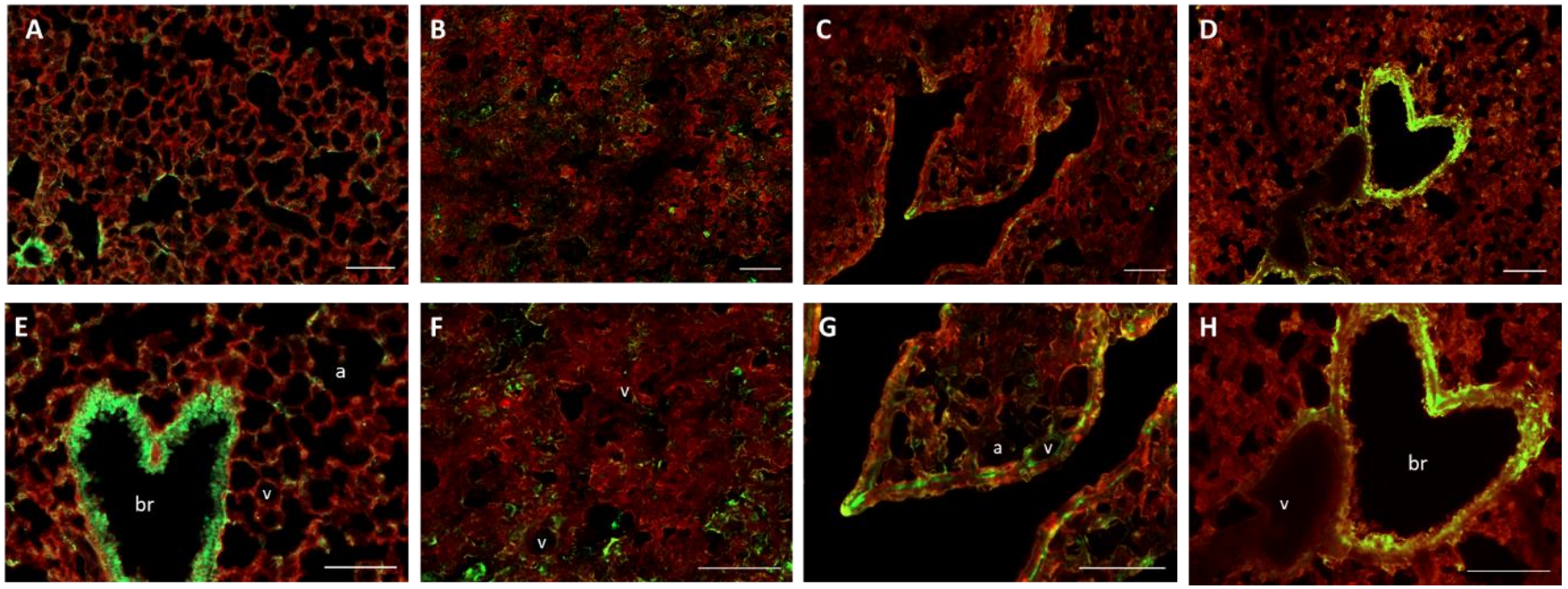

Figure 4.17. Fluorescence images of tamoxifen and bleomycin treated double transgenic adult mice, 14 days after bleomycin treatment. Lungs were isolated from double transgenic mice containing the mT/mG reporter construct (Muzumdar *et al.*, 2007) *and Col1α2-CreER^{T2} gene. Tamoxifen was administered to all mice on days 1, 3 &5, after a 7-day interval a single OA challenge of 0.375 ng/g bleomycin was administered (B - D, F - H). Tissues were collected 14 days after bleomycin treatment. Tissues were imaged at 10x magnification (A - D) and 20x magnification (E - H). Col1α2-CreER^{T2} activity is indicated by EGFP signal. Tissues were imaged using a Zeiss Axio Observer apotome microscope and Axio Cam MR R3 camera. FITC (519 nm) and mCherry (610 nm) fluorescence channels were used to identify tdTomato and EGFP expression. Anatomical features are noted as: a- alveoli, v- blood vessels, br- bronchioles. Scale bars represent 100 µm.*

4.6 Discussion

This chapter described the generation of three new double transgenic mouse lines. The purpose of the first two of these mouse lines, Col1α2-CCN2fl and ROSA-CCN2 was to bring about the loss of function of CCN2 in fibroblast cells, using the Col1α2-CreER^{T2} previously generated by the Bou-Gharios lab (Bou-Gharios *et al.*, 1996; De Val *et al.*, 2002) and in a ubiquitous manner using a Gt(ROSA)26Sortm1-CreER^{T2}, (ROSA-CreER^{T2}) (Ventura *et al.*, 2007). Site specific gain and loss of function animals under the spatio temporal control of tamoxifen inducible CreER^{T2} have been an essential tool for the study of specific proteins and their roles in development, homeostasis and disease pathology (Gierut, Jacks and Haigis, 2014). The protein of interest in this research, CCN2, has previously been identified as an essential for normal embryonic development (Lambi *et al.*, 2012), therefore loss of function must be timed to adulthood. Single transgenic mice possessing the CCN2 floxed allele (Liu *et al.*, 2011), were bred with single transgenic animals expressing the Col1α2-CreER^{T2}. Littermate breeding was maintained to establish a colony of double transgenic animals, homologous for the CCN2 floxed allele, and positive for Col1α2-CreER^{T2}, identified in the following discussion as 'Col1α2-CCN2fl'. The same breeding strategy was adopted to generate a homologous CCN2 floxed, expressing ROSA-CreER^{T2} double transgenic mouse line, identified in the following discussion as 'ROSA-CCN2fl'.

The third new line was developed to characterise the expression profile of the newly generated shorter fibroblast-specific enhancer; Col1α2-CreER^{T2}, utilising the dual fluorescence reporter construct reported by (Muzumdar *et al.*, 2007). Previous research has used the LacZ reporter system to assess the activity of this CreER^{T2} (De Val *et al.*, 2002; Ponticos *et al.*, 2004). The research presented here aimed to reproduce these expression patterns using a dual fluorescent reporter. Single transgenic animals for the mT/mG dual fluorescent reporter construct were bred with single transgenic animals expressing the Col1α2-CreER^{T2}. Littermate breeding was maintained to establish a colony of double transgenic animals, homologous for the mT/mG dual fluorescent reporter construct, and positive for Col1α2-CreER^{T2}.

The first experiments in this chapter described the genotyping strategies developed to identify the transgenes in offspring from the loss of function CCN2 transgenic lines (Col1α2-CCN2fl and ROSA-CCN2fl). Ear punch biopsies were taken from every animal and the DNA was extracted and assessed for transgene expression by PCR. Biopsy location also served as a means of identifying individual animals. Genotyping results (Figure 4.4) were generated for

every animal for both transgenes. Double transgenic animals were identified and used for breeding or for loss of function experiments described in chapter 5. This strategy was reproducible and consistent for the duration of these experiments.

Once double transgenic lines were established, lungs from these mice were extracted and examined by histology to assess whether the presence of the transgenes presented with a defective phenotype (Figure 4.5). Both double transgenic lines were assessed for morphological differences in the lungs, no phenotypes were observed for either strain.

The next series of experiments aimed to induce recombination of the CCN2 floxed gene by administration of tamoxifen. The first strategy for inducing CCN2 knock out, used primary fibroblast cells isolated from double transgenic animals from both the Col1α2-CCN2fl and ROSA-CCN2fl mouse lines. Active metabolite 4-OHT was added to a final concentration of 100 nM, as described in literature for primary fibroblast cultures (Schmidt *et al.*, 2002; Jaskelioff *et al.*, 2010). Cells were assessed 12 hr after 4-OHT administration. Extensive cell death was observed (Figure 4.6). It was not apparent as to why this occurred. Multiple replicates following the same protocol resulted in the same response. No samples for recombination analysis were obtained from any cell culture experiments, therefore recombination was assessed *in vivo*.

Mice were administered tamoxifen via I.P. injection on experimental days 1, 3 and 5. Tail snips were isolated, and DNA extracted for PCR analysis 7 days after the final tamoxifen dose was administered. Visualisation of the DNA gel confirmed that this regime of tamoxifen dosing was sufficient to induce recombination of the CCN2 floxed gene in *vivo* (Figure 4.4). Non-floxed CCN2 alleles were not affected and animals negative for $CreER^{T2}$ showed no response to tamoxifen treatment.

Concentration of tamoxifen was dependent on the transgenic line. Col1α2-CCN2fl mice were administered a dose of 0.025 mg/g. Animals from the ROSA-CCN2 colony experienced increased incidence of adverse effects when administered the 0.025 mg/g dose (data not shown). This was resolved when a dose of 0.0125 mg/g was substituted. CCN2 is implicated in the wound healing process (Hall-Glenn and Lyons, 2011; Ramazani *et al.*, 2018), and it was postulated that the efficiency of the ROSA-$CreER^{T2}$ in removing CCN2 may have prevented

proper healing response in these animals following tamoxifen injection at 0.025 ng/g. This concept was examined further and will be discussed further in the next results chapter. Results for recombination in Figure 4.4 are from ROSA-CCN2fl animals treated with 0.0125 ng/g tamoxifen, therefore this concentration was still sufficient to induce recombination *in vivo*.

To confirm the DNA recombination resulted in knock down of the CCN2 gene, RNA was extracted from the lungs of male and female animals from both the Col1α2-CCN2fl and ROSA-CCN2fl lines and assessed by RT-qPCR for transcription levels of CCN2. Tamoxifen treated lungs were compared to control lungs isolated from untreated littermates and non-transgenic animals of the same background. Inclusion of non-transgenic animal samples was used to confirm that there was no difference in CCN2 transcription owing to the presence of the CCN2 floxed transgene and/or $CreER^{T2}$ genes. No difference was observed.

Col1α2-CCN2fl colony results required assessing on a gender specific basis as a differential response to tamoxifen was observed between male and female animals. Males demonstrated a reduction in CCN2 transcription at all timepoints. Decreases in CCN2 transcript abundance of 0.15, 0.40 and 0.60-fold were observed at days 7, 14 and 28 respectively. Females demonstrated an initial peak in transcription at day 7, with a 3-fold increase in transcription, followed by a 0.4-fold decrease in transcript abundance by day 14 day, in line with the results seen in male animals. CCN2 removal was targeted to fibroblast cells in this line so the partial reduction in transcription observed was expected. It is not known why female and male mice demonstrated different responses at 7 days. Analysis using this loss of function colony in the next results chapter examined the transcriptional differences in a gender specific manner based on these results.

The ROSA-CCN2fl colony demonstrated a complete ablation of CCN2 transcription activity at 14 days. Research using this loss of function colony was planned for a timepoint of 14 days only so no further timepoints were assessed. However as complete recombination was identified by DNA analysis it is likely that cessation of CCN2 transcription had already occurred by 7 days and would be unlikely to resume at later timepoints. No differences were identified between genders. However, based on the results from the Col1α2-CCN2fl colony that analyses of loss of function experiments presented in the next results chapter would analyse qPCR results on a gender specific basis for both Col1α2-CCN2fl and ROSA-CCN2fl colonies.

To determine if these transcriptional changes were translated to a reduction in protein expression, antibody staining for CCN2 was carried out on lungs isolated 14 days after tamoxifen administration from mice from both Col1α2-CCNfl and ROSA-CCN2fl colonies. Antibody staining patterns were compared to an untreated control lung for localisation and prevalence of CCN2.

A reduction of staining in the bronchioles of the Col1α2-CCN2fl was noted. Staining in regions surrounding alveoli was seen with a similar expression to control. This was not unexpected as CCN2 has been shown to be expressed by many different cell types including epithelial cells, vascular smooth muscle cells (VSMCs), as well as fibroblasts (Moussad and Brigstock, 2000; Chang *et al.*, 2004; Yu *et al.*, 2009; Bai *et al.*, 2013). Background staining was notably darker in lungs isolated from the Col1α2-CCN2fl colony. In lungs isolated from mice where CCN2 was targeted ubiquitously, no staining was observed. Commercially available antibodies for CCN2 have been difficult to optimise, with researchers within the CCN2 field opting to generate their own in-house antibodies (Wang, McLennan and Twigg, 2011; Charrier *et al.*, 2014). These staining results were deemed appropriate and it was concluded that I.P. injection of tamoxifen was sufficient to induce recombination of the CCN2 floxed gene in *vivo* that resulted in a knock down of protein expression.

CCN2 knock down was demonstrated both at the transcriptional level and the protein level. The efficiency of this reduction was dependent on the CreER^{T2} specificity. These results concluded the first and second aims of this chapter to establish and characterise the double transgenic mouse colonies, containing the floxed CCN2 transgene and a ubiquitously expressed ROSA26CreER^{T2} (ROSA-CCN2fl), or a fibroblast specific tamoxifen-inducible CreER^{T2} (Col1α2-CCN2fl).

To address the third aim of this research chapter, to characterise the expression of the Col1α2-CreER^{T2}, experiments were carried out using the third new double transgenic mouse colony, expressing the mT/mG dual fluorescent reporter construct (Col1α2-R26TmG).

The first experiments using this mouse colony investigated the expression patterns of Col1α2-CreER^{T2} expression during embryonic development. Pregnant females were Sch1 by cervical dislocation and embryos were collected at developmental days E13.5 and E15.5. A single I.P. dose of 3 mg tamoxifen was administered to pregnant females at embryonic developmental stages E11.5 and E13.5 for Col1α2-CreER^{T2} expression analysis at E13.5 and E15.5 respectively. Control embryos were collected at the same developmental stages from untreated females for comparison.

Expression of the mT/mG reporter was confirmed by fluorescence imaging, control embryos at both E13.5 and E15.5 emitted red fluorescent signal, which was confirmed to by synonymous with tissue deposition by subsequent staining of the sections with H & E. To ensure no Col1α2-CreER^{T2} activity occurred spontaneously, sections were examined at higher magnification. No expression was seen.

EGFP fluorescent signal was used as a readout for Col1α2-CreER^{T2} activity when assessing samples that were administered tamoxifen. Serial sections were analysed for EGFP signal at E13.5 and E15.5. Activation of the CreER^{T2} was confirmed by observation of EGFP signal at both developmental stages. The expression patterns observed were comparable to those described by (De Val *et al.*, 2002), with EGFP signal seen in the skull bone, dermal layer of the skin, liver, ribs, lungs, and kidney. Single cell populations exhibiting EGFP signal were identified when these sections were observed at higher magnification.

Col1α2-CreER^{T2} expression was then analysed in adult tissue. Mice of ≥ 6 weeks of age were administered tamoxifen and tissues were isolated and examined for tdTomato and EGFP signal 7 days and 3 months after tamoxifen. Tissues were isolated from untreated littermate animals for comparison. No EGFP signal was found in any tissue collected from untreated mice.

Analysis of these sections demonstrated expression matching that described previously for homeostatic adult tissue (Ponticos *et al.*, 2004). Manne, Markova, Siracusa, & Jimenez, (2013) described the expression patterns of collagen for skin and lung, and the results shown for EGFP expression in the skin and lung reproduce this expression pattern faithfully. EGFP localisation in tissues isolated at 3 months was previously reported in Li, Horwell, Chu, de Crombrugghe, & Bou-Gharios, (2017). Skin and kidney expression was identical to that seen at 7 days, in fact there was no difference in EGFP signalling / Col1α2-CreER^{T2} activity when comparing skin and lung samples collected at 7 or 90 days (3 months).

The final experiment in this chapter investigated the expression pattern of Col1α2-CreER^{T2} when the lungs were subject to injury using the bleomycin model of fibrosis described in chapter 3. Animals were administered a single dose of bleomycin following the protocol developed in chapter 3. Lungs were extracted for analysis at day 14. This protocol was described and Col1α2-CreER^{T2} activity examined using β-galactosidase activity by Ponticos et al., (2004). Increased tdTomato signalling was seen, revealing a loss of usual morphology as expected and characteristic of bleomycin treated lungs. Regions of EGFP signalling could be identified within the tdTomato signal. Individual EGFP expressing cells were visualised

surrounding vessels and lining alveoli. This expression pattern was consistent with the expression pattern reported by Ponticos et al., (2004).

4.7 Summary

The research in this chapter aimed to establish and characterise two double transgenic mouse colonies, containing the floxed CCN2 transgene and a ubiquitously expressed ROSA26CreER^{T2} (ROSA-CCN2fl), or a fibroblast specific tamoxifen-inducible CreER^{T2} (Col1α2-CCN2fl) for use in loss of functional CCN2 experiments (reported in Chapter 5). This was achieved by developing genotyping strategies to identify animals containing the desired transgenes. Subsequent breeding pairs were chosen based on these results and littermates were interbred to produce offspring that were homologous for the floxed CCN2 gene, and positive for one of the two CreER^{T2} (ROSA26CreER^{T2} or Col1α2-CCN2fl).

A tamoxifen dosing regime was then assessed for recombination of the CCN2 floxed gene both *in vitro* and *in vivo*. *In vitro* studies failed to yield any data. *In vivo*, recombination of the CCN2 floxed gene was demonstrated at the DNA, transcriptional and translational level for both the fibroblast specific (Col1α2-CCN2fl) and ubiquitously targeting (ROSA-CCN2fl) animal lines.

This research also aimed to characterise the expression profile of the Col1α2-CreER^{T2} using a dual fluorescent (mT/mG) reporter construct. Mice containing the mT/mG reporter construct described by Muzumdar et al., (2007), were bred with mice containing the Col1α2-CreER^{T2}. Littermate breeding pairs were maintained to produce a double transgenic mouse colony that was homozygous for the mT/mG reporter construct, and positive for Col1α2-CreER^{T2}. These animals were then used for lineage tracing experiments to determine the expression pattern of the Col1α2-CreER^{T2} during development and during adulthood. This new shorter collagen enhancer expressed more widely in almost all fibroblast compared with the previous Cre ER^{T1} generated by (Denton *et al.*, 2001).

5. Investigating the Effects of CCN2 Loss of Function on the Initiation and Propagation of Fibrosis using a Bleomycin Model of IPF

5.1 Fibrotic disease

Fibrosis is characterised by excessive accumulation of ECM and is the end result of chronic inflammation arising from a number of stimuli including persistent infections, chemical insults, and tissue injury (Wynn, 2008). In IPF this accumulation of ECM is localised to the lung resulting in destruction of its normal architecture, ultimately leading to organ failure and death (Sime and O'reilly, 2001; Biernacka, Dobaczewski and Frangogiannis, 2011; Kolb, Gauldie and Bellaye, 2016).

At the cellular level, the key mediators of fibrosis are the fibroblast and their profibrotic phenotype, the myofibroblast. The myofibroblast serves as the primary collagen-producing cell during wound healing and fibrosis (Klingberg, Hinz and White, 2013). During the repair process fibroblasts are stimulated to differentiate into their active, ECM synthesising myofibroblast phenotype (Kuhn and McDonald, 1991; Kolb, Gauldie and Bellaye, 2016). One of the current hypotheses is that a state of chronic inflammation and recurrent micro-damage leads to dysregulation in the fibroplasia phase of the tissue repair process (Wynn, 2008). The traditional view was that these activated myofibroblasts derive from resident fibroblast populations. However, recent evidence suggests that fibroblasts may originate from other cellular sources, such as pericytes (Lin *et al.*, 2008), mesenchymal cells (Misharin *et al.*, 2017) and epithelium (Krenning, Zeisberg and Kalluri, 2010).

TGF-β is known to be a key mediator of fibrogenesis and is capable of driving the activation of the myofibroblast (Chen *et al.*, 2009; Midgley *et al.*, 2013; Tomcik *et al.*, 2015). Although this makes TGF-β an attractive therapeutic target for IPF, the pleiotropic roles it plays in tissue homeostasis (Xu *et al.*, 2018), immunity (Travis and Sheppard, 2014) and cell proliferation (Huang and Huang, 2005) raise concerns that too many potential side effects may be caused by targeting TGF-β signalling (Biernacka, Dobaczewski and Frangogiannis, 2011). Therefore, research has explored downstream mediators of TGF-β signalling as candidates for therapeutic intervention.

CCN2 has been proposed to be a key downstream mediator of the profibrotic effects of TGF-β, and its role in fibrosis has been investigated independently of TGF-β (Sonnylal *et al.*, 2010). CCN2 has consistently been shown to be upregulated in connective disease in the lung (Allen and Spiteri, 2002), in tandem with TGF-β upregulation (Lasky *et al.*, 1998; Xu *et al.*, 2006). CCN2 is known to be a key mediator of many of the signalling pathways associated with fibrosis, such as activating cell adhesion and migration (Bradham *et al.*, 1991), angiogenesis

(Babic, Chen and Lau, 1999), myofibroblast activation (Tsai *et al.*, 2018), and extracellular matrix deposition and remodelling (Lipson *et al.*, 2012). A monoclonal antibody to CCN2, currently in clinical development (FG-3019) has demonstrated the ability to reverse the fibrosis in various murine models of fibrosis (Koshman *et al.*, 2015; Bickelhaupt *et al.*, 2017) and is showing promising efficacy in human trials (Raghu *et al.*, 2012, 2016; Picozzi *et al.*, 2016).

5.2 Chapter Aims

The aims of this chapter were as follows:

1) Investigate the effects of fibroblast specific removal of CCN2 in a bleomycin model of IPF.

In the previous chapter a double transgenic mouse line was generated that was homologous for the CCN2 floxed allele, and positive for Col1α2-CreER^{T2}, (Col1α2-CCN2fl). This research used this transgenic mouse line in conjunction with the bleomycin model of IPF that was generated in Chapter 3 to achieve the following objectives:

- Identify if the fibroblast specific removal of CCN2 results in a phenotype in the lung. µCt analysis, histology and qPCR were used to assess lung samples from Col1α2-CCN2fl mice, at time points 7, 14 and 28 days post treatment with tamoxifen.
- Identify if there is an altered response in the rate of fibrosis formation when CCN2 is removed from fibroblasts prior to treatment with bleomycin. µCt analysis, histology and qPCR were used to assess lung samples from Col1α2-CCN2fl mice, at time points 7, 14 and 28 days post treatment with tamoxifen and bleomycin.

2) Investigate the effects of ubiquitous removal of CCN2 in a bleomycin model of idiopathic pulmonary fibrosis (IPF) and compare this to the response seen in Col1α2-CCN2fl mice at 14 days post bleomycin treatment.

In the previous chapter a second double transgenic mouse line was generated that was homologous for the CCN2 floxed allele, and positive for ubiquitously expressed ROSA-CreER^{T2}, (ROSA-CCN2fl). This research used this transgenic mouse line in conjunction with the bleomycin model of IPF that was generated in Chapter 3 to achieve the following objectives:

- Identify if the ubiquitous removal of CCN2 results in a phenotype in the lung. µCt analysis, histology and qPCR were used to assess lung samples from ROSA-CCN2fl mice, at a time point of 14 days post treatment with tamoxifen.
- Identify if there is an altered response in the rate of fibrosis formation when CCN2 is removed from all cells prior to treatment with bleomycin. µCt analysis, histology and qPCR were used to assess lung samples from ROSA-CCN2fl mice, at a time points of 14 days post treatment with tamoxifen and bleomycin.

5.3 Phenotypic analysis of lungs from tamoxifen treated Col1α2-CreER^{T2}

The first experiments in this research characterised the responses to tamoxifen treatment in the Col1α2-CCN2fl double transgenic mouse line. Experimental day 1 was considered as 7 days after tamoxifen dosing was completed. This was to ensure analyses in these studies were directly comparable to later experiments when a 7-day recovery period was required prior to bleomycin treatment. Tamoxifen injection activated recombination of the CCN2fl gene by Col1α2-CreER^{T2}.

Male and female mice from the Col1α2-CCN2fl were aged to ≥6 weeks and administered three I.P. 0.025 mg/g injections of tamoxifen as described in methods section 2.5.1. On experimental days 7, 14 and 28 animals were culled by Sch1 by overdose of Pentobarbital prepared for µCT scanning as per methods section 2.6. No morphological differences in the lungs were observed by µCT analysis at any time point (Figure 5.1).

Closer examination of the morphology of the lungs was carried out by histological analysis. A lobe from experimental lungs was isolated immediately after µCT scanning and processed for histology following the protocol described in methods section 2.8. Sections of 5 µm were stained with H & E, or Goldner's trichrome stains. Protocols can be found in methods section 2.8.

H & E stain was used to identify anatomical features of the lung including the bronchioles, alveoli and blood vessels. A stitched image taken at 10x magnification was used to visually assess the whole lung lobe section (Figure 5.2), where scale bars represent 1 mm. For closer analysis of the morphology of the lung, individual images were taken at 10x magnification (Figure 5.3), scale bars represent 200 µm. Single cell epithelial lining of the alveoli was identifiable at 10x magnification for all samples (Figure 5.3). Blood vessels were seen associated with the bronchioles as well as being dispersed throughout the alveoli. No differences in morphology were identified when comparing lung lobes treated with tamoxifen to an untreated control lung.

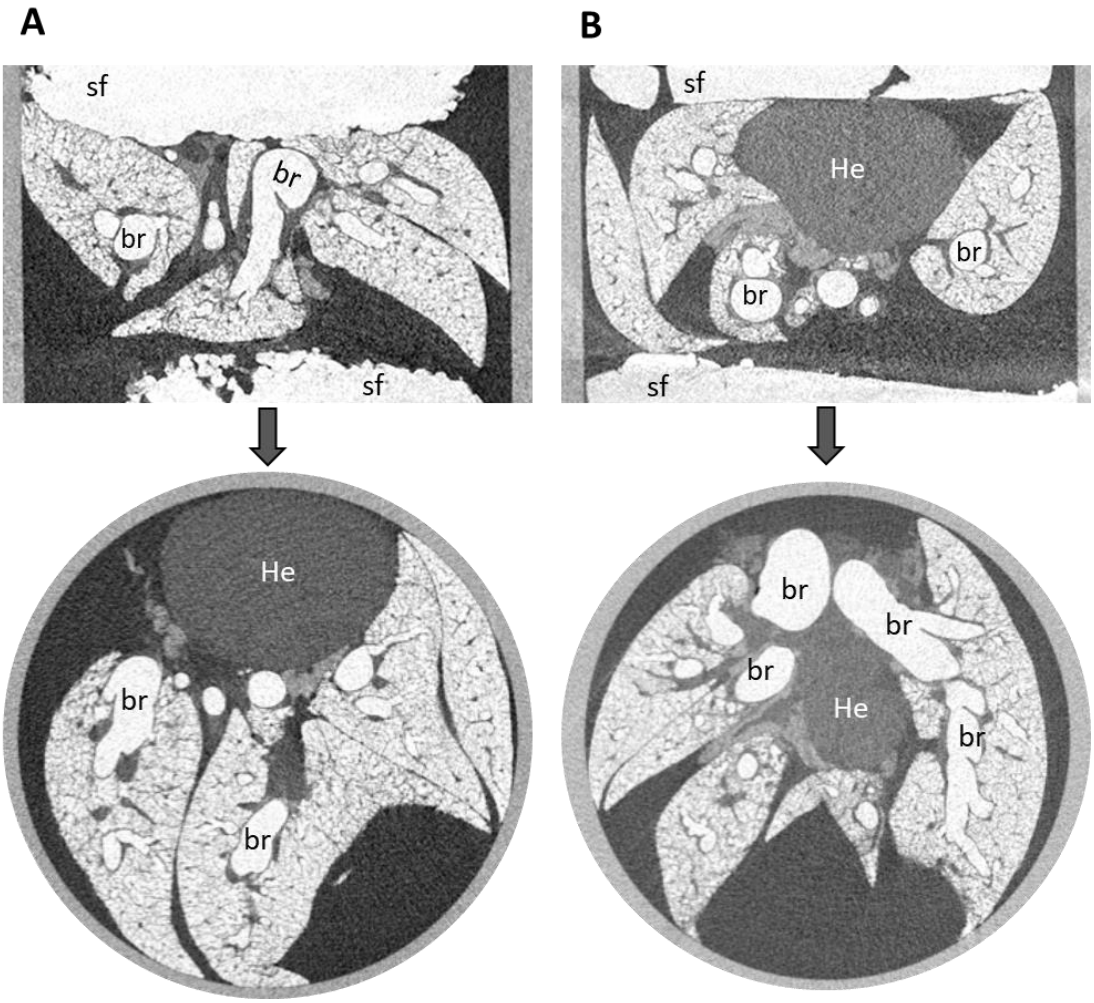
A
sf
br
br
sf
He
br
br
br
B
sf
He
br
br
sf
br
br
br
He
br

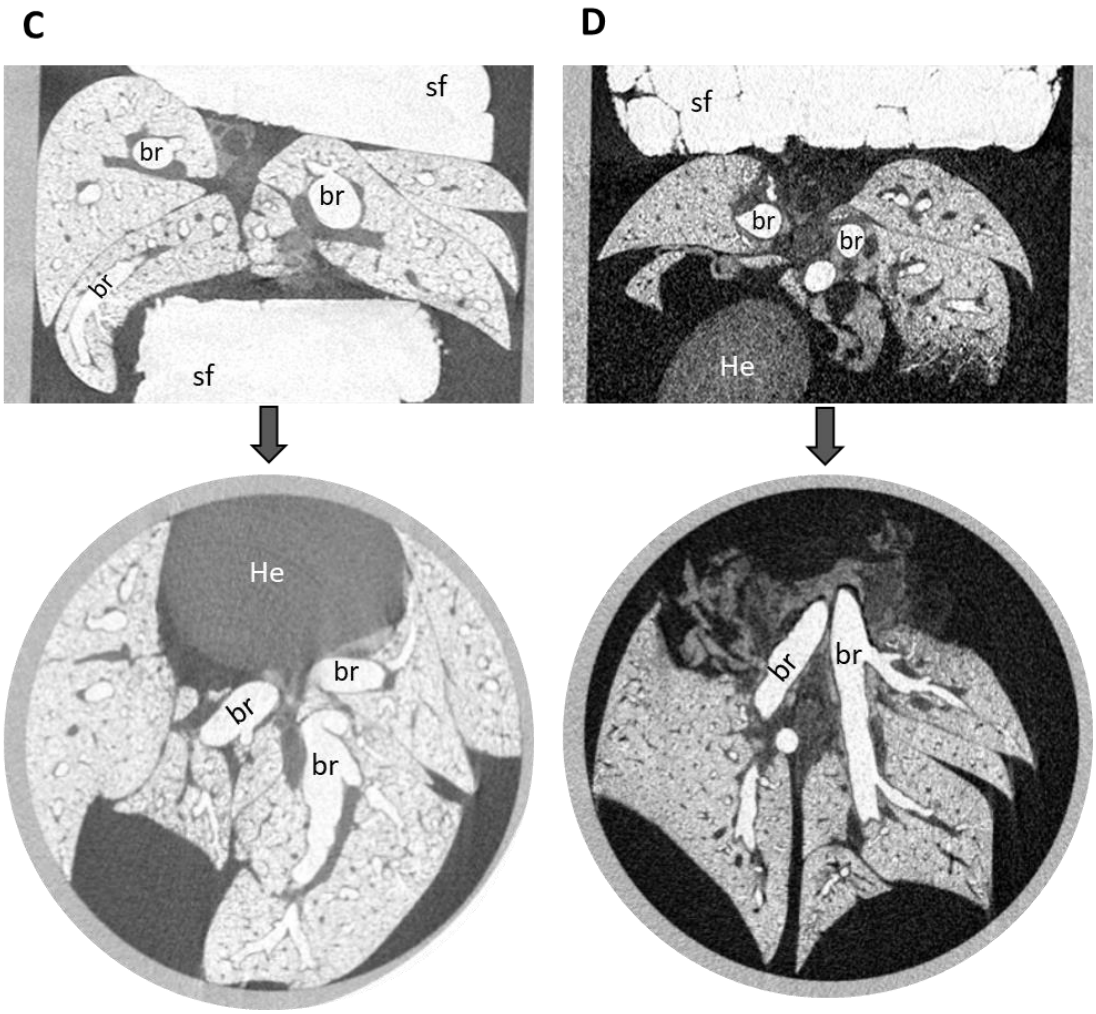

Figure 5.1. µCT scans of unfixed, inflated mouse lungs isolated from tamoxifen treated Col1α2-CCN2fl mice at 7, 14 and 28 Days. Animals were administered 3x doses of tamoxifen at 0.025 ng/g. A week's recovery period was given before experimental day 1. Animals were Sch1 by overdose of Pentobarbital, the lungs manually inflated prior to extraction. Isolated lungs were then suspended between pieces of Styrofoam (sf) in 3 – 5 % (wt / vol) KI contrast agent for µCT scanning. Lungs were scanned using a SkyScan 1272 µCT system at a resolution of 20 µm (0.25 mm aluminium filter, 0.3 ° rotation step). Images were reconstructed using Skyscan Nrecon software and visualised using DataViewer. Tamoxifen treatment causes loss of CCN2 in fibroblasts. Anatomical features are identified by the following: br- bronchioles, He- heart. Representative images from whole lung 3D scans are shown using DataViewer software. Example scans for lungs collected at the following timepoints are A) Untreated, B) Experimental day 7, C) Experimental day 14, D) Experimental day 28.

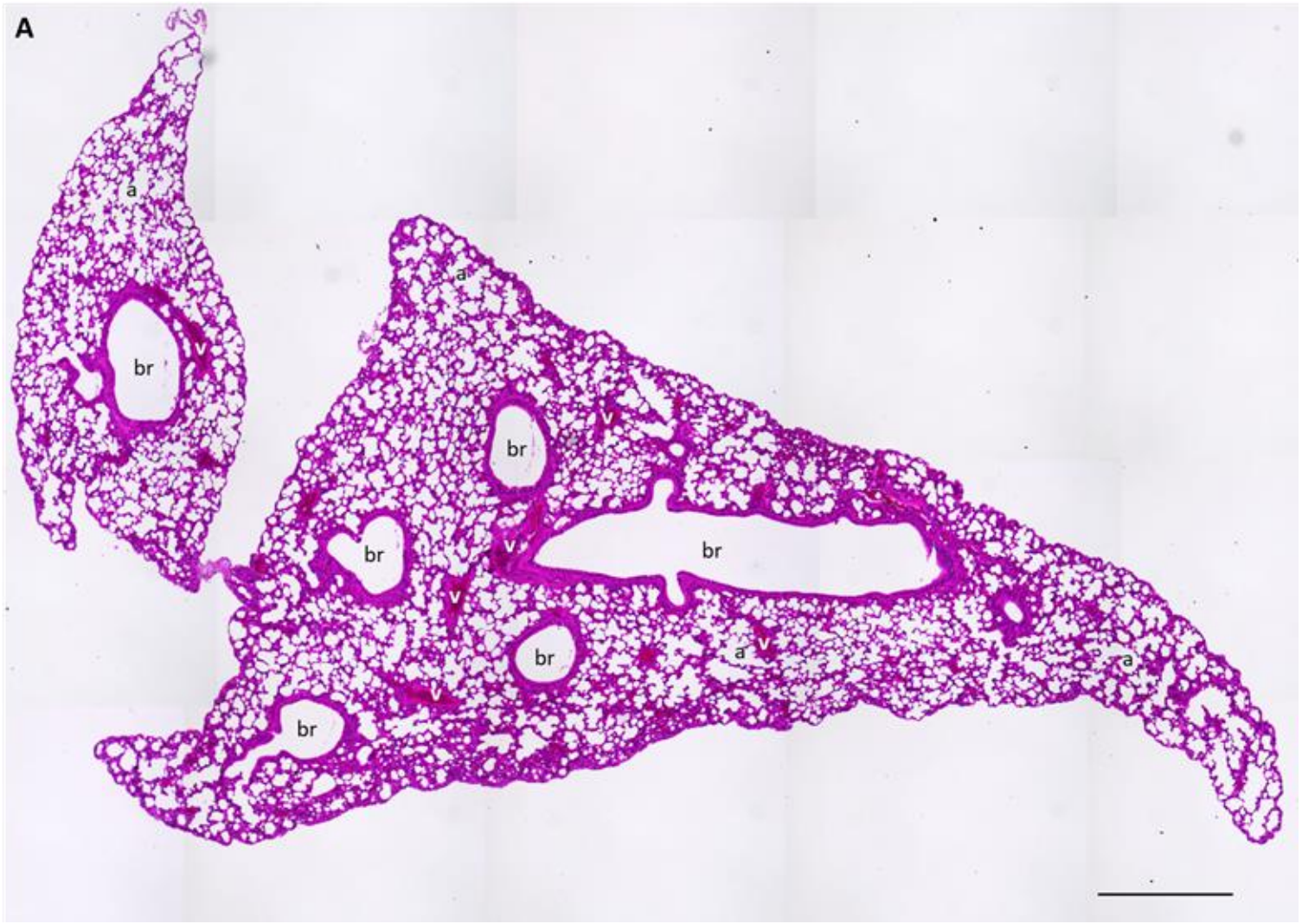
A
a
br
v
a
br
br
v
br
v
a
v
a
br
v
br

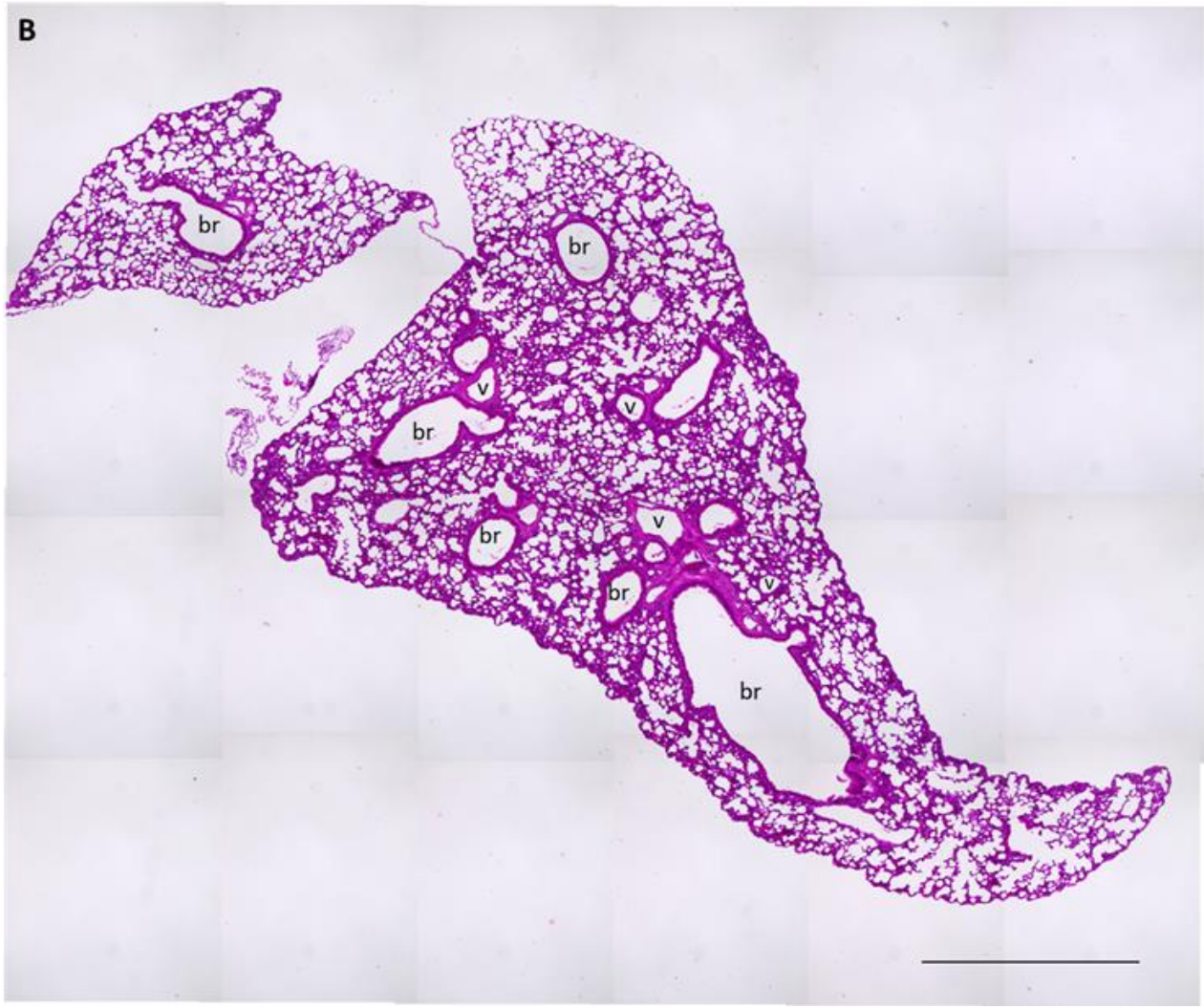
B
br
br
v
v
br
br
v
br
v
br

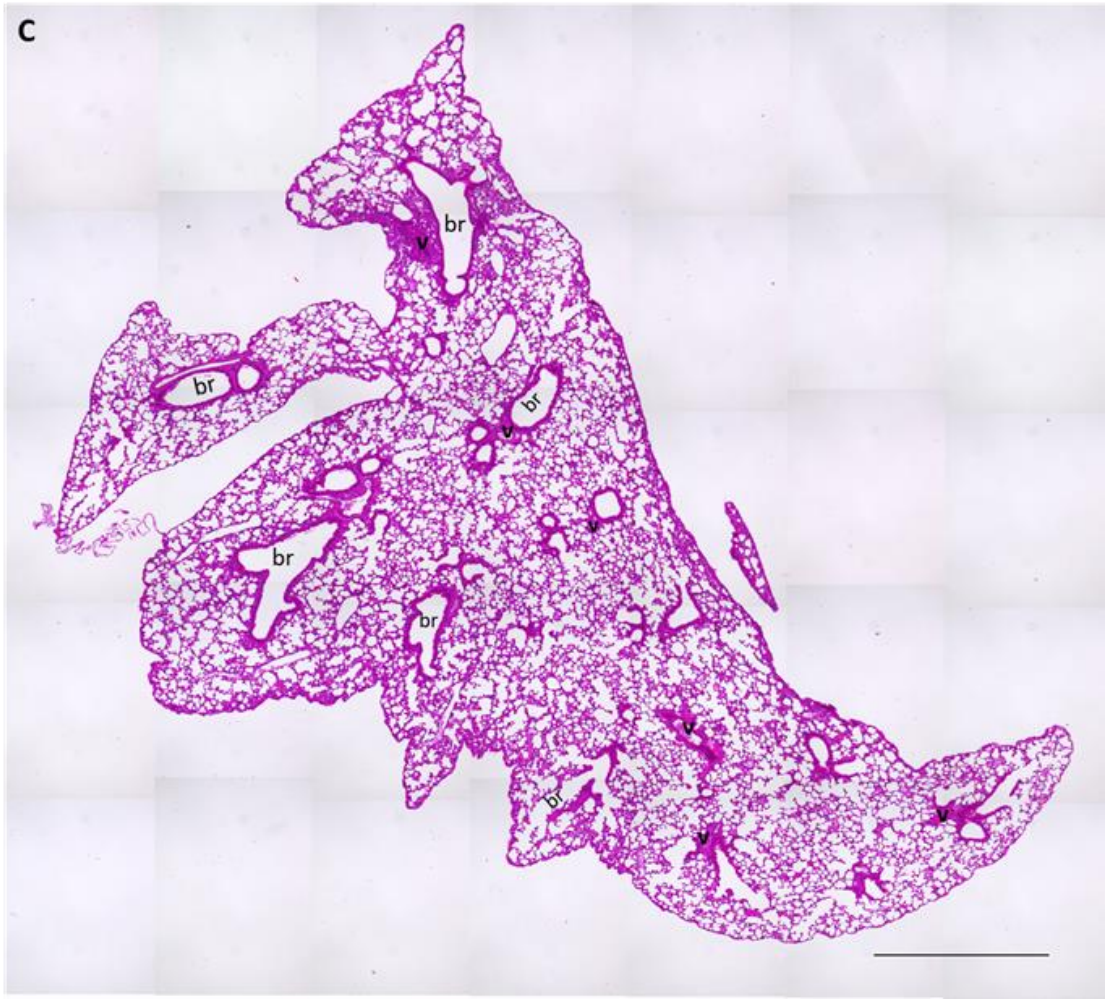
C
br
v

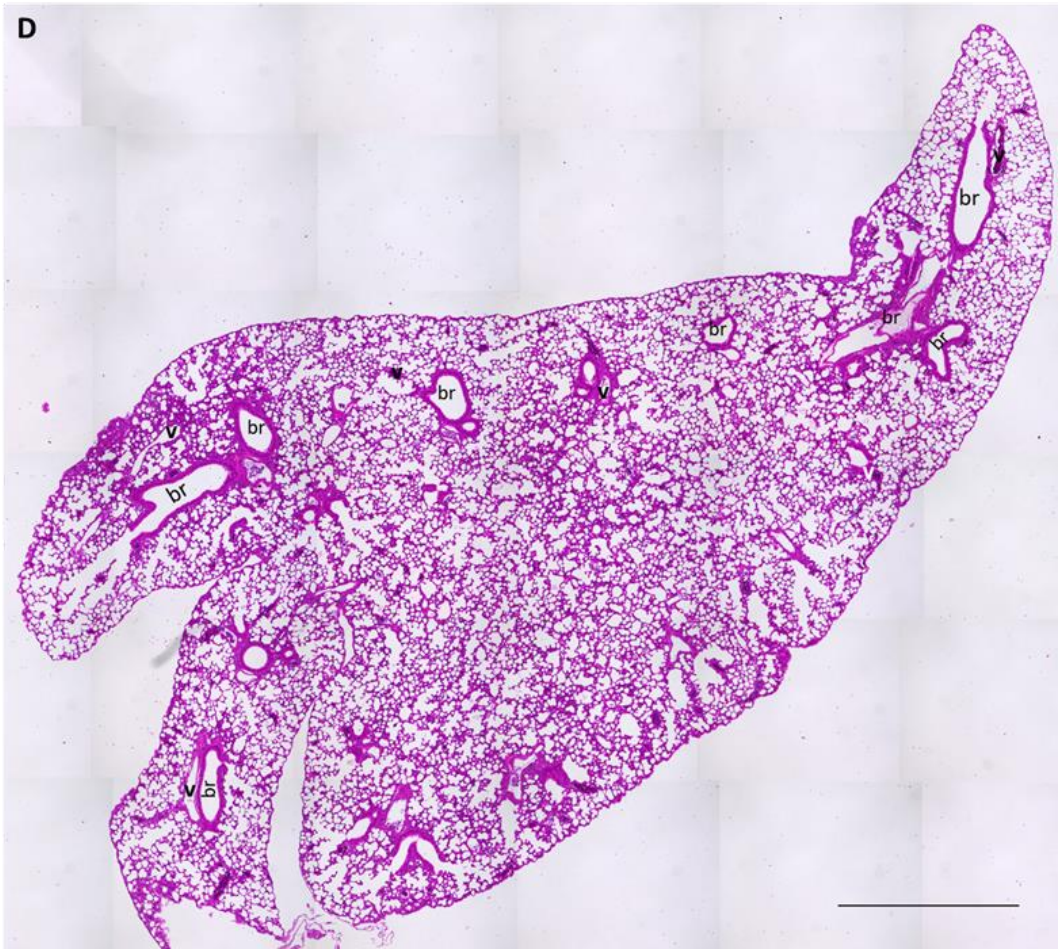

Figure 5.2. Histological evaluation of whole lung lobe samples lungs isolated from tamoxifen treated Col1α2-CCN2fl mice at 7, 14 and 28 Days using H & E stain. Lungs were isolated immediately after Sch1 by anaesthetic overdose and manually inflated for scanning, using a SkyScan 1272 µCT system at a resolution of 20 µm (0.25 mm aluminium filter, 0.3 ° rotation step). Lungs were processed for wax histology and stained with H & E. Anatomical features are identified as follows: a- alveoli, br- bronchioles, v- blood vessels. All images were taken at 10x magnification. A) Untreated, B) Experimental day 7, C) Experimental day 14, D) Experimental day 28. Scale bars represent 1 mm.

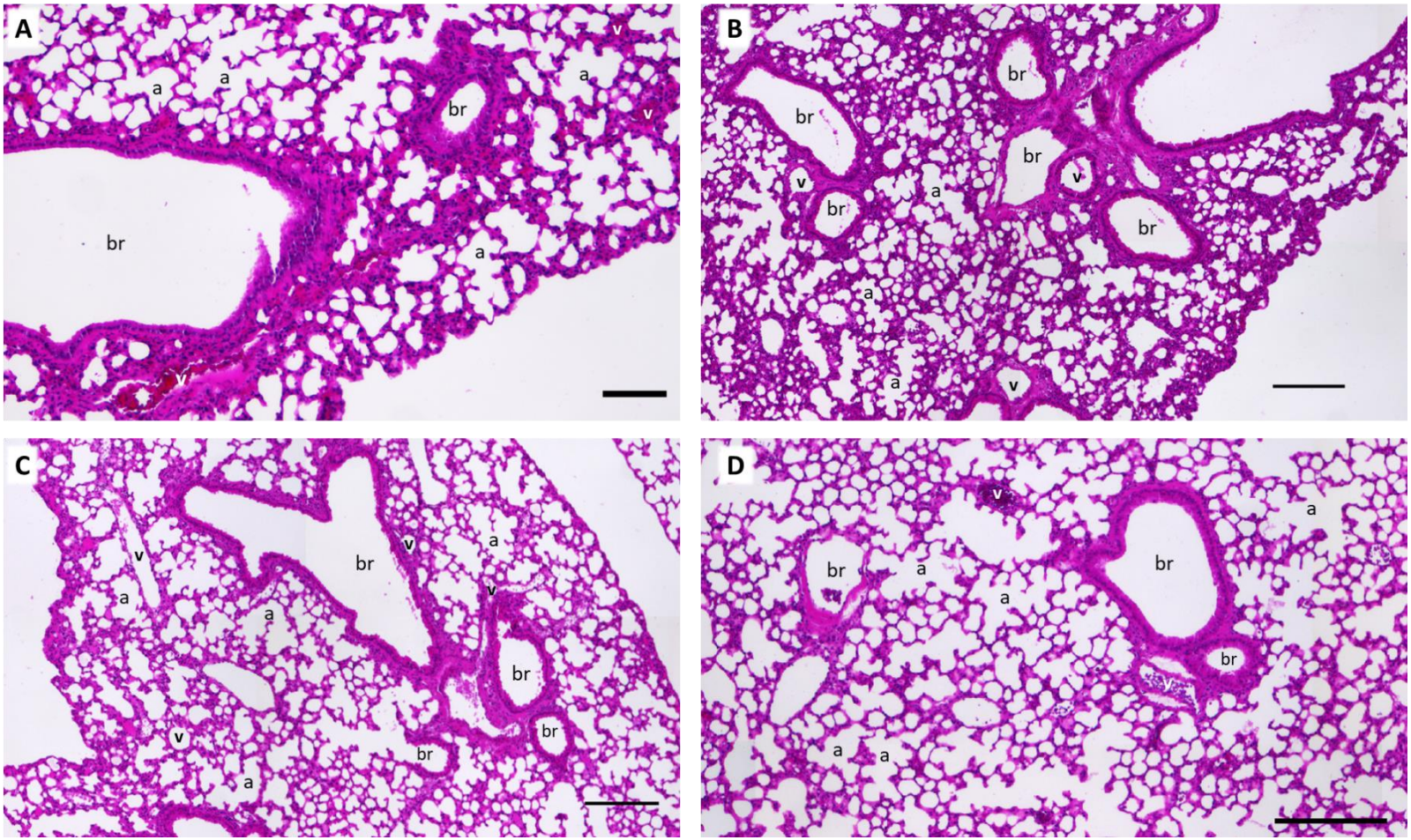

Figure 5.3. Histological evaluation of lung samples isolated from tamoxifen treated Col1α2-CCN2fl mice at 7, 14 and 28 days using H & E stain. Lungs were isolated immediately after Sch1 by anaesthetic overdose and manually inflated for scanning, using a SkyScan 1272 µCT system at a resolution of 20 µm (0.25 mm aluminium filter, 0.3 ° rotation step). Lungs were processed for wax histology and stained with H & E. Anatomical features are identified as follows: a- alveoli, br- bronchioles, v- blood vessels. All images were taken at 10x magnification. A) Untreated, B) Experimental day 7, C) Experimental day 14, D) Experimental day 28. Scale bars represent 200 µm.

Goldner's trichrome stain was used to identify collagen deposits from muscular tissues. Cell nuclei appear black, cytoplasm - red and collagen - green. A stitched image taken at 10 x magnification was used to visually assess the presence of collagen across in the whole lung lobe lung section (Figure 5.4), where scale bars represent 1 mm. For closer analysis of the morphology of the lung, individual images were taken at 10x magnification (Figure 5.5), scale bars represent 200 µm. Anatomical features of the lung are identified in the figure as: bronchioles, alveoli and blood vessels.

Collagen is a major constituent of the pulmonary interstitium and major structures including the bronchioles, blood vessels alveoli and bronchioles. Therefore, some green staining of these structures was anticipated and seen in both control and tamoxifen treated lungs (Figure 5.5). Red staining inside bronchioles demonstrates the presence of the epithelial cells lining these structures. No differences in morphology were identified when comparing lung lobes treated with tamoxifen to an untreated control lung.

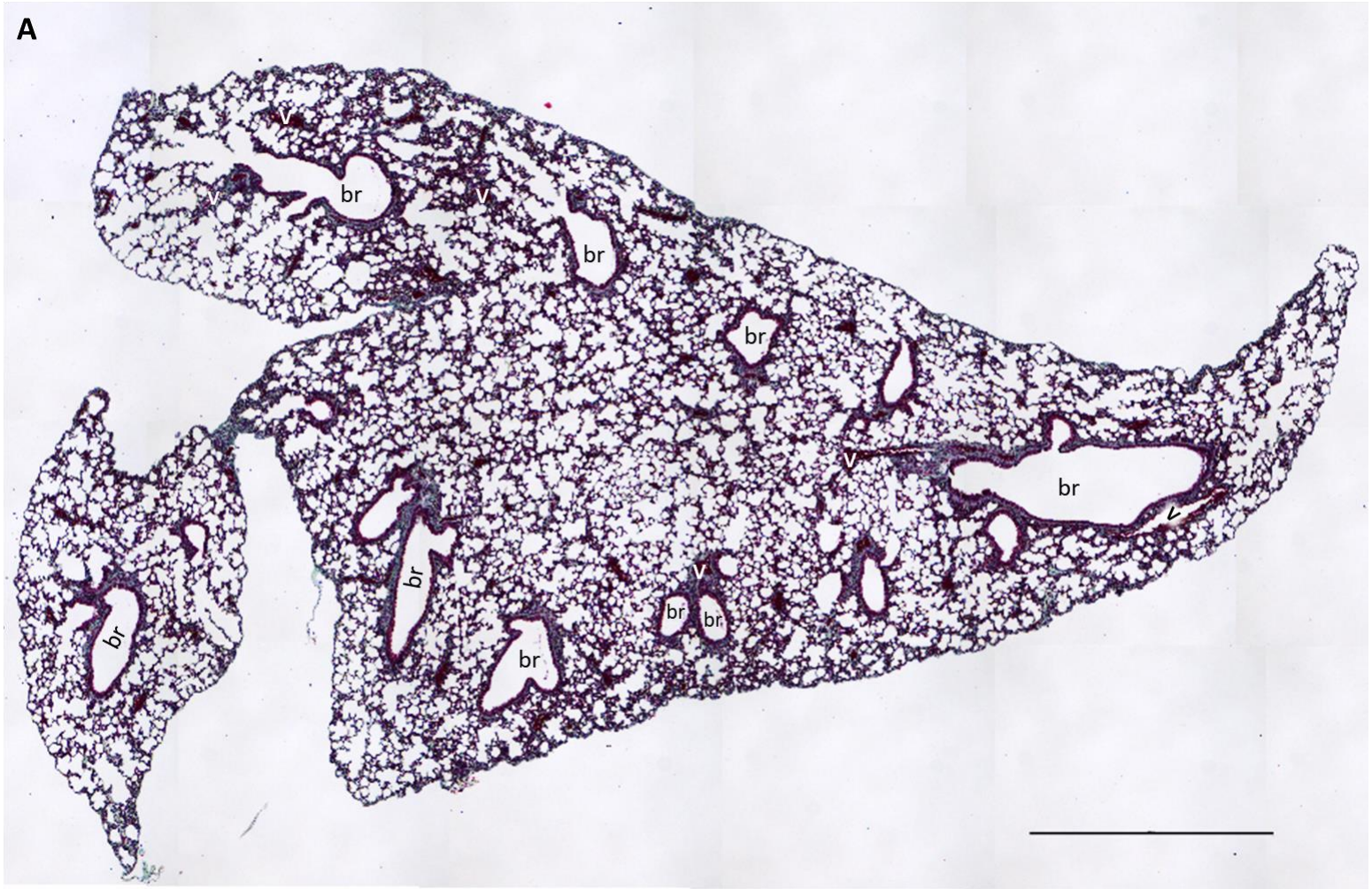
A
v
v
br
v
br
br
v
br
v
br
br
br
br
br
v
br
br

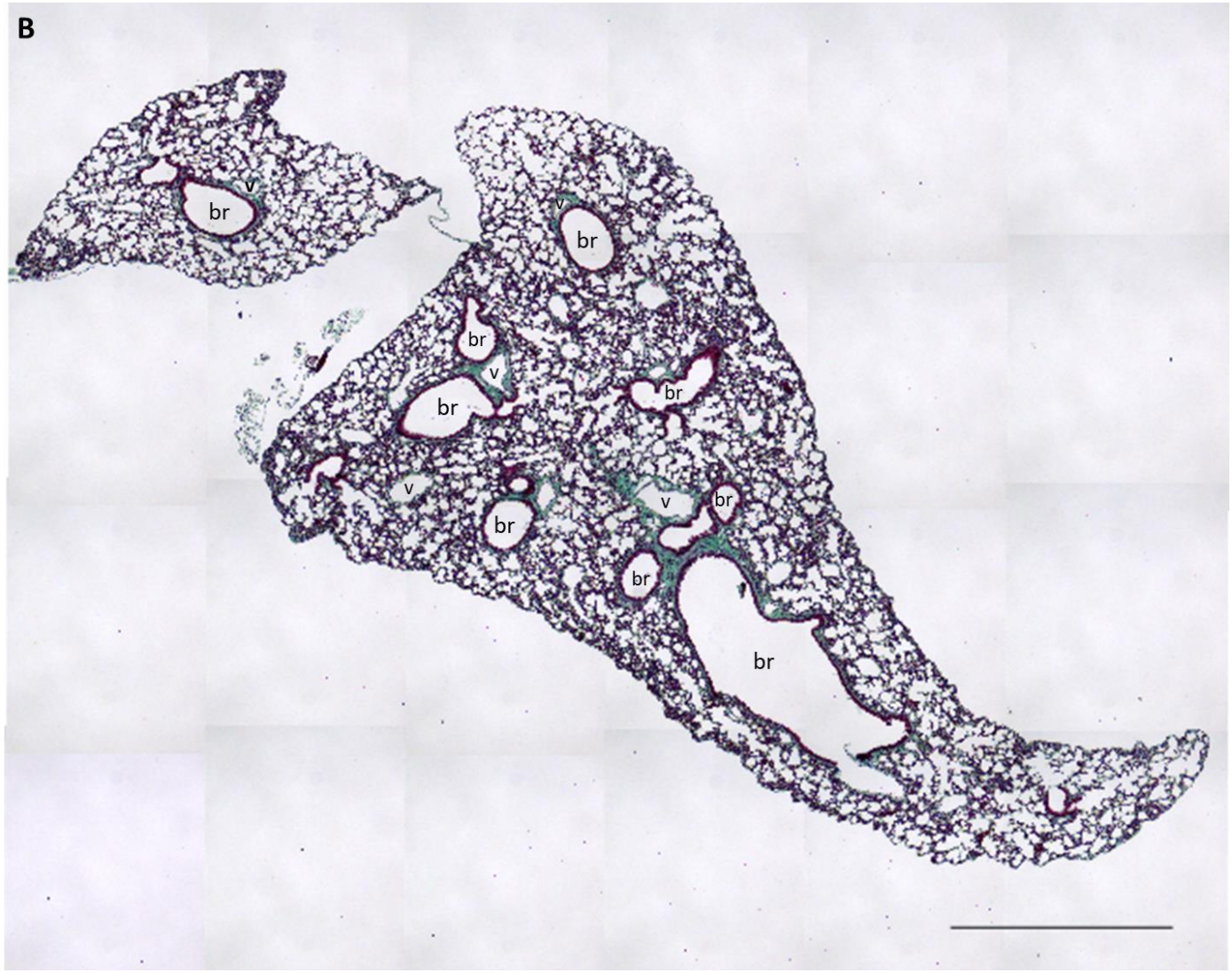
B
v
br
v
br
br
v
br
br
v
br
v
br
br
br
br

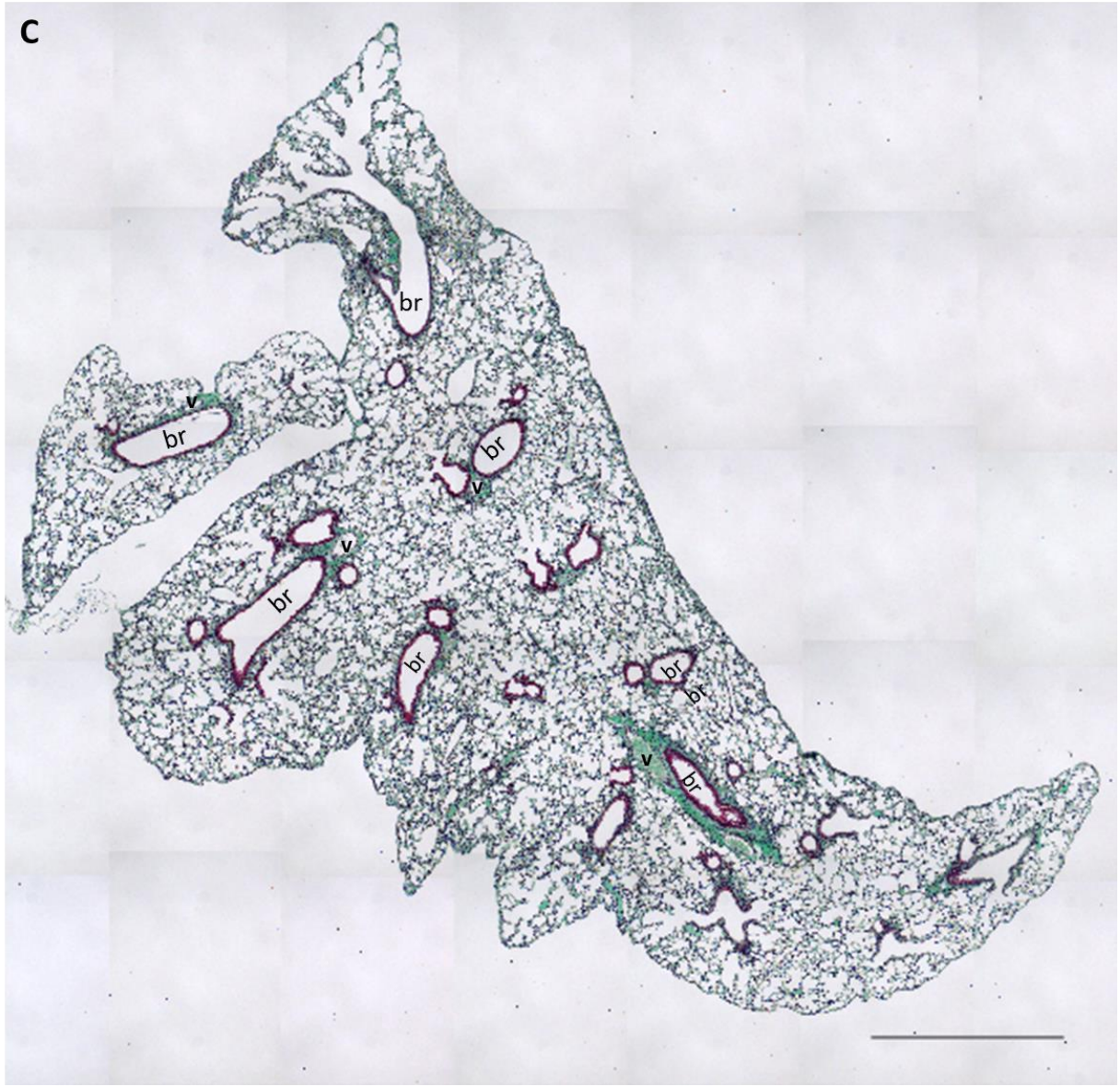
C
br
v
br
br
v
v
br
br
br
br
v
br

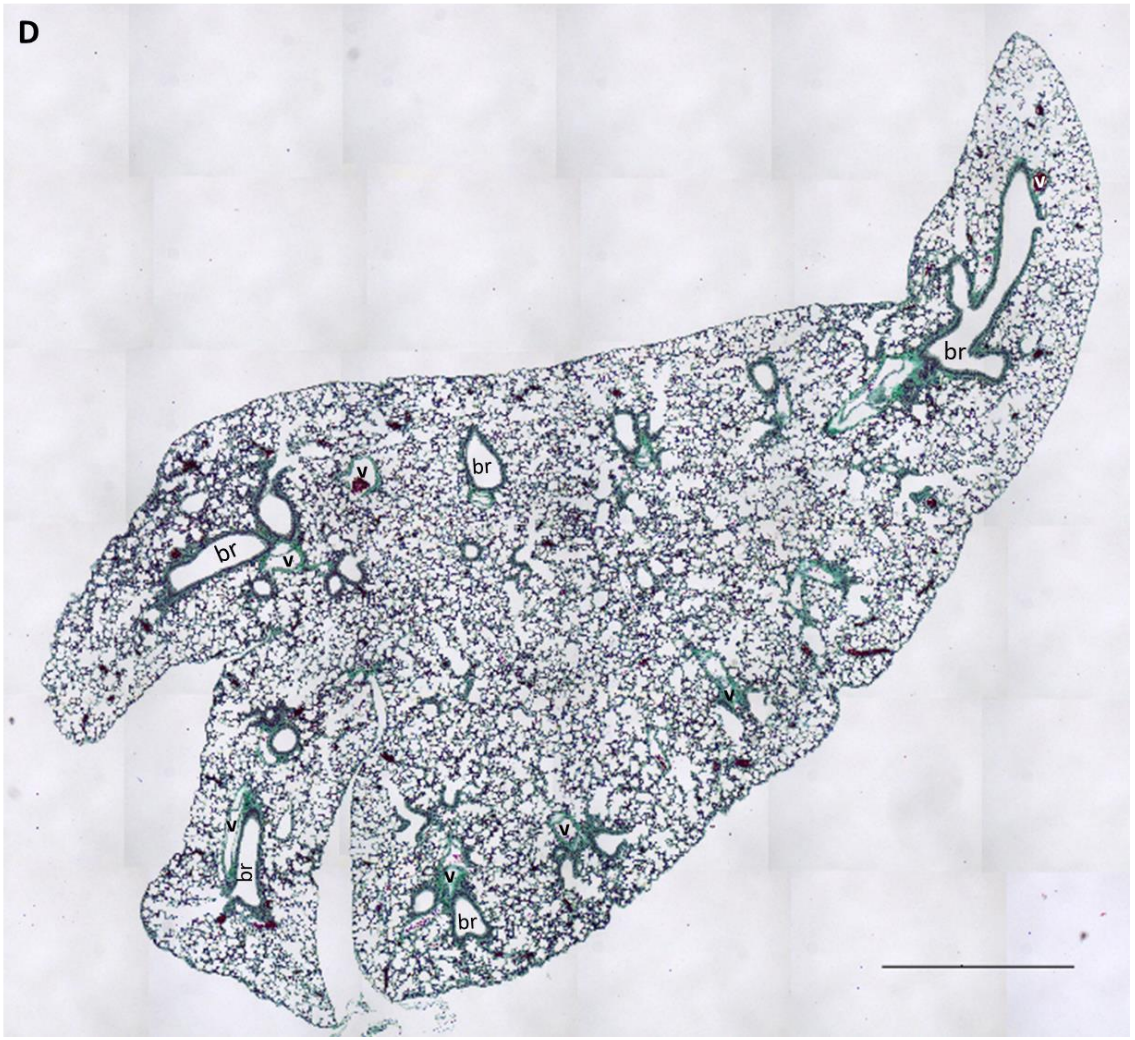

Figure 5.4. Histological evaluation of whole lung lobe samples lungs isolated from tamoxifen treated Col1α2-CCN2fl mice at 7, 14 and 28 Days using Goldner's trichrome stain. Lungs were isolated immediately after Sch1 by anaesthetic overdose and manually inflated for scanning, using a SkyScan 1272 µCT system at a resolution of 20 µm (0.25 mm aluminium filter, 0.3 ° rotation step). Lungs were processed for wax histology and stained with H & E. Anatomical features are identified as follows: a- alveoli, br- bronchioles, v- blood vessels. All images were taken at 10x magnification. A) Untreated, B) Experimental day 7, C) Experimental day 14, D) Experimental day 28. Scale bars represent 1 mm.

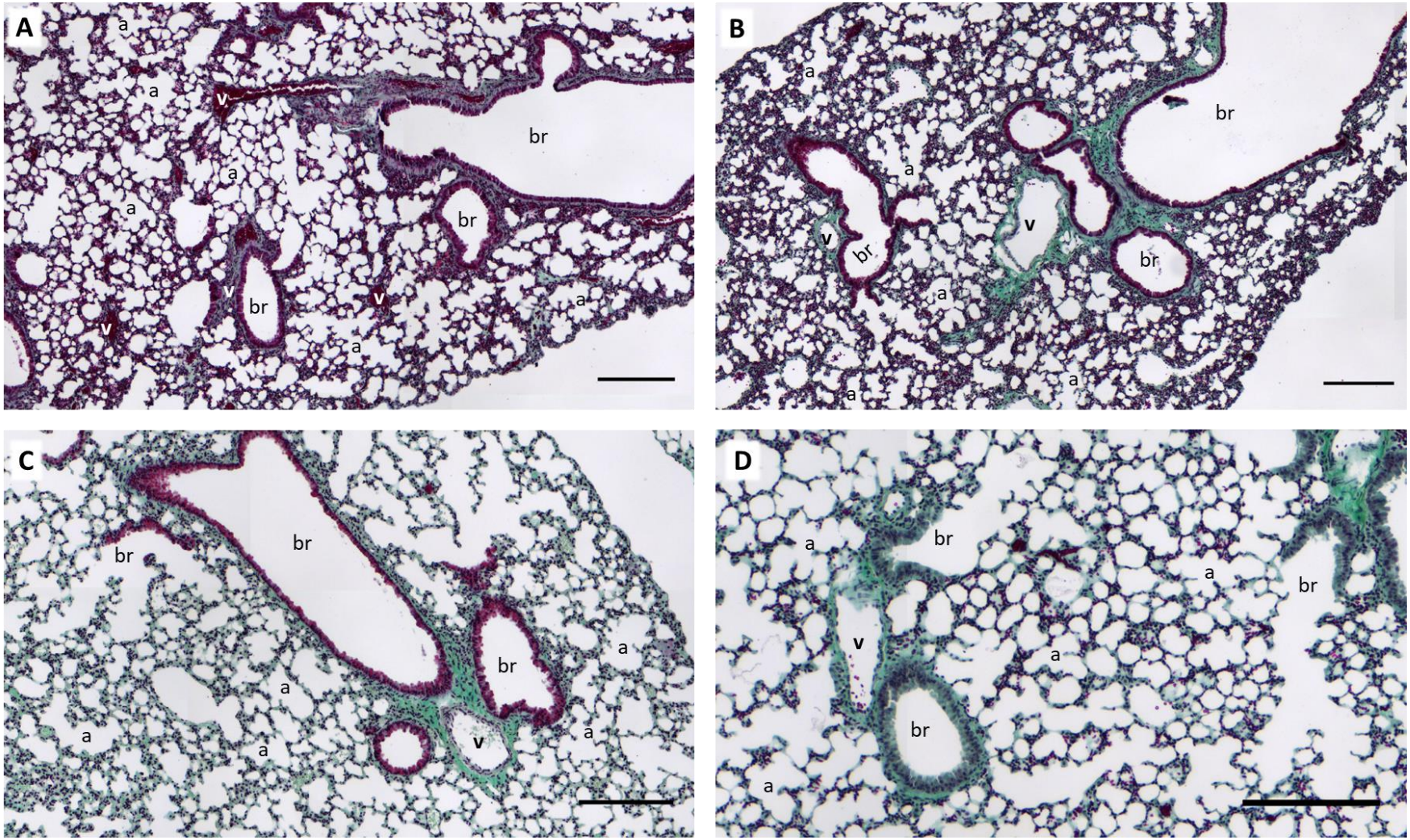

Figure 5.5. Histological evaluation of lung samples isolated from tamoxifen treated Col1α2-CCN2fl mice at 7, 14 and 28 Days using Goldner's trichrome stain. Lungs were isolated immediately after Sch1 by anaesthetic overdose and manually inflated for scanning, using a SkyScan 1272 µCT system at a resolution of 20 µm (0.25 mm aluminium filter, 0.3 ° rotation step). Lungs were processed for wax histology and stained with H & E. Anatomical features are identified as follows: a- alveoli, br- bronchioles, v- blood vessels. All images were taken at 10x magnification. A) Untreated, B) Experimental day 7, C) Experimental day 14, D) Experimental day 28. Scale bars represent 200 µm.

The gene expression levels of Collagen I (*COL1α2),* Collagen III *(COL3)* and Fibronectin E-DA (*FN-EDA)* gene transcription was quantified by PCR analysis on the remaining lobes of the lungs (Figure 5.6). These proteins are all constituents of the ECM in the lung and were selected for analysis due to their association with fibrotic lung phenotypes. Sample cycle threshold (Ct) values were normalised to untreated animals of the same background and are expressed as a fold change using the ΔΔCt method. Significance was determined using a one-way ANOVA, and Tukey's post hoc test for correction for multiple testing was performed using GraphPad Prism. *P*-values below 0.05 were considered statistically significant. Samples from male and female mice were analysed independently.

In male animals no difference in transcription of *COL1α2* and *FN-EDA* was observed at any of the experimental time points (Figure 5.6 A & C). Statistically significant increase ($P < 0.0001$) in *COL3* was observed at experimental day 7 (Figure 5.6). In female animals, Figure 5.6 D – F) statistically significant reduction ($P < 000.1$) in *COL1α2* (D) and *COL3* (E) transcription was observed at experimental day 14. At experimental day 7 a statistically significant increase in *FN-EDA* was observed ($P < 000.1$), followed by a statistically significant reduction ($P < 0.05$) at experimental day 14 (Figure 5.6, F). The ΔΔCt fold change of *FN*-EDA between 7 and 14 days was also found to be statistically significant ($P < 0.0001$), (Figure 5.6, F). These analyses showed that although no phenotype manifested at any time point, there were alterations in gene transcription of Collagen I, Collagen III and Fibronectin ED-A when CCN2 was removed from fibroblasts over a 28-day experimental period.

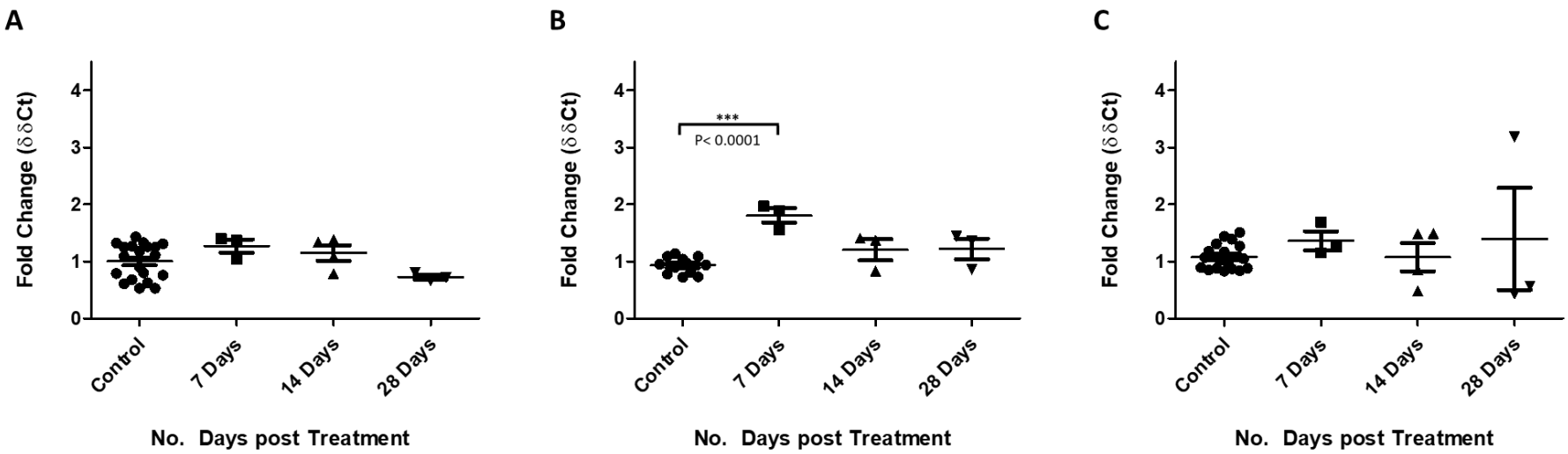
A
B
C
Fold Change (δδCt)
0
1
2
3
4
***
P< 0.0001
Control
7 Days
14 Days
28 Days
No. Days post Treatment

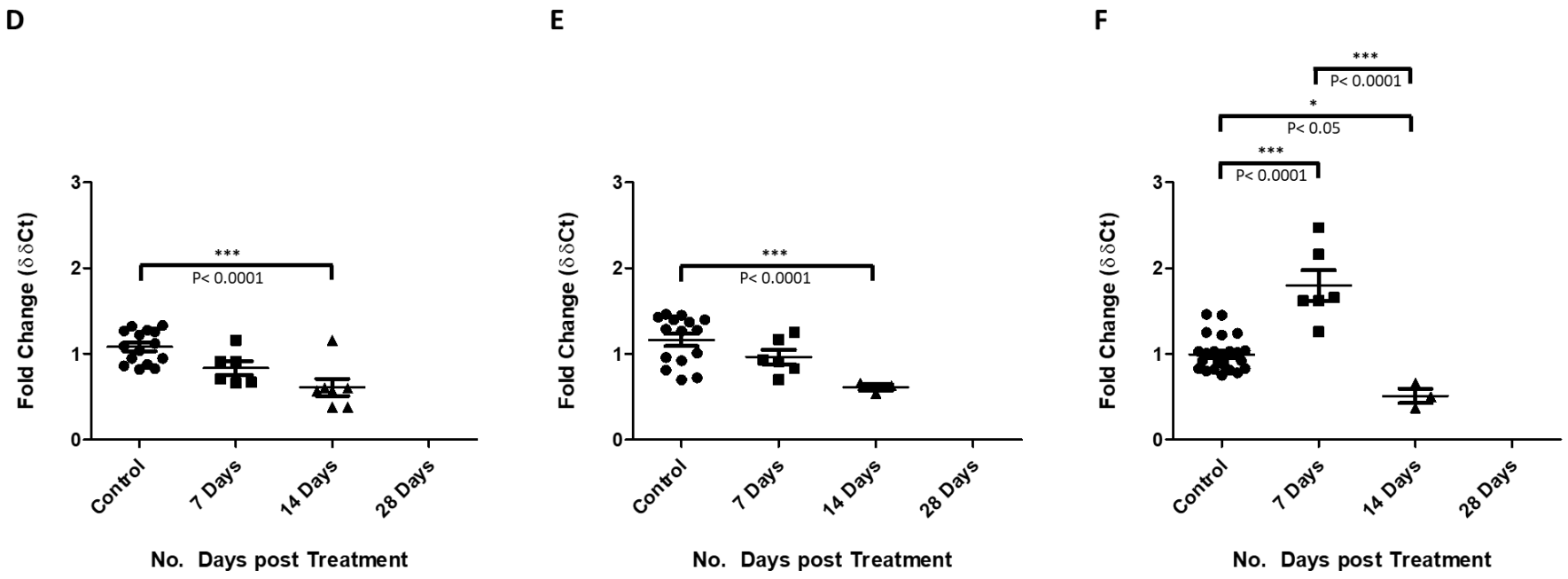

Figure 5.6. RT-qPCR analysis of COL1α2, COL3 and FN-EDA expression in lung samples isolated from tamoxifen treated Col1α2-CCN2fl mice at 7, 14 and 28 Days. ΔΔCt analysis of COL1α2 (A & D), COL3 (B & E) and FN-EDA (C & F) mRNA in double transgenic animals homozygous for CCN2 floxed gene and positive for fibroblast specific Col1α2-CreER^{T2}. (A - C) Male mice, (D - F), Female mice. RNA was extracted from whole lungs, after µCT scanning. Samples were collected on experimental days 7, 14 and 28 days. ΔΔCt fold change results are plotted, significance was determined using a one-way ANOVA, and Tukey's post hoc test. Significance and associated p-value are indicated by (*).

5.4 Investigating the effects of fibroblast specific loss of function of CCN2, in a bleomycin model of IPF using the tamoxifen-inducible double transgenic Col1α2-CCN2fl mouse line

The next series of experiments aimed to determine if the removal of CCN2 from fibroblast cells affected the fibrosis formed using the bleomycin model of IPF described in chapter 4 with Col1α2-CCN2fl double transgenic mouse line. Timepoints of 7, 14 and 28 days after bleomycin administration were investigated. Experimental day 1 was considered as 7 days after tamoxifen dosing was completed.

Male and female mice from the Col1α2-CCN2fl were aged to ≥6 weeks and administered with three I.P. 0.025 mg/g injections of tamoxifen as described in methods section 2.5.1. Tamoxifen treatment induced recombination of the CCN2 gene and ultimately caused the loss of function of CCN2 from fibroblast cells. A 7-day recovery period was required following tamoxifen treatment. Research reported in chapter 4 confirmed that this period was sufficient for CCN2 protein expression to be reduced. A single dose of bleomycin (0.375 ng/g) was then administered by OA as described in methods section 2.5.2. On experimental days 7, 14 and 28 animals were Sch1 by overdose of Pentobarbital and prepared for µCT scanning as per methods section 2.6. A single lobe was isolated after µCT scanning and processed for paraffin wax histology. The remaining lung tissue was snap frozen and RNA was extracted following the protocol in methods section 2.7.2. Littermate animals were administered the bleomycin treatment in the absence of tamoxifen for direct comparison of the extent of fibrosis at experimental timepoints. These mice are described as wild type (WT) for these results as the expression of CCN2 was unaltered. Animals where CCN2 loss of function was induced are referred to as 'CCN2 k/o'.

Visual assessment of the µCT scans (Figure 5.7) showed the expected progression for developing fibrosis in the bleomycin model across the 28-day experimental period for both tamoxifen treated and control animals. Early fibrotic focal regions were observed at 7 days (Figure 5.7, B, red arrows), numerous regions of established fibrosis at 14 days (Figure 5.7, C, red arrows), followed by apparent resolution by 28 days (Figure 5.7, D, red arrows). The extent of fibrosis identified at 14 days in CCN2 k/o lungs appeared to be reduced when compared to WT lungs (Figure 5.7 C & D, red arrows).

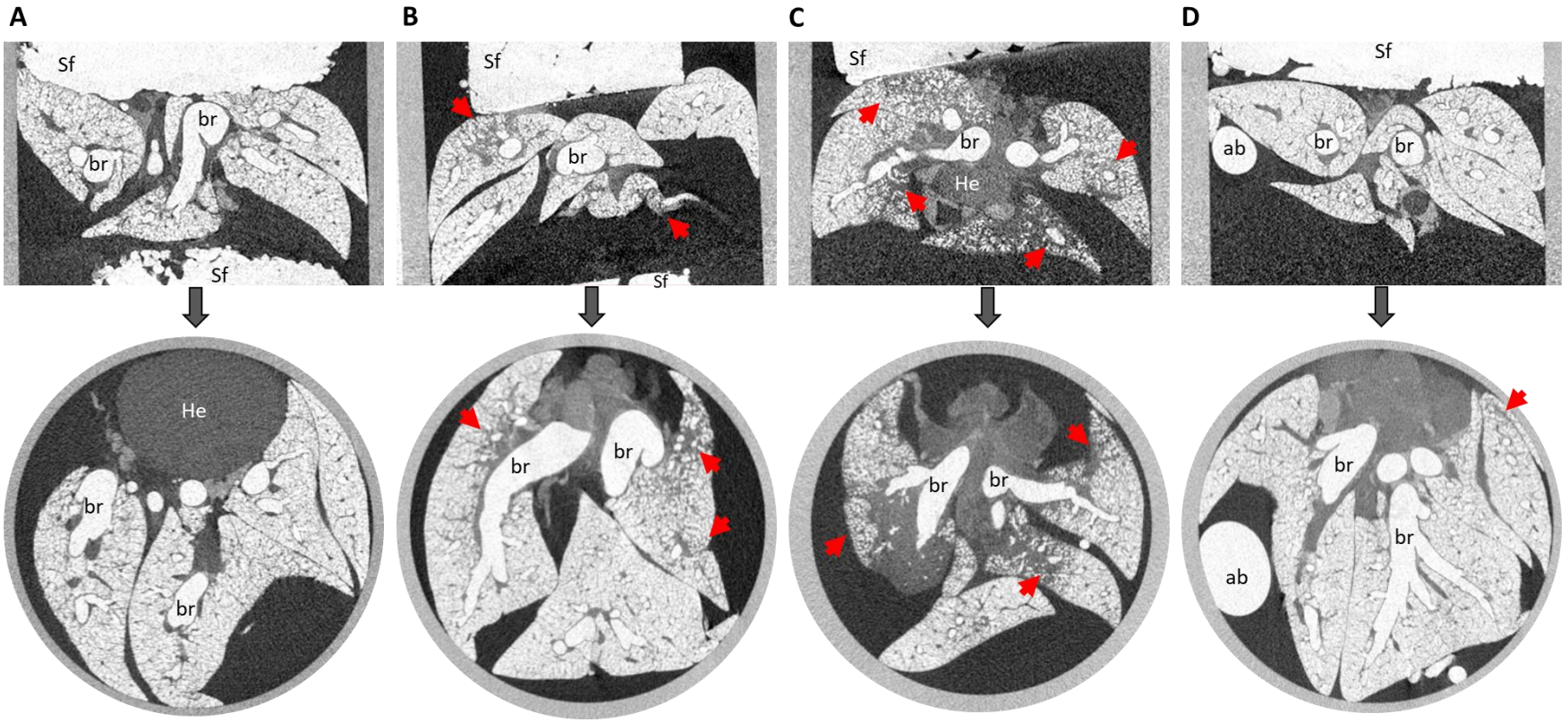
A
Sf
br
br
Sf
He
br
br
B
Sf
br
Sf
br
br
C
Sf
br
He
br
br
D
Sf
ab
br
br
br
br
ab

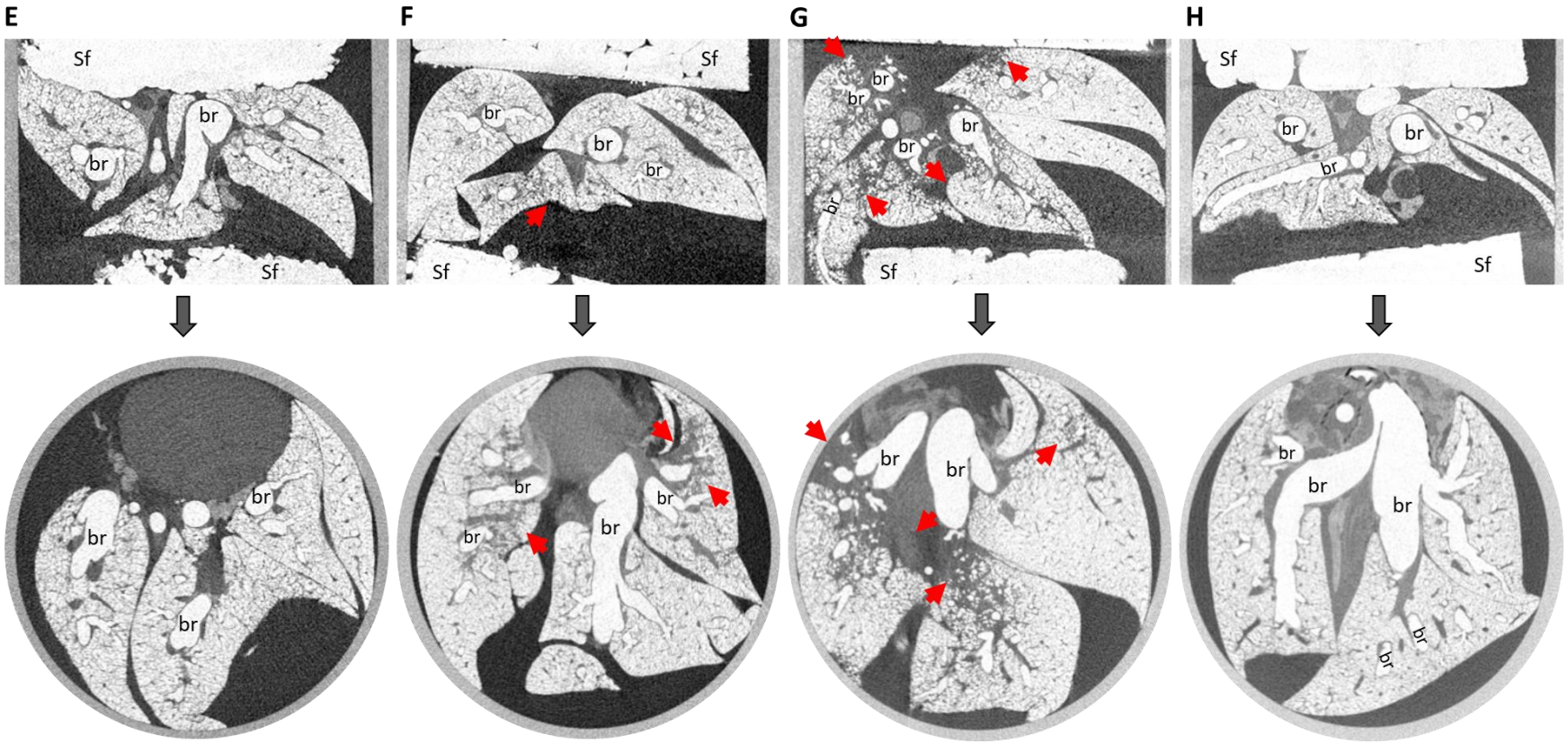

Figure 5.7. µCT scans of unfixed, inflated mouse lungs isolated from tamoxifen and bleomycin treated Col1α2-CCN2fl mice at 7, 14 and 28 Days. Animals were administered 3x doses of tamoxifen at 0.025 ng/g. A week's recovery period was given before experimental day 1. Animals were Sch1 by overdose of pentobarbital, and the lungs manually inflated prior to extraction. Isolated lungs were then suspended between pieces of Styrofoam (sf) in 3 – 5 % (wt / vol) KI contrast agent for µCT scanning. Lungs were scanned using a SkyScan 1272 µCT system at a resolution of 20 µm (0.25 mm aluminium filter, 0.3 ° rotation step). Images were reconstructed using Skyscan Nrecon software and visualised using DataViewer. Anatomical features are identified by the following: br- bronchioles, He- heart. Air bubbles are marked as-ab. Representative images from whole lung 3D scans are shown using DataViewer software. A – D) Example scans from mice treated with bleomycin only, A) Untreated, B) Experimental day 7, C) Experimental day 14, D) Experimental day 28. E-H) Example scans from mice treated with tamoxifen before bleomycin treatment. E) Untreated, F) Experimental day 7, G) Experimental day 14, H) Experimental day 28. Red arrows indicate regions of fibrosis.

Closer examination of the morphology of the lungs was carried out by histological analysis. A lobe from experimental lungs was isolated immediately after µCT scanning and processed for histology following the protocol described in methods section 2.8. Sections of 5 µm were stained with H & E, or Goldner's trichrome stains. Protocols can be found in methods section 2.8.

H & E stain was used to identify anatomical features of the lung including the bronchioles, alveoli and blood vessels. Representative images taken at 10x magnification are shown in (Figure 5.8), scale bars represent 200 µm. Regions identified as fibrotic, from visual assessment of the µCT scans, were found to correspond to tissue deposits in H & E stained sections (Figure 5.8, black arrows). In sections from experimental day 7 (Figure 5.8, B & E) fibrotic foci were observed (black arrows) in lungs where CCN2 loss of function was induced in fibroblasts and in WT lungs. At 14 days, large regions of tissue deposits were identified in both WT and CCN2. These were more extensive than those observed at 7 days (Figure 5.8). Examination of sections at 28 days revealed some regions of fibrosis remained (Figure 5.8, D & G). These were not as frequent or extensive as those seen at day 14. Increase in tissue volume of the section was associated with an altered morphology of alveoli. A thickening in the cells lining the alveoli was observed in regions adjacent to tissue deposits (Figure 5.8). Staining with Goldner's Trichrome (Figure 5.9) indicated that these tissue deposits consisted of collagen, as corresponding regions of sections stained green. An increase in green staining was observed in corresponding patterns those described for H & E staining. Regions of fibrosis were closely associated with the bronchioles, with tissue deposition observed and fibrotic foci formation occurring most frequently in the immediate vicinity of the bronchioles. Increased nuclear staining was observed in all lungs that were treated with bleomycin when compared to the untreated lung (Figure 5.8 and Figure 5.9). This was observed at the greatest extent in lungs isolated at experimental day 14 in tissue deposits (black arrows) surrounding bronchioles.

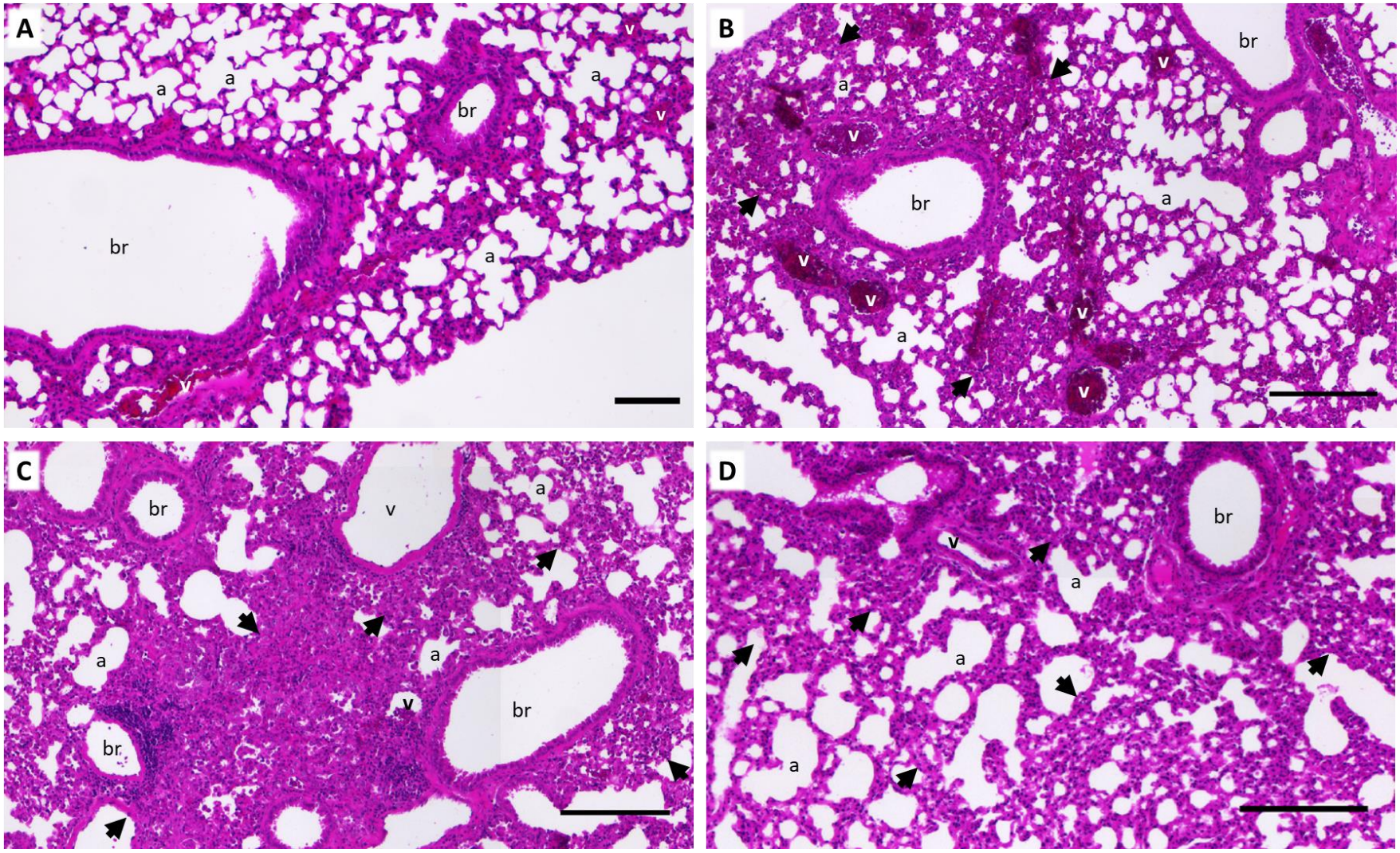
A
a
a
br
v
a
v
br
a
v
B
br
a
v
v
br
a
v
v
v
a
v
C
br
v
a
a
a
v
br
br
D
br
v
a
a
a

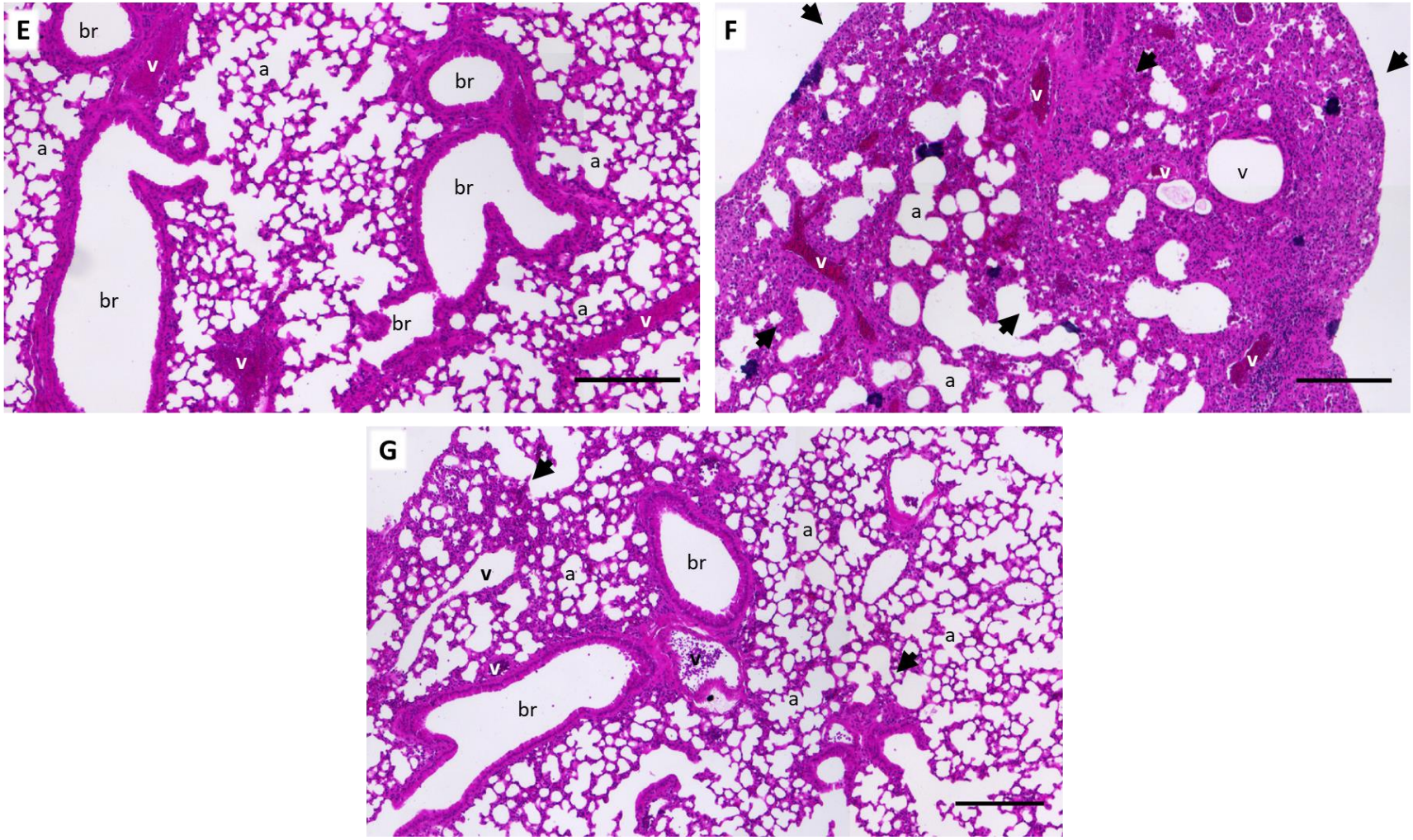

Figure 5.8. Histological evaluation of lung samples isolated from Col1α2-CCN2fl mice at 7, 14 and 28 days post tamoxifen and bleomycin treatment using H & E stain. Lungs were isolated immediately after Sch1 by anaesthetic overdose and manually inflated for scanning, using a SkyScan 1272 µCT system at a resolution of 20µm (0.25mm aluminium filter, 0.3° rotation step). Lungs were processed for wax histology and stained with H & E. Anatomical features are identified as follows: a- alveoli, br- bronchioles, v- blood vessels, black arrows indicate regions of fibrosis. All images were taken at 10x magnification. A) Untreated, B - D) Bleomycin treated only, Experimental days 7, 14, and 28 respectively. E - G) Tamoxifen followed by bleomycin treatments, Experimental days 7, 14, and 28 respectively. Scale bars represent 200 µm.

Goldner's trichrome stain was used to identify collagen deposits from muscular tissues. Cell nuclei appear black, cytoplasm - red and collagen - green. Images were taken at 10x magnification (Figure 5.9), scale bars represent 200 µm. Anatomical features of the lung are identified in the figure as: bronchioles (br), alveoli (a) and blood vessels (v). Collagen is a major constituent of the pulmonary interstitium and major structures including the bronchioles, blood vessels, alveoli and bronchioles. Therefore, green staining of these structures was anticipated and seen in all lungs (Figure 5.9). Red staining inside bronchioles demonstrates the presence of the epithelial cells lining these structures. The same morphology as described for the H & E stained images was noted, with the additional comment that tissue deposits were stained green, supporting the notion that these are fibrotic tissue deposits of ECM.

In sections from experimental day 7 (Figure 5.9, B & E) fibrotic foci exhibited similar staining patterns, intensity and localisation (red arrows) in lungs from CCN2 k/o animals compared to WT lungs. At 14 days, large regions of tissue deposits were identified in both WT and CCN2 (Figure 5.9 C & F). These were more extensive than those observed at 7 days, and fibrotic foci were observed forming in close proximity to bronchioles. Sections from CCN2 k/o animals appeared to show a subtle reduction in staining and instance of foci formation (Figure 5.9, F). Examination of sections at 28 days identified some regions of fibrosis remained (Figure 5.9, D & G, red arrows). These were not as frequent or extensive as those seen at day 14. Resolution of fibrosis was apparent in sections from both normal and transgenic animals at 28 days. No significant differences in staining were noted at any time point when directly comparing fibroblast CCN2 k/o with WT.

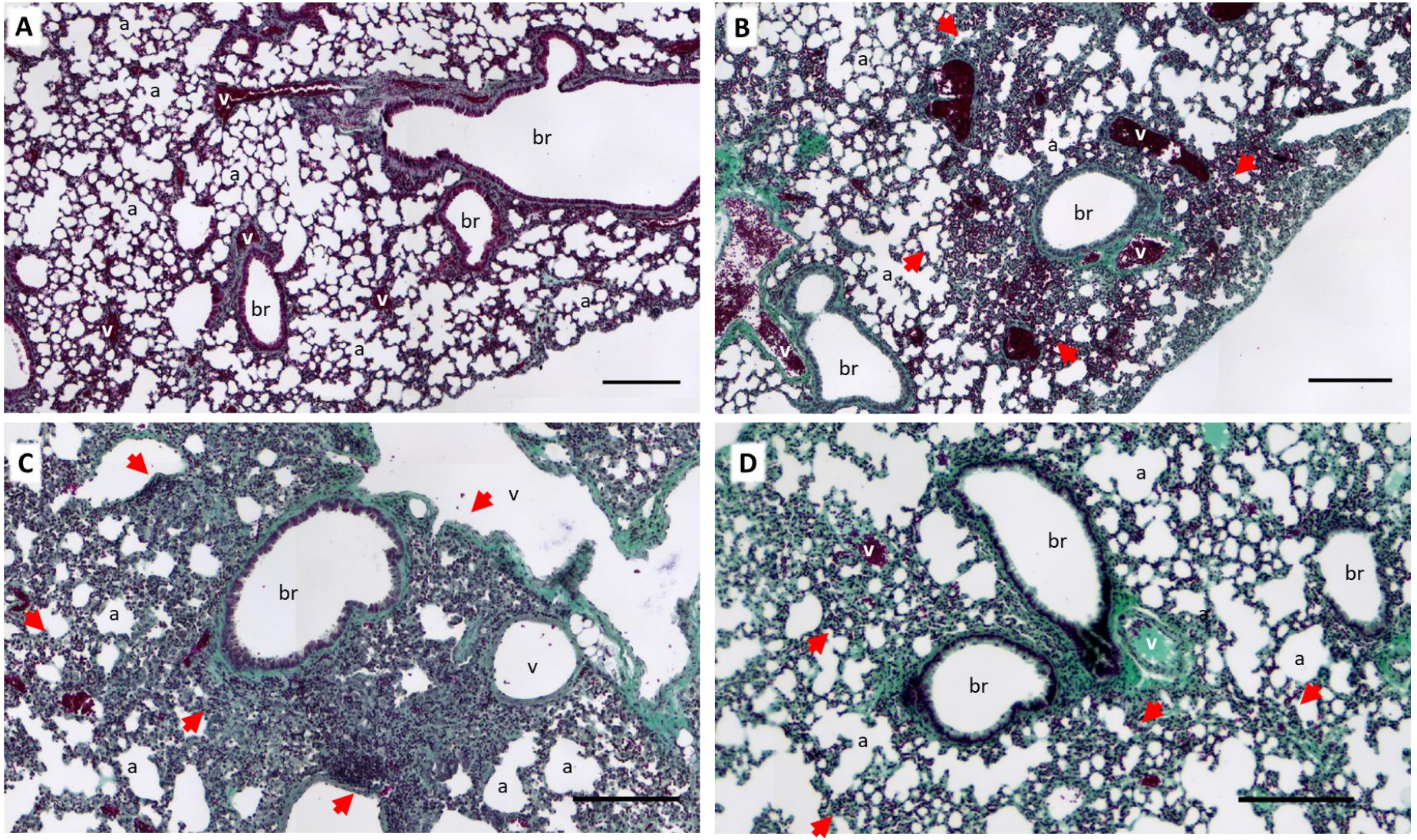
A
a
a
v
br
a
a
br
v
v
br
v
a
v
a
B
a
a
v
br
v
a
v
br
C
v
br
a
v
a
a
a
D
a
br
v
br
a
v
a
br
a

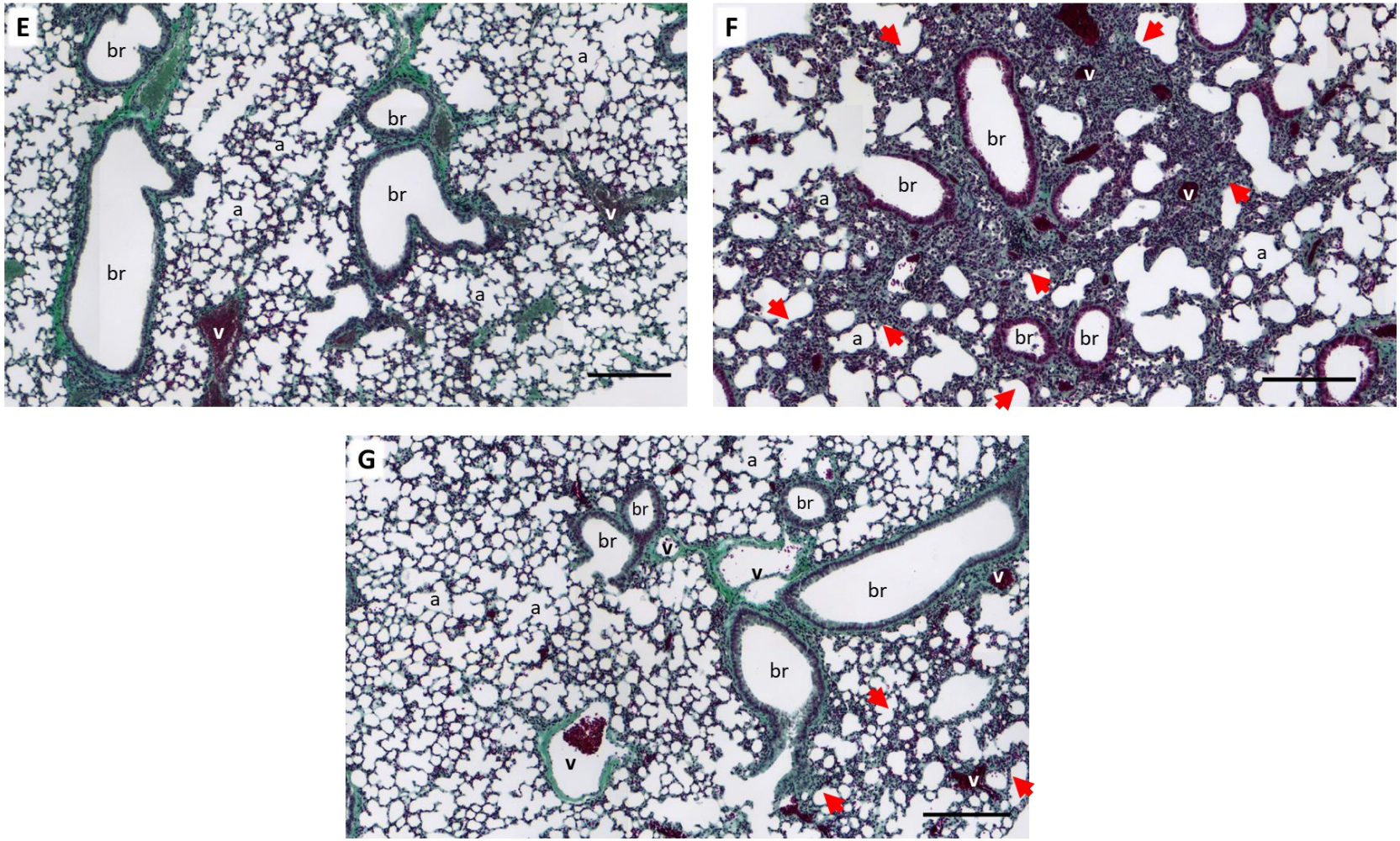

Figure 5.9. Histological evaluation of lung samples isolated from Col1α2-CCN2fl mice at 7, 14 and 28 days post tamoxifen and bleomycin treatment using Goldner's trichrome stain. Lungs were isolated immediately after Sch1 by anaesthetic overdose and manually inflated for scanning, using a SkyScan 1272 µCT system at a resolution of 20 µm (0.25 mm aluminium filter, 0.3 ° rotation step). Lungs were processed for wax histology and stained with H & E. Anatomical features are identified as follows: a- alveoli, br- bronchioles, v- blood vessels, red arrows indicate regions of fibrosis. All images were taken at 10 x magnification. A) Untreated, B - D) Bleomycin treated only, Experimental days 7, 14, and 28 respectively. E - G) Tamoxifen followed by bleomycin treatments, Experimental days 7, 14, and 28 respectively. Scale bars represent 200 µm.

Collagen I (*COL1α2),* Collagen III *(COL3)* and Fibronectin – EDA (*FN-EDA)* gene transcription was examined by qPCR analysis of the remaining lobes of the lungs (Figure 5.10). These proteins are all constituents of the ECM in the lung and were selected for analysis due to their association with fibrotic lung phenotypes. Sample cycle threshold (Ct) values were normalised to untreated animals of the same background and are expressed as a fold change using the ΔΔCt method. Significance was determined using a one-way ANOVA, and Tukey's post hoc test for correction for multiple testing was performed using GraphPad Prism. *P*-values below 0.05 were considered statistically significant. Samples from male and female mice were analysed independently.

Analysis of WT male animals (Figure 5.10, A & C), identified a statistically significant upregulation of *COL1α2, COL3* and *FN-EDA* transcription between control and bleomycin treated lungs at 14 days ($P < 0.0001$). No statistically significant difference in the ΔΔCt fold change was observed between control and WT bleomycin treated lungs at 28 days. The reduction in transcription (decrease in mean ΔΔCt) of *COL1α2, COL3* and *FN-EDA* between 14 and 28 days was found to be statistically significant ($P < 0.05$).

Analysis of CCN2 k/o male animals (Figure 5.10 D - F), identified a statistically significant upregulation of *COL1α2* (D)*,* transcription between control and bleomycin treated lungs at 7 ($P < 0.05$), 14 ($P < 0.0001$) and 28 days ($P < 0.0001$). Analysis of *COL3* transcription (Figure 5.10, E) identified a statistically significant upregulation of *COL3,* transcription between control and bleomycin treated lungs at 7 ($P < 0.0001$), 14 ($P < 0.0001$) and 28 days ($P < 0.0001$). Analysis of *FN-EDA* transcription identified a statistically significant increase in ΔΔCt between control and bleomycin treated lungs at 7 ($P < 0.01$), 14 ($P < 0.0001$) and 28 days ($P < 0.01$) (Figure 5.10, F). The change in transcription of *COL1α2, COL3* and *FN-EDA* between experimental timepoints was not found to be statistically significant.

Analysis of WT female animals (Figure 5.11, A - C), identified no statistically significant changes in transcription of *COL1α2* (A) or *COL3* (B). A statistically significant upregulation of *FN-EDA* transcription was observed between control and bleomycin treated lungs at 7 days ($P < 0.0001$) and 14 days ($P < 0.05$) (Figure 5.11, C). The reduction in transcription of *FN-EDA* between 7 and 14 days, and 7 and 28 days was also found to be statistically significant ($P < 0.01$, $P < 0.01$) (Figure 5.11, F). No statistically significant difference in *FN-EDA* transcription was observed between 14 and 28 days (Figure 5.11, F).

Analysis of CCN2 k/o female animals (Figure 5.11, D - F), identified no statistically significant differences in *COL1α2,* transcription between control and bleomycin treated lungs (Figure

5.11, D). A statistically significant decrease in transcription of *COL1α2* was observed between 7 and 28 days ($P < 0.05$) (Figure 5.11, D). No statistically significant differences were observed between other time points (Figure 5.11, D). No statistically significant differences were observed at any time point for *COL3* transcription (Figure 5.11, E). Analysis of *FN-EDA* transcription (Figure 5.11, F) identified a statistically significant upregulation of *FN-EDA* transcription between control and bleomycin treated lungs at 7 ($P < 0.01$), 14 ($P < 0.01$) and 28 days ($P < 0.05$). identified a statistically significant upregulation of *COL1α2,* transcription between control and bleomycin treated lungs at 7 ($P < 0.01$), 14 ($P < 0.0001$) and 28 days ($P < 0.01$). The change in transcription of *FN-EDA* between experimental timepoints was not found to be statistically significant.

The average ΔΔCt values are presented in (Table 5.1). In both male and female mice where CCN2 was removed from fibroblasts prior to bleomycin treatment, the average ΔΔCt value for each gene was reduced when compared to a WT at 14 days. At 28 Days the ΔΔCt values for females are similar, with the exception of *FN-EDA,* where CCN2 k/o shows a slight increase in ΔΔCt compared to WT counterparts. In male mice CCN2 removal from fibroblasts resulted in a higher ΔΔCt value at 28 days than observed for WT mice. In male mice the highest fold increases in gene transcription were observed at the 14-day time point. In female mice the highest fold increases in gene transcription were observed at the 14-day time point.

Based on the fibrotic phenotype and transcriptional changes identified in animals collected at 14 days, it was decided that this timepoint would be used to compare the effects of a ubiquitous knock out of CCN2 with the fibroblast specific knock out of CCN2, in the bleomycin model of IPF.

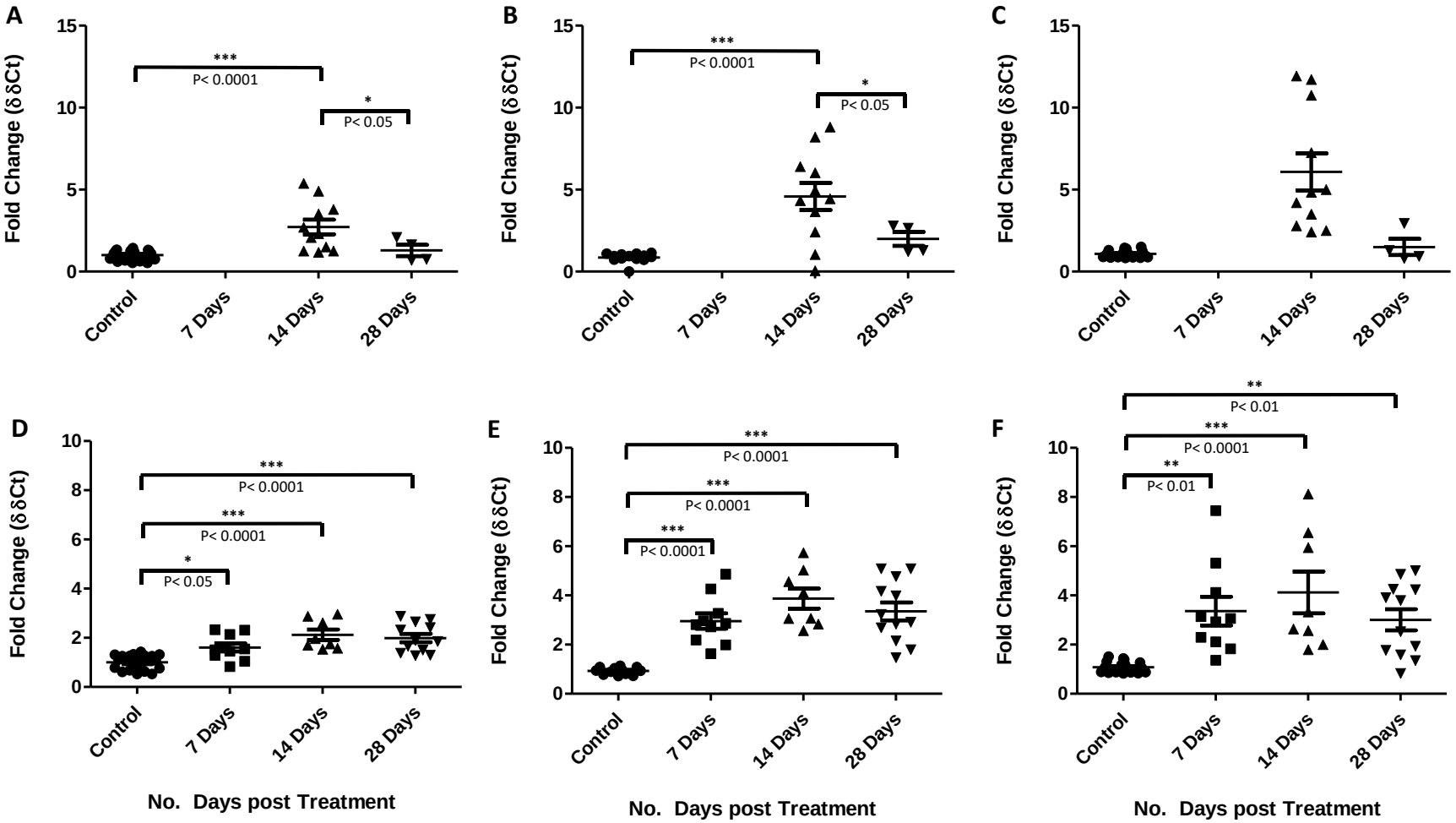

Figure 5.10. RT-qPCR analysis of COL1α2, COL3 and FN-EDA expression in lung samples isolated from tamoxifen and bleomycin treated male Col1α2-CCN2fl mice at 7, 14 and 28 days. ΔΔCt analysis of COL1α2 (A & D), COL3 (B & E) and FN-EDA (C & F) mRNA in double transgenic animals homozygous for CCN2 floxed gene and positive for fibroblast specific Col1α2-CreER^{T2}. (A - C) Bleomycin treated only, (D - F), Tamoxifen and bleomycin treated mice. RNA was extracted from whole lungs, after µCT scanning. Samples were collected on experimental days 7, 14 and 28 days. ΔΔCt fold change results are plotted, significance was determined using a one-way ANOVA, and Tukey's post hoc test. Significance and associated p-value are indicated by (*).

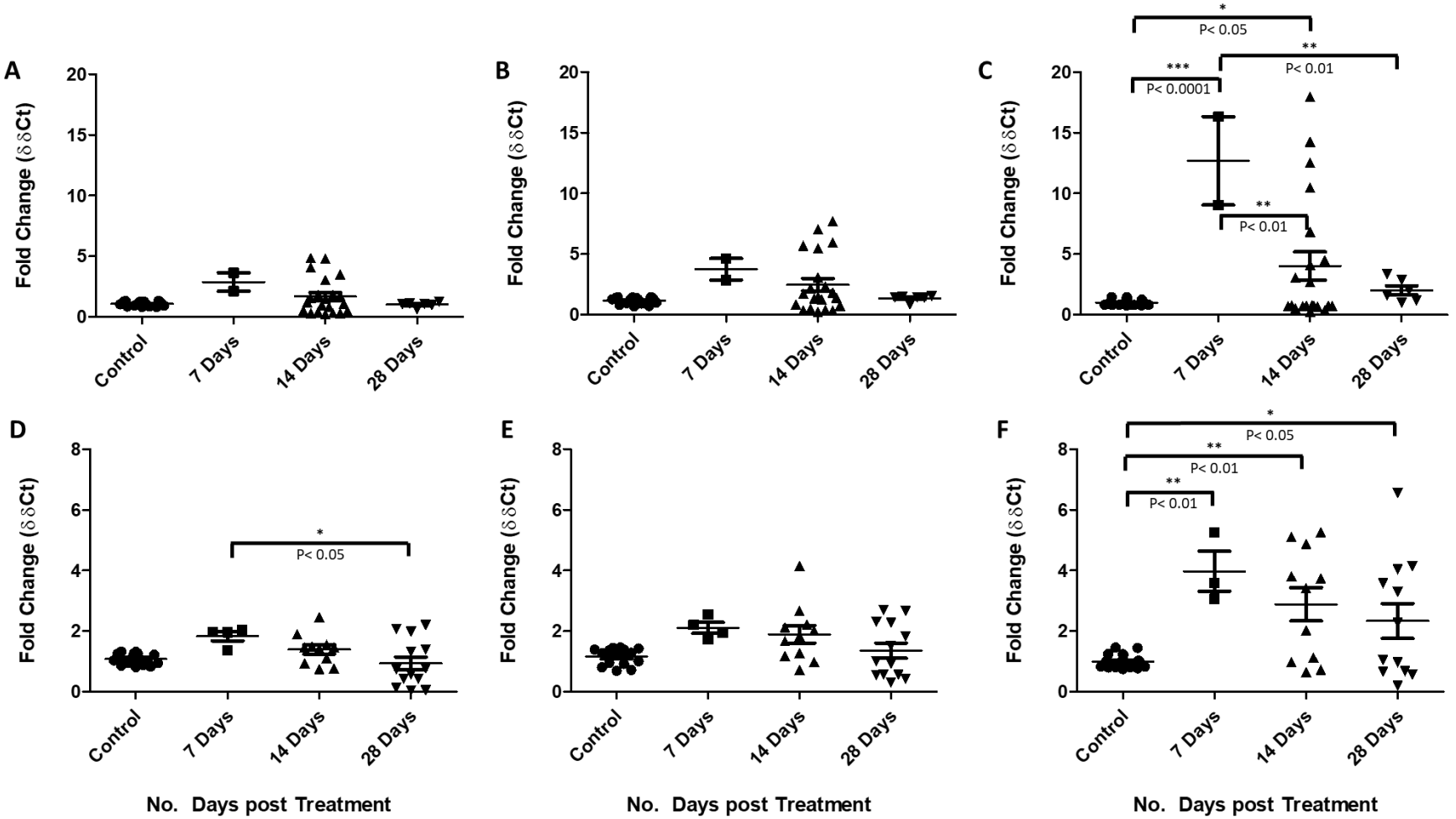

Figure 5.11. RT-qPCR analysis of COL1α2, COL3 and FN-EDA expression in lung samples isolated from tamoxifen and bleomycin treated Female Col1α2-CCN2fl mice at 7, 14 and 28 days. ΔΔCt analysis of COL1α2 (A & D), COL3 (B & E) and FN-EDA (C & F) mRNA in double transgenic animals homozygous for CCN2 floxed gene and positive for fibroblast specific Col1α2-CreER^{T2}. (A - C) Bleomycin treated only, (D - F), Tamoxifen and bleomycin treated mice. RNA was extracted from whole lungs, after µCT scanning. Samples were collected on experimental days 7, 14 and 28 days. ΔΔCt fold change results are plotted, significance was determined using a one-way ANOVA, and Tukey's post hoc test. Significance and associated p-value are indicated by (*).

Table 5.1. Summary table of mean ΔΔCt values COL1α2, COL3 and FN-EDA gene expression. Lung samples were isolated from tamoxifen and bleomycin treated Col1α2-CCN2fl mice (FB CCN2 k/o) and bleomycin alone treated mice (WT) at 7, 14 and 28 Days after bleomycin administration. The number of animals in each treatment group (n =) and mean ΔΔCt fold change is shown for each timepoint.

Gene of interest	Mouse strain	7 Days			14 Days			28 Days		
		n =	Avg. ΔΔCt	Std. Dev	n =	Avg. ΔΔCt	Std. Dev	n =	Avg. ΔΔCt	Std. Dev
COL I	WT	-	-	-	11	3	1.50	4	1.29	0.6900
	FB CCN2 k/o	10	1.61	0.51	8	2	0.60	12	1.99	0.59
COL III	WT	-	-	-	11	5	2.74	4	1.99	0.85
	FB CCN2 k/o	10	2.96	0.15	8	4	1.16	12	3.35	1.26
FN-EDA	WT	-	-	-	11	6	3.73	4	1.50	0.99
	FB CCN2 k/o	10	3.36	1.84	8	4	2.40	12	3.01	1.49

Female

Gene of interest	Mouse strain	7 Days			14 Days			28 Days		
		n =	Avg. ΔΔCt	Std. Dev	n =	Avg. ΔΔCt	Std. Dev	n =	Avg. ΔΔCt	Std. Dev
COL I	WT	4	2.88	1.08	11	1.69	1.50	13	1.02	0.20
	FB CCN2 k/o	2	1.84	0.31	21	1.40	0.50	6	0.94	0.78
COL III	WT	2	3.75	1.26	21	2.47	2.38	6	1.37	0.26
	FB CCN2 k/o	4	2.11	0.36	11	1.90	0.95	13	1.36	0.90
FN-EDA	WT	2	12.69	5.16	21	4.01	5.30	6	2.00	0.94
	FB CCN2 k/o	3	3.98	1.14	11	2.89	1.83	12	2.34	1.98

5.5 Comparing the effects of fibroblast specific loss of function of CCN2, with a ubiquitous loss of function of CCN2 in a bleomycin model of IPF using the tamoxifen-inducible double transgenic Col1α2-CCN2fl and ROSA-CCN2fl mouse line

The subsequent series of experiments aimed to determine if there was a differential response in fibrosis formation when loss of function of CCN2 was induced in a fibroblast specific (Col1α2-CCN2fl) or ubiquitous (ROSA-CCN2fl) manner, prior to the administration of bleomycin. A timepoint of 14 days after bleomycin administration was investigated. Experimental day 1 was considered as 7 days after tamoxifen dosing was completed.

Male and female mice from the ROSA-CCN2fl mouse colony were aged to ≥6 weeks and administered three I.P. 0.025 mg/g injections of tamoxifen as described in methods section 2.5.1. Tamoxifen treatment induced recombination of the CCN2 gene and ultimately caused the loss of function of CCN2 from all cells (ROSA-CCN2fl). A 7-day recovery period was required following tamoxifen treatment. Research reported in chapter 4 confirmed that this period was sufficient for CCN2 protein expression to be completely stopped. A single dose of bleomycin (0.375 ng/g) was then administered by OA as described in methods section 2.5.2. On experimental day 14 animals were Sch1 by overdose of Pentobarbital and prepared for µCT scanning as per methods section 2.6. A single lobe was isolated after µCT scanning and processed for paraffin wax histology. The remaining lung tissue was snap frozen and RNA was extracted following the protocol in methods section 2.7.2. Littermate animals were administered the bleomycin treatment in the absence of tamoxifen for direct comparison of the extent of fibrosis at 14 days where CCN2 activity was unmodified.

The results from these experiments were compared to the previously described results in animals where CCN2 loss of function was induced in fibroblasts. Where loss of function of CCN2 was induced in fibroblasts prior to bleomycin administration, animals are referred to as ‘Fb k/o’ (Col1α2-CCN2fl double transgenic line). Animals where CCN2 loss of function was induced in all cells prior to bleomycin administration are referred to as ‘Ub k/o’ (ROSA-CCN2fl double transgenic line).

Visual comparison of the µCT scans (Figure 5.12) showed no difference in phenotype of WT animals from Col1α2-CCN2fl (A) and ROSA-CCN2fl (E) double transgenic mouse lines. The response to bleomycin in WT animals was not observed to be different between Col1α2-CCN2fl (C) and ROSA-CCN2fl (G) double transgenic mouse lines. No difference in phenotype between WT and Fb k/o mice was observed when loss of function of CCN2 was induced without subsequent challenge with bleomycin (Figure 5.12, B). In Ub k/o animals where loss

of function of CCN2 was induced without subsequent challenge with bleomycin small regions of fibrosis were observed in subpleural regions of the lungs (Figure 5.12, F, red arrows). The extent of fibrosis identified at 14 days in Fb k/o lungs (Figure 5.12, D, red arrows) appeared to be reduced when compared to WT lungs (Figure 5.12, C & G). The µCT scans of Ub k/o mice (Figure 5.12, H) showed far more extensive fibrosis than both WT and Fb k/o mice (Figure 5.12, C, D & G). Large dense regions of tissue were observed in the lungs, accompanied by a loss of identifiable anatomical features excluding the bronchioles. Very few regions of suspected functional tissue could be identified (Figure 15.12, H, green arrows).

H & E stain was used to identify anatomical features of the lung including the bronchioles, alveoli and blood vessels. Representative images taken at 10x magnification are shown in (Figure 5.13), scale bars represent 200 µm. Regions identified as fibrotic, from visual assessment of the µCT scans, were found to correspond to tissue deposits in H & E stained sections (Figure 5.13, black arrows). Regions of fibrosis (black arrows) were closely associated with the bronchioles, with tissue deposition observed and fibrotic foci formation occurring most frequently in the immediate vicinity of the bronchioles. Increased nuclear staining was observed in all lungs that were treated with bleomycin (Figure 5.13, C, D, G & H) when compared to the untreated lung (Figure 5.13 A). Tissue samples from Ub k/o mice (Figure 5.13, H) confirmed that the morphology identified in the µCT scan (Figure 5.12, H) was accurately represented as tissue deposition was extensive in these sections.

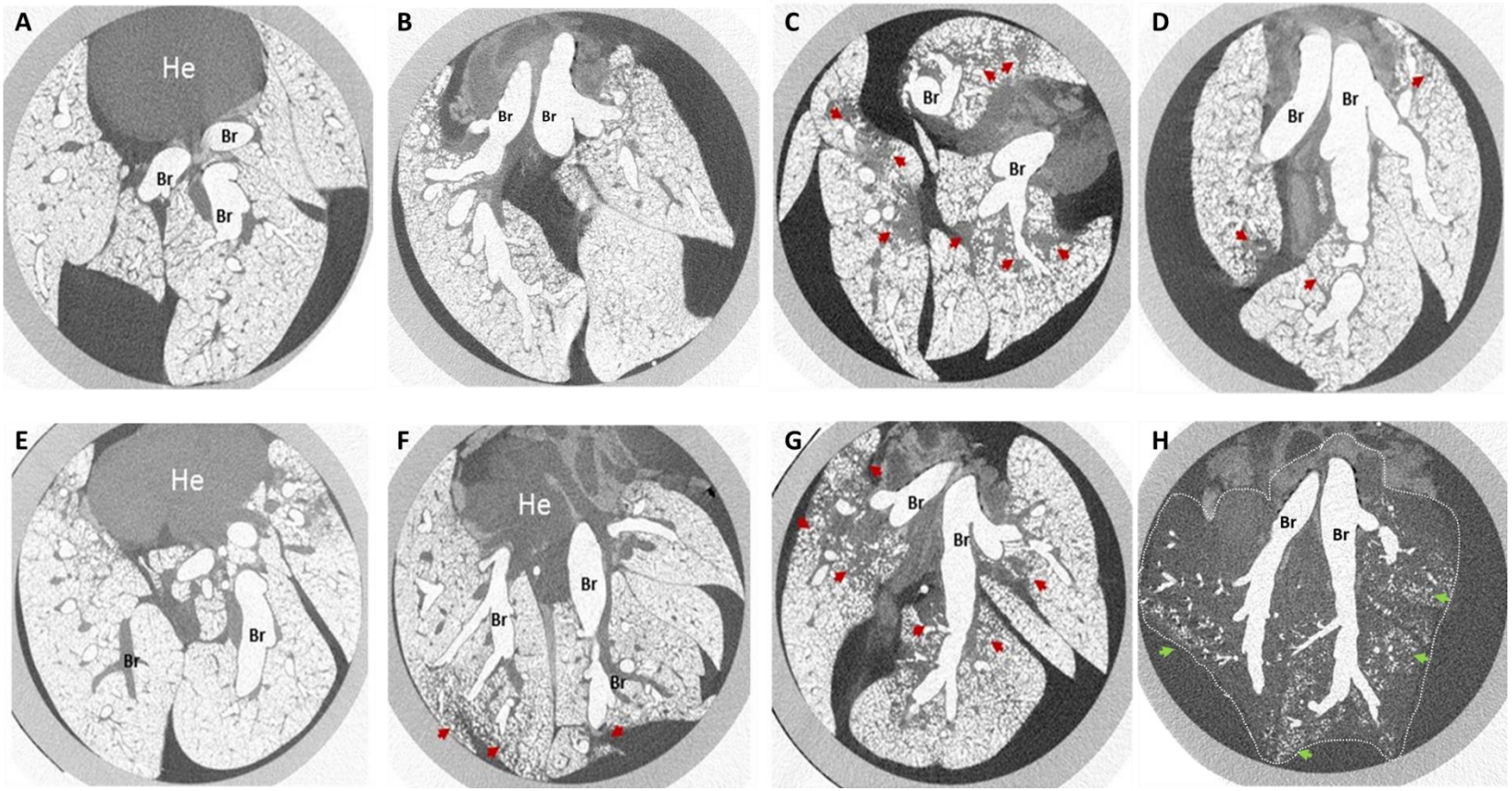

Figure 5.12. µCT scans of unfixed, inflated mouse lungs isolated from tamoxifen and bleomycin treated Col1α2-CCN2fl mice and ROSA-CCN2fl mice at experimental day 14. Animals were administered 3x doses of tamoxifen at 0.025 ng/g. A week's recovery period was given before experimental day 1. Animals were Sch1 by overdose of Pentobarbital, the lungs manually inflated prior to extraction. Isolated lungs were then suspended between pieces of Styrofoam (sf) in 3 – 5 % (wt / v) KI contrast agent for µCT scanning. Lungs were scanned using a SkyScan 1272 µCT system at a resolution of 20 µm (0.25 mm aluminium filter, 0.3 ° rotation step). Images were reconstructed using Skyscan Nrecon software and visualised using DataViewer. Tamoxifen treatment causes loss of CCN2 in fibroblasts in Col1α2-CCN2fl mice and a ubiquitous removal of CCN2 in ROSA-CCN2fl mice. Anatomical features are identified by the following: br- bronchioles, He- heart. Representative images from whole lung 3D scans are shown using DataViewer software. A) Untreated Col1α2-CCN2fl mouse, B) Tamoxifen treated Col1α2-CCN2fl mouse, C) Bleomycin treated Col1α2-CCN2fl mouse, D) Tamoxifen and Bleomycin treated Col1α2-CCN2fl mouse, E) Untreated ROSA-CCN2fl mouse, F) Tamoxifen treated ROSA-CCN2fl mouse, G) Bleomycin treated ROSA-CCN2fl mouse, H) Tamoxifen and Bleomycin treated ROSA-CCN2fl mouse. Red arrows indicate fibrosis, green arrows indicate regions of normal tissue morphology.

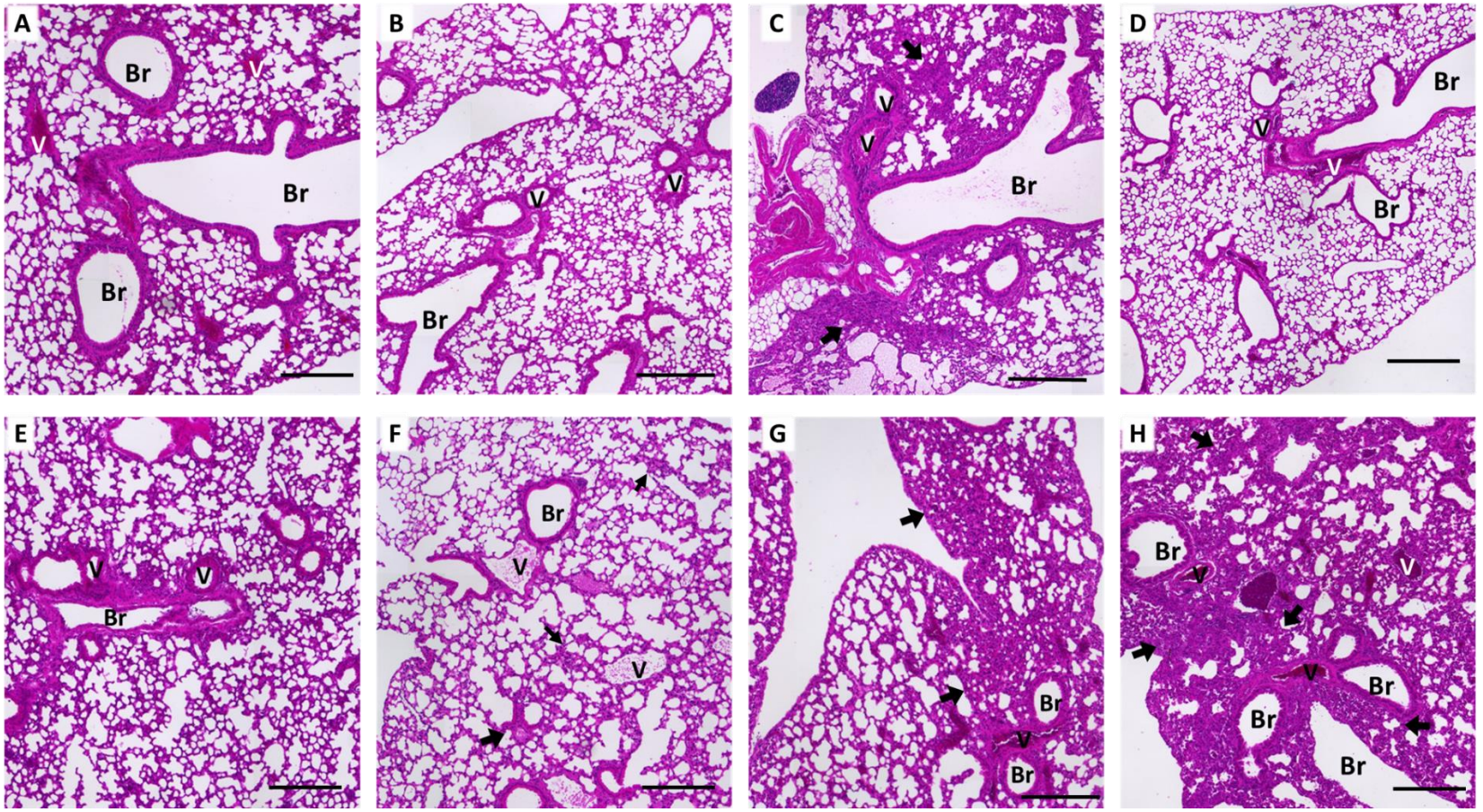

Figure 5.13. Histological evaluation of lung samples isolated from tamoxifen and bleomycin treated Col1α2-CCN2fl and ROSA-CCN2fl mice at experimental day 14 using H & E stain. Lungs were isolated immediately after Sch1 by anaesthetic overdose and manually inflated for scanning, using a SkyScan 1272 µCT system at a resolution of 20 µm (0.25 mm aluminium filter, 0.3 ° rotation step). After scanning a single lobe was isolated, processed for wax histology, sectioned to 5 µm and stained with H & E. Tamoxifen treatment causes loss of CCN2 in fibroblasts in Col1α2-CCN2fl mice and a ubiquitous removal of CCN2 in ROSA-CCN2fl mice. Anatomical features are identified as follows: a- alveoli, br- bronchioles, v- blood vessels, black arrows indicate regions of fibrosis. All images were taken at 10x magnification. A) Untreated Col1α2-CCN2fl mouse, B) Tamoxifen treated Col1α2-CCN2fl mouse, C) Bleomycin treated Col1α2-CCN2fl mouse, D) Tamoxifen and Bleomycin treated mouse, E) Untreated ROSA-CCN2fl mouse, F) Tamoxifen treated ROSA-CCN2fl mouse, G) Bleomycin treated ROSA-CCN2fl mouse, H) Tamoxifen and Bleomycin treated ROSA-CCN2fl mouse. Scale bars represent 200 µm.

Goldner's trichrome stain was used to identify collagen deposits from muscular tissues. Images were taken at 10x magnification (Figure 5.14), scale bars represent 200 µm. Anatomical features of the lung are identified in the figure as: bronchioles (br), alveoli (a) and blood vessels (v). Green staining of the blood vessels, alveoli and bronchioles was anticipated and seen in all lungs (Figure 5.14). Red staining inside bronchioles demonstrates the presence of the epithelial cells lining these structures. The same morphology as described for the H & E stained images was noted, with the additional comment that tissue deposits were stained green, supporting the notion that these are fibrotic tissue deposits of ECM.

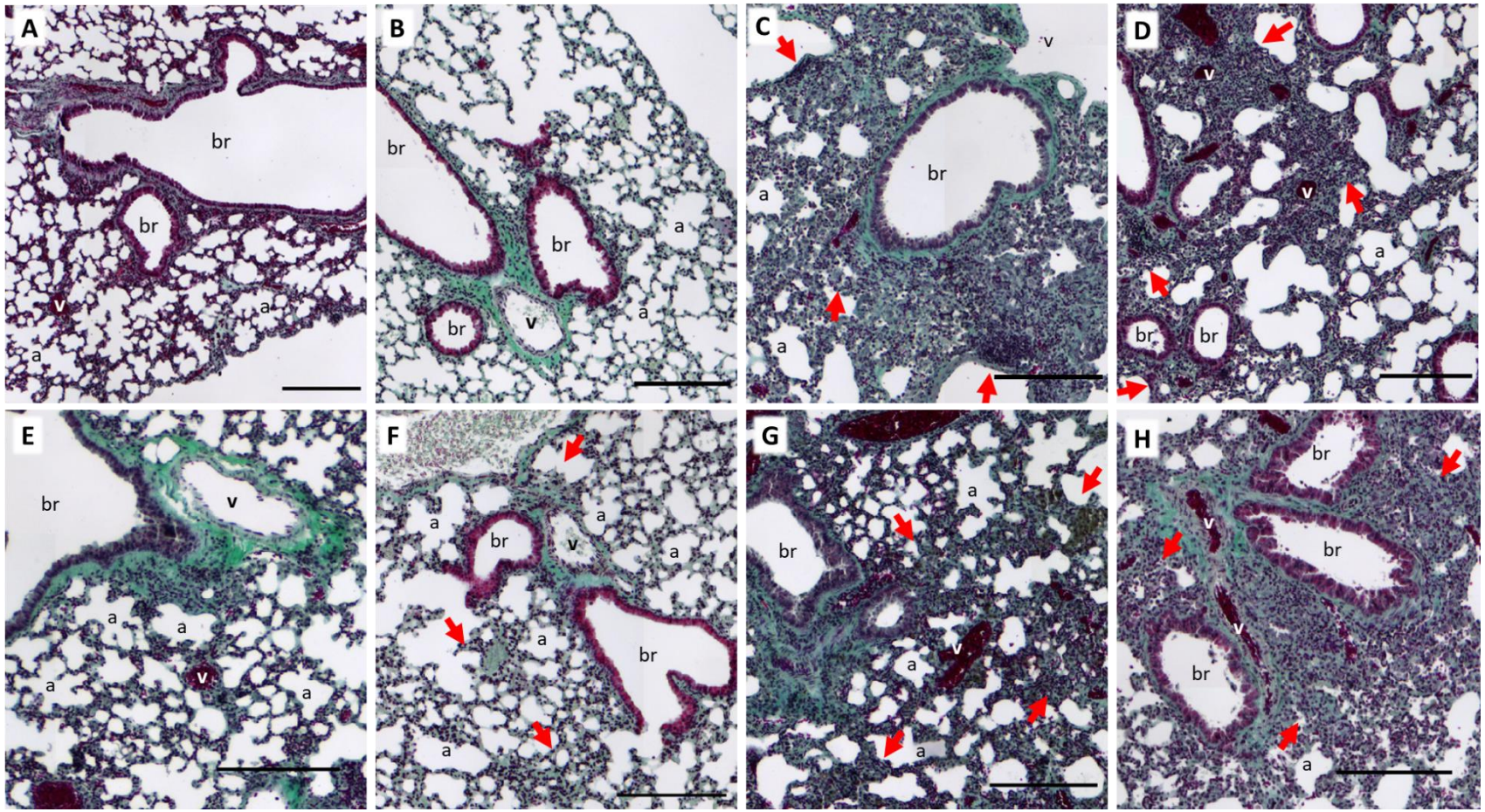

Figure 5.14. Histological evaluation of lung samples isolated from tamoxifen and bleomycin treated Col1α2-CCN2fl and ROSA-CCN2fl mice at experimental day 14 using Goldner's trichrome stain. Lungs were isolated immediately after Sch1 by anaesthetic overdose and manually inflated for scanning, using a SkyScan 1272 µCT system at a resolution of 20 µm (0.25 mm aluminium filter, 0.3 ° rotation step). After scanning a single lobe was isolated, processed for wax histology, sectioned to 5 µm and stained with H & E. Tamoxifen treatment causes loss of CCN2 in fibroblasts in Col1α2-CCN2fl mice and a ubiquitous removal of CCN2 in ROSA-CCN2fl mice. Anatomical features are identified as follows: a- alveoli, br- bronchioles, v- blood vessels, red arrows indicate regions of fibrosis. All images were taken at 10x magnification. A) Untreated Col1α2-CCN2fl mouse, B) Tamoxifen treated Col1α2-CCN2fl mouse, C) Bleomycin treated Col1α2-CCN2fl mouse, D) Tamoxifen and Bleomycin treated mouse, E) Untreated ROSA-CCN2fl mouse, F) Tamoxifen treated ROSA-CCN2fl mouse, G) Bleomycin treated ROSA-CCN2fl mouse, H) Tamoxifen and Bleomycin treated ROSA-CCN2fl mouse. Scale bars represent 200 µm.

The levels of Collagen I (*COL1α2),* Collagen III *(COL3)* and Fibronectin – EDA (*FN-EDA)* gene transcription in the remaining lobes of the lungs were examined by qPCR analysis (Figure 5.15). These proteins are all constituents of the ECM in the lung and were selected for analysis due to their association with fibrotic lung phenotypes. Sample cycle threshold (Ct) values were normalised to untreated animals of the same background and are expressed as a fold change using the ΔΔCt method. Significance was determined using a one-way ANOVA, and Tukey's post hoc test for correction for multiple testing was performed using GraphPad Prism. *P*-values below 0.05 were considered statistically significant. Samples from male and female mice were analysed independently. The first analysis compared the lungs from mice administered tamoxifen only.

In male mice, as previously described, no statistically significant difference in ΔΔCt was observed for *COL1α2, COL3* or *FN-EDA* (Figure 5.15, A – C respectively) when CCN2 was removed from fibroblast cells (Col1α2-CCN2fl). A statistically significant increase in *COL1α2* transcription ($P < 0.05$) was observed compared to control when CCN2 was removed from all cells (Figure 5.15, A). A statistically significant increase in *COL3* transcription was observed compared to control, ($P < 0.0001$) and compared to Fb k/o ($P < 0.0001$) when CCN2 was removed from all cells (FIGURE B). No statistically significant difference in the ΔΔCt fold change was observed for *FN-EDA* (Figure 5.15, C).

In female mice, statistically significant decreases in ΔΔCt were observed for *COL1α2, COL3* and *FN-EDA* (Figure 5.15, D - F respectively). When CCN2 was removed from fibroblast cells statistically significant reductions were seen in *COL1α2* ($P < 0.0001$)*, COL3* ($P < 0.01$) and *FN-EDA* ($P < 0.0001$) transcription when compared to control (Figure 5.15, D - F respectively). The same result was observed when CCN2 was removed from all cells, with statistically significant reductions observed in *COL1α2* ($P < 0.0001$)*, COL3* ($P < 0.0001$) and *FN-EDA* ($P < 0.0001$) transcription when compared to control (Figure 5.15, D - F respectively). A statistically significant difference was observed between the ΔΔCt values of Fb k/o compared to Ub k/o for all genes; *COL1α2* ($P < 0.01$)*, COL3* ($P < 0.05$) and *FN-EDA* ($P < 0.05$), (Figure 5.15, D – E).

The second analysis compared the lungs from mice administered both tamoxifen and bleomycin treatments. The effects of bleomycin in WT lungs was compared with the response in lungs where CCN2 was removed in fibroblasts (Fb k/o) or ubiquitously (Ub k/o).

In male mice, there were no statistically significant differences in mean ΔΔCt for *COL1α2* or *FN-EDA* (Figure 5.16, A & C). A statistically significant increase in mean ΔΔCt for *COL3* was

observed when Fb k/o was compared to Ub k/o ($P < 0.05$) (Figure 5.16, B). No statistically significant differences in mean ΔΔCt for *COL3* transcription was observed when Fb k/o and Ub k/o were compared to control.

In female mice, there were no statistically significant differences in mean ΔΔCt for *COL1α2* or *COL3* (Figure 5.16, D & E). Statistically significant reductions in ΔΔCt for *FN-EDA* were observed when Fb k/o and Ub k/o were compared to control ($P < 0.05$, $P < 0.01$). No statistically significant difference was observed when Fb k/o and Ub k/o ΔΔCt was compared.

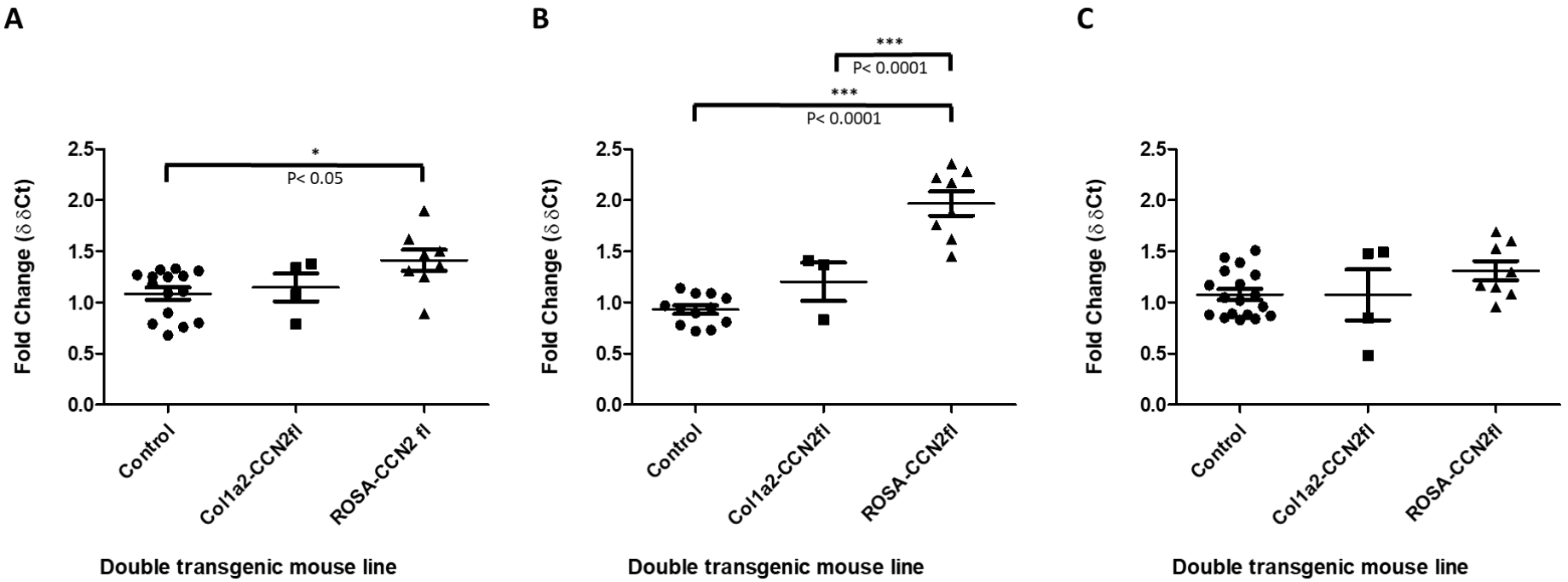
A
B
C
Fold Change (δδCt)
2.5
2.0
1.5
1.0
0.5
0.0
*
P< 0.05
***
P< 0.0001
***
P< 0.0001
Control
Col1a2-CCN2fl
ROSA-CCN2 fl
ROSA-CCN2fl
Double transgenic mouse line

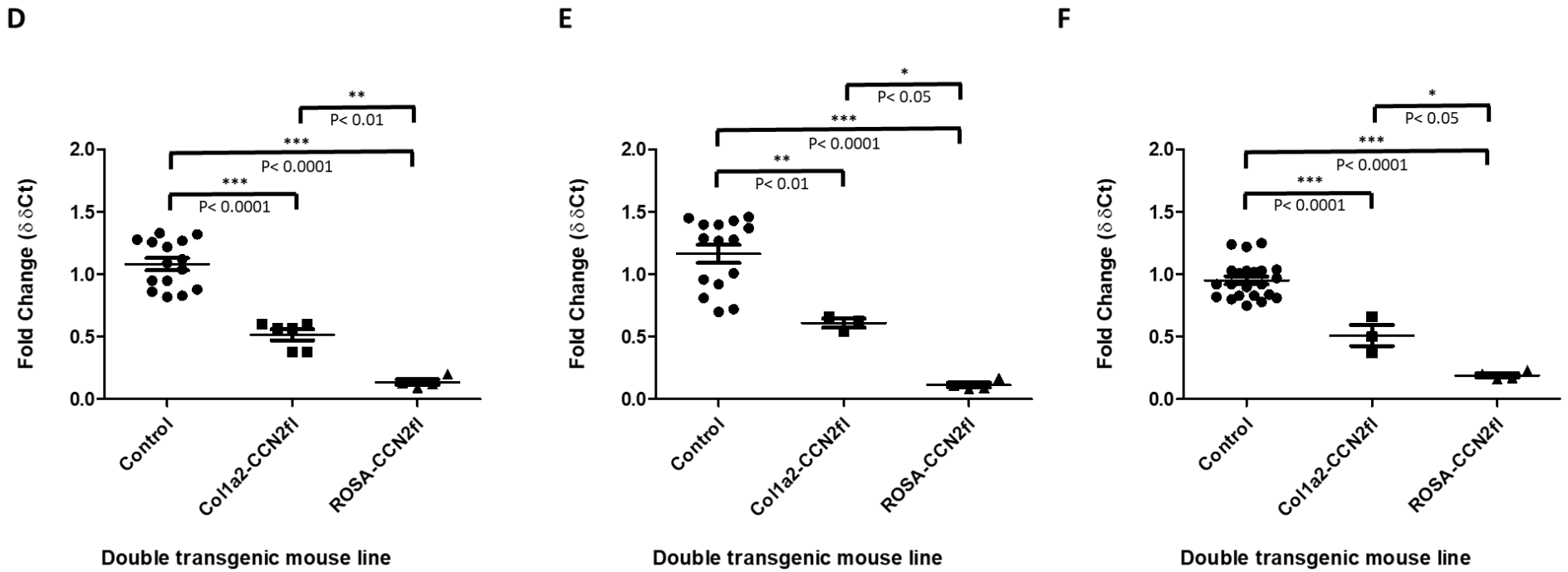

Figure 5.15. RT-qPCR analysis of COL1α2, COL3 and FN-EDA expression in lung samples isolated from tamoxifen treated Col1α2-CCN2fl and ROSA-CCN2fl mice at experimental day 14. ΔΔCt analysis of COL1α2 (A & D), COL3 (B & E) and FN-EDA (C & F). Lungs were isolated immediately after Sch1 by anaesthetic overdose and manually inflated for scanning, using a SkyScan 1272 µCT system at a resolution of 20 µm (0.25 mm aluminium filter, 0.3 ° rotation step). After scanning a single lobe was isolated for histology, the remainder of the lung was snap frozen and RNA extracted. Tamoxifen treatment causes loss of CCN2 in fibroblasts in Col1α2-CCN2fl mice and a ubiquitous removal of CCN2 in ROSA-CCN2fl mice. A - C) Male mice, D - F), Female mice. ΔΔCt fold change results are plotted, significance was determined using a one-way ANOVA, and Tukey's post hoc test. Significance and associated p-value are indicated by (*).

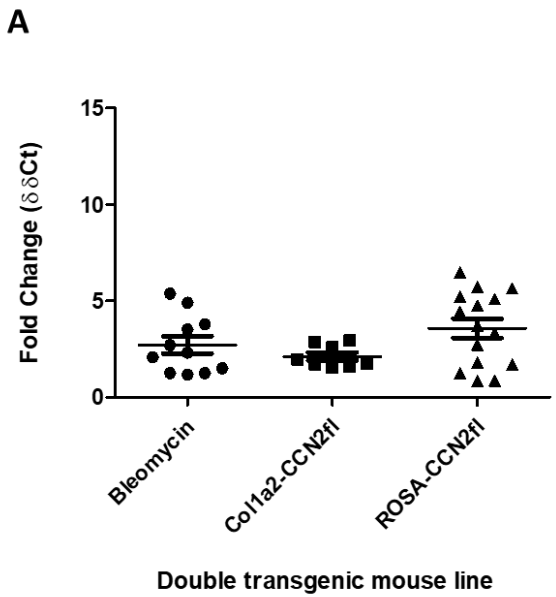
A
Fold Change (δδCt)
15
10
5
0
Bleomycin
Col1a2-CCN2fl
ROSA-CCN2fl
Double transgenic mouse line

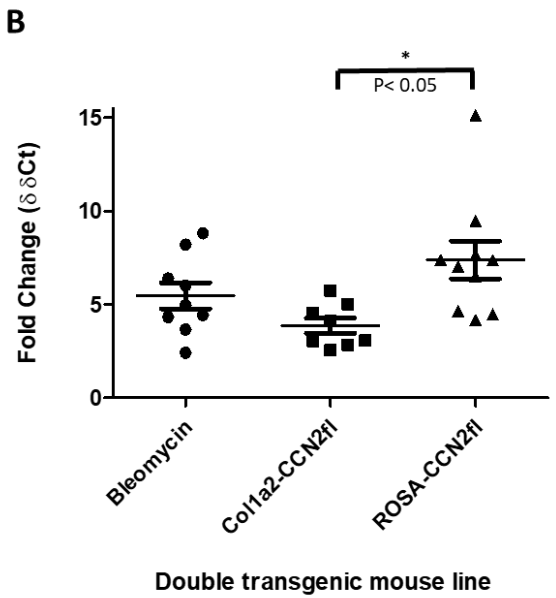
B
*
P< 0.05
Fold Change (δδCt)
15
10
5
0
Bleomycin
Col1a2-CCN2fl
ROSA-CCN2fl
Double transgenic mouse line

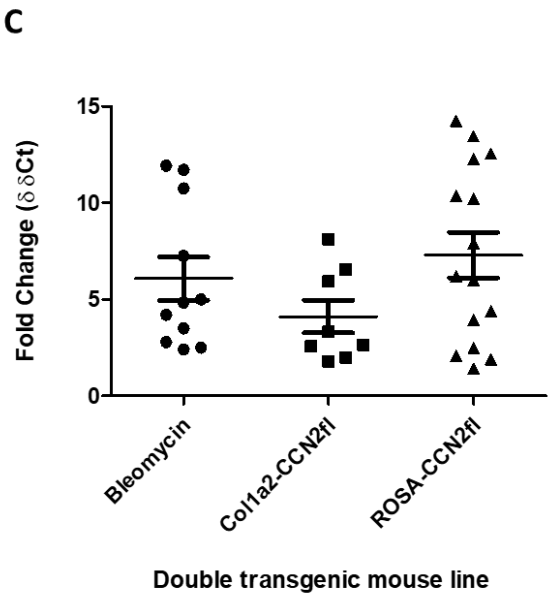
C
Fold Change (δδCt)
15
10
5
0
Bleomycin
Col1a2-CCN2fl
ROSA-CCN2fl
Double transgenic mouse line

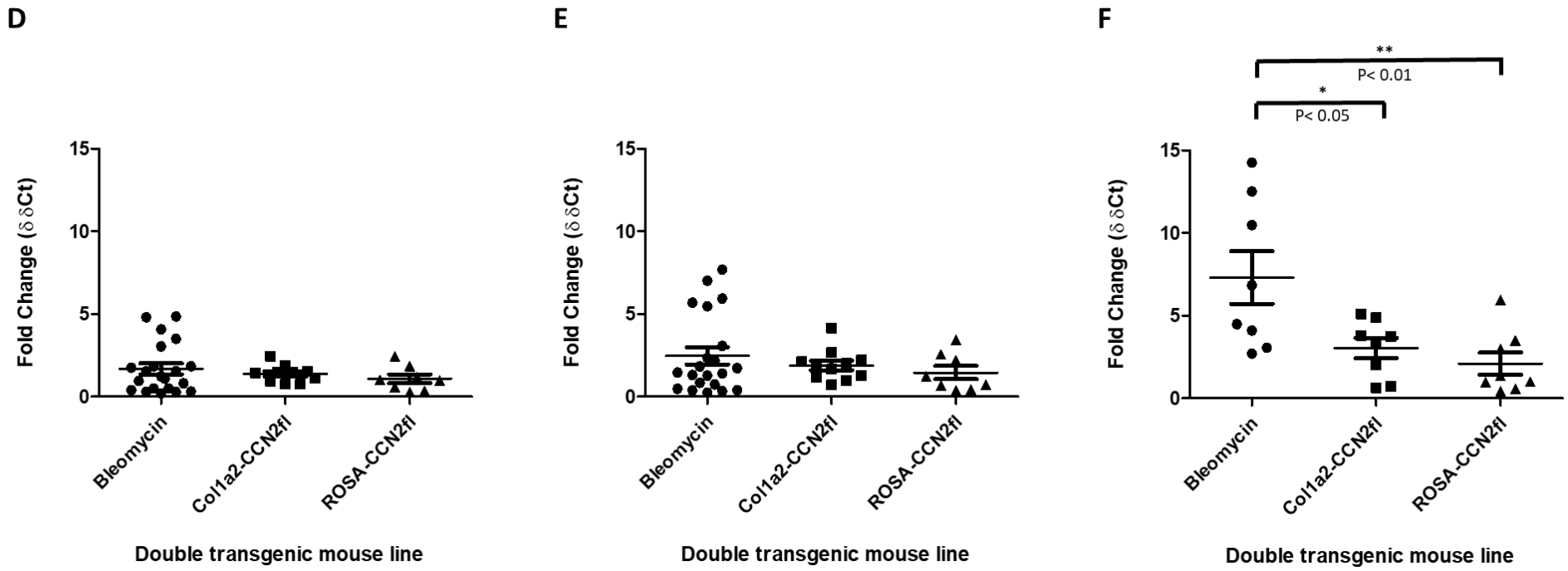

Figure 5.16. RT-qPCR analysis of COL1α2, COL3 and FN-EDA expression in lung samples isolated from tamoxifen and bleomycin treated Col1α2-CCN2fl and ROSA-CCN2fl mice at experimental day 14. ΔΔCt analysis of COL1α2 (A & D), COL3 (B & E) and FN-EDA (C & F). Lungs were isolated immediately after Sch1 by anaesthetic overdose and manually inflated for scanning, using a SkyScan 1272 µCT system at a resolution of 20 µm (0.25 mm aluminium filter, 0.3 ° rotation step). After scanning a single lobe was isolated for histology, the remainder of the lung was snap frozen and RNA extracted. Tamoxifen treatment causes loss of CCN2 in fibroblasts in Col1α2-CCN2fl mice and a ubiquitous removal of CCN2 in ROSA-CCN2fl mice. A - C) Male mice, D - F), Female mice. ΔΔCt fold change results are plotted, significance was determined using a one-way ANOVA, and Tukey's post hoc test. Significance and associated p-value are indicated by (*).

5.6 Discussion

This chapter presents the first original data on the effects of loss of function of CCN2 from fibroblast cells and from all cells in adult mice using two novel, inducible, double transgenic mouse lines; Col1α2-CCN2fl and ROSA-CCN2. This research also investigated the effects of these of loss of function phenotypes in a murine model of IPF. Myofibroblast are the primary collagen-producing cell in fibrosis (Klingberg, Hinz and White, 2013). Activation of fibroblasts to this profibrotic phenotype has been shown to be under the control of TGF-β CCN2 signalling (Shi-Wen, Leask and Abraham, 2008). Inhibition of CCN2 signalling has been shown to have anti-fibrotic effects in various murine models of fibrosis (Koshman *et al.*, 2015; Bickelhaupt *et al.*, 2017), and in human clinical trials (Raghu *et al.*, 2012, 2016; Picozzi *et al.*, 2016). It was therefore hypothesised that the loss of function of CCN2 would provide a preventative effect on the formation of fibrosis in response to bleomycin.

The first experiments in this chapter described the phenotype in the lung, induced by fibroblast specific removal of CCN2 across a period of 28 days. No difference in the gross morphology of the lungs was observed at any timepoint by qualitative evaluation of the lungs (Figure 5.1 - 5.5). This was not unexpected as CCN2 is expression and activity is limited during adulthood under normal homeostasis (Ramazani *et al.*, 2018) and phenotypes resulting from knock out models of CCN2 are usually observed in response to injury (Liu *et al.*, 2011; Wang *et al.*, 2014; Tracy, Minasian and Caterson, 2016; Bickelhaupt *et al.*, 2017).

RT-qPCR analysis of the lungs found no statistically significant difference in transcription of *COL1α2* or *FN-EDA* in male mice (Figure 5.6, A & C). A statistically significant increase ($P < 0.0001$) in *COL3* was observed at experimental day 7 only (Figure 5.6, B). In female animals statistically significant differences in transcription of *COL1α2, COL3* and *FN-EDA* were observed across the experimental time period (Figure 5.6, D – F). Female and male mice have been shown to exhibit different responses to tamoxifen (Falke *et al.*, 2017). It is believed to be a result of the hormone responses seen in these animals as the 4-OHT metabolite of tamoxifen has been shown to elicit responses from endogenous estrogen receptors (Robinson *et al.*, 1991; Delle *et al.*, 2012; Kim *et al.*, 2014; Falke *et al.*, 2017). As such, it was not surprising to note different responses in response to tamoxifen induced removal of CCN2 between male and female animals. What was unusual was the opposing trends apparent between the two sexes. In male mice the general trend observed was an increase in average ΔΔCt value, whereas in females this was reversed with general reduction in average ΔΔCt, with the exception of *FN-EDA* at 7 days (FIGURE 5.6). These analyses showed that although

no physical phenotype manifested, loss of function of CCN2 in fibroblasts was sufficient to cause statistically significant differences in gene transcription of Collagen I, Collagen III and Fibronectin ED-A.

The next series of experiments aimed to determine if the removal of CCN2 from fibroblast cells affected the fibrosis formed using the bleomycin model of IPF. Visual assessment of the µCT scans (Figure 5.7) showed the expected progression for developing fibrosis in the bleomycin model across the 28-day experimental period for both tamoxifen treated and control animals (Izbicki *et al.*, 2002). The extent of fibrosis identified at 14 days using µCT and histological analysis (Figure 5.7 - 5.9) was found to be reduced in lungs where CCN2 was removed from fibroblasts prior to bleomycin administration. This was considered an encouraging result, as previous literature using different models of CCN2 loss of function in different cell types has described similar protective effects in models of IPF (Gao and Brigstock, 2004; Xu *et al.*, 2006; Shi-Wen, Leask and Abraham, 2008; Brigstock, 2009; Ponticos *et al.*, 2009; Jun and Lau, 2011; Liu *et al.*, 2011; Rittié *et al.*, 2011; Kubota and Takigawa, 2015).

Analysis of WT male animals (Figure 5.10, A & C), identified a statistically significant upregulation of *COL1α2, COL3* and *FN-EDA* transcription between control and bleomycin treated lungs at 14 days ($P < 0.0001$). No statistically significant difference in the ΔΔCt fold change was observed between control and WT bleomycin treated lungs at 28 days. Analysis of male animals where CCN2 was removed from fibroblasts before bleomycin treatment (Fb k/o) identified a statistically significant upregulation of *COL1α2, COL3* and *FN-EDA* transcription between control and bleomycin treated lungs at all timepoints (Figure 5.10, D – F). The extent of fibrosis observed in the lungs of both WT and Fb k/o mice correlated with the trend in ΔΔCt changes. Peak expression of *COL1α2, COL3* and *FN-EDA* was observed at day 14, where the greatest extent of fibrosis was observed. When the average ΔΔCt was compared (Table 5.1), it was found that the increase in gene expressions seen at 14 days were reduced in Fb k/o mice and increased at 28 days when compared to WT responses. Differential expression of *COL1α2, COL3* and *FN-EDA* has been described in the bleomycin model of IPF (Swiderski *et al.*, 1998; Cabrera *et al.*, 2013), the trends in transcriptional changes and their associated phenotypes were found to be comparable to those of this research.

Analysis of WT female animals identified no statistically significant changes in transcription of *COL1α2* or *COL3* (Figure 5.11, A - C). A statistically significant upregulation of *FN-EDA*

transcription was observed at 7 and 14 days. Analysis of CCN2 k/o female animals identified no statistically significant changes in transcription of *COL1α2* or *COL3* when compared to control (Figure 5.11, D - F). Analysis of *FN-EDA* transcription (Figure 5.11, F) identified statistically significant changes in ΔΔCt at all timepoints. When the average ΔΔCt was compared (Table 5.1), it was found that for all genes (*COL1α2, COL3* and *FN-EDA*) the average ΔΔCt at every time point. Both male and female animals exhibited a peak in translational increase of *COL1α2, COL3* and *FN-EDA* followed by reductions in later timepoints. In females this peak in transcriptional activity was observed at 7 days, whereas in males it was observed at 14 days. The expression for male animals was expected (Swiderski *et al.*, 1998; Cabrera *et al.*, 2013). Whereas the peak in transcriptional activity in females was surprising as this timepoint is usually associated with the resolution of inflammation rather than exponential matrix deposition (Izbicki *et al.*, 2002) and was not reflected in the phenotype of the lungs. It has been shown that male and female mice respond differently to bleomycin treatment (Gharaee-Kermani *et al.*, 2005; Voltz *et al.*, 2008; Redente *et al.*, 2011) therefore it was not surprising to find differences in the expression profiles between the two sexes. However, these differences were not identified in qualitative analyses and no obvious distinction was made in the pathologies observed for male or female animals. The conclusions from these results were that removal of CCN2 from fibroblasts prior to treatment with bleomycin demonstrated a less extensive fibrosis at 14 days than WT counterparts. A reduction in ECM associated genes (*COL1, COL3* and *FN-EDA*) was observed in both male and female animals when compared with WT.

Based on the phenotype response to bleomycin, the subsequent series of experiments used a 14-day timepoint to examine the response in fibrosis formation when loss of function of CCN2 was induced in a ubiquitous (ROSA-CCN2fl) manner. This was compared to fibroblast specific removal of CCN2. Both fibroblast specific (Fb k/o) and ubiquitous (Ub k/o) loss of function models were activated prior to the administration of bleomycin. The effect of loss of function of CCN2 was compared to WT lungs treated with bleomycin.

Visual comparison of the gross morphology by μCT (Figure 5.12) and histological analysis (Figure 5.13 and Figure 5.14) of the lungs showed no difference in phenotype of untreated WT animals from Col1α2-CCN2fl or ROSA-CCN2fl mouse lines. No difference in baseline response to bleomycin was observed for either mouse line. In Ub k/o animals where ubiquitous loss of function of CCN2 was induced without subsequent challenge with bleomycin, small regions of fibrosis were observed in subpleural regions of the lungs (Figure 5.12, F, red arrows). This was an unexpected observation as no difference in phenotype was

observed in Fb k/o mice. The fibrosis was observed by both µCT and histological analysis (Figure 5.12 - 5.14).

RT-qPCR analysis on the remaining lobes of the lungs in male mice found a statistically significant increase in *COL1α2* and *COL3* transcription in Ub k/o where the effect of loss of CCN2 function was examined independently from bleomycin injury. This was interesting as these results provided further evidence that the tissue regions apparent in the µCT and histological analysis were likely to be a 'spontaneous' fibrosis. It was interesting to find that although the average ΔΔCt value was higher in Ub k/o than Fb k/o lungs for all genes (Figure 5.15, A - C), this increase was only statistically significant for collagen III transcription, yet a fibrotic phenotype was observed for Ub k/o and not Fb k/o.

In female mice, statistically significant decreases in ΔΔCt were observed for *COL1α2, COL3* and *FN-EDA* (Figure 5.15, D - F respectively) for both Fb k/o and Ub k/o where the effect of loss of CCN2 function was examined independently from bleomycin injury. A statistically significant difference was also observed between the ΔΔCt values of Fb k/o compared to Ub k/o for all genes (Figure 5.15, D – E).

These results were of interest as the appearance of early fibrosis in the subpleural regions of the lung was observed in Ub k/o mice of both genders, even though genetic profiles from RT-qPCR analysis revealed contradictory alterations to gene expression of collagen I, III and fibronectin ED-A. The localisation of the fibrosis was comparable to that of human patients presenting with IPF, whereby usual IIP honeycombing patterns are generally identified in subpleural regions of the lungs by CT scan (Society, 2002; Travis *et al.*, 2013; Lynch *et al.*, 2018).

The RT-qPCR results from lungs from mice administered both tamoxifen and bleomycin treatments were then analysed.

In male mice, there were no statistically significant differences in mean ΔΔCt for *COL1α2, COL3* or *FN-EDA* (Figure 5.16, A & C) when either a Fb k/o or Ub k/o was compared to WT response to bleomycin. Although not statistically significant, the mean ΔΔCt values for Ub k/o mice compared to WT and Fb k/o were consistently higher. Mean ΔΔCt for each treatment group and gene were ***COL1α2***: WT = 2.72, Fb = 2.12, Ub = 3.51; ***COL3***: WT = 5.47, Fb = 3.87, Ub = 7.39; ***FN*-EDA**: WT = 6.09, Fb = 4.12, Ub = 7.3. The variation in response of individuals within each group is likely the reason these differences were not statistically significant.

In female mice, there were no statistically significant differences in mean ΔΔCt for *COL1α2* or *COL3* (Figure 5.16, D & E). Statistically significant reductions in ΔΔCt for *FN-EDA* were observed in both Fb k/o and Ub k/o when compared to control. No statistically significant difference was observed when Fb k/o and Ub k/o ΔΔCt was compared. However conversely to the males, the mean ΔΔCt values for Ub k/o mice compared to WT and Fb k/o were consistently lower. Mean ΔΔCt for each treatment group and gene were ***COL1α2***: WT = 1.69, Fb = 1.39, Ub = 1.09; ***COL3***: WT = 2.47, Fb = 1.90, Ub = 1.50; ***FN*-EDA**: WT = 7.31, Fb = 3.05, Ub = 2.01.

It is of interest to note that the opposing expression profiles between sexes were also observed when bleomycin treatment followed CCN2 loss of function. The difference in response to bleomycin treatment described by Gharaee-Kermani *et a*l., (2005); Redente et al., (2011) and Voltz et al., (2008) identified a protective effect of tamoxifen in females administered bleomycin and other fibrotic agents. When the mean ΔΔCt values of males were compared with females (Figure 5.16) this phenomenon could be implied based on qPCR results. However, no difference between the phenotypes in male and female mice were noted during qualitative analyses.

5.6 Summary

This chapter presented the first research using the two double transgenic mouse colonies, containing the floxed CCN2 transgene and a ubiquitously expressed ROSA26CreER^{T2} (ROSA-CCN2fl), or the fibroblast specific tamoxifen-inducible CreER^{T2} (Col1α2-CCN2fl), in conjunction with the bleomycin model of IPF. The loss of function of CCN2 in a fibroblast specific manner did not present any observed phenotype in the lung when no injury was induced. Where bleomycin induced fibrosis was induced, fibroblast specific loss of CCN2 was found to convey a protective effect. Reductions in the extent of fibrosis observed in the lung were observed at 14 days. A decrease in the level of upregulation in transcription of associated ECM components; collagen I, collagen III and fibronectin ED-A was also observed in Fb k/o mouse lungs challenged with bleomycin, although this was not found to be statistically significant from these experiments. This was the first time that fibroblast cells were specifically targeted using the Col1α2-CreER^{T2} in the bleomycin model of IPF. Alternative CCN2 knock-outs in different cells and tissues show that cell specific loss of function of CCN2 conveys similar levels of protection when examined in the context of fibrosis. The loss of function of CCN2 in a ubiquitous manner resulted in a grossly exacerbated response to bleomycin injury, with extensive fibrosis throughout the lung by 14

days. This contradicted the current dogma that the mechanism of action of CCN2 is predominantly profibrotic in the pathogenesis of fibrosis. Ubiquitous removal of CCN2 without injury identified small early regions of fibrosis forming in the sub pleural regions of the lung by experimental day 14. This was both unexpected and interesting as it highlighted a previously underappreciated role of CCN2 as an inhibitor of tissue fibrosis. It also presented the potential for ubiquitous removal of CCN2 to be used as a new model system for IPF.

6. General Discussion

As early as 1935, reports of clinical cases describe patients presenting with extreme and progressive dyspnoea and cough, accompanied by clubbing of the fingers and toes. The histological findings upon autopsy reported excessive proliferation of fibrous tissue in the interstitium as a common feature in these patients (Hamman and Rich, 1933; 1935; Homolka, 1987). Although termed interstitial non-purulent pneumonia at the time, the disease described is known today as IPF. IPF is a chronic, progressive and ultimately lethal disease of the lung with no known cause (Raghu *et al.*, 2011). Incidence and mortality appear to be on the rise, and prevalence is expected to increase with the aging population (Ley and Collard, 2013). The 5 – year survival rate for IPF is worse than a number of cancers including breast, prostate and skin (Vancheri *et al.*, 2010). An increase in basic and clinical research in recent decades has led to the development and approval of two new drugs for IPF, Nintedanib (Wollin *et al.*, 2014; Drugs, 2016) and Pirfenidone (NICE, 2013; King *et al.*, 2014), with a third (FG-3019 / Pamrevlumab) currently undergoing clinical assessment (Raghu *et al.*, 2016; Lipson *et al.*, 2017). However, the pathobiology of IPF still remains elusive and there is an ever more pressing need to understand the molecular processes behind this disease to identify potential therapeutic targets for this disease (Hui Hoo and B Whyte, 2012).

Animal models of IPF have been an essential tool for investigating the pathology and mechanisms underlying this disease (Roberts *et al.*, 1995; Moore and Hogaboam, 2008; Schaefer *et al.*, 2011; Wollin *et al.*, 2014; Marenzana and Vande Velde, 2015; Qian *et al.*, 2016; Masopust, Sivula and Jameson, 2017). Although limited by their inability to encapsulate the full range of features present in human disease, they remain a useful means for examining key physiological traits and as a screening platform for candidate pharmaceutical molecules. Of these models, the most widely used for IPF is bleomycin. With the recent success of Nintedanib and Pirfenidone being approved in human trials following pre-clinical assessment using the bleomycin model of IPF (Schaefer *et al.*, 2011; Wollin *et al.*, 2014) it was decided that this research for this thesis would utilise this technique to investigate the role of CCN2 in IPF.

The first attempt to reproduce a previously established protocol for bleomycin induces IPF (Ponticos *et al.*, 2009) resulted in a severe response to bleomycin treatment in around 25 % of the animals. This was not anticipated and lead to animals being culled earlier than their designated time points. An alternative protocol was developed using a lower dose of bleomycin which proved to be far better tolerated and was reproducible between mice. The fibrosis observed was comparable in both progression and morphology to that described in the literature (Adamson and Bowden, 1974; Izbicki *et al.*, 2002; Lakatos *et al.*, 2006; Egger *et*

al., 2013). It was uncertain as to why the earlier dose was so poorly tolerated and no definitive conclusions were reached as to why the mice demonstrated such an exacerbated response. However, the results from this study highlighted several key issues in the experimental design, primarily the need to assess the extent of fibrosis throughout the entire lung prior to isolating individual lobes from the lung for differential analysis. As such the options for whole lung imaging techniques available at the University of Liverpool were assessed and the *ex-vivo* Bruker SkyScan 1272 µCT scanner was decided to be suitable. Initially a chemical dehydration method was used to examine the morphology of the lungs, however it was not feasible to analyse these samples for the genetic profile of transgenic animals. Therefore, a novel protocol was established that enabled scanning of the lungs immediately after Sch1 of the animal without the need for chemical fixatives. The results in this thesis demonstrated that a comparable level of detail to that obtained from dehydrated scans was achieved, and with the assistance of Professor Rob Van 'T Hof, a macro was developed that was able to quantify the level of fibrosis in the lungs. Subsequent histological analysis confirmed that the suspected regions of fibrosis observed using the µCT scanner were in fact collagenous tissue. It was concluded that the model was sufficient to produce a visible fibrosis in mice by 14 days and that imaging and analysis protocols developed during this research were suitable for identifying and quantifying this. These protocols are the first to describe a method using an *ex-vivo* scanner whereby the same lungs can be used for both a qualitative and quantitative analysis. Typically researchers using *ex-vivo* µCT scans will chemically fix the samples required for scanning (Sharir, Ramniceanu and Brumfeld, 2011; Downey *et al.*, 2012; Scotton *et al.*, 2013), requiring larger experimental group sizes if genetic analysis is required. The major limitation from *ex-vivo* analysis is the requirement for Sch1 of the animal at designated timepoints. The basic assumption remains that animals culled and assessed at earlier timepoints would have continued to express the same phenotypes seen in animals that continued on study. The new gold-standard for this technique describes the use of *in-vivo* µCT scanning, whereby the same animal can be assessed longitudinally. The rise in availability and reduction in costs of the benchtop *in-vivo* µCT scanners has led to an increase in literature describing this scanning technique for the assessment of bleomycin induced IPF (Cavanaugh *et al.*, 2006; Driehuys and Hedlund, 2007; Johnson, 2008; Schambach *et al.*, 2010; Misharin *et al.*, 2017; Ruscitti *et al.*, 2017). The University of Liverpool has recently purchased an *in-vivo* scanner, as such the application of *ex-vivo* scanning of bleomycin treated lungs is likely to be replaced in favour of *in-vivo* imaging. However, the research to develop the bleomycin model at the University will remain relevant for future research in this area.

The 4th chapter in this thesis focussed on the development of three novel, tamoxifen - inducible, double transgenic mouse lines. Two of these mouse lines were designed to instigate a loss of CCN2 function in either a ubiquitous manner, or in fibroblast cells only. The third utilised the dual-fluorescent reporter line described by (Muzumdar *et al.*, 2007) to characterise the fibroblast specific Col1α2 - CreER^{T2} generated by the Bou-Gharios lab (Bou-Gharios *et al.*, 1996; De Val *et al.*, 2002; Ponticos *et al.*, 2004). In this research we presented the original data for assessing the levels of CCN2 k/o achieved when recombination of the CCN2 was induced by tamoxifen administration. In chapter 5 the effects of these phenotypes were assessed in conjunction with the bleomycin IPF model.

CCN2 is known to be a contributor of IPF in patients and animal models of lung fibrosis and has been identified as a key downstream mediator of the effects of the known master regulator of repair TGF – β Leask and Abraham, 2006; Shi-wen *et al.*, 2006; Arnott *et al.*, 2007; Ponticos *et al.*, 2009; Holmes *et al.*, 2001; Leask *et al.*, 2003; Geisinger *et al.*, 2012. As such, CCN2 has been proposed as a therapeutic target in IPF as well as a possible biomarker for companion diagnostics for treatment of this disease. It was proposed that the cellular propagator of fibrosis was the fibroblast owing to its key role in ECM production and deposition. Research in patients with IPF identified increased levels of CCN2 in a number of cell types including fibroblasts (Plantier et al., 2016) bronchoalveolar lavage cells (Allen et al., 1999), plasma (Kono et al., 2011) and general lung tissue (Pan et al., 2001). However, as fibroblasts were the only cells identified as capable of generating ECM components it was hypothesised that the removal of CCN2 from fibroblasts would prove beneficial. Animal models of IPF have also shown CCN2 is increased in fibroblasts (Lasky et al., 1998; Liu et al., 2011; Yang et al., 2014; Ashley et al., 2017). Knock out animal models of CCN2 have demonstrated the presence of fewer myofibroblasts and reductions in ECM disposition, indicating that CCN2 is necessary for induction of fibrosis in these animals (Liu et al 2011). This thesis aimed to investigate this hypothesis further by targeting CCN2 for removal in fibroblast cells and in all cells using the bleomycin model of IPF utilising the newly generated tamoxifen - inducible double transgenic animal models described above.

Research in the Bou-Gharios lab had previously identified a 1.5 kb enhancer sequence upstream of the transcriptional start site of the *COL1α2* gene (Bou-Gharios *et al.*, 1996; De Val *et al.*, 2002). This was used to generate a tamoxifen-inducible CreERT2 mouse line (Col1α2CreER^{T2}) (Ponticos *et al.*, 2004, 2009). Research in this thesis aimed to characterise the expression profile of the Col1α2-CreER^{T2} using a dual fluorescent (mT/mG) reporter construct. Mice containing the mT/mG reporter construct described by Muzumdar et al.,

(2007), were bred with mice containing the Col1α2-CreER^{T2}. Littermate breeding pairs were maintained to produce a double transgenic mouse colony that was homozygous for the mT/mG reporter construct, and positive for Col1α2-CreER^{T2}. These animals were then used for lineage tracing experiments to determine the expression pattern of the Col1α2-CreER^{T2} during development and during adulthood. This new shorter collagen enhancer was found to express more widely in almost all fibroblast compared with the previous CreER^{T1} generated by (Denton *et al.*, 2001).

This Col1α2CreER^{T2} was then used to generate a new tamoxifen-inducible double transgenic mouse line capable of removing CCN2 from fibroblasts. The removal of CCN2 specifically in fibroblasts using the Col1α2 - CreER^{T2} has not previously been described in conjunction with the IPF bleomycin model, therefore we generated this mouse to investigate whether the protective effects seen in other cell specific k/o models of CCN2 would be true in this transgenic system.

No difference in the gross morphology of the lungs was observed at any timepoint by qualitative evaluation of the lungs when CCN2 was removed from fibroblast cells. This was not unexpected owing to the limited expression and activity of CCN2 during adulthood under normal homeostasis (Ramazani *et al.*, 2018). No injury was induced for these analyses and phenotypes resulting from knock out models of CCN2 are usually observed in response to injury (Liu *et al.*, 2011; Wang *et al.*, 2014; Tracy, Minasian and Caterson, 2016; Bickelhaupt *et al.*, 2017). Therefore, the next experiments investigated if the removal of CCN2 from fibroblast cells demonstrated any effect on the formation of fibrosis bleomycin model of IPF. Although not statistically significant these results found that the extent of fibrosis identified at 14 days was visibly reduced, and genetic analyses showed a decrease in transcription of collagen I, collagen III and fibronectin ED-A. This was considered an encouraging result, as these results were comparable to the literature (Gao and Brigstock, 2004; Xu *et al.*, 2006; Shi-Wen, Leask and Abraham, 2008; Brigstock, 2009; Ponticos *et al.*, 2009; Jun and Lau, 2011; Liu *et al.*, 2011; Rittié *et al.*, 2011; Kubota and Takigawa, 2015) and suggested that targeting CCN2 in IPF patients should have a beneficial therapeutic effect.

Based on these promising results, the ubiquitous k/o of CCN2 was assessed for efficacy in reducing fibrosis at 14 days. It was hypothesised that the protective effects demonstrated by the fibroblast k/o of CCN2 would convey a greater level of protection when CCN2 was removed from all cells. However, the resulting fibrosis in mice where CCN2 was removed ubiquitously was grossly exacerbated. In many cases the fibrosis extended to such a degree

that it was astonishing that the mice were not exhibiting any signs of an adverse response and in some animals the fact that they remained able to breathe was wholly impressive. The second result of interest in these mice was that a fibrosis was seen developing in animals where bleomycin was not administered. At 14 days small regions of fibrosis were identified in the subpleural regions of the lungs. These results raise several questions regarding the roles that CCN2 plays both in fibrosis and in normal lung homeostasis.

This research has demonstrated that deleting CCN2 from fibroblasts can cause an amelioration in the pathology of fibrosis at 14 days. This is considered a favourable result, especially when considering that anti-CCN2 antibodies are currently in clinical trials in the form of monoclonal antibody, FG-3109 (Pamrevlumab). Interestingly current results from these trials appear promising, with a double-blind placebo - controlled trial demonstrating significantly reduced decline of the forced vital capacity in patients treated with Pamrevlumab compared to placebo treatment. Efficacy and tolerance are also proving positive with no current adverse events being reported (Raghu et al., 2016; Lipson et al., 2017).

Survival rates in several animal models of fibrosis are also improved following removal of CCN2 in fibroblasts, and demonstrate a reduction in the expression of ECM components and preservation of alveolar epithelial cell morphology (Bickelhaupt et al., 2017). Yet when CCN2 was removed from all cells, the results were entirely contradictory with a rapid progression of fibrosis occurring with bleomycin and even occurring spontaneously when CCN2 was simply removal from all cells. This leads to the next question posed by this data; if not fibroblasts, then which cells are secreting and responding to CCN2 in order to elicit a fibrotic response when this protein is removed from the microenvironment? Misharin et al., (2017) recently reported that monocyte derived alveolar macrophages and tissue resident alveolar macrophages demonstrate distinct roles during the development of lung fibrosis. Both of which were found to secrete large amount of CCN2. Using a genetic lineage tracing system, they showed that deletion of monocyte derived alveolar macrophages after their recruitment to the lung in a bleomycin model of IPF markedly attenuated the severity of fibrosis. The differentiation from monocyte to alveolar macrophage would appear to be the target for any anti-fibrotic intervention as this is reportedly the stage where a fibrotic phenotype can be instigated. Incomplete differentiation between the phenotypes has been shown to lead to increased expression of pro-fibrotic genes. The persistence of these partially differentiated macrophages in the lung microenvironment is likely to play a part in the

initiation and propagation of fibrosis (Landsman, Varol and Jung, 2007; Lavin et al., 2014). These results now point the spotlight to the macrophage rather than the fibroblast as the cellular mediator of fibrotic responses.

To address this hypothesis a series of experiments was designed that would utilise a cell sorting technique to isolate the different cell populations from the lung for individual analysis. The experiments in this thesis used a whole lung homogenate therefore it wasn't possible to determine which cells were producing the ECM in the absence of the ubiquitous model of CCN2 knock out and bleomycin model retrospectively. Unfortunately, time constraints meant that these experiments were not completed during this PhD but would provide valuable mechanistic information with regards to the reasons the ROSA-CCN2fl mice responded so poorly to bleomycin. It would also be interesting to maintain the animals only treated with tamoxifen to later timepoints to see if the fibrosis continued to develop from the subpleural regions into a pathology similar to that of humans. If this could be proven this would present the ROSA-CCN2fl mouse as a new model system to study IPF.

The other interesting finding of these study which has yet to be discussed, was the difference between males and females when examining the transcriptional responses of the ECM genes to CCN2 knock out. Although the phenotypes were comparable, the underlying molecular changes seen were contradictory. With converse increases and decreases in transcription observed for all the analyses in this research. Many diseases show differential prevalence between the sexes, and in fact IPF is one such disease, with an increased prevalence in males (Strongman, Kausar and Maher, 2018). Many examples of differences between the sexes in animal models are described in the literature however very little research exists on the biological and molecular mechanisms driving this response. It would be interesting to assess hormone response pathways in these mouse models to see if any gender related differences could be elucidated.

In summary, the studies reported in this thesis presented novel findings on the role of CCN2 in the pathogenesis of fibrosis. Two novel transgenic mouse lines were established for the genetic manipulation of CCN2 *in vivo.* These were used in conjunction with the bleomycin model, which was established for the first time at the University of Liverpool. The results from these experiments unveiled unexpected results and raised further questions as to the role CCN2 plays in homeostatic regulation of ECM production by demonstrating a potent anti-fibrotic effect of CCN2. When removed from all cells a 'spontaneous' fibrosis was observed and when challenged with bleomycin, a grossly exacerbated response was seen resulting in

extensive fibrosis. A third transgenic mouse line was used to characterise the expression profile of a fibroblast specific CreER^{T2} developed by the Bou-Gharios lab group and found that the fibroblast specificity was prevalent in a wider population of Fibroblasts than described previously.

7. References

Abrams, G. D., Bauer, H. and Sprinz, H. (1963) 'Influence of the normal flora on mucosal morphology and cellular renewal in the ileum. A comparison of germ-free and conventional mice.', *Laboratory investigation; a journal of technical methods and pathology*. United States, 12, pp. 355–364.

Adamson, I. (1976) 'Pulmonary toxicity of bleomycin', *Environmental Health Perspectives*, 16, pp. 119–125. Available at: http://www.ncbi.nlm.nih.gov/pmc/articles/PMC1475236/.

Adamson, I. Y. R. and Bowden, D. H. (1974) 'The Pathogenesis of Bleomycin-Induced Pulmonary Fibrosis in Mice', *The American Journal of Pathology*, 77(2), pp. 185–198. Available at: http://www.ncbi.nlm.nih.gov/pmc/articles/PMC1910906/.

Albert, R. K., Spiro, S. G. and Jett, J. R. (2008) *Clinical respiratory medicine*, *Clinical Respiratory Medicine*. doi: 10.1016/B978-0-323-04825-5.X1000-8.

Allen, J. T. *et al.* (1999) 'Enhanced insulin-like growth factor binding protein-related protein 2 (connective tissue growth factor) expression in patients with idiopathic pulmonary fibrosis and pulmonary sarcoidosis', *American Journal of Respiratory Cell and Molecular Biology*, 21(6), pp. 693–700. doi: 10.1165/ajrcmb.21.6.3719.

Allen, J. T. and Spiteri, M. A. (2002) 'Growth factors in idiopathic pulmonary fibrosis: relative roles.', *Respiratory research*. England, 3, p. 13.

Allen, M. J. *et al.* (2001) 'Polysaccharide Recognition by Surfactant Protein D: Novel Interactions of a C-Type Lectin with Nonterminal Glucosyl Residues', *Biochemistry*. American Chemical Society, 40(26), pp. 7789–7798. doi: 10.1021/bi002901q.

Armstrong, J. D. *et al.* (1982) 'Lung tissue volume estimated by simultaneous radiographic and helium dilution methods.', *Thorax*, 37(9), pp. 676–679. Available at: http://www.ncbi.nlm.nih.gov/pmc/articles/PMC459405/.

Arnott, J. A. *et al.* (2007) 'Connective tissue growth factor (CTGF/CCN2) is a downstream mediator for TGF-??1-induced extracellular matrix production in osteoblasts', *Journal of Cellular Physiology*, 210(3), pp. 843–852. doi: 10.1002/jcp.20917.

Ashley, S. L. *et al.* (2017) 'Periostin regulates fibrocyte function to promote myofibroblast differentiation and lung fibrosis', *Mucosal Immunology*. Nature Publishing Group, 10(2), pp. 341–351. doi: 10.1038/mi.2016.61.

Babic, A. M., Chen, C. C. and Lau, L. F. (1999) 'Fisp12/mouse connective tissue growth factor mediates endothelial cell adhesion and migration through integrin alphavbeta3, promotes endothelial cell survival, and induces angiogenesis in vivo.', *Molecular and cellular biology*. United States, 19(4), pp. 2958–2966.

Babinet, C. (2000) 'Transgenic mice: an irreplaceable tool for the study of mammalian development and biology.', *Journal of the American Society of Nephrology : JASN*. United States, 11 Suppl 1, pp. S88-94.

Bach, J.-F. (2017) 'The hygiene hypothesis in autoimmunity: the role of pathogens and commensals', *Nature Reviews Immunology*. Nature Publishing Group, a division of Macmillan Publishers Limited. All Rights Reserved., 18, p. 105. Available at: https://doi.org/10.1038/nri.2017.111.

Badea, T. C., Wang, Y. and Nathans, J. (2003) 'A noninvasive genetic/pharmacologic strategy for visualizing cell morphology and clonal relationships in the mouse.', *The Journal of neuroscience : the official journal of the Society for Neuroscience*. United States, 23(6), pp. 2314–2322.

Bai, K.-J. *et al.* (2013) 'Thrombin-induced CCN2 expression in human lung fibroblasts requires the c-Src/JAK2/STAT3 pathway', *Journal of Leukocyte Biology*, 93(1), pp. 101–112. doi: 10.1189/jlb.0911449.

Ballinger, M. N. and Christman, J. W. (2016) 'Pulmonary macrophages: Overlooked and underappreciated', *American Journal of Respiratory Cell and Molecular Biology*, 54(1), pp. 1–2. doi: 10.1165/rcmb.2015-0270ED.

Bantsimba-Malanda, C. *et al.* (2010) 'A role for dendritic cells in bleomycin-induced pulmonary fibrosis in mice?', *American Journal of Respiratory and Critical Care Medicine*, 182(3), pp. 385–395. doi: 10.1164/rccm.200907-1164OC.

Barbarin, V. *et al.* (2005) 'The role of pro- and anti-inflammatory responses in silica-induced lung fibrosis.', *Respiratory research*. England, 6, p. 112. doi: 10.1186/1465-9921-6-112.

Barkauskas, C. E. *et al.* (2013) 'Type 2 alveolar cells are stem cells in adult lung.', *The Journal of clinical investigation*. United States, 123(7), pp. 3025–3036. doi: 10.1172/JCI68782.

Bateman, E. D. *et al.* (1983) 'Cryptogenic fibrosing alveolitis: Prediction of fibrogenic activity from immunohistochemical studies of collagen types in lung biopsy specimens', *Thorax*, 38(2), pp. 93–101. doi: 10.1136/thx.38.2.93.

Bauer, J. S. and Link, T. M. (2009) 'Advances in osteoporosis imaging.', *European journal of radiology*. Ireland, 71(3), pp. 440–449. doi: 10.1016/j.ejrad.2008.04.064.

Baum, J. and Duffy, H. S. (2011) 'Fibroblasts and Myofibroblasts: What Are We Talking About?', *Journal of Cardiovascular Pharmacology*. doi: 10.1097/FJC.0b013e3182116e39.

Bejvl, I. *et al.* (2013) 'Analysis of plasma surfactant protein D levels in lung transplant recipients.', *Transplant infectious disease : an official journal of the Transplantation Society*. Denmark, 15(6), pp. 645–651. doi: 10.1111/tid.12132.

Berngard, S. C. and Afshar, K. (2016) 'Idiopathic pulmonary fibrosis: Past, present, future-a review from Talmadge King's ATS 2016 presentation', *Journal of Thoracic Disease*, 8(7), pp. S559–S561. doi: 10.21037/jtd.2016.07.31.

Beura, L. K. *et al.* (2016) 'Normalizing the environment recapitulates adult human immune traits in laboratory mice.', *Nature*. England, 532(7600), pp. 512–516. doi: 10.1038/nature17655.

Bickelhaupt, S. *et al.* (2017) 'Effects of CTGF Blockade on Attenuation and Reversal of Radiation-Induced Pulmonary Fibrosis', *JNCI: Journal of the National Cancer Institute*. Oxford University Press, 109(8). doi: 10.1093/jnci/djw339.

Bienkowski, R. S., Baum, B. J. and Crystal, R. G. (1978) 'Fibroblasts degrade newly synthesised collagen within the cell before secretion.', *Nature*. England, 276(5686), pp. 413–416.

Biernacka, A., Dobaczewski, M. and Frangogiannis, N. G. (2011) 'TGF-beta signaling in fibrosis.', *Growth factors (Chur, Switzerland)*. England, 29(5), pp. 196–202. doi: 10.3109/08977194.2011.595714.

Bou-Gharios, G. *et al.* (1996) 'A potent far-upstream enhancer in the mouse proα2(I) collagen gene regulates expression of reporter genes in transgenic mice', *Journal of Cell Biology*, 134(5), pp. 1333–1344. doi: 10.1083/jcb.134.5.1333.

Bradham, D. M. *et al.* (1991) 'Connective tissue growth factor: a cysteine-rich mitogen secreted by human vascular endothelial cells is related to the SRC-induced immediate early

gene product CEF-10.', *The Journal of cell biology*. United States, 114(6), pp. 1285–1294.

Braun, R. K. *et al.* (1996) 'Comparison of two models of bleomycin-induced lung fibrosis in mouse on the level of leucocytes and T cell subpopulations in bronchoalveolar lavage', *Comparative Haematology International*. Springer-Verlag, 6(3), pp. 141–148. doi: 10.1007/BF00368457.

Brigstock, D. R. (1999) 'The Connective Tissue Growth Factor / Cysteine-', *Endocrine Reviews*, 20(June), pp. 189–206.

Brigstock, D. R. *et al.* (2003) 'Proposal for a unified CCN nomenclature.', *Molecular pathology : MP*. England, 56(2), pp. 127–128.

Brigstock, D. R. (2009) 'Strategies for blocking the fibrogenic actions of connective tissue growth factor (CCN2): From pharmacological inhibition in vitro to targeted siRNA therapy in vivo', *Journal of Cell Communication and Signaling*, 3(1), pp. 5–18. doi: 10.1007/s12079-009-0043-9.

Bryda, E. C. (2013) 'The Mighty Mouse: the impact of rodents on advances in biomedical research', *Missouri medicine*. Journal of the Missouri State Medical Association, 110(3), pp. 207–211. Available at: https://www.ncbi.nlm.nih.gov/pubmed/23829104.

Buchholz, F. *et al.* (1996) 'Different Thermostabilities of FLP and Cre Recombinases: Implications for Applied Site-Specific Recombination', *Nucleic Acids Research*, 24(21), pp. 4256–4262. Available at: http://dx.doi.org/10.1093/nar/24.21.4256.

Byrne, A. J., Maher, T. M. and Lloyd, C. M. (2016) 'Pulmonary Macrophages: A New Therapeutic Pathway in Fibrosing Lung Disease?', *Trends in Molecular Medicine*. Elsevier Ltd, 22(4), pp. 303–316. doi: 10.1016/j.molmed.2016.02.004.

Cabrera, S. *et al.* (2013) 'Gene expression profiles reveal molecular mechanisms involved in the progression and resolution of bleomycin-induced lung fibrosis.', *American journal of physiology. Lung cellular and molecular physiology*. United States, 304(9), pp. L593-601. doi: 10.1152/ajplung.00320.2012.

Capecchi, M. R. (1989) 'The new mouse genetics: Altering the genome by gene targeting', *Trends in Genetics*. Elsevier Current Trends, 5, pp. 70–76. doi: 10.1016/0168-9525(89)90029-2.

Cavanaugh, D. *et al.* (2006) 'Quantification of Bleomycin-Induced Murine Lung Damage In Vivo With Micro-Computed Tomography', *Academic Radiology*, 13(12), pp. 1505–1512. doi: 10.1016/j.acra.2006.08.011.

Chang, C.-C. *et al.* (2004) 'Connective tissue growth factor and its role in lung adenocarcinoma invasion and metastasis.', *Journal of the National Cancer Institute*. United States, 96(5), pp. 364–375.

Charrier, A. *et al.* (2014) 'Regulation of pancreatic inflammation by connective tissue growth factor (CTGF/CCN2)', *Immunology*, 141(4), pp. 564–576. doi: 10.1111/imm.12215.

Chaudhary, N. I., Schnapp, A. and Park, J. E. (2006) 'Pharmacologic differentiation of inflammation and fibrosis in the rat bleomycin model.', *American journal of respiratory and critical care medicine*. United States, 173(7), pp. 769–776. doi: 10.1164/rccm.200505-717OC.

Chen, H. *et al.* (2009) 'TGF-beta induces fibroblast activation protein expression; fibroblast activation protein expression increases the proliferation, adhesion, and migration of HO-

8910PM [corrected].', *Experimental and molecular pathology*. Netherlands, 87(3), pp. 189–194. doi: 10.1016/j.yexmp.2009.09.001.

Chen, J. *et al.* (2008) 'Mechanistic studies on bleomycin-mediated DNA damage: Multiple binding modes can result in double-stranded DNA cleavage', *Nucleic Acids Research*, 36(11), pp. 3781–3790. doi: 10.1093/nar/gkn302.

Clarke, G. *et al.* (2013) 'The microbiome-gut-brain axis during early life regulates the hippocampal serotonergic system in a sex-dependent manner.', *Molecular psychiatry*. England, 18(6), pp. 666–673. doi: 10.1038/mp.2012.77.

Cohn, L. A. *et al.* (2004) 'Identification and characterization of an idiopathic pulmonary fibrosis-like condition in cats.', *Journal of veterinary internal medicine*. United States, 18(5), pp. 632–641.

Coultas, D. B. *et al.* (1994) 'The epidemiology of interstitial lung diseases.', *American Journal of Respiratory and Critical Care Medicine*, 150(4), pp. 967–972. doi: 10.1164/ajrccm.150.4.7921471.

Crapo, J. D. *et al.* (1983) 'Morphometric characteristics of cells in the alveolar region of mammalian lungs.', *The American review of respiratory disease*. United States, 128(2 Pt 2), pp. S42-6. doi: 10.1164/arrd.1983.128.2P2.S42.

Crowell, R. E. *et al.* (1992) 'Alveolar and interstitial macrophage populations in the murine lung.', *Experimental lung research*. England, 18(4), pp. 435–446.

Culver, B. H. (2012) *Respiratory Mechanics*. Fourth Edi, *Clinical Respiratory Medicine: Fourth Edition*. Fourth Edi. Elsevier Inc. doi: 10.1016/B978-1-4557-0792-8.00003-9.

Cyphert, J. M. *et al.* (2012) 'Long-term response of rats to single intratracheal exposure of Libby amphibole or amosite.', *Journal of toxicology and environmental health. Part A*. England, 75(3), pp. 183–200. doi: 10.1080/15287394.2012.641203.

Dancer, R. C. A., Wood, A. M. and Thickett, D. R. (2011) 'Metalloproteinases in idiopathic pulmonary fibrosis', *European Respiratory Journal*, pp. 1461–1467. doi: 10.1183/09031936.00024711.

Davis, G. S., Leslie, K. O. and Hemenway, D. R. (1998) 'Silicosis in mice: effects of dose, time, and genetic strain.', *Journal of environmental pathology, toxicology and oncology : official organ of the International Society for Environmental Toxicology and Cancer*. United States, 17(2), pp. 81–97.

Delle, H. *et al.* (2012) 'Antifibrotic effect of tamoxifen in a model of progressive renal disease.', *Journal of the American Society of Nephrology : JASN*. United States, 23(1), pp. 37–48. doi: 10.1681/ASN.2011010046.

Denton, C. P. *et al.* (2001) 'Activation of a fibroblast-specific enhancer of the proα2(I) collagen gene in tight-skin mice', *Arthritis and Rheumatism*, 44(3), pp. 712–722. doi: 10.1002/1529-0131(200103)44:3<712::AID-ANR121>3.0.CO;2-1.

Dong, Y. *et al.* (2015) 'Blocking follistatin-like 1 attenuates bleomycin-induced pulmonary fibrosis in mice', *The Journal of Experimental Medicine*, 212(2), p. 235 LP-252. Available at: http://jem.rupress.org/content/212/2/235.abstract.

Downey, C. M. *et al.* (2012) 'Quantitative Ex-Vivo Micro-Computed Tomographic Imaging of Blood Vessels and Necrotic Regions within Tumors', *PLoS ONE*. Edited by G. Wang. Public Library of Science, 7(7), p. e41685. doi: 10.1371/journal.pone.0041685.

Driehuys, B. and Hedlund, L. W. (2007) 'Imaging Techniques for Small Animal Models of Pulmonary Disease: MR Microscopy', *Toxicologic Pathology*, 35(1), pp. 49–58. doi: 10.1080/01926230601132048.

Drugs, N. E. W. (2016) 'Nintedanib Lung cancer Ramucirumab', 39(2), pp. 62–63.

Egger, C. *et al.* (2013) 'Administration of Bleomycin via the Oropharyngeal Aspiration Route Leads to Sustained Lung Fibrosis in Mice and Rats as Quantified by UTE-MRI and Histology', *PLoS ONE*, 8(5). doi: 10.1371/journal.pone.0063432.

Exposito, J. Y. *et al.* (2010) 'The fibrillar collagen family', *International Journal of Molecular Sciences*, 11(2), pp. 407–426. doi: 10.3390/ijms11020407.

Falke, L. L. *et al.* (2017) 'Tamoxifen for induction of Cre-recombination may confound fibrosis studies in female mice.', *Journal of cell communication and signaling*. Netherlands, 11(2), pp. 205–211. doi: 10.1007/s12079-017-0390-x.

Fehrenbach, H. (2001) 'Alveolar epithelial type II cell: defender of the alveolus revisited', *Respiratory Research*. BioMed Central, 2(1), pp. 33–46. doi: 10.1186/rr36.

Feil, S., Valtcheva, N. and Feil, R. (2009) 'Inducible Cre Mice', in. Humana Press, pp. 343–363. doi: 10.1007/978-1-59745-471-1_18.

Finke, J. *et al.* (1993) 'An improved strategy and a useful housekeeping gene for RNA analysis from formalin-fixed, paraffin-embedded tissues by PCR.', *BioTechniques*. England, 14(3), pp. 448–453.

Fleischman, R. W. *et al.* (1971) 'Bleomycin-induced interstitial pneumonia in dogs', *Thorax*, 26(6), pp. 675–682. Available at: http://www.ncbi.nlm.nih.gov/pmc/articles/PMC472381/.

Fox, J. G. *et al.* (2006) *The Mouse in Biomedical Research, Volume 4 : Immunology.* Elsevier.

Gao, R. and Brigstock, D. R. (2004) 'Connective tissue growth factor (CCN2) induces adhesion of rat activated hepatic stellate cells by binding of its C-terminal domain to integrin alpha(v)beta(3) and heparan sulfate proteoglycan.', *The Journal of biological chemistry*. American Society for Biochemistry and Molecular Biology, 279(10), pp. 8848–55. doi: 10.1074/jbc.M313204200.

Garcia-Sancho, C. *et al.* (2011) 'Familial pulmonary fibrosis is the strongest risk factor for idiopathic pulmonary fibrosis.', *Respiratory medicine*. England, 105(12), pp. 1902–1907. doi: 10.1016/j.rmed.2011.08.022.

Geisinger, M. T. *et al.* (2012) 'Ets-1 is essential for connective tissue growth factor (CTGF/CCN2) induction by TGF-??1 in osteoblasts', *PLoS ONE*, 7(4). doi: 10.1371/journal.pone.0035258.

Gelse, K., Poschl, E. and Aigner, T. (2003) 'Collagens--structure, function, and biosynthesis.', *Advanced drug delivery reviews*. Netherlands, 55(12), pp. 1531–1546.

Gharaee-Kermani, M. *et al.* (2005) 'Gender-based differences in bleomycin-induced pulmonary fibrosis.', *The American journal of pathology*. United States, 166(6), pp. 1593–1606. doi: 10.1016/S0002-9440(10)62470-4.

Gierut, J. J., Jacks, T. E. and Haigis, K. M. (2014) 'Strategies to achieve conditional gene mutation in mice.', *Cold Spring Harbor protocols*. United States, 2014(4), pp. 339–349. doi: 10.1101/pdb.top069807.

Gilhodes, J. C. *et al.* (2017) 'Quantification of pulmonary fibrosis in a bleomycin mouse

model using automated histological image analysis', *PLoS ONE*. doi: 10.1371/journal.pone.0170561.

Giménez, A. *et al.* (no date) 'Dysregulated Collagen Homeostasis by Matrix Stiffening and TGF-β1 in Fibroblasts from Idiopathic Pulmonary Fibrosis Patients: Role of FAK/Akt'. doi: 10.3390/ijms18112431.

Gonzalez, R. F., Allen, L. and Dobbs, L. G. (2009) 'Rat alveolar type I cells proliferate, express OCT-4, and exhibit phenotypic plasticity in vitro.', *American journal of physiology. Lung cellular and molecular physiology*. United States, 297(6), pp. L1045-55. doi: 10.1152/ajplung.90389.2008.

Gordon, M. K. and Hahn, R. A. (2010) 'Collagens', *Cell and Tissue Research*, 339(1), pp. 247–257. doi: 10.1007/s00441-009-0844-4.

Gordon, S. (2008) 'Elie Metchnikoff: father of natural immunity.', *European journal of immunology*. Germany, 38(12), pp. 3257–3264. doi: 10.1002/eji.200838855.

Gribbin, J. *et al.* (2006) 'Incidence and mortality of idiopathic pulmonary fibrosis and sarcoidosis in the UK.', *Thorax*. England, 61(11), pp. 980–985. doi: 10.1136/thx.2006.062836.

Gui, Y.-S. *et al.* (2012) 'SPC-Cre-ERT2 transgenic mouse for temporal gene deletion in alveolar epithelial cells.', *PloS one*. United States, 7(9), p. e46076. doi: 10.1371/journal.pone.0046076.

Guilliams, M. *et al.* (2013) 'Alveolar macrophages develop from fetal monocytes that differentiate into long-lived cells in the first week of life via GM-CSF.', *The Journal of experimental medicine*. United States, 210(10), pp. 1977–1992. doi: 10.1084/jem.20131199.

Guiot, J. *et al.* (2017) 'STATE OF THE ART REVIEW Blood Biomarkers in Idiopathic Pulmonary Fibrosis', *Lung*, 195, pp. 273–280. doi: 10.1007/s00408-017-9993-5.

Guo, L. *et al.* (2015) 'Hypoxia-Induced Epithelial-Mesenchymal Transition Is Involved in Bleomycin-Induced Lung Fibrosis.', *BioMed research international*. United States, 2015, p. 232791. doi: 10.1155/2015/232791.

Hall-Glenn, F. and Lyons, K. M. (2011) 'Roles for CCN2 in normal physiological processes', *Cellular and Molecular Life Sciences*, pp. 3209–3217. doi: 10.1007/s00018-011-0782-7.

Hamman, L. and Rich, A. R. (1935) 'Fulminating Diffuse Interstitial Fibrosis of the Lungs.', *Transactions of the American Clinical and Climatological Association*. United States, 51, pp. 154–163.

Han, M. *et al.* (2018) 'Small Animal Models of Respiratory Viral Infection Related to Asthma', *Viruses*. MDPI, 10(12), p. 682. doi: 10.3390/v10120682.

Harlotte, C. *et al.* (2002) *The New England Journal of Medicine ENVIRONMENTAL EXPOSURE TO ENDOTOXIN AND ITS RELATION TO ASTHMA IN SCHOOL-AGE CHILDREN*, *N Engl J Med*. Available at: www.nejm.org (Accessed: 16 October 2018).

Hashimoto, Y. *et al.* (1998) 'Expression of the Elm1 gene, a novel gene of the CCN (connective tissue growth factor, Cyr61/Cef10, and neuroblastoma overexpressed gene) family, suppresses In vivo tumor growth and metastasis of K-1735 murine melanoma cells.', *The Journal of experimental medicine*. United States, 187(3), pp. 289–296.

Haston, C. K. (2012) 'Mouse genetic approaches applied to the normal tissue radiation

response.', *Frontiers in oncology*. Switzerland, 2, p. 94. doi: 10.3389/fonc.2012.00094.

Herchenhan, A. *et al.* (2015) 'Lysyl Oxidase Activity Is Required for Ordered Collagen Fibrillogenesis by Tendon Cells.', *The Journal of biological chemistry*. American Society for Biochemistry and Molecular Biology, 290(26), pp. 16440–50. doi: 10.1074/jbc.M115.641670.

Herzog, E. L. *et al.* (2014) 'Review: interstitial lung disease associated with systemic sclerosis and idiopathic pulmonary fibrosis: how similar and distinct?', *Arthritis & rheumatology (Hoboken, N.J.)*. United States, 66(8), pp. 1967–1978. doi: 10.1002/art.38702.

Holbourn, K. P., Acharya, K. R. and Perbal, B. (2008a) 'The CCN family of proteins: structure-function relationships', *Trends in Biochemical Sciences*, 33(10), pp. 461–473. doi: 10.1016/j.tibs.2008.07.006.

Holbourn, K. P., Acharya, K. R. and Perbal, B. (2008b) 'The CCN family of proteins: structure-function relationships', *Trends in Biochemical Sciences*, pp. 461–473. doi: 10.1016/j.tibs.2008.07.006.

Holmes, A. *et al.* (2001) 'CTGF and SMADs, Maintenance of Scleroderma Phenotype Is Independent of SMAD Signaling', *Journal of Biological Chemistry*. American Society for Biochemistry and Molecular Biology, 276(14), pp. 10594–10601. doi: 10.1074/jbc.M010149200.

Homolka, J. (1987) 'Idiopathic pulmonary fibrosis: a historical review', *Cmaj*, 137(11), pp. 1003–1005. doi: 10.1007/978-1-62703-682-5_1.

Huang, S. S. and Huang, J. S. (2005) 'TGF-beta control of cell proliferation.', *Journal of cellular biochemistry*. United States, 96(3), pp. 447–462. doi: 10.1002/jcb.20558.

Hubbard, J. S., Chen, P. H. and Boyd, K. L. (2017) 'Effects of Repeated Intraperitoneal Injection of Pharmaceutical-grade and Nonpharmaceutical-grade Corn Oil in Female C57BL/6J Mice.', *Journal of the American Association for Laboratory Animal Science : JAALAS*. United States, 56(6), pp. 779–785.

Hubbard, R. *et al.* (1996) 'Mortality rates from cryptogenic fibrosing alveolitis in seven countries.', *Thorax*. England, 51(7), pp. 711–716.

Hui Hoo, Z. and B Whyte, M. K. (2012) 'Idiopathic pulmonary fibrosis THE PATHOPHYSIOLOGY OF IPF', *Thorax*, 67(8), pp. 742–6. doi: 10.1136/thoraxjnl-2011-200515.

Hulmes, D. J. S. (2008) 'Collagen diversity, synthesis and assembly', *Collagen: Structure and Mechanics*, pp. 15–47. doi: 10.1007/978-0-387-73906-9_2.

'Idiopathic pulmonary fibrosis in adults: diagnosis and management | Guidance and guidelines | NICE' (no date). NICE. Available at: https://www.nice.org.uk/guidance/cg163 (Accessed: 16 August 2018).

Irvin, C. G. and Bates, J. H. T. (2003) 'Measuring the lung function in the mouse: The challenge of size', *Respiratory Research*, 4, pp. 1–9. doi: 10.1186/rr199.

Ivkovic, S. *et al.* (2003) 'Connective tissue growth factor coordinates chondrogenesis and angiogenesis during skeletal development', *Development*, 130(12), p. 2779 LP-2791. Available at: http://dev.biologists.org/content/130/12/2779.abstract.

Izbicki, G. *et al.* (2002) 'Time course of bleomycin-induced lung fibrosis', *International Journal of Experimental Pathology*, 83(3), pp. 111–119. doi: 10.1046/j.1365-2613.2002.00220.x.

Jackson Laboratories (no date) *Jackson Laboratories Mouse Genome Informatics*. Available at: http://www.informatics.jax.org/ (Accessed: 25 October 2018).

Jakubovic, B. D. *et al.* (2013) 'Methotrexate-induced pulmonary toxicity.', *Canadian respiratory journal*. Egypt, 20(3), pp. 153–155. doi: 10.1155/2013/527912.

Janssen, W. J. *et al.* (2011) 'Fas determines differential fates of resident and recruited macrophages during resolution of acute lung injury.', *American journal of respiratory and critical care medicine*. United States, 184(5), pp. 547–560. doi: 10.1164/rccm.201011-1891OC.

Jaskelioff, M. *et al.* (2010) 'Telomerase reactivation reverses tissue degeneration in aged telomerase-deficient mice', *Nature*. Nature Publishing Group, a division of Macmillan Publishers Limited. All Rights Reserved., 469, p. 102. Available at: http://dx.doi.org/10.1038/nature09603.

Johnson, C. T. B. and M. D. and D. W. H. and G. A. (2008) 'In vivo small-animal imaging using micro-CT and digital subtraction angiography', *Physics in Medicine & Biology*, 53(19), p. R319. Available at: http://stacks.iop.org/0031-9155/53/i=19/a=R01.

Johnston, I. *et al.* (1990) *Rising mortality from cryptogenic fibrosing alveolitis*, *BMJ (Clinical research ed.)*. doi: 10.1136/bmj.301.6759.1017.

Joliot, V. *et al.* (1992) 'Proviral rearrangements and overexpression of a new cellular gene (nov) in myeloblastosis-associated virus type 1-induced nephroblastomas.', *Molecular and Cellular Biology*, 12(1), pp. 10–21. Available at: http://www.ncbi.nlm.nih.gov/pmc/articles/PMC364064/.

Jun, J. Il and Lau, L. F. (2011) 'Taking aim at the extracellular matrix: CCN proteins as emerging therapeutic targets', *Nature Reviews Drug Discovery*. doi: 10.1038/nrd3599.

Kadler, K. E. *et al.* (2007) 'Collagens at a glance', *Journal of Cell Science*, 120, pp. 1955–1958. doi: 10.1242/jcs.03453.

Kim, D. *et al.* (2014) 'Tamoxifen ameliorates renal tubulointerstitial fibrosis by modulation of estrogen receptor alpha-mediated transforming growth factor-beta1/Smad signaling pathway.', *Nephrology, dialysis, transplantation : official publication of the European Dialysis and Transplant Association - European Renal Association*. England, 29(11), pp. 2043–2053. doi: 10.1093/ndt/gfu240.

Kim, D. S. (2006) 'Classification and Natural History of the Idiopathic Interstitial Pneumonias', *Proceedings of the American Thoracic Society*, 3(4), pp. 285–292. doi: 10.1513/pats.200601-005TK.

King, T. E. J. *et al.* (2001) 'Idiopathic pulmonary fibrosis: relationship between histopathologic features and mortality.', *American journal of respiratory and critical care medicine*. United States, 164(6), pp. 1025–1032. doi: 10.1164/ajrccm.164.6.2001056.

King, T. E. J. *et al.* (2014) 'A phase 3 trial of pirfenidone in patients with idiopathic pulmonary fibrosis.', *The New England journal of medicine*. United States, 370(22), pp. 2083–2092. doi: 10.1056/NEJMoa1402582.

Kirk, J. M. *et al.* (1984) 'Quantitation of types I and III collagen in biopsy lung samples from patients with cryptogenic fibrosing alveolitis.', *Collagen and related research*. Germany, 4(3), pp. 169–182.

Klingberg, F., Hinz, B. and White, E. S. (2013) 'The myofibroblast matrix: implications for

tissue repair and fibrosis.', *The Journal of pathology*. England, 229(2), pp. 298–309. doi: 10.1002/path.4104.

Kolb, M., Gauldie, J. and Bellaye, P. S. (2016) 'Editorial: Extracellular Matrix: The Common Thread of Disease Progression in Fibrosis?', *Arthritis and Rheumatology*, 68(5), pp. 1053–1056. doi: 10.1002/art.39569.

Kono, M. *et al.* (2011) 'Plasma CCN2 (connective tissue growth factor; CTGF) is a potential biomarker in idiopathic pulmonary fibrosis (IPF)', *Clinica Chimica Acta*. Elsevier, 412(23–24), pp. 2211–2215. doi: 10.1016/J.CCA.2011.08.008.

Kopf, M., Schneider, C. and Nobs, S. P. (2014) 'The development and function of lung-resident macrophages and dendritic cells', *Nature Immunology*. Nature Publishing Group, a division of Macmillan Publishers Limited. All Rights Reserved., 16, p. 36. Available at: http://dx.doi.org/10.1038/ni.3052.

Koshman, Y. E. *et al.* (2015) 'Connective tissue growth factor regulates cardiac function and tissue remodeling in a mouse model of dilated cardiomyopathy.', *Journal of molecular and cellular cardiology*. England, 89(Pt B), pp. 214–222. doi: 10.1016/j.yjmcc.2015.11.003.

Krenning, G., Zeisberg, E. M. and Kalluri, R. (2010) 'The origin of fibroblasts and mechanism of cardiac fibrosis.', *Journal of cellular physiology*. United States, 225(3), pp. 631–637. doi: 10.1002/jcp.22322.

Kubota, S. and Takigawa, M. (2015) 'Cellular and molecular actions of CCN2/CTGF and its role under physiological and pathological conditions', *Clinical Science*, 128(3), pp. 181–196. doi: 10.1042/CS20140264.

Kuhn, C. and McDonald, J. A. (1991) 'The roles of the myofibroblast in idiopathic pulmonary fibrosis. Ultrastructural and immunohistochemical features of sites of active extracellular matrix synthesis.', *The American journal of pathology*. United States, 138(5), pp. 1257–1265.

Kurundkar, A. R. *et al.* (2016) 'The matricellular protein CCN1 enhances TGF-β1/SMAD3-dependent profibrotic signaling in fibroblasts and contributes to fibrogenic responses to lung injury', *FASEB Journal*, 30(6), pp. 2135–2150. doi: 10.1096/fj.201500173.

Lakatos, H. F. *et al.* (2006) 'Oropharyngeal aspiration of a silica suspension produces a superior model of silicosis in the mouse when compared to intratracheal instillation', *Experimental Lung Research*, 32(5), pp. 181–199. doi: 10.1080/01902140600817465.

Lambi, A. G. *et al.* (2012) 'The Skeletal site-specific role of connective tissue growth factor in prenatal osteogenesis', *Developmental Dynamics*, 241(12), pp. 1944–1959. doi: 10.1002/dvdy.23888.

Lan, Y. W. *et al.* (2015) 'Hypoxia-preconditioned mesenchymal stem cells attenuate bleomycin-induced pulmonary fibrosis', *Stem Cell Research and Therapy*. Stem Cell Research & Therapy, 6(1), pp. 1–17. doi: 10.1186/s13287-015-0081-6.

Landsman, L., Varol, C. and Jung, S. (2007) 'Distinct differentiation potential of blood monocyte subsets in the lung.', *Journal of immunology (Baltimore, Md. : 1950)*. United States, 178(4), pp. 2000–2007.

Laskin, D. L. *et al.* (2011) 'Macrophages and tissue injury: agents of defense or destruction?', *Annual review of pharmacology and toxicology*. United States, 51, pp. 267–288. doi: 10.1146/annurev.pharmtox.010909.105812.

Laskin, D. L., Malaviya, R. and Laskin, J. D. (2015) *Pulmonary Macrophages*. Second Edi, *Comparative Biology of the Normal Lung: Second Edition*. Second Edi. Elsevier Inc. doi: 10.1016/B978-0-12-404577-4.00032-1.

Lasky, J. A. *et al.* (1998) 'Connective tissue growth factor mRNA expression is upregulated in bleomycin-induced lung fibrosis.', *The American journal of physiology*. United States, 275(2 Pt 1), pp. L365-71.

Lau, L. F. and Nathans, D. (1987) 'Expression of a set of growth-related immediate early genes in BALB/c 3T3 cells: coordinate regulation with c-fos or c-myc.', *Proceedings of the National Academy of Sciences of the United States of America*. United States, 84(5), pp. 1182–1186.

Lavin, Y. *et al.* (2014) 'Tissue-resident macrophage enhancer landscapes are shaped by the local microenvironment.', *Cell*. United States, 159(6), pp. 1312–1326. doi: 10.1016/j.cell.2014.11.018.

Lawson, W. E. *et al.* (2005) 'Characterization of fibroblast-specific protein 1 in pulmonary fibrosis', *American Journal of Respiratory and Critical Care Medicine*, 171(8), pp. 899–907. doi: 10.1164/rccm.200311-1535OC.

Leask, A. *et al.* (2003) 'Connective tissue growth factor gene regulation. Requirements for its induction by transforming growth factor-beta 2 in fibroblasts.', *The Journal of biological chemistry*, 278(15), pp. 13008–15. doi: 10.1074/jbc.M210366200.

Leask, A. (2009) 'CIHR Group in Skeletal Development and Remodeling, Division of Oral Biology, Department of Physiology and Pharmacology, Schulich School of Medicine and Dentistry, University of Western Ontario, Dental Sciences Building, London ON N6A 5C1', *Matrix*, pp. 115–122.

Leask, A. and Abraham, D. J. (2006) 'All in the CCN family: essential matricellular signaling modulators emerge from the bunker', *Journal of Cell Science*, 119(23), pp. 4803–4810. doi: 10.1242/jcs.03270.

Leask, A., Denton, C. P. and Abraham, D. J. (2004) 'Insights into the molecular mechanism of chronic fibrosis: the role of connective tissue growth factor in scleroderma.', *The Journal of investigative dermatology*. United States, 122(1), pp. 1–6. doi: 10.1046/j.0022-202X.2003.22133.x.

Leeman, K. T., Fillmore # †, C. M. and Kim, C. F. (2014) 'Lung Stem and Progenitor Cells in Tissue Homeostasis and Disease'. doi: 10.1016/B978-0-12-416022-4.00008-1.

Leeming, D. J. *et al.* (2012) 'Biomarker Insights O r I g I n A L r e S e A r c h serological Investigation of the collagen Degradation Profile of Patients with Chronic Obstructive Pulmonary Disease or Idiopathic Pulmonary Fibrosis', *Biomarker Insights*, 7, p. 7. doi: 10.4137/BMI.S9415.

Lehnert, B. E., Valdez, Y. E. and Holland, L. M. (1985) 'Pulmonary macrophages: alveolar and interstitial populations.', *Experimental lung research*. England, 9(3–4), pp. 177–190.

Leu, S.-J., Lam, S. C.-T. and Lau, L. F. (2002) 'Pro-angiogenic activities of CYR61 (CCN1) mediated through integrins alphavbeta3 and alpha6beta1 in human umbilical vein endothelial cells.', *The Journal of biological chemistry*. United States, 277(48), pp. 46248–46255. doi: 10.1074/jbc.M209288200.

Levitzky, M. G. (2007a) *Function and structure of the respiratory system*, *Lange physiology series pulmonary physiology*.

Levitzky, M. G. (2007b) *Levitzky's Pulmonary Physiology (Lange Physiology)-McGraw-Hill Medical (2007)*, *Lange physiology series pulmonary physiology*. doi: 10.1036/0071437754.

Ley, B. and Collard, H. R. (2013) 'Epidemiology of idiopathic pulmonary fibrosis', *Clinical Epidemiology*, 5(1), pp. 483–492. doi: 10.2147/CLEP.S54815.

Li, I. M. H. *et al.* (2017) 'Characterization of mesenchymal-fibroblast cells using the Col1a2 promoter/enhancer', in *Methods in Molecular Biology*, pp. 139–161. doi: 10.1007/978-1-4939-7113-8_10.

Liegeois, M. *et al.* (2018) 'The interstitial macrophage: A long-neglected piece in the puzzle of lung immunity', *Cellular Immunology*. Elsevier, 330(February), pp. 91–96. doi: 10.1016/j.cellimm.2018.02.001.

Lin, S.-L. *et al.* (2008) 'Pericytes and perivascular fibroblasts are the primary source of collagen-producing cells in obstructive fibrosis of the kidney.', *The American journal of pathology*. United States, 173(6), pp. 1617–1627. doi: 10.2353/ajpath.2008.080433.

Lindahl, G. E. *et al.* (2013) 'Microarray profiling reveals suppressed interferon stimulated gene program in fibroblasts from scleroderma-associated interstitial lung disease', *Respiratory Research*. Respiratory Research, 14(1), p. 1. doi: 10.1186/1465-9921-14-80.

Lindenschmidt, R. C. *et al.* (1986) 'Intratracheal versus intravenous administration of bleomycin in mice: acute effects.', *Toxicology and applied pharmacology*. United States, 85(1), pp. 69–77.

Lipson, K. *et al.* (2017) 'Therapeutic pamrevlumab (FG-3019) is more effective than pirfenidone or nintedanib in a mouse radiation-induced lung fibrosis model', *European Respiratory Journal*, 50(suppl 61). Available at: http://erj.ersjournals.com/content/50/suppl_61/PA908.abstract.

Lipson, K. E. *et al.* (2012) 'CTGF is a central mediator of tissue remodeling and fibrosis and its inhibition can reverse the process of fibrosis', *Fibrogenesis & Tissue Repair*. doi: 10.1186/1755-1536-5-S1-S24.

Liu, S. *et al.* (2011) 'CCN2 is required for bleomycin-induced skin fibrosis in mice', *Arthritis and Rheumatism*, 63(1), pp. 239–246. doi: 10.1002/art.30074.

Liu, Y.-M., Nepali, K. and Liou, J.-P. (2017) 'Idiopathic Pulmonary Fibrosis: Current Status, Recent Progress, and Emerging Targets', *Journal of Medicinal Chemistry*. American Chemical Society, 60(2), pp. 527–553. doi: 10.1021/acs.jmedchem.6b00935.

Liu, Z. *et al.* (2018) 'Short-term tamoxifen treatment has long-term effects on metabolism in high-fat diet-fed mice with involvement of Nmnat2 in POMC neurons', *FEBS Letters*, 592, pp. 3305–3316. doi: 10.1002/1873-3468.13240.

Lopez-Larraza, D., De Luca, J. C. and Bianchi, N. O. (1990) 'The kinetics of DNA damage by bleomycin in mammalian cells.', *Mutation research*. Netherlands, 232(1), pp. 57–61.

Luczynski, P. *et al.* (2016) 'Growing up in a Bubble: Using Germ-Free Animals to Assess the Influence of the Gut Microbiota on Brain and Behavior.', *The international journal of neuropsychopharmacology*. Oxford University Press, 19(8). doi: 10.1093/ijnp/pyw020.

Lynch, D. A. *et al.* (2018) 'Diagnostic criteria for idiopathic pulmonary fibrosis: a Fleischner Society White Paper', *The Lancet Respiratory Medicine*. Elsevier Ltd, 6(2), pp. 138–153. doi: 10.1016/S2213-2600(17)30433-2.

Malik, A. R., Liszewska, E. and Jaworski, J. (2015) 'Matricellular proteins of the

Cyr61/CTGF/NOV (CCN) family and the nervous system', *Frontiers in Cellular Neuroscience*, 9. doi: 10.3389/fncel.2015.00237.

Manne, J. *et al.* (2013) 'Collagen content in skin and internal organs of the tight skin mouse: an animal model of scleroderma.', *Biochemistry research international*. United States, 2013, p. 436053. doi: 10.1155/2013/436053.

Marciniak, S. J. and Lomas, D. A. (2012) *Basic Aspects of Cellular and Molecular Biology*. Fourth Edi, *Clinical Respiratory Medicine: Fourth Edition*. Fourth Edi. Elsevier Inc. doi: 10.1016/B978-1-4557-0792-8.00002-7.

Marenzana, M. and Vande Velde, G. (2015) 'Refine, reduce, replace: Imaging of fibrosis and arthritis in animal models', *Best Practice and Research: Clinical Rheumatology*, 29(6), pp. 715–740. doi: 10.1016/j.berh.2016.02.001.

Martin-Mosquero, C. *et al.* (2006) 'Increased collagen deposition correlated with lung destruction in human emphysema.', *Histology and histopathology*. Spain, 21(8), pp. 823–828. doi: 10.14670/HH-21.823.

Martinez, F. O. *et al.* (2008) 'Macrophage activation and polarization.', *Frontiers in bioscience : a journal and virtual library*. United States, 13, pp. 453–461.

Masopust, D., Sivula, C. P. and Jameson, S. C. (2017) 'Of Mice, Dirty Mice, and Men: Using Mice To Understand Human Immunology.', *Journal of immunology (Baltimore, Md. : 1950)*. United States, 199(2), pp. 383–388. doi: 10.4049/jimmunol.1700453.

Masuda, N. *et al.* (1999) 'Analysis of chemical modification of RNA from formalin-fixed samples and optimization of molecular biology applications for such samples.', *Nucleic acids research*. England, 27(22), pp. 4436–4443.

Maus, U. A. *et al.* (2006) 'Resident alveolar macrophages are replaced by recruited monocytes in response to endotoxin-induced lung inflammation.', *American journal of respiratory cell and molecular biology*. United States, 35(2), pp. 227–235. doi: 10.1165/rcmb.2005-0241OC.

McAnulty, R. J. and Laurent, G. J. (1987) 'Collagen synthesis and degradation in vivo. Evidence for rapid rates of collagen turnover with extensive degradation of newly synthesized collagen in tissues of the adult rat.', *Collagen and related research*. Germany, 7(2), pp. 93–104.

Metzger, D. *et al.* (1995) 'Conditional site-specific recombination in mammalian cells using a ligand-dependent chimeric Cre recombinase.', *Proceedings of the National Academy of Sciences of the United States of America*. United States, 92(15), pp. 6991–6995.

Midgley, A. C. *et al.* (2013) 'Transforming growth factor-β1 (TGF-β1)-stimulated fibroblast to myofibroblast differentiation is mediated by hyaluronan (HA)-facilitated epidermal growth factor receptor (EGFR) and CD44 co-localization in lipid rafts.', *The Journal of biological chemistry*. American Society for Biochemistry and Molecular Biology, 288(21), pp. 14824–38. doi: 10.1074/jbc.M113.451336.

Miller, E. J. (1985) 'The structure of fibril-forming collagens.', *Annals of the New York Academy of Sciences*. United States, 460, pp. 1–13.

Minutti, C. M. *et al.* (2017) 'Tissue-specific contribution of macrophages to wound healing', *Seminars in Cell and Developmental Biology*. Elsevier Ltd, 61, pp. 3–11. doi: 10.1016/j.semcdb.2016.08.006.

Misharin, A. V. *et al.* (2017) 'Monocyte-derived alveolar macrophages drive lung fibrosis and persist in the lung over the life span', *The Journal of Experimental Medicine*, 214(8), pp. 2387–2404. doi: 10.1084/jem.20162152.

Moeller, A. *et al.* (2008) 'NIH Public Access', *The international journal of biochemistry & cell biology*, 40(3), pp. 362–382. doi: 10.1038/jid.2014.371.

Moeller, A. *et al.* (2008) 'The bleomycin animal model: A useful tool to investigate treatment options for idiopathic pulmonary fibrosis?', *The International Journal of Biochemistry & Cell Biology*, 40(3), pp. 362–382. doi: 10.1016/j.biocel.2007.08.011.

Mondrinos, M. J. *et al.* (2013) *Lungs*. Fourth Edi, *Principles of Tissue Engineering: Fourth Edition*. Fourth Edi. Elsevier. doi: 10.1016/B978-0-12-398358-9.00074-4.

Moore, B. B. *et al.* (2005) 'CCR2-mediated recruitment of fibrocytes to the alveolar space after fibrotic injury.', *The American journal of pathology*. United States, 166(3), pp. 675–684. doi: 10.1016/S0002-9440(10)62289-4.

Moore, B. B. and Hogaboam, C. M. (2008) 'Murine models of pulmonary fibrosis', *American Journal of Physiology-Lung Cellular and Molecular Physiology*. American Physiological Society, 294(2), pp. L152–L160. doi: 10.1152/ajplung.00313.2007.

Morrisey, E. E. and Hogan, B. L. M. (2010) 'Preparing for the First Breath: Genetic and Cellular Mechanisms in Lung Development', *Dev Cell*, 18(1), pp. 8–23. doi: 10.1016/j.devcel.2009.12.010.

Moshai, E. F. *et al.* (2014) 'Targeting the hedgehog-glioma-associated oncogene homolog pathway inhibits bleomycin-induced lung fibrosis in mice.', *American journal of respiratory cell and molecular biology*. United States, 51(1), pp. 11–25. doi: 10.1165/rcmb.2013-0154OC.

Mosser, D. M. and Edwards, J. P. (2008) 'Exploring the full spectrum of macrophage activation.', *Nature reviews. Immunology*. England, 8(12), pp. 958–969. doi: 10.1038/nri2448.

Moussad, E. E. and Brigstock, D. R. (2000) 'Connective tissue growth factor: what's in a name?', *Molecular genetics and metabolism*. United States, 71(1–2), pp. 276–292. doi: 10.1006/mgme.2000.3059.

MRC (2001) 'Mice and medicines', online article accessed 15/02/2019

Muller, R. *et al.* (1998) 'Morphometric analysis of human bone biopsies: a quantitative structural comparison of histological sections and micro-computed tomography.', *Bone*. United States, 23(1), pp. 59–66.

Murray, L. A. *et al.* (2009) 'Fibroblasts', *Asthma and COPD*, pp. 193–200. doi: 10.1016/B978-0-12-374001-4.00015-8.

Murray, P. J. and Wynn, T. A. (2011) 'Protective and pathogenic functions of macrophage subsets.', *Nature reviews. Immunology*. England, 11(11), pp. 723–737. doi: 10.1038/nri3073.

von Mutius, E. (2007) 'Allergies, infections and the hygiene hypothesis - The epidemiological evidence', *Immunobiology*, 212(6), pp. 433–439. doi: 10.1016/j.imbio.2007.03.002.

Muzumdar, M. D. *et al.* (2007) 'A global double-fluorescent cre reporter mouse', *Genesis*. doi: 10.1002/dvg.20335.

Nagy, A. (2000) ‘Cre recombinase: the universal reagent for genome tailoring.’, *Genesis (New York, N.Y. : 2000)*. United States, 26(2), pp. 99–109.

Nagy, A., Mar, L. and Watts, G. (2009) ‘Creation and use of a cre recombinase transgenic database.’, *Methods in molecular biology (Clifton, N.J.)*. United States, 530, pp. 365–378. doi: 10.1007/978-1-59745-471-1_19.

Nakanishi, H. *et al.* (2012) ‘Convergent signaling in the regulation of connective tissue growth factor in malignant mesothelioma: TGFβ signaling and defects in the Hippo signaling cascade’, *Cell Cycle*, 11(18), pp. 3373–3379. doi: 10.4161/cc.21397.

Navaratnam, V. *et al.* (2011) ‘The rising incidence of idiopathic pulmonary fibrosis in the U.K.’, *Thorax*. England, 66(6), pp. 462–467. doi: 10.1136/thx.2010.148031.

Navarro, S. and Driscoll, B. (2017) ‘Regeneration of the Aging Lung: A Mini-Review’, *Gerontology*. doi: 10.1159/000451081.

Ni, S. *et al.* (2015) ‘Bone marrow mesenchymal stem cells protect against bleomycin-induced pulmonary fibrosis in rat by activating Nrf2 signaling’, *International Journal of Clinical and Experimental Pathology*. e-Century Publishing Corporation, 8(7), pp. 7752–7761. Available at: http://www.ncbi.nlm.nih.gov/pmc/articles/PMC4555668/.

NICE (2013) *Pirfenidone for treating idiopathic pulmonary fibrosis*. Available at: https://www.nice.org.uk/guidance/ta504/documents/final-appraisal-determination-document (Accessed: 16 August 2018).

Nomellini, V. and Chen, H. (2012) *Murray and Nadel’s Textbook of Respiratory Medicine*, *Journal of Surgical Research*. doi: 10.1016/j.jss.2011.08.019.

Novak, A. *et al.* (2000) ‘Z/EG, a double reporter mouse line that expresses enhanced green fluorescent protein upon Cre-mediated excision.’, *Genesis (New York, N.Y. : 2000)*. United States, 28(3–4), pp. 147–155.

Ochs, M. *et al.* (2004) ‘The number of alveoli in the human lung.’, *American journal of respiratory and critical care medicine*. United States, 169(1), pp. 120–124. doi: 10.1164/rccm.200308-1107OC.

Omoto, S. *et al.* (2004) ‘Expression and localization of connective tissue growth factor (CTGF/Hcs24/CCN2) in osteoarthritic cartilage.’, *Osteoarthritis and cartilage*. England, 12(10), pp. 771–778. doi: 10.1016/j.joca.2004.06.009.

Ono, N. *et al.* (2014) ‘A subset of chondrogenic cells provides early mesenchymal progenitors in growing bones’, *Nature Cell Biology*. Nature Publishing Group, 16, p. 1157. Available at: http://dx.doi.org/10.1038/ncb3067.

Padilla-Carlin, D. J. *et al.* (2011) ‘Pulmonary inflammatory and fibrotic responses in Fischer 344 rats after intratracheal instillation exposure to Libby amphibole.’, *Journal of toxicology and environmental health. Part A*. England, 74(17), pp. 1111–1132. doi: 10.1080/15287394.2011.586940.

Pan, L. H. *et al.* (2001) ‘Type II alveolar epithelial cells and interstitial fibroblasts express connective tissue growth factor in IPF.’, *The European respiratory journal*. England, 17(6), pp. 1220–1227.

Paun, A. *et al.* (2010) ‘Combined Tlr2 and Tlr4 deficiency increases radiation-induced pulmonary fibrosis in mice.’, *International journal of radiation oncology, biology, physics*. United States, 77(4), pp. 1198–1205. doi: 10.1016/j.ijrobp.2009.12.065.

Peão, M. N. *et al.* (1993) 'Anatomy of Clara cell secretion: surface changes observed by scanning electron microscopy.', *Journal of Anatomy*, 182(Pt 3), pp. 377–388. Available at: http://www.ncbi.nlm.nih.gov/pmc/articles/PMC1259811/.

Pennica, D. *et al.* (1998) 'WISP genes are members of the connective tissue growth factor family that are up-regulated in wnt-1-transformed cells and aberrantly expressed in human colon tumors.', *Proceedings of the National Academy of Sciences of the United States of America*. United States, 95(25), pp. 14717–14722.

Perbal, B. (2013) 'CCN proteins: A centralized communication network.', *Journal of cell communication and signaling*. Netherlands, 7(3), pp. 169–177. doi: 10.1007/s12079-013-0193-7.

Phan, S. H. and Kunkel, S. L. (1992) 'Lung cytokine production in bleomycin-induced pulmonary fibrosis.', *Experimental lung research*. England, 18(1), pp. 29–43. doi: 10.3109/01902149209020649.

Picozzi, V. J. *et al.* (2016) *FG-3019, A Human Monoclonal Antibody to Connective Tissue Growth Factor, Combined with Chemotherapy in Patients with Locally Advanced or Metastatic Pancreatic Ductal Adenocarcinoma*. Available at: https://www.omicsonline.org/open-access/fg3019-a-human-monoclonal-antibody-to-connective-tissue-growth-factorcombined-with-chemotherapy-in-patients-with-locally-advanced.pdf (Accessed: 27 October 2018).

Planque, N. and Perbal, B. (2003) 'A structural approach to the role of CCN (CYR61/CTGF/NOV) proteins in tumourigenesis.', *Cancer cell international*. England, 3(1), p. 15. doi: 10.1186/1475-2867-3-15.

Plantier, L. *et al.* (2016) 'Transcriptome of Cultured Lung Fibroblasts in Idiopathic Pulmonary Fibrosis: Meta-Analysis of Publically Available Microarray Datasets Reveals Repression of Inflammation and Immunity Pathways', *International Journal of Molecular Sciences*, 17(12), p. 2091. doi: 10.3390/ijms17122091.

Ponticos, M. *et al.* (2004) 'Col1a2 enhancer regulates collagen activity during development and in adult tissue repair', 22, pp. 619–628. doi: 10.1016/j.matbio.2003.12.002.

Ponticos, M. *et al.* (2009) 'Pivotal role of connective tissue growth factor in lung fibrosis: MAPK-dependent transcriptional activation of type I collagen', *Arthritis and Rheumatism*, 60(7), pp. 2142–2155. doi: 10.1002/art.24620.

Qian, H. S. *et al.* (2016) 'Quantification and comparison of anti-fibrotic therapies by polarized SRM and SHG-based morphometry in rat UUO model', *PLoS ONE*, 11(6), pp. 1–13. doi: 10.1371/journal.pone.0156734.

Raghu, G. *et al.* (2011) 'An official ATS/ERS/JRS/ALAT statement: idiopathic pulmonary fibrosis: evidence-based guidelines for diagnosis and management.', *American journal of respiratory and critical care medicine*. United States, 183(6), pp. 788–824. doi: 10.1164/rccm.2009-040GL.

Raghu, G. *et al.* (2012) 'Phase 2 trial of FG-3019, anti-CTGF monoclonal antibody, in idiopathic pulmonary fibrosis (IPF): Preliminary safety and efficacy results', *European Respiratory Journal*, 40(Suppl 56). Available at: http://erj.ersjournals.com/content/40/Suppl_56/2819.abstract.

Raghu, G. *et al.* (2016) 'FG-3019 anti-connective tissue growth factor monoclonal antibody: results of an open-label clinical trial in IPF', *European Respiratory Journal*. Available at:

http://erj.ersjournals.com/content/early/2016/03/10/13993003.01030-2015.abstract.

Raghu, G., Nicholson, A. G. and Lynch, D. (2008) 'The classification, natural history and radiological/histological appearance of idiopathic pulmonary fibrosis and the other idiopathic interstitial pneumonias', *European Respiratory Review*, 17(109), pp. 108–115. doi: 10.1183/09059180.00010902.

Ramazani, Y. *et al.* (2018) 'Connective tissue growth factor (CTGF) from basics to clinics', *Matrix Biology*. Elsevier, 68–69, pp. 44–66. doi: 10.1016/J.MATBIO.2018.03.007.

Ramshaw, J. A. M., Shah, N. K. and Brodsky, B. (1998) 'Gly-X-Y tripeptide frequencies in collagen: A context for host-guest triple-helical peptides', *Journal of Structural Biology*, 122(1–2), pp. 86–91. doi: 10.1006/jsbi.1998.3977.

Rasmussen, D. L. and Pfau, J. C. (2012) 'Asbestos activates CH12.LX B-lymphocytes via macrophage signaling.', *Journal of immunotoxicology*. England, 9(2), pp. 129–140. doi: 10.3109/1547691X.2011.631953.

Redente, E. F. *et al.* (2011) 'Age and sex dimorphisms contribute to the severity of bleomycin-induced lung injury and fibrosis.', *American journal of physiology. Lung cellular and molecular physiology*. United States, 301(4), pp. L510-8. doi: 10.1152/ajplung.00122.2011.

Reinert, T. *et al.* (2013) 'Bleomycin-Induced Lung Injury', *Journal of Cancer Research*. Hindawi, 2013, pp. 1–9. doi: 10.1155/2013/480608.

Ricard-Blum, S. (2011) 'The Collagen Family', *Cold Spring Harbor Perspectives in Biology*, 3(1), pp. 1–19. doi: 10.1101/cshperspect.a004978.

Richeldi, L. *et al.* (2014) 'Efficacy and safety of nintedanib in idiopathic pulmonary fibrosis.', *The New England journal of medicine*. United States, 370(22), pp. 2071–2082. doi: 10.1056/NEJMoa1402584.

Richeldi, L., Collard, H. R. and Jones, M. G. (2017) 'Idiopathic pulmonary fibrosis', *The Lancet*, 389(10082), pp. 1941–1952. doi: 10.1016/S0140-6736(17)30866-8.

Rittié, L. *et al.* (2011) 'Spatial-temporal modulation of CCN proteins during wound healing in human skin in vivo', *Journal of Cell Communication and Signaling*, 5(1), pp. 69–80. doi: 10.1007/s12079-010-0114-y.

Robbe, A. *et al.* (2015) 'Intratracheal Bleomycin Aerosolization: The Best Route of Administration for a Scalable and Homogeneous Pulmonary Fibrosis Rat Model?', *BioMed Research International*. Hindawi, 2015, pp. 1–10. doi: 10.1155/2015/198418.

Roberts, S. N. *et al.* (1995) 'A novel model for human interstitial lung disease: hapten-driven lung fibrosis in rodents.', *The Journal of pathology*. England, 176(3), pp. 309–318. doi: 10.1002/path.1711760313.

Robinson, S. P. *et al.* (1991) 'Metabolites, pharmacodynamics, and pharmacokinetics of tamoxifen in rats and mice compared to the breast cancer patient.', *Drug metabolism and disposition: the biological fate of chemicals*. United States, 19(1), pp. 36–43.

Rock, J. R. *et al.* (2011) 'Multiple stromal populations contribute to pulmonary fibrosis without evidence for epithelial to mesenchymal transition', *Proceedings of the National Academy of Sciences*, 108(52), pp. E1475–E1483. doi: 10.1073/pnas.1117988108.

Roggli, V. L. *et al.* (2010) 'Pathology of asbestosis- An update of the diagnostic criteria: Report of the asbestosis committee of the college of american pathologists and pulmonary

pathology society.', *Archives of pathology & laboratory medicine*. United States, 134(3), pp. 462–480. doi: 10.1043/1543-2165-134.3.462.

Roy, S. R. *et al.* (2003) 'Bacterial DNA in house and farm barn dust', *Journal of Allergy and Clinical Immunology*, 112(3), pp. 571–578. doi: 10.1016/S0091-6749(03)01863-3.

Ruscitti, F. *et al.* (2017) 'Longitudinal assessment of bleomycin-induced lung fibrosis by Micro-CT correlates with histological evaluation in mice.', *Multidisciplinary respiratory medicine*. England, 12, p. 8. doi: 10.1186/s40248-017-0089-0.

Schaefer, C. J. *et al.* (2011) 'Antifibrotic activities of pirfenidone in animal models.', *European respiratory review : an official journal of the European Respiratory Society*. England, 20(120), pp. 85–97. doi: 10.1183/09059180.00001111.

Schambach, S. J. *et al.* (2010) 'Application of micro-CT in small animal imaging', *Methods*. Academic Press, 50(1), pp. 2–13. doi: 10.1016/J.YMETH.2009.08.007.

Schmidt, M. *et al.* (2002) 'Cell Cycle Inhibition by FoxO Forkhead Transcription Factors Involves Downregulation of Cyclin D', *Molecular and Cellular Biology*, 22(22), pp. 7842–7852. doi: 10.1128/MCB.22.22.7842-7852.2002.

Schrier, D. J., Kunkel, R. G. and Phan, S. H. (1983) 'The role of strain variation in murine bleomycin-induced pulmonary fibrosis.', *The American review of respiratory disease*. United States, 127(1), pp. 63–66. doi: 10.1164/arrd.1983.127.1.63.

Schwenk, F. *et al.* (1998) 'Temporally and spatially regulated somatic mutagenesis in mice.', *Nucleic acids research*. England, 26(6), pp. 1427–1432.

Scotton, C. J. *et al.* (2009) 'Increased local expression of coagulation factor X contributes to the fibrotic response in human and murine lung injury.', *The Journal of clinical investigation*. United States, 119(9), pp. 2550–2563. doi: 10.1172/JCI33288.

Scotton, C. J. *et al.* (2013) 'Ex vivo micro-computed tomography analysis of bleomycin-induced lung fibrosis for preclinical drug evaluation', *European Respiratory Journal*, 42(6), pp. 1633–1645. doi: 10.1183/09031936.00182412.

Scotton, C. J. and Chambers, R. C. (2010) 'Bleomycin revisited: towards a more representative model of IPF?' doi: 10.1152/ajplung.00258.2010.

Sebring, R. J. and Lehnert, B. E. (1992) 'Morphometric comparisons of rat alveolar macrophages, pulmonary interstitial macrophages, and blood monocytes.', *Experimental lung research*. England, 18(4), pp. 479–496.

Selman, M. *et al.* (1986) 'Concentration, biosynthesis and degradation of collagen in idiopathic pulmonary fibrosis', *Thorax*, 41(5), pp. 355–359. doi: 10.1136/thx.41.5.355.

Selman, M., King, T. E. and Pardo, A. (2001) 'Idiopathic pulmonary fibrosis: prevailing and evolving hypotheses about its pathogenesis and implications for therapy.', *Annals of internal medicine*. United States, 134(2), pp. 136–151.

Seyer, J. M., Kang, A. H. and Rodnan, G. (1981) 'Investigation of type i and type iii collagens of the lung in progressive systemic sclerosis', *Arthritis & Rheumatism*, 24(4), pp. 625–631. doi: 10.1002/art.1780240410.

Sharir, A., Ramniceanu, G. and Brumfeld, V. (2011) 'High resolution 3D imaging of ex-vivo biological samples by micro CT.', *Journal of visualized experiments : JoVE*. United States, (52). doi: 10.3791/2688.

Shi-wen, X. *et al.* (2006) 'CCN2 is necessary for adhesive responses to transforming growth factor-beta1 in embryonic fibroblasts.', *The Journal of biological chemistry*. United States, 281(16), pp. 10715–10726. doi: 10.1074/jbc.M511343200.

Shi-Wen, X., Leask, A. and Abraham, D. (2008) 'Regulation and function of connective tissue growth factor/CCN2 in tissue repair, scarring and fibrosis.', *Cytokine & growth factor reviews*. England, 19(2), pp. 133–144. doi: 10.1016/j.cytogfr.2008.01.002.

Sidik, K. and Smerdon2, M. J. (1990) *Bleomycin-induced DNA Damage and Repair in Human Cells Permeabilized with Lysophosphatidylcholine1*, *CANCER RESEARCH*. Available at: http://cancerres.aacrjournals.org/content/canres/50/5/1613.full.pdf (Accessed: 22 October 2018).

Sime, P. J. and O'reilly, K. M. A. (2001) 'Fibrosis of the lung and other tissues: New concepts in pathogenesis and treatment', *Clinical Immunology*, 99(3), pp. 308–319. doi: 10.1006/clim.2001.5008.

Smith, B. L., Bauer, G. B. and Povirk, L. F. (1994) 'DNA damage induced by bleomycin, neocarzinostatin, and melphalan in a precisely positioned nucleosome. Asymmetry in protection at the periphery of nucleosome-bound DNA', *Journal of Biological Chemistry*, 269(48), pp. 30587–30594. doi: 10.1161/STROKEAHA.106.478156.

Society, A. T. (2010) 'Interstitial Lung Disease', *Breathing in America: Diseases, Progress, and Hope*, (10), pp. 99–108. doi: 10.1159/000068408.

Society, A. T. S. R. (2002) 'American Thoracic Society American Thoracic Society / European Respiratory Society International Multidisciplinary Consensus Classification of the Idiopathic Interstitial Pneumonias', *American Journal of Respiratory and Critical Care Medicine*, 166(6), pp. 518–626. doi: 10.1183/09031936.02.00492002.

Sonnylal, S. *et al.* (2010) 'Selective expression of connective tissue growth factor in fibroblasts in vivo promotes systemic tissue fibrosis', *Arthritis and Rheumatism*, 62(5), pp. 1523–1532. doi: 10.1002/art.27382.

Srinivasan, M., Sedmak, D. and Jewell, S. (2002) 'Effect of fixatives and tissue processing on the content and integrity of nucleic acids.', *The American journal of pathology*. United States, 161(6), pp. 1961–1971. doi: 10.1016/S0002-9440(10)64472-0.

Stelekati, E. and Wherry, E. J. (2012) 'Chronic Bystander Infections and Immunity to Unrelated Antigens', *Cell Host & Microbe*. Cell Press, 12(4), pp. 458–469. doi: 10.1016/J.CHOM.2012.10.001.

Stone, K. C. *et al.* (1992) 'Allometric relationships of cell numbers and size in the mammalian lung.', *American journal of respiratory cell and molecular biology*. United States, 6(2), pp. 235–243. doi: 10.1165/ajrcmb/6.2.235.

Strachan, D. P. (1989) 'Household Size', *BMJ : British Medical Journal*, 299(November), pp. 1259–1260. doi: 10.1136/bmj.299.6710.1259.

Strongman, H., Kausar, I. and Maher, T. M. (2018) 'Incidence, Prevalence, and Survival of Patients with Idiopathic Pulmonary Fibrosis in the UK', *Advances in Therapy*. Springer Healthcare, 35(5), pp. 724–736. doi: 10.1007/s12325-018-0693-1.

Suarez, C. J., Dintzis, S. M. and Frevert, C. W. (2012) 'Respiratory', *Comparative Anatomy and Histology*, pp. 121–134. doi: 10.1016/B978-0-12-381361-9.00009-3.

Swiderski, R. E. *et al.* (1998) 'Differential expression of extracellular matrix remodeling

genes in a murine model of bleomycin-induced pulmonary fibrosis', *The American Journal of Pathology*, 152(3), pp. 821–828. doi: 10.1016/S0169-7218(11)02412-9.

Tanjore, H. *et al.* (2009) 'Contribution of epithelial-derived fibroblasts to bleomycin-induced lung fibrosis', *American Journal of Respiratory and Critical Care Medicine*, 180(7), pp. 657–665. doi: 10.1164/rccm.200903-0322OC.

The Jackson Laboratory (no date) *Mouse Genetics - The mouse as a model for human disease.* Available at: https://www.jax.org/personalized-medicine/why-mouse-genetics# (Accessed: 15 March 2019).

Thickett, D. R. *et al.* (2014) 'Improving care for patients with idiopathic pulmonary fibrosis (IPF) in the UK: A round table discussion', *Thorax*, 69(12), pp. 1136–1140. doi: 10.1136/thoraxjnl-2014-206284.

Thrall, R. S. *et al.* (1979) 'Bleomycin-induced pulmonary fibrosis in the rat: inhibition by indomethacin.', *The American journal of pathology*. United States, 95(1), pp. 117–130.

Tomasek, J. J. *et al.* (2005) 'Regulation of α-Smooth Muscle Actin Expression in Granulation Tissue Myofibroblasts Is Dependent on the Intronic CArG Element and the Transforming Growth Factor-β1 Control Element', *The American Journal of Pathology*. Elsevier, 166(5), pp. 1343–1351. doi: 10.1016/S0002-9440(10)62353-X.

Tomcik, M. *et al.* (2015) 'S100A4 amplifies TGF-β-induced fibroblast activation in systemic sclerosis.', *Annals of the rheumatic diseases*. BMJ Publishing Group Ltd, 74(9), pp. 1748–55. doi: 10.1136/annrheumdis-2013-204516.

Tracy, L. E., Minasian, R. A. and Caterson, E. J. (2016) 'Extracellular Matrix and Dermal Fibroblast Function in the Healing Wound', *Advances in Wound Care*, 5(3), pp. 119–136. doi: 10.1089/wound.2014.0561.

Travis, M. A. and Sheppard, D. (2014) 'TGF-beta activation and function in immunity.', *Annual review of immunology*. United States, 32, pp. 51–82. doi: 10.1146/annurev-immunol-032713-120257.

Travis, W. D. *et al.* (2013) 'An official American Thoracic Society/European Respiratory Society statement: Update of the international multidisciplinary classification of the idiopathic interstitial pneumonias', *American Journal of Respiratory and Critical Care Medicine*, 188(6), pp. 733–748. doi: 10.1164/rccm.201308-1483ST.

Tsai, C. C. *et al.* (2018) 'Essential role of connective tissue growth factor (CTGF) in transforming growth factor-β1 (TGF-β1)-induced myofibroblast transdifferentiation from Graves' orbital fibroblasts', *Scientific Reports*. Springer US, 8(1), pp. 1–10. doi: 10.1038/s41598-018-25370-3.

Tsukui, T. *et al.* (2013) 'Qualitative Rather than Quantitative Changes Are Hallmarks of Fibroblasts in Bleomycin-Induced Pulmonary Fibrosis', *The American Journal of Pathology*. doi: 10.1016/j.ajpath.2013.06.005.

Tyrrell, L., Elias, J. and Longley, J. (1995) 'Detection of specific mRNAs in routinely processed dermatopathology specimens.', *The American Journal of dermatopathology*. United States, 17(5), pp. 476–483.

Umezawa, H. *et al.* (1967) 'Studies on bleomycin.', *Cancer*. United States, 20(5), pp. 891–895.

De Val, S. *et al.* (2002) 'Identification of the key regions within the mouse Pro-α2(I) collagen

gene far-upstream enhancer', *Journal of Biological Chemistry*, 277(11), pp. 9286–9292. doi: 10.1074/jbc.M111040200.

Vancheri, C. *et al.* (2010) 'Idiopathic pulmonary fibrosis: A disease with similarities and links to cancer biology', *European Respiratory Journal*, 35(3), pp. 496–504. doi: 10.1183/09031936.00077309.

Ventura, A. *et al.* (2007) 'Restoration of p53 function leads to tumour regression in vivo', *Nature*, 445(7128), pp. 661–665. doi: 10.1038/nature05541.

Voltz, J. W. *et al.* (2008) 'Male sex hormones exacerbate lung function impairment after bleomycin-induced pulmonary fibrosis.', *American journal of respiratory cell and molecular biology*. United States, 39(1), pp. 45–52. doi: 10.1165/rcmb.2007-0340OC.

Wang, C. *et al.* (2014) 'Inhibition of Wnt/ -catenin signaling promotes epithelial differentiation of mesenchymal stem cells and repairs bleomycin-induced lung injury', *AJP: Cell Physiology*, 307(3), pp. C234–C244. doi: 10.1152/ajpcell.00366.2013.

Wang, S. and Hubmayr, R. D. (2011) 'Type I alveolar epithelial phenotype in primary culture.', *American journal of respiratory cell and molecular biology*. United States, 44(5), pp. 692–699. doi: 10.1165/rcmb.2009-0359OC.

Wang, X. *et al.* (2015) 'Blocking the Wnt/β-catenin pathway by lentivirus-mediated short hairpin RNA targeting β-catenin gene suppresses silica-induced lung fibrosis in mice', *International Journal of Environmental Research and Public Health*, 12(9), pp. 10739–10754. doi: 10.3390/ijerph120910739.

Wang, X., McLennan, S. V. and Twigg, S. M. (2011) 'CCN-2 is up-regulated by and mediates effects of matrix bound advanced glycated end-products in human renal mesangial cells', *Journal of Cell Communication and Signaling*. Springer Netherlands, 5(3), pp. 193–200. doi: 10.1007/s12079-011-0137-z.

Wang, Y. *et al.* (2015) 'Maresin 1 inhibits epithelial-to-mesenchymal transition in vitro and attenuates bleomycin induced lung fibrosis in vivo', *Shock*, 44(5), pp. 496–502. doi: 10.1097/SHK.0000000000000446.

Ward, H. E. and Nicholas, T. E. (1984) 'Alveolar type I and type II cells.', *Australian and New Zealand journal of medicine*. Australia, 14(5 Suppl 3), pp. 731–734.

Van De Water, L., Varney, S. and Tomasek, J. J. (2013) 'Mechanoregulation of the Myofibroblast in Wound Contraction, Scarring, and Fibrosis: Opportunities for New Therapeutic Intervention', *Advances in Wound Care*, 2(4), pp. 122–141. doi: 10.1089/wound.2012.0393.

Van 'T Hof, R. J. *et al.* (2017) 'Open source software for semi-automated histomorphometry of bone resorption and formation parameters.', *Bone*. United States, 99, pp. 69–79. doi: 10.1016/j.bone.2017.03.051.

Webb, J. A. and Armstrong, J. (2002) 'Chronic idiopathic pulmonary fibrosis in a West Highland white terrier.', *The Canadian veterinary journal = La revue veterinaire canadienne*. Canada, 43(9), pp. 703–705.

Weinberger, S. E., Cockrill, B. A. and Mandel, J. (2014) 'Pulmonary Anatomy and Physiology', in *Principles of Pulmonary Medicine*. doi: 10.1016/B978-1-4557-2532-8.00001-3.

Williams, K. J. *et al.* (2007) 'Equine multinodular pulmonary fibrosis: a newly recognized

herpesvirus-associated fibrotic lung disease.', *Veterinary pathology*. United States, 44(6), pp. 849–862. doi: 10.1354/vp.44-6-849.

Williamson, J. D., Sadofsky, L. R. and Hart, S. P. (2015) 'The pathogenesis of bleomycin-induced lung injury in animals and its applicability to human idiopathic pulmonary fibrosis', *Experimental Lung Research*, 41(2), pp. 57–73. doi: 10.3109/01902148.2014.979516.

Wills-karp, M., Santeliz, J. and Karp, C. L. (2001) 'Revisiting the hygiene hypothesis', *Nature Reviews Immunology*, (November), pp. 69–74. doi: 10.1038/35095579.

Wolkove, N. and Baltzan, M. (2009) 'Amiodarone pulmonary toxicity.', *Canadian respiratory journal*. Egypt, 16(2), pp. 43–48. doi: 10.1155/2009/282540.

Wollin, L. *et al.* (2014) 'Antifibrotic and anti-inflammatory activity of the tyrosine kinase inhibitor nintedanib in experimental models of lung fibrosis.', *The Journal of pharmacology and experimental therapeutics*. United States, 349(2), pp. 209–220. doi: 10.1124/jpet.113.208223.

Wolters, P. J. *et al.* (2018) 'Time for a change: is idiopathic pulmonary fibrosis still idiopathic and only fibrotic? HHS Public Access Author manuscript', *Lancet Respir Med*, 6(2), pp. 154–160. doi: 10.1016/S2213-2600(18)30007-9.

Wolters, P. J., Collard, H. R. and Jones, K. D. (2014) 'Pathogenesis of idiopathic pulmonary fibrosis.', *Annual review of pathology*, 9, pp. 157–79. doi: 10.1146/annurev-pathol-012513-104706.

Wong, M. H., Chapin, O. C. and Johnson, M. D. (2012) 'LPS-Stimulated Cytokine Production in Type I Cells Is Modulated by the Renin–Angiotensin System', *American Journal of Respiratory Cell and Molecular Biology*. American Thoracic Society, 46(5), pp. 641–650. doi: 10.1165/rcmb.2011-0289OC.

Wostmann, B. S. *et al.* (1970) 'Serum proteins and lymphoid tissues in germ-free mice fed a chemically defined, water soluble, low molecular weight diet.', *Immunology*. England, 19(3), pp. 443–448.

Wu, Q. *et al.* (2016) 'Members of the Cyr61/CTGF/NOV Protein Family: Emerging Players in Hepatic Progenitor Cell Activation and Intrahepatic Cholangiocarcinoma', *Gastroenterology Research and Practice*. doi: 10.1155/2016/2313850.

Wynn, T. A. (2008) 'Cellular and molecular mechanisms of fibrosis.', *The Journal of pathology*. England, 214(2), pp. 199–210. doi: 10.1002/path.2277.

Wynn, T. A., Chawla, A. and Pollard, J. W. (2013) 'Macrophage biology in development, homeostasis and disease.', *Nature*. England, 496(7446), pp. 445–455. doi: 10.1038/nature12034.

Xu, S. W. *et al.* (2006) 'CCN2 is necessary for adhesive responses to transforming growth factor-β1 in embryonic fibroblasts', *Journal of Biological Chemistry*, 281(16), pp. 10715–10726. doi: 10.1074/jbc.M511343200.

Xu, X. *et al.* (2018) 'Transforming growth factor-beta in stem cells and tissue homeostasis.', *Bone research*. China, 6, p. 2. doi: 10.1038/s41413-017-0005-4.

Yamamoto, K. *et al.* (2012) 'Type I alveolar epithelial cells mount innate immune responses during pneumococcal pneumonia.', *Journal of immunology (Baltimore, Md. : 1950)*. United States, 189(5), pp. 2450–2459. doi: 10.4049/jimmunol.1200634.

Yang, J. *et al.* (2014) 'Activated alveolar epithelial cells initiate fibrosis through autocrine

and paracrine secretion of connective tissue growth factor', *AJP: Lung Cellular and Molecular Physiology*, 306(8), pp. L786–L796. doi: 10.1152/ajplung.00243.2013.

Yatomi, M. *et al.* (2015) '17(R)-resolvin D1 ameliorates bleomycin-induced pulmonary fibrosis in mice.', *Physiological reports*. United States, 3(12). doi: 10.14814/phy2.12628.

Yeger, H. and Perbal, B. (2007) 'The ccn family of genes: A perspective on ccn biology and therapeutic potential', *Journal of Cell Communication and Signaling*. doi: 10.1007/s12079-008-0022-6.

Yona, S. *et al.* (2013) 'Fate mapping reveals origins and dynamics of monocytes and tissue macrophages under homeostasis.', *Immunity*. United States, 38(1), pp. 79–91. doi: 10.1016/j.immuni.2012.12.001.

Yu, C.-C. *et al.* (2009) 'Thrombin-induced connective tissue growth factor expression in human lung fibroblasts requires the ASK1/JNK/AP-1 pathway.', *Journal of immunology (Baltimore, Md. : 1950)*. United States, 182(12), pp. 7916–7927. doi: 10.4049/jimmunol.0801582.

Zhang, R. *et al.* (1998) 'Identification of rCop-1, a new member of the CCN protein family, as a negative regulator for cell transformation', *Mol Cell Biol*, 18(10), pp. 6131–6141. doi: 10.1128/MCB.18.10.6131.

Zhang, Y., Kaminski, N. and Simmons, R. P. (2012) 'Biomarkers in idiopathic pulmonary fibrosis'. doi: 10.1097/MCP.0b013e328356d03c.

Zhong, Z. A. *et al.* (2015) 'Optimizing tamoxifen-inducible Cre/loxp system to reduce tamoxifen effect on bone turnover in long bones of young mice.', *Bone*. NIH Public Access, 81, pp. 614–619. doi: 10.1016/j.bone.2015.07.034.

Zhou, W. and Wang, Y. (2016) 'Candidate genes of idiopathic pulmonary fibrosis: Current evidence and research', *Application of Clinical Genetics*, 9(August 2015), pp. 5–13. doi: 10.2147/TACG.S61999.

Zhu, M. *et al.* (2008) 'Tamoxifen-inducible Cre-recombination in articular chondrocytes of adult Col2a1-CreER(T2) transgenic mice.', *Osteoarthritis and cartilage*. England, 16(1), pp. 129–130. doi: 10.1016/j.joca.2007.08.001.

Van 'T Hof, R. J. *et al.* (2017) 'Open source software for semi-automated histomorphometry of bone resorption and formation parameters.', *Bone*. United States, 99, pp. 69–79. doi: 10.1016/j.bone.2017.03.051.

Abrams, G. D., Bauer, H. and Sprinz, H. (1963) 'Influence of the normal flora on mucosal morphology and cellular renewal in the ileum. A comparison of germ-free and conventional mice.', *Laboratory investigation; a journal of technical methods and pathology*. United States, 12, pp. 355–364.

Adamson, I. (1976) 'Pulmonary toxicity of bleomycin', *Environmental Health Perspectives*, 16, pp. 119–125. Available at: http://www.ncbi.nlm.nih.gov/pmc/articles/PMC1475236/.

Adamson, I. Y. R. and Bowden, D. H. (1974) 'The Pathogenesis of Bleomycin-Induced Pulmonary Fibrosis in Mice', *The American Journal of Pathology*, 77(2), pp. 185–198. Available at: http://www.ncbi.nlm.nih.gov/pmc/articles/PMC1910906/.

Albert, R. K., Spiro, S. G. and Jett, J. R. (2008) *Clinical respiratory medicine*, *Clinical Respiratory Medicine*. doi: 10.1016/B978-0-323-04825-5.X1000-8.

Allen, J. T. *et al.* (1999) 'Enhanced insulin-like growth factor binding protein-related protein

2 (connective tissue growth factor) expression in patients with idiopathic pulmonary fibrosis and pulmonary sarcoidosis', *American Journal of Respiratory Cell and Molecular Biology*, 21(6), pp. 693–700. doi: 10.1165/ajrcmb.21.6.3719.

Allen, J. T. and Spiteri, M. A. (2002) 'Growth factors in idiopathic pulmonary fibrosis: relative roles.', *Respiratory research*. England, 3, p. 13.

Allen, M. J. *et al.* (2001) 'Polysaccharide Recognition by Surfactant Protein D: Novel Interactions of a C-Type Lectin with Nonterminal Glucosyl Residues', *Biochemistry*. American Chemical Society, 40(26), pp. 7789–7798. doi: 10.1021/bi002901q.

Armstrong, J. D. *et al.* (1982) 'Lung tissue volume estimated by simultaneous radiographic and helium dilution methods.', *Thorax*, 37(9), pp. 676–679. Available at: http://www.ncbi.nlm.nih.gov/pmc/articles/PMC459405/.

Arnott, J. A. *et al.* (2007) 'Connective tissue growth factor (CTGF/CCN2) is a downstream mediator for TGF-??1-induced extracellular matrix production in osteoblasts', *Journal of Cellular Physiology*, 210(3), pp. 843–852. doi: 10.1002/jcp.20917.

Ashley, S. L. *et al.* (2017) 'Periostin regulates fibrocyte function to promote myofibroblast differentiation and lung fibrosis', *Mucosal Immunology*. Nature Publishing Group, 10(2), pp. 341–351. doi: 10.1038/mi.2016.61.

Babic, A. M., Chen, C. C. and Lau, L. F. (1999) 'Fisp12/mouse connective tissue growth factor mediates endothelial cell adhesion and migration through integrin alphavbeta3, promotes endothelial cell survival, and induces angiogenesis in vivo.', *Molecular and cellular biology*. United States, 19(4), pp. 2958–2966.

Babinet, C. (2000) 'Transgenic mice: an irreplaceable tool for the study of mammalian development and biology.', *Journal of the American Society of Nephrology : JASN*. United States, 11 Suppl 1, pp. S88-94.

Bach, J.-F. (2017) 'The hygiene hypothesis in autoimmunity: the role of pathogens and commensals', *Nature Reviews Immunology*. Nature Publishing Group, a division of Macmillan Publishers Limited. All Rights Reserved., 18, p. 105. Available at: https://doi.org/10.1038/nri.2017.111.

Badea, T. C., Wang, Y. and Nathans, J. (2003) 'A noninvasive genetic/pharmacologic strategy for visualizing cell morphology and clonal relationships in the mouse.', *The Journal of neuroscience : the official journal of the Society for Neuroscience*. United States, 23(6), pp. 2314–2322.

Bai, K.-J. *et al.* (2013) 'Thrombin-induced CCN2 expression in human lung fibroblasts requires the c-Src/JAK2/STAT3 pathway', *Journal of Leukocyte Biology*, 93(1), pp. 101–112. doi: 10.1189/jlb.0911449.

Ballinger, M. N. and Christman, J. W. (2016) 'Pulmonary macrophages: Overlooked and underappreciated', *American Journal of Respiratory Cell and Molecular Biology*, 54(1), pp. 1–2. doi: 10.1165/rcmb.2015-0270ED.

Bantsimba-Malanda, C. *et al.* (2010) 'A role for dendritic cells in bleomycin-induced pulmonary fibrosis in mice?', *American Journal of Respiratory and Critical Care Medicine*, 182(3), pp. 385–395. doi: 10.1164/rccm.200907-1164OC.

Barbarin, V. *et al.* (2005) 'The role of pro- and anti-inflammatory responses in silica-induced lung fibrosis.', *Respiratory research*. England, 6, p. 112. doi: 10.1186/1465-9921-6-112.

Barkauskas, C. E. *et al.* (2013) 'Type 2 alveolar cells are stem cells in adult lung.', *The Journal of clinical investigation*. United States, 123(7), pp. 3025–3036. doi: 10.1172/JCI68782.

Bateman, E. D. *et al.* (1983) 'Cryptogenic fibrosing alveolitis: Prediction of fibrogenic activity from immunohistochemical studies of collagen types in lung biopsy specimens', *Thorax*, 38(2), pp. 93–101. doi: 10.1136/thx.38.2.93.

Bauer, J. S. and Link, T. M. (2009) 'Advances in osteoporosis imaging.', *European journal of radiology*. Ireland, 71(3), pp. 440–449. doi: 10.1016/j.ejrad.2008.04.064.

Baum, J. and Duffy, H. S. (2011) 'Fibroblasts and Myofibroblasts: What Are We Talking About?', *Journal of Cardiovascular Pharmacology*. doi: 10.1097/FJC.0b013e3182116e39.

Bejvl, I. *et al.* (2013) 'Analysis of plasma surfactant protein D levels in lung transplant recipients.', *Transplant infectious disease : an official journal of the Transplantation Society*. Denmark, 15(6), pp. 645–651. doi: 10.1111/tid.12132.

Berngard, S. C. and Afshar, K. (2016) 'Idiopathic pulmonary fibrosis: Past, present, future-a review from Talmadge King's ATS 2016 presentation', *Journal of Thoracic Disease*, 8(7), pp. S559–S561. doi: 10.21037/jtd.2016.07.31.

Beura, L. K. *et al.* (2016) 'Normalizing the environment recapitulates adult human immune traits in laboratory mice.', *Nature*. England, 532(7600), pp. 512–516. doi: 10.1038/nature17655.

Bickelhaupt, S. *et al.* (2017) 'Effects of CTGF Blockade on Attenuation and Reversal of Radiation-Induced Pulmonary Fibrosis', *JNCI: Journal of the National Cancer Institute*. Oxford University Press, 109(8). doi: 10.1093/jnci/djw339.

Bienkowski, R. S., Baum, B. J. and Crystal, R. G. (1978) 'Fibroblasts degrade newly synthesised collagen within the cell before secretion.', *Nature*. England, 276(5686), pp. 413–416.

Biernacka, A., Dobaczewski, M. and Frangogiannis, N. G. (2011) 'TGF-beta signaling in fibrosis.', *Growth factors (Chur, Switzerland)*. England, 29(5), pp. 196–202. doi: 10.3109/08977194.2011.595714.

Bou-Gharios, G. *et al.* (1996) 'A potent far-upstream enhancer in the mouse proα2(I) collagen gene regulates expression of reporter genes in transgenic mice', *Journal of Cell Biology*, 134(5), pp. 1333–1344. doi: 10.1083/jcb.134.5.1333.

Bradham, D. M. *et al.* (1991) 'Connective tissue growth factor: a cysteine-rich mitogen secreted by human vascular endothelial cells is related to the SRC-induced immediate early gene product CEF-10.', *The Journal of cell biology*. United States, 114(6), pp. 1285–1294.

Braun, R. K. *et al.* (1996) 'Comparison of two models of bleomycin-induced lung fibrosis in mouse on the level of leucocytes and T cell subpopulations in bronchoalveolar lavage', *Comparative Haematology International*. Springer-Verlag, 6(3), pp. 141–148. doi: 10.1007/BF00368457.

Brigstock, D. R. (1999) 'The Connective Tissue Growth Factor / Cysteine-', *Endocrine Reviews*, 20(June), pp. 189–206.

Brigstock, D. R. *et al.* (2003) 'Proposal for a unified CCN nomenclature.', *Molecular pathology : MP*. England, 56(2), pp. 127–128.

Brigstock, D. R. (2009) 'Strategies for blocking the fibrogenic actions of connective tissue growth factor (CCN2): From pharmacological inhibition in vitro to targeted siRNA therapy in

vivo', *Journal of Cell Communication and Signaling*, 3(1), pp. 5–18. doi: 10.1007/s12079-009-0043-9.

Bryda, E. C. (2013) 'The Mighty Mouse: the impact of rodents on advances in biomedical research', *Missouri medicine*. Journal of the Missouri State Medical Association, 110(3), pp. 207–211. Available at: https://www.ncbi.nlm.nih.gov/pubmed/23829104.

Buchholz, F. *et al.* (1996) 'Different Thermostabilities of FLP and Cre Recombinases: Implications for Applied Site-Specific Recombination', *Nucleic Acids Research*, 24(21), pp. 4256–4262. Available at: http://dx.doi.org/10.1093/nar/24.21.4256.

Byrne, A. J., Maher, T. M. and Lloyd, C. M. (2016) 'Pulmonary Macrophages: A New Therapeutic Pathway in Fibrosing Lung Disease?', *Trends in Molecular Medicine*. Elsevier Ltd, 22(4), pp. 303–316. doi: 10.1016/j.molmed.2016.02.004.

Cabrera, S. *et al.* (2013) 'Gene expression profiles reveal molecular mechanisms involved in the progression and resolution of bleomycin-induced lung fibrosis.', *American journal of physiology. Lung cellular and molecular physiology*. United States, 304(9), pp. L593-601. doi: 10.1152/ajplung.00320.2012.

Capecchi, M. R. (1989) 'The new mouse genetics: Altering the genome by gene targeting', *Trends in Genetics*. Elsevier Current Trends, 5, pp. 70–76. doi: 10.1016/0168-9525(89)90029-2.

Cavanaugh, D. *et al.* (2006) 'Quantification of Bleomycin-Induced Murine Lung Damage In Vivo With Micro-Computed Tomography', *Academic Radiology*, 13(12), pp. 1505–1512. doi: 10.1016/j.acra.2006.08.011.

Chang, C.-C. *et al.* (2004) 'Connective tissue growth factor and its role in lung adenocarcinoma invasion and metastasis.', *Journal of the National Cancer Institute*. United States, 96(5), pp. 364–375.

Charrier, A. *et al.* (2014) 'Regulation of pancreatic inflammation by connective tissue growth factor (CTGF/CCN2)', *Immunology*, 141(4), pp. 564–576. doi: 10.1111/imm.12215.

Chaudhary, N. I., Schnapp, A. and Park, J. E. (2006) 'Pharmacologic differentiation of inflammation and fibrosis in the rat bleomycin model.', *American journal of respiratory and critical care medicine*. United States, 173(7), pp. 769–776. doi: 10.1164/rccm.200505-717OC.

Chen, H. *et al.* (2009) 'TGF-beta induces fibroblast activation protein expression; fibroblast activation protein expression increases the proliferation, adhesion, and migration of HO-8910PM [corrected].', *Experimental and molecular pathology*. Netherlands, 87(3), pp. 189–194. doi: 10.1016/j.yexmp.2009.09.001.

Chen, J. *et al.* (2008) 'Mechanistic studies on bleomycin-mediated DNA damage: Multiple binding modes can result in double-stranded DNA cleavage', *Nucleic Acids Research*, 36(11), pp. 3781–3790. doi: 10.1093/nar/gkn302.

Clarke, G. *et al.* (2013) 'The microbiome-gut-brain axis during early life regulates the hippocampal serotonergic system in a sex-dependent manner.', *Molecular psychiatry*. England, 18(6), pp. 666–673. doi: 10.1038/mp.2012.77.

Cohn, L. A. *et al.* (2004) 'Identification and characterization of an idiopathic pulmonary fibrosis-like condition in cats.', *Journal of veterinary internal medicine*. United States, 18(5), pp. 632–641.

Coultas, D. B. *et al.* (1994) 'The epidemiology of interstitial lung diseases.', *American Journal of Respiratory and Critical Care Medicine*, 150(4), pp. 967–972. doi: 10.1164/ajrccm.150.4.7921471.

Crapo, J. D. *et al.* (1983) 'Morphometric characteristics of cells in the alveolar region of mammalian lungs.', *The American review of respiratory disease*. United States, 128(2 Pt 2), pp. S42-6. doi: 10.1164/arrd.1983.128.2P2.S42.

Crowell, R. E. *et al.* (1992) 'Alveolar and interstitial macrophage populations in the murine lung.', *Experimental lung research*. England, 18(4), pp. 435–446.

Culver, B. H. (2012) *Respiratory Mechanics*. Fourth Edi, *Clinical Respiratory Medicine: Fourth Edition*. Fourth Edi. Elsevier Inc. doi: 10.1016/B978-1-4557-0792-8.00003-9.

Cyphert, J. M. *et al.* (2012) 'Long-term response of rats to single intratracheal exposure of Libby amphibole or amosite.', *Journal of toxicology and environmental health. Part A*. England, 75(3), pp. 183–200. doi: 10.1080/15287394.2012.641203.

Dancer, R. C. A., Wood, A. M. and Thickett, D. R. (2011) 'Metalloproteinases in idiopathic pulmonary fibrosis', *European Respiratory Journal*, pp. 1461–1467. doi: 10.1183/09031936.00024711.

Davis, G. S., Leslie, K. O. and Hemenway, D. R. (1998) 'Silicosis in mice: effects of dose, time, and genetic strain.', *Journal of environmental pathology, toxicology and oncology : official organ of the International Society for Environmental Toxicology and Cancer*. United States, 17(2), pp. 81–97.

Delle, H. *et al.* (2012) 'Antifibrotic effect of tamoxifen in a model of progressive renal disease.', *Journal of the American Society of Nephrology : JASN*. United States, 23(1), pp. 37–48. doi: 10.1681/ASN.2011010046.

Denton, C. P. *et al.* (2001) 'Activation of a fibroblast-specific enhancer of the proα2(I) collagen gene in tight-skin mice', *Arthritis and Rheumatism*, 44(3), pp. 712–722. doi: 10.1002/1529-0131(200103)44:3<712::AID-ANR121>3.0.CO;2-1.

Dong, Y. *et al.* (2015) 'Blocking follistatin-like 1 attenuates bleomycin-induced pulmonary fibrosis in mice', *The Journal of Experimental Medicine*, 212(2), p. 235 LP-252. Available at: http://jem.rupress.org/content/212/2/235.abstract.

Downey, C. M. *et al.* (2012) 'Quantitative Ex-Vivo Micro-Computed Tomographic Imaging of Blood Vessels and Necrotic Regions within Tumors', *PLoS ONE*. Edited by G. Wang. Public Library of Science, 7(7), p. e41685. doi: 10.1371/journal.pone.0041685.

Driehuys, B. and Hedlund, L. W. (2007) 'Imaging Techniques for Small Animal Models of Pulmonary Disease: MR Microscopy', *Toxicologic Pathology*, 35(1), pp. 49–58. doi: 10.1080/01926230601132048.

Drugs, N. E. W. (2016) 'Nintedanib Lung cancer Ramucirumab', 39(2), pp. 62–63.

Egger, C. *et al.* (2013) 'Administration of Bleomycin via the Oropharyngeal Aspiration Route Leads to Sustained Lung Fibrosis in Mice and Rats as Quantified by UTE-MRI and Histology', *PLoS ONE*, 8(5). doi: 10.1371/journal.pone.0063432.

Exposito, J. Y. *et al.* (2010) 'The fibrillar collagen family', *International Journal of Molecular Sciences*, 11(2), pp. 407–426. doi: 10.3390/ijms11020407.

Falke, L. L. *et al.* (2017) 'Tamoxifen for induction of Cre-recombination may confound fibrosis studies in female mice.', *Journal of cell communication and signaling*. Netherlands,

11(2), pp. 205–211. doi: 10.1007/s12079-017-0390-x.

Fehrenbach, H. (2001) 'Alveolar epithelial type II cell: defender of the alveolus revisited', *Respiratory Research*. BioMed Central, 2(1), pp. 33–46. doi: 10.1186/rr36.

Feil, S., Valtcheva, N. and Feil, R. (2009) 'Inducible Cre Mice', in. Humana Press, pp. 343–363. doi: 10.1007/978-1-59745-471-1_18.

Finke, J. *et al.* (1993) 'An improved strategy and a useful housekeeping gene for RNA analysis from formalin-fixed, paraffin-embedded tissues by PCR.', *BioTechniques*. England, 14(3), pp. 448–453.

Fleischman, R. W. *et al.* (1971) 'Bleomycin-induced interstitial pneumonia in dogs', *Thorax*, 26(6), pp. 675–682. Available at: http://www.ncbi.nlm.nih.gov/pmc/articles/PMC472381/.

Fox, J. G. *et al.* (2006) *The Mouse in Biomedical Research, Volume 4 : Immunology.* Elsevier.

Gao, R. and Brigstock, D. R. (2004) 'Connective tissue growth factor (CCN2) induces adhesion of rat activated hepatic stellate cells by binding of its C-terminal domain to integrin alpha(v)beta(3) and heparan sulfate proteoglycan.', *The Journal of biological chemistry*. American Society for Biochemistry and Molecular Biology, 279(10), pp. 8848–55. doi: 10.1074/jbc.M313204200.

Garcia-Sancho, C. *et al.* (2011) 'Familial pulmonary fibrosis is the strongest risk factor for idiopathic pulmonary fibrosis.', *Respiratory medicine*. England, 105(12), pp. 1902–1907. doi: 10.1016/j.rmed.2011.08.022.

Geisinger, M. T. *et al.* (2012) 'Ets-1 is essential for connective tissue growth factor (CTGF/CCN2) induction by TGF-??1 in osteoblasts', *PLoS ONE*, 7(4). doi: 10.1371/journal.pone.0035258.

Gelse, K., Poschl, E. and Aigner, T. (2003) 'Collagens--structure, function, and biosynthesis.', *Advanced drug delivery reviews*. Netherlands, 55(12), pp. 1531–1546.

Gharaee-Kermani, M. *et al.* (2005) 'Gender-based differences in bleomycin-induced pulmonary fibrosis.', *The American journal of pathology*. United States, 166(6), pp. 1593–1606. doi: 10.1016/S0002-9440(10)62470-4.

Gierut, J. J., Jacks, T. E. and Haigis, K. M. (2014) 'Strategies to achieve conditional gene mutation in mice.', *Cold Spring Harbor protocols*. United States, 2014(4), pp. 339–349. doi: 10.1101/pdb.top069807.

Gilhodes, J. C. *et al.* (2017) 'Quantification of pulmonary fibrosis in a bleomycin mouse model using automated histological image analysis', *PLoS ONE*. doi: 10.1371/journal.pone.0170561.

Giménez, A. *et al.* (no date) 'Dysregulated Collagen Homeostasis by Matrix Stiffening and TGF-β1 in Fibroblasts from Idiopathic Pulmonary Fibrosis Patients: Role of FAK/Akt'. doi: 10.3390/ijms18112431.

Gonzalez, R. F., Allen, L. and Dobbs, L. G. (2009) 'Rat alveolar type I cells proliferate, express OCT-4, and exhibit phenotypic plasticity in vitro.', *American journal of physiology. Lung cellular and molecular physiology*. United States, 297(6), pp. L1045-55. doi: 10.1152/ajplung.90389.2008.

Gordon, M. K. and Hahn, R. A. (2010) 'Collagens', *Cell and Tissue Research*, 339(1), pp. 247–257. doi: 10.1007/s00441-009-0844-4.

Gordon, S. (2008) 'Elie Metchnikoff: father of natural immunity.', *European journal of immunology*. Germany, 38(12), pp. 3257–3264. doi: 10.1002/eji.200838855.

Gribbin, J. *et al.* (2006) 'Incidence and mortality of idiopathic pulmonary fibrosis and sarcoidosis in the UK.', *Thorax*. England, 61(11), pp. 980–985. doi: 10.1136/thx.2006.062836.

Gui, Y.-S. *et al.* (2012) 'SPC-Cre-ERT2 transgenic mouse for temporal gene deletion in alveolar epithelial cells.', *PloS one*. United States, 7(9), p. e46076. doi: 10.1371/journal.pone.0046076.

Guilliams, M. *et al.* (2013) 'Alveolar macrophages develop from fetal monocytes that differentiate into long-lived cells in the first week of life via GM-CSF.', *The Journal of experimental medicine*. United States, 210(10), pp. 1977–1992. doi: 10.1084/jem.20131199.

Guiot, J. *et al.* (2017) 'STATE OF THE ART REVIEW Blood Biomarkers in Idiopathic Pulmonary Fibrosis', *Lung*, 195, pp. 273–280. doi: 10.1007/s00408-017-9993-5.

Guo, L. *et al.* (2015) 'Hypoxia-Induced Epithelial-Mesenchymal Transition Is Involved in Bleomycin-Induced Lung Fibrosis.', *BioMed research international*. United States, 2015, p. 232791. doi: 10.1155/2015/232791.

Hall-Glenn, F. and Lyons, K. M. (2011) 'Roles for CCN2 in normal physiological processes', *Cellular and Molecular Life Sciences*, pp. 3209–3217. doi: 10.1007/s00018-011-0782-7.

Hamman, L. and Rich, A. R. (1935) 'Fulminating Diffuse Interstitial Fibrosis of the Lungs.', *Transactions of the American Clinical and Climatological Association*. United States, 51, pp. 154–163.

Han, M. *et al.* (2018) 'Small Animal Models of Respiratory Viral Infection Related to Asthma', *Viruses*. MDPI, 10(12), p. 682. doi: 10.3390/v10120682.

Harlotte, C. *et al.* (2002) *The New England Journal of Medicine ENVIRONMENTAL EXPOSURE TO ENDOTOXIN AND ITS RELATION TO ASTHMA IN SCHOOL-AGE CHILDREN*, *N Engl J Med*. Available at: www.nejm.org (Accessed: 16 October 2018).

Hashimoto, Y. *et al.* (1998) 'Expression of the Elm1 gene, a novel gene of the CCN (connective tissue growth factor, Cyr61/Cef10, and neuroblastoma overexpressed gene) family, suppresses In vivo tumor growth and metastasis of K-1735 murine melanoma cells.', *The Journal of experimental medicine*. United States, 187(3), pp. 289–296.

Haston, C. K. (2012) 'Mouse genetic approaches applied to the normal tissue radiation response.', *Frontiers in oncology*. Switzerland, 2, p. 94. doi: 10.3389/fonc.2012.00094.

Herchenhan, A. *et al.* (2015) 'Lysyl Oxidase Activity Is Required for Ordered Collagen Fibrillogenesis by Tendon Cells.', *The Journal of biological chemistry*. American Society for Biochemistry and Molecular Biology, 290(26), pp. 16440–50. doi: 10.1074/jbc.M115.641670.

Herzog, E. L. *et al.* (2014) 'Review: interstitial lung disease associated with systemic sclerosis and idiopathic pulmonary fibrosis: how similar and distinct?', *Arthritis & rheumatology (Hoboken, N.J.)*. United States, 66(8), pp. 1967–1978. doi: 10.1002/art.38702.

Holbourn, K. P., Acharya, K. R. and Perbal, B. (2008a) 'The CCN family of proteins: structure-function relationships', *Trends in Biochemical Sciences*, 33(10), pp. 461–473. doi: 10.1016/j.tibs.2008.07.006.

Holbourn, K. P., Acharya, K. R. and Perbal, B. (2008b) 'The CCN family of proteins: structure-function relationships', *Trends in Biochemical Sciences*, pp. 461–473. doi: 10.1016/j.tibs.2008.07.006.

Holmes, A. *et al.* (2001) 'CTGF and SMADs, Maintenance of Scleroderma Phenotype Is Independent of SMAD Signaling', *Journal of Biological Chemistry*. American Society for Biochemistry and Molecular Biology, 276(14), pp. 10594–10601. doi: 10.1074/jbc.M010149200.

Homolka, J. (1987) 'Idiopathic pulmonary fibrosis: a historical review', *Cmaj*, 137(11), pp. 1003–1005. doi: 10.1007/978-1-62703-682-5_1.

Huang, S. S. and Huang, J. S. (2005) 'TGF-beta control of cell proliferation.', *Journal of cellular biochemistry*. United States, 96(3), pp. 447–462. doi: 10.1002/jcb.20558.

Hubbard, J. S., Chen, P. H. and Boyd, K. L. (2017) 'Effects of Repeated Intraperitoneal Injection of Pharmaceutical-grade and Nonpharmaceutical-grade Corn Oil in Female C57BL/6J Mice.', *Journal of the American Association for Laboratory Animal Science : JAALAS*. United States, 56(6), pp. 779–785.

Hubbard, R. *et al.* (1996) 'Mortality rates from cryptogenic fibrosing alveolitis in seven countries.', *Thorax*. England, 51(7), pp. 711–716.

Hui Hoo, Z. and B Whyte, M. K. (2012) 'Idiopathic pulmonary fibrosis THE PATHOPHYSIOLOGY OF IPF', *Thorax*, 67(8), pp. 742–6. doi: 10.1136/thoraxjnl-2011-200515.

Hulmes, D. J. S. (2008) 'Collagen diversity, synthesis and assembly', *Collagen: Structure and Mechanics*, pp. 15–47. doi: 10.1007/978-0-387-73906-9_2.

'Idiopathic pulmonary fibrosis in adults: diagnosis and management | Guidance and guidelines | NICE' (no date). NICE. Available at: https://www.nice.org.uk/guidance/cg163 (Accessed: 16 August 2018).

Irvin, C. G. and Bates, J. H. T. (2003) 'Measuring the lung function in the mouse: The challenge of size', *Respiratory Research*, 4, pp. 1–9. doi: 10.1186/rr199.

Ivkovic, S. *et al.* (2003) 'Connective tissue growth factor coordinates chondrogenesis and angiogenesis during skeletal development', *Development*, 130(12), p. 2779 LP-2791. Available at: http://dev.biologists.org/content/130/12/2779.abstract.

Izbicki, G. *et al.* (2002) 'Time course of bleomycin-induced lung fibrosis', *International Journal of Experimental Pathology*, 83(3), pp. 111–119. doi: 10.1046/j.1365-2613.2002.00220.x.

Jackson Laboratories (no date) *Jackson Laboratories Mouse Genome Informatics*. Available at: http://www.informatics.jax.org/ (Accessed: 25 October 2018).

Jakubovic, B. D. *et al.* (2013) 'Methotrexate-induced pulmonary toxicity.', *Canadian respiratory journal*. Egypt, 20(3), pp. 153–155. doi: 10.1155/2013/527912.

Janssen, W. J. *et al.* (2011) 'Fas determines differential fates of resident and recruited macrophages during resolution of acute lung injury.', *American journal of respiratory and critical care medicine*. United States, 184(5), pp. 547–560. doi: 10.1164/rccm.201011-1891OC.

Jaskelioff, M. *et al.* (2010) 'Telomerase reactivation reverses tissue degeneration in aged telomerase-deficient mice', *Nature*. Nature Publishing Group, a division of Macmillan Publishers Limited. All Rights Reserved., 469, p. 102. Available at:

http://dx.doi.org/10.1038/nature09603.

Johnson, C. T. B. and M. D. and D. W. H. and G. A. (2008) 'In vivo small-animal imaging using micro-CT and digital subtraction angiography', *Physics in Medicine & Biology*, 53(19), p. R319. Available at: http://stacks.iop.org/0031-9155/53/i=19/a=R01.

Johnston, I. *et al.* (1990) *Rising mortality from cryptogenic fibrosing alveolitis*, *BMJ (Clinical research ed.)*. doi: 10.1136/bmj.301.6759.1017.

Joliot, V. *et al.* (1992) 'Proviral rearrangements and overexpression of a new cellular gene (nov) in myeloblastosis-associated virus type 1-induced nephroblastomas.', *Molecular and Cellular Biology*, 12(1), pp. 10–21. Available at: http://www.ncbi.nlm.nih.gov/pmc/articles/PMC364064/.

Jun, J. Il and Lau, L. F. (2011) 'Taking aim at the extracellular matrix: CCN proteins as emerging therapeutic targets', *Nature Reviews Drug Discovery*. doi: 10.1038/nrd3599.

Kadler, K. E. *et al.* (2007) 'Collagens at a glance', *Journal of Cell Science*, 120, pp. 1955–1958. doi: 10.1242/jcs.03453.

Kim, D. *et al.* (2014) 'Tamoxifen ameliorates renal tubulointerstitial fibrosis by modulation of estrogen receptor alpha-mediated transforming growth factor-beta1/Smad signaling pathway.', *Nephrology, dialysis, transplantation : official publication of the European Dialysis and Transplant Association - European Renal Association*. England, 29(11), pp. 2043–2053. doi: 10.1093/ndt/gfu240.

Kim, D. S. (2006) 'Classification and Natural History of the Idiopathic Interstitial Pneumonias', *Proceedings of the American Thoracic Society*, 3(4), pp. 285–292. doi: 10.1513/pats.200601-005TK.

King, T. E. J. *et al.* (2001) 'Idiopathic pulmonary fibrosis: relationship between histopathologic features and mortality.', *American journal of respiratory and critical care medicine*. United States, 164(6), pp. 1025–1032. doi: 10.1164/ajrccm.164.6.2001056.

King, T. E. J. *et al.* (2014) 'A phase 3 trial of pirfenidone in patients with idiopathic pulmonary fibrosis.', *The New England journal of medicine*. United States, 370(22), pp. 2083–2092. doi: 10.1056/NEJMoa1402582.

Kirk, J. M. *et al.* (1984) 'Quantitation of types I and III collagen in biopsy lung samples from patients with cryptogenic fibrosing alveolitis.', *Collagen and related research*. Germany, 4(3), pp. 169–182.

Klingberg, F., Hinz, B. and White, E. S. (2013) 'The myofibroblast matrix: implications for tissue repair and fibrosis.', *The Journal of pathology*. England, 229(2), pp. 298–309. doi: 10.1002/path.4104.

Kolb, M., Gauldie, J. and Bellaye, P. S. (2016) 'Editorial: Extracellular Matrix: The Common Thread of Disease Progression in Fibrosis?', *Arthritis and Rheumatology*, 68(5), pp. 1053–1056. doi: 10.1002/art.39569.

Kono, M. *et al.* (2011) 'Plasma CCN2 (connective tissue growth factor; CTGF) is a potential biomarker in idiopathic pulmonary fibrosis (IPF)', *Clinica Chimica Acta*. Elsevier, 412(23–24), pp. 2211–2215. doi: 10.1016/J.CCA.2011.08.008.

Kopf, M., Schneider, C. and Nobs, S. P. (2014) 'The development and function of lung-resident macrophages and dendritic cells', *Nature Immunology*. Nature Publishing Group, a division of Macmillan Publishers Limited. All Rights Reserved., 16, p. 36. Available at:

http://dx.doi.org/10.1038/ni.3052.

Koshman, Y. E. *et al.* (2015) 'Connective tissue growth factor regulates cardiac function and tissue remodeling in a mouse model of dilated cardiomyopathy.', *Journal of molecular and cellular cardiology*. England, 89(Pt B), pp. 214–222. doi: 10.1016/j.yjmcc.2015.11.003.

Krenning, G., Zeisberg, E. M. and Kalluri, R. (2010) 'The origin of fibroblasts and mechanism of cardiac fibrosis.', *Journal of cellular physiology*. United States, 225(3), pp. 631–637. doi: 10.1002/jcp.22322.

Kubota, S. and Takigawa, M. (2015) 'Cellular and molecular actions of CCN2/CTGF and its role under physiological and pathological conditions', *Clinical Science*, 128(3), pp. 181–196. doi: 10.1042/CS20140264.

Kuhn, C. and McDonald, J. A. (1991) 'The roles of the myofibroblast in idiopathic pulmonary fibrosis. Ultrastructural and immunohistochemical features of sites of active extracellular matrix synthesis.', *The American journal of pathology*. United States, 138(5), pp. 1257–1265.

Kurundkar, A. R. *et al.* (2016) 'The matricellular protein CCN1 enhances TGF-β1/SMAD3-dependent profibrotic signaling in fibroblasts and contributes to fibrogenic responses to lung injury', *FASEB Journal*, 30(6), pp. 2135–2150. doi: 10.1096/fj.201500173.

Lakatos, H. F. *et al.* (2006) 'Oropharyngeal aspiration of a silica suspension produces a superior model of silicosis in the mouse when compared to intratracheal instillation', *Experimental Lung Research*, 32(5), pp. 181–199. doi: 10.1080/01902140600817465.

Lambi, A. G. *et al.* (2012) 'The Skeletal site-specific role of connective tissue growth factor in prenatal osteogenesis', *Developmental Dynamics*, 241(12), pp. 1944–1959. doi: 10.1002/dvdy.23888.

Lan, Y. W. *et al.* (2015) 'Hypoxia-preconditioned mesenchymal stem cells attenuate bleomycin-induced pulmonary fibrosis', *Stem Cell Research and Therapy*. Stem Cell Research & Therapy, 6(1), pp. 1–17. doi: 10.1186/s13287-015-0081-6.

Landsman, L., Varol, C. and Jung, S. (2007) 'Distinct differentiation potential of blood monocyte subsets in the lung.', *Journal of immunology (Baltimore, Md. : 1950)*. United States, 178(4), pp. 2000–2007.

Laskin, D. L. *et al.* (2011) 'Macrophages and tissue injury: agents of defense or destruction?', *Annual review of pharmacology and toxicology*. United States, 51, pp. 267–288. doi: 10.1146/annurev.pharmtox.010909.105812.

Laskin, D. L., Malaviya, R. and Laskin, J. D. (2015) *Pulmonary Macrophages*. Second Edi, *Comparative Biology of the Normal Lung: Second Edition*. Second Edi. Elsevier Inc. doi: 10.1016/B978-0-12-404577-4.00032-1.

Lasky, J. A. *et al.* (1998) 'Connective tissue growth factor mRNA expression is upregulated in bleomycin-induced lung fibrosis.', *The American journal of physiology*. United States, 275(2 Pt 1), pp. L365-71.

Lau, L. F. and Nathans, D. (1987) 'Expression of a set of growth-related immediate early genes in BALB/c 3T3 cells: coordinate regulation with c-fos or c-myc.', *Proceedings of the National Academy of Sciences of the United States of America*. United States, 84(5), pp. 1182–1186.

Lavin, Y. *et al.* (2014) 'Tissue-resident macrophage enhancer landscapes are shaped by the

local microenvironment.', *Cell*. United States, 159(6), pp. 1312–1326. doi: 10.1016/j.cell.2014.11.018.

Lawson, W. E. *et al.* (2005) 'Characterization of fibroblast-specific protein 1 in pulmonary fibrosis', *American Journal of Respiratory and Critical Care Medicine*, 171(8), pp. 899–907. doi: 10.1164/rccm.200311-1535OC.

Leask, A. *et al.* (2003) 'Connective tissue growth factor gene regulation. Requirements for its induction by transforming growth factor-beta 2 in fibroblasts.', *The Journal of biological chemistry*, 278(15), pp. 13008–15. doi: 10.1074/jbc.M210366200.

Leask, A. (2009) 'CIHR Group in Skeletal Development and Remodeling, Division of Oral Biology, Department of Physiology and Pharmacology, Schulich School of Medicine and Dentistry, University of Western Ontario, Dental Sciences Building, London ON N6A 5C1', *Matrix*, pp. 115–122.

Leask, A. and Abraham, D. J. (2006) 'All in the CCN family: essential matricellular signaling modulators emerge from the bunker', *Journal of Cell Science*, 119(23), pp. 4803–4810. doi: 10.1242/jcs.03270.

Leask, A., Denton, C. P. and Abraham, D. J. (2004) 'Insights into the molecular mechanism of chronic fibrosis: the role of connective tissue growth factor in scleroderma.', *The Journal of investigative dermatology*. United States, 122(1), pp. 1–6. doi: 10.1046/j.0022-202X.2003.22133.x.

Leeman, K. T., Fillmore # †, C. M. and Kim, C. F. (2014) 'Lung Stem and Progenitor Cells in Tissue Homeostasis and Disease'. doi: 10.1016/B978-0-12-416022-4.00008-1.

Leeming, D. J. *et al.* (2012) 'Biomarker Insights O r I g I n A L r e S e A r c h serological Investigation of the collagen Degradation Profile of Patients with Chronic Obstructive Pulmonary Disease or Idiopathic Pulmonary Fibrosis', *Biomarker Insights*, 7, p. 7. doi: 10.4137/BMI.S9415.

Lehnert, B. E., Valdez, Y. E. and Holland, L. M. (1985) 'Pulmonary macrophages: alveolar and interstitial populations.', *Experimental lung research*. England, 9(3–4), pp. 177–190.

Leu, S.-J., Lam, S. C.-T. and Lau, L. F. (2002) 'Pro-angiogenic activities of CYR61 (CCN1) mediated through integrins alphavbeta3 and alpha6beta1 in human umbilical vein endothelial cells.', *The Journal of biological chemistry*. United States, 277(48), pp. 46248–46255. doi: 10.1074/jbc.M209288200.

Levitzky, M. G. (2007a) *Function and structure of the respiratory system*, *Lange physiology series pulmonary physiology*.

Levitzky, M. G. (2007b) *Levitzky's Pulmonary Physiology (Lange Physiology)-McGraw-Hill Medical (2007)*, *Lange physiology series pulmonary physiology*. doi: 10.1036/0071437754.

Ley, B. and Collard, H. R. (2013) 'Epidemiology of idiopathic pulmonary fibrosis', *Clinical Epidemiology*, 5(1), pp. 483–492. doi: 10.2147/CLEP.S54815.

Li, I. M. H. *et al.* (2017) 'Characterization of mesenchymal-fibroblast cells using the Col1a2 promoter/enhancer', in *Methods in Molecular Biology*, pp. 139–161. doi: 10.1007/978-1-4939-7113-8_10.

Liegeois, M. *et al.* (2018) 'The interstitial macrophage: A long-neglected piece in the puzzle of lung immunity', *Cellular Immunology*. Elsevier, 330(February), pp. 91–96. doi: 10.1016/j.cellimm.2018.02.001.

Lin, S.-L. *et al.* (2008) 'Pericytes and perivascular fibroblasts are the primary source of collagen-producing cells in obstructive fibrosis of the kidney.', *The American journal of pathology*. United States, 173(6), pp. 1617–1627. doi: 10.2353/ajpath.2008.080433.

Lindahl, G. E. *et al.* (2013) 'Microarray profiling reveals suppressed interferon stimulated gene program in fibroblasts from scleroderma-associated interstitial lung disease', *Respiratory Research*. Respiratory Research, 14(1), p. 1. doi: 10.1186/1465-9921-14-80.

Lindenschmidt, R. C. *et al.* (1986) 'Intratracheal versus intravenous administration of bleomycin in mice: acute effects.', *Toxicology and applied pharmacology*. United States, 85(1), pp. 69–77.

Lipson, K. *et al.* (2017) 'Therapeutic pamrevlumab (FG-3019) is more effective than pirfenidone or nintedanib in a mouse radiation-induced lung fibrosis model', *European Respiratory Journal*, 50(suppl 61). Available at: http://erj.ersjournals.com/content/50/suppl_61/PA908.abstract.

Lipson, K. E. *et al.* (2012) 'CTGF is a central mediator of tissue remodeling and fibrosis and its inhibition can reverse the process of fibrosis', *Fibrogenesis & Tissue Repair*. doi: 10.1186/1755-1536-5-S1-S24.

Liu, S. *et al.* (2011) 'CCN2 is required for bleomycin-induced skin fibrosis in mice', *Arthritis and Rheumatism*, 63(1), pp. 239–246. doi: 10.1002/art.30074.

Liu, Y.-M., Nepali, K. and Liou, J.-P. (2017) 'Idiopathic Pulmonary Fibrosis: Current Status, Recent Progress, and Emerging Targets', *Journal of Medicinal Chemistry*. American Chemical Society, 60(2), pp. 527–553. doi: 10.1021/acs.jmedchem.6b00935.

Liu, Z. *et al.* (2018) 'Short-term tamoxifen treatment has long-term effects on metabolism in high-fat diet-fed mice with involvement of Nmnat2 in POMC neurons', *FEBS Letters*, 592, pp. 3305–3316. doi: 10.1002/1873-3468.13240.

Lopez-Larraza, D., De Luca, J. C. and Bianchi, N. O. (1990) 'The kinetics of DNA damage by bleomycin in mammalian cells.', *Mutation research*. Netherlands, 232(1), pp. 57–61.

Luczynski, P. *et al.* (2016) 'Growing up in a Bubble: Using Germ-Free Animals to Assess the Influence of the Gut Microbiota on Brain and Behavior.', *The international journal of neuropsychopharmacology*. Oxford University Press, 19(8). doi: 10.1093/ijnp/pyw020.

Lynch, D. A. *et al.* (2018) 'Diagnostic criteria for idiopathic pulmonary fibrosis: a Fleischner Society White Paper', *The Lancet Respiratory Medicine*. Elsevier Ltd, 6(2), pp. 138–153. doi: 10.1016/S2213-2600(17)30433-2.

Malik, A. R., Liszewska, E. and Jaworski, J. (2015) 'Matricellular proteins of the Cyr61/CTGF/NOV (CCN) family and the nervous system', *Frontiers in Cellular Neuroscience*, 9. doi: 10.3389/fncel.2015.00237.

Manne, J. *et al.* (2013) 'Collagen content in skin and internal organs of the tight skin mouse: an animal model of scleroderma.', *Biochemistry research international*. United States, 2013, p. 436053. doi: 10.1155/2013/436053.

Marciniak, S. J. and Lomas, D. A. (2012) *Basic Aspects of Cellular and Molecular Biology*. Fourth Edi, *Clinical Respiratory Medicine: Fourth Edition*. Fourth Edi. Elsevier Inc. doi: 10.1016/B978-1-4557-0792-8.00002-7.

Marenzana, M. and Vande Velde, G. (2015) 'Refine, reduce, replace: Imaging of fibrosis and arthritis in animal models', *Best Practice and Research: Clinical Rheumatology*, 29(6), pp.

715–740. doi: 10.1016/j.berh.2016.02.001.

Martin-Mosquero, C. *et al.* (2006) 'Increased collagen deposition correlated with lung destruction in human emphysema.', *Histology and histopathology*. Spain, 21(8), pp. 823–828. doi: 10.14670/HH-21.823.

Martinez, F. O. *et al.* (2008) 'Macrophage activation and polarization.', *Frontiers in bioscience : a journal and virtual library*. United States, 13, pp. 453–461.

Masopust, D., Sivula, C. P. and Jameson, S. C. (2017) 'Of Mice, Dirty Mice, and Men: Using Mice To Understand Human Immunology.', *Journal of immunology (Baltimore, Md. : 1950)*. United States, 199(2), pp. 383–388. doi: 10.4049/jimmunol.1700453.

Masuda, N. *et al.* (1999) 'Analysis of chemical modification of RNA from formalin-fixed samples and optimization of molecular biology applications for such samples.', *Nucleic acids research*. England, 27(22), pp. 4436–4443.

Maus, U. A. *et al.* (2006) 'Resident alveolar macrophages are replaced by recruited monocytes in response to endotoxin-induced lung inflammation.', *American journal of respiratory cell and molecular biology*. United States, 35(2), pp. 227–235. doi: 10.1165/rcmb.2005-0241OC.

McAnulty, R. J. and Laurent, G. J. (1987) 'Collagen synthesis and degradation in vivo. Evidence for rapid rates of collagen turnover with extensive degradation of newly synthesized collagen in tissues of the adult rat.', *Collagen and related research*. Germany, 7(2), pp. 93–104.

Metzger, D. *et al.* (1995) 'Conditional site-specific recombination in mammalian cells using a ligand-dependent chimeric Cre recombinase.', *Proceedings of the National Academy of Sciences of the United States of America*. United States, 92(15), pp. 6991–6995.

Midgley, A. C. *et al.* (2013) 'Transforming growth factor-β1 (TGF-β1)-stimulated fibroblast to myofibroblast differentiation is mediated by hyaluronan (HA)-facilitated epidermal growth factor receptor (EGFR) and CD44 co-localization in lipid rafts.', *The Journal of biological chemistry*. American Society for Biochemistry and Molecular Biology, 288(21), pp. 14824–38. doi: 10.1074/jbc.M113.451336.

Miller, E. J. (1985) 'The structure of fibril-forming collagens.', *Annals of the New York Academy of Sciences*. United States, 460, pp. 1–13.

Minutti, C. M. *et al.* (2017) 'Tissue-specific contribution of macrophages to wound healing', *Seminars in Cell and Developmental Biology*. Elsevier Ltd, 61, pp. 3–11. doi: 10.1016/j.semcdb.2016.08.006.

Misharin, A. V. *et al.* (2017) 'Monocyte-derived alveolar macrophages drive lung fibrosis and persist in the lung over the life span', *The Journal of Experimental Medicine*, 214(8), pp. 2387–2404. doi: 10.1084/jem.20162152.

Moeller, A. *et al.* (2008) 'NIH Public Access', *The international journal of biochemistry & cell biology*, 40(3), pp. 362–382. doi: 10.1038/jid.2014.371.

Moeller, A. *et al.* (2008) 'The bleomycin animal model: A useful tool to investigate treatment options for idiopathic pulmonary fibrosis?', *The International Journal of Biochemistry & Cell Biology*, 40(3), pp. 362–382. doi: 10.1016/j.biocel.2007.08.011.

Mondrinos, M. J. *et al.* (2013) *Lungs*. Fourth Edi, *Principles of Tissue Engineering: Fourth Edition*. Fourth Edi. Elsevier. doi: 10.1016/B978-0-12-398358-9.00074-4.

Moore, B. B. *et al.* (2005) 'CCR2-mediated recruitment of fibrocytes to the alveolar space after fibrotic injury.', *The American journal of pathology*. United States, 166(3), pp. 675–684. doi: 10.1016/S0002-9440(10)62289-4.

Moore, B. B. and Hogaboam, C. M. (2008) 'Murine models of pulmonary fibrosis', *American Journal of Physiology-Lung Cellular and Molecular Physiology*. American Physiological Society, 294(2), pp. L152–L160. doi: 10.1152/ajplung.00313.2007.

Morrisey, E. E. and Hogan, B. L. M. (2010) 'Preparing for the First Breath: Genetic and Cellular Mechanisms in Lung Development', *Dev Cell*, 18(1), pp. 8–23. doi: 10.1016/j.devcel.2009.12.010.

Moshai, E. F. *et al.* (2014) 'Targeting the hedgehog-glioma-associated oncogene homolog pathway inhibits bleomycin-induced lung fibrosis in mice.', *American journal of respiratory cell and molecular biology*. United States, 51(1), pp. 11–25. doi: 10.1165/rcmb.2013-0154OC.

Mosser, D. M. and Edwards, J. P. (2008) 'Exploring the full spectrum of macrophage activation.', *Nature reviews. Immunology*. England, 8(12), pp. 958–969. doi: 10.1038/nri2448.

Moussad, E. E. and Brigstock, D. R. (2000) 'Connective tissue growth factor: what's in a name?', *Molecular genetics and metabolism*. United States, 71(1–2), pp. 276–292. doi: 10.1006/mgme.2000.3059.

MRC (2001) 'Mice and medicines', p.

Muller, R. *et al.* (1998) 'Morphometric analysis of human bone biopsies: a quantitative structural comparison of histological sections and micro-computed tomography.', *Bone*. United States, 23(1), pp. 59–66.

Murray, L. A. *et al.* (2009) 'Fibroblasts', *Asthma and COPD*, pp. 193–200. doi: 10.1016/B978-0-12-374001-4.00015-8.

Murray, P. J. and Wynn, T. A. (2011) 'Protective and pathogenic functions of macrophage subsets.', *Nature reviews. Immunology*. England, 11(11), pp. 723–737. doi: 10.1038/nri3073.

von Mutius, E. (2007) 'Allergies, infections and the hygiene hypothesis - The epidemiological evidence', *Immunobiology*, 212(6), pp. 433–439. doi: 10.1016/j.imbio.2007.03.002.

Muzumdar, M. D. *et al.* (2007) 'A global double-fluorescent cre reporter mouse', *Genesis*. doi: 10.1002/dvg.20335.

Nagy, A. (2000) 'Cre recombinase: the universal reagent for genome tailoring.', *Genesis (New York, N.Y. : 2000)*. United States, 26(2), pp. 99–109.

Nagy, A., Mar, L. and Watts, G. (2009) 'Creation and use of a cre recombinase transgenic database.', *Methods in molecular biology (Clifton, N.J.)*. United States, 530, pp. 365–378. doi: 10.1007/978-1-59745-471-1_19.

Nakanishi, H. *et al.* (2012) 'Convergent signaling in the regulation of connective tissue growth factor in malignant mesothelioma: TGFβ signaling and defects in the Hippo signaling cascade', *Cell Cycle*, 11(18), pp. 3373–3379. doi: 10.4161/cc.21397.

Navaratnam, V. *et al.* (2011) 'The rising incidence of idiopathic pulmonary fibrosis in the U.K.', *Thorax*. England, 66(6), pp. 462–467. doi: 10.1136/thx.2010.148031.

Navarro, S. and Driscoll, B. (2017) 'Regeneration of the Aging Lung: A Mini-Review', *Gerontology*. doi: 10.1159/000451081.

Ni, S. *et al.* (2015) 'Bone marrow mesenchymal stem cells protect against bleomycin-induced pulmonary fibrosis in rat by activating Nrf2 signaling', *International Journal of Clinical and Experimental Pathology*. e-Century Publishing Corporation, 8(7), pp. 7752–7761. Available at: http://www.ncbi.nlm.nih.gov/pmc/articles/PMC4555668/.

NICE (2013) *Pirfenidone for treating idiopathic pulmonary fibrosis*. Available at: https://www.nice.org.uk/guidance/ta504/documents/final-appraisal-determination-document (Accessed: 16 August 2018).

Nomellini, V. and Chen, H. (2012) *Murray and Nadel's Textbook of Respiratory Medicine*, *Journal of Surgical Research*. doi: 10.1016/j.jss.2011.08.019.

Novak, A. *et al.* (2000) 'Z/EG, a double reporter mouse line that expresses enhanced green fluorescent protein upon Cre-mediated excision.', *Genesis (New York, N.Y. : 2000)*. United States, 28(3–4), pp. 147–155.

Ochs, M. *et al.* (2004) 'The number of alveoli in the human lung.', *American journal of respiratory and critical care medicine*. United States, 169(1), pp. 120–124. doi: 10.1164/rccm.200308-1107OC.

Omoto, S. *et al.* (2004) 'Expression and localization of connective tissue growth factor (CTGF/Hcs24/CCN2) in osteoarthritic cartilage.', *Osteoarthritis and cartilage*. England, 12(10), pp. 771–778. doi: 10.1016/j.joca.2004.06.009.

Ono, N. *et al.* (2014) 'A subset of chondrogenic cells provides early mesenchymal progenitors in growing bones', *Nature Cell Biology*. Nature Publishing Group, 16, p. 1157. Available at: http://dx.doi.org/10.1038/ncb3067.

Padilla-Carlin, D. J. *et al.* (2011) 'Pulmonary inflammatory and fibrotic responses in Fischer 344 rats after intratracheal instillation exposure to Libby amphibole.', *Journal of toxicology and environmental health. Part A*. England, 74(17), pp. 1111–1132. doi: 10.1080/15287394.2011.586940.

Pan, L. H. *et al.* (2001) 'Type II alveolar epithelial cells and interstitial fibroblasts express connective tissue growth factor in IPF.', *The European respiratory journal*. England, 17(6), pp. 1220–1227.

Paun, A. *et al.* (2010) 'Combined Tlr2 and Tlr4 deficiency increases radiation-induced pulmonary fibrosis in mice.', *International journal of radiation oncology, biology, physics*. United States, 77(4), pp. 1198–1205. doi: 10.1016/j.ijrobp.2009.12.065.

Peão, M. N. *et al.* (1993) 'Anatomy of Clara cell secretion: surface changes observed by scanning electron microscopy.', *Journal of Anatomy*, 182(Pt 3), pp. 377–388. Available at: http://www.ncbi.nlm.nih.gov/pmc/articles/PMC1259811/.

Pennica, D. *et al.* (1998) 'WISP genes are members of the connective tissue growth factor family that are up-regulated in wnt-1-transformed cells and aberrantly expressed in human colon tumors.', *Proceedings of the National Academy of Sciences of the United States of America*. United States, 95(25), pp. 14717–14722.

Perbal, B. (2013) 'CCN proteins: A centralized communication network.', *Journal of cell communication and signaling*. Netherlands, 7(3), pp. 169–177. doi: 10.1007/s12079-013-0193-7.

Phan, S. H. and Kunkel, S. L. (1992) 'Lung cytokine production in bleomycin-induced pulmonary fibrosis.', *Experimental lung research*. England, 18(1), pp. 29–43. doi: 10.3109/01902149209020649.

Picozzi, V. J. *et al.* (2016) *FG-3019, A Human Monoclonal Antibody to Connective Tissue Growth Factor, Combined with Chemotherapy in Patients with Locally Advanced or Metastatic Pancreatic Ductal Adenocarcinoma*. Available at: https://www.omicsonline.org/open-access/fg3019-a-human-monoclonal-antibody-to-connective-tissue-growth-factorcombined-with-chemotherapy-in-patients-with-locally-advanced.pdf (Accessed: 27 October 2018).

Planque, N. and Perbal, B. (2003) 'A structural approach to the role of CCN (CYR61/CTGF/NOV) proteins in tumourigenesis.', *Cancer cell international*. England, 3(1), p. 15. doi: 10.1186/1475-2867-3-15.

Plantier, L. *et al.* (2016) 'Transcriptome of Cultured Lung Fibroblasts in Idiopathic Pulmonary Fibrosis: Meta-Analysis of Publically Available Microarray Datasets Reveals Repression of Inflammation and Immunity Pathways', *International Journal of Molecular Sciences*, 17(12), p. 2091. doi: 10.3390/ijms17122091.

Ponticos, M. *et al.* (2004) 'Col1a2 enhancer regulates collagen activity during development and in adult tissue repair', 22, pp. 619–628. doi: 10.1016/j.matbio.2003.12.002.

Ponticos, M. *et al.* (2009) 'Pivotal role of connective tissue growth factor in lung fibrosis: MAPK-dependent transcriptional activation of type I collagen', *Arthritis and Rheumatism*, 60(7), pp. 2142–2155. doi: 10.1002/art.24620.

Qian, H. S. *et al.* (2016) 'Quantification and comparison of anti-fibrotic therapies by polarized SRM and SHG-based morphometry in rat UUO model', *PLoS ONE*, 11(6), pp. 1–13. doi: 10.1371/journal.pone.0156734.

Raghu, G. *et al.* (2011) 'An official ATS/ERS/JRS/ALAT statement: idiopathic pulmonary fibrosis: evidence-based guidelines for diagnosis and management.', *American journal of respiratory and critical care medicine*. United States, 183(6), pp. 788–824. doi: 10.1164/rccm.2009-040GL.

Raghu, G. *et al.* (2012) 'Phase 2 trial of FG-3019, anti-CTGF monoclonal antibody, in idiopathic pulmonary fibrosis (IPF): Preliminary safety and efficacy results', *European Respiratory Journal*, 40(Suppl 56). Available at: http://erj.ersjournals.com/content/40/Suppl_56/2819.abstract.

Raghu, G. *et al.* (2016) 'FG-3019 anti-connective tissue growth factor monoclonal antibody: results of an open-label clinical trial in IPF', *European Respiratory Journal*. Available at: http://erj.ersjournals.com/content/early/2016/03/10/13993003.01030-2015.abstract.

Raghu, G., Nicholson, A. G. and Lynch, D. (2008) 'The classification, natural history and radiological/histological appearance of idiopathic pulmonary fibrosis and the other idiopathic interstitial pneumonias', *European Respiratory Review*, 17(109), pp. 108–115. doi: 10.1183/09059180.00010902.

Ramazani, Y. *et al.* (2018) 'Connective tissue growth factor (CTGF) from basics to clinics', *Matrix Biology*. Elsevier, 68–69, pp. 44–66. doi: 10.1016/J.MATBIO.2018.03.007.

Ramshaw, J. A. M., Shah, N. K. and Brodsky, B. (1998) 'Gly-X-Y tripeptide frequencies in collagen: A context for host-guest triple-helical peptides', *Journal of Structural Biology*, 122(1–2), pp. 86–91. doi: 10.1006/jsbi.1998.3977.

Rasmussen, D. L. and Pfau, J. C. (2012) 'Asbestos activates CH12.LX B-lymphocytes via macrophage signaling.', *Journal of immunotoxicology*. England, 9(2), pp. 129–140. doi: 10.3109/1547691X.2011.631953.

Redente, E. F. *et al.* (2011) 'Age and sex dimorphisms contribute to the severity of bleomycin-induced lung injury and fibrosis.', *American journal of physiology. Lung cellular and molecular physiology*. United States, 301(4), pp. L510-8. doi: 10.1152/ajplung.00122.2011.

Reinert, T. *et al.* (2013) 'Bleomycin-Induced Lung Injury', *Journal of Cancer Research*. Hindawi, 2013, pp. 1–9. doi: 10.1155/2013/480608.

Ricard-Blum, S. (2011) 'The Collagen Family', *Cold Spring Harbor Perspectives in Biology*, 3(1), pp. 1–19. doi: 10.1101/cshperspect.a004978.

Richeldi, L. *et al.* (2014) 'Efficacy and safety of nintedanib in idiopathic pulmonary fibrosis.', *The New England journal of medicine*. United States, 370(22), pp. 2071–2082. doi: 10.1056/NEJMoa1402584.

Richeldi, L., Collard, H. R. and Jones, M. G. (2017) 'Idiopathic pulmonary fibrosis', *The Lancet*, 389(10082), pp. 1941–1952. doi: 10.1016/S0140-6736(17)30866-8.

Rittié, L. *et al.* (2011) 'Spatial-temporal modulation of CCN proteins during wound healing in human skin in vivo', *Journal of Cell Communication and Signaling*, 5(1), pp. 69–80. doi: 10.1007/s12079-010-0114-y.

Robbe, A. *et al.* (2015) 'Intratracheal Bleomycin Aerosolization: The Best Route of Administration for a Scalable and Homogeneous Pulmonary Fibrosis Rat Model?', *BioMed Research International*. Hindawi, 2015, pp. 1–10. doi: 10.1155/2015/198418.

Roberts, S. N. *et al.* (1995) 'A novel model for human interstitial lung disease: hapten-driven lung fibrosis in rodents.', *The Journal of pathology*. England, 176(3), pp. 309–318. doi: 10.1002/path.1711760313.

Robinson, S. P. *et al.* (1991) 'Metabolites, pharmacodynamics, and pharmacokinetics of tamoxifen in rats and mice compared to the breast cancer patient.', *Drug metabolism and disposition: the biological fate of chemicals*. United States, 19(1), pp. 36–43.

Rock, J. R. *et al.* (2011) 'Multiple stromal populations contribute to pulmonary fibrosis without evidence for epithelial to mesenchymal transition', *Proceedings of the National Academy of Sciences*, 108(52), pp. E1475–E1483. doi: 10.1073/pnas.1117988108.

Roggli, V. L. *et al.* (2010) 'Pathology of asbestosis- An update of the diagnostic criteria: Report of the asbestosis committee of the college of american pathologists and pulmonary pathology society.', *Archives of pathology & laboratory medicine*. United States, 134(3), pp. 462–480. doi: 10.1043/1543-2165-134.3.462.

Roy, S. R. *et al.* (2003) 'Bacterial DNA in house and farm barn dust', *Journal of Allergy and Clinical Immunology*, 112(3), pp. 571–578. doi: 10.1016/S0091-6749(03)01863-3.

Ruscitti, F. *et al.* (2017) 'Longitudinal assessment of bleomycin-induced lung fibrosis by Micro-CT correlates with histological evaluation in mice.', *Multidisciplinary respiratory medicine*. England, 12, p. 8. doi: 10.1186/s40248-017-0089-0.

Schaefer, C. J. *et al.* (2011) 'Antifibrotic activities of pirfenidone in animal models.', *European respiratory review : an official journal of the European Respiratory Society*. England, 20(120), pp. 85–97. doi: 10.1183/09059180.00001111.

Schambach, S. J. *et al.* (2010) 'Application of micro-CT in small animal imaging', *Methods*. Academic Press, 50(1), pp. 2–13. doi: 10.1016/J.YMETH.2009.08.007.

Schmidt, M. *et al.* (2002) 'Cell Cycle Inhibition by FoxO Forkhead Transcription Factors Involves Downregulation of Cyclin D', *Molecular and Cellular Biology*, 22(22), pp. 7842–7852. doi: 10.1128/MCB.22.22.7842-7852.2002.

Schrier, D. J., Kunkel, R. G. and Phan, S. H. (1983) 'The role of strain variation in murine bleomycin-induced pulmonary fibrosis.', *The American review of respiratory disease*. United States, 127(1), pp. 63–66. doi: 10.1164/arrd.1983.127.1.63.

Schwenk, F. *et al.* (1998) 'Temporally and spatially regulated somatic mutagenesis in mice.', *Nucleic acids research*. England, 26(6), pp. 1427–1432.

Scotton, C. J. *et al.* (2009) 'Increased local expression of coagulation factor X contributes to the fibrotic response in human and murine lung injury.', *The Journal of clinical investigation*. United States, 119(9), pp. 2550–2563. doi: 10.1172/JCI33288.

Scotton, C. J. *et al.* (2013) 'Ex vivo micro-computed tomography analysis of bleomycin-induced lung fibrosis for preclinical drug evaluation', *European Respiratory Journal*, 42(6), pp. 1633–1645. doi: 10.1183/09031936.00182412.

Scotton, C. J. and Chambers, R. C. (2010) 'Bleomycin revisited: towards a more representative model of IPF?' doi: 10.1152/ajplung.00258.2010.

Sebring, R. J. and Lehnert, B. E. (1992) 'Morphometric comparisons of rat alveolar macrophages, pulmonary interstitial macrophages, and blood monocytes.', *Experimental lung research*. England, 18(4), pp. 479–496.

Selman, M. *et al.* (1986) 'Concentration, biosynthesis and degradation of collagen in idiopathic pulmonary fibrosis', *Thorax*, 41(5), pp. 355–359. doi: 10.1136/thx.41.5.355.

Selman, M., King, T. E. and Pardo, A. (2001) 'Idiopathic pulmonary fibrosis: prevailing and evolving hypotheses about its pathogenesis and implications for therapy.', *Annals of internal medicine*. United States, 134(2), pp. 136–151.

Seyer, J. M., Kang, A. H. and Rodnan, G. (1981) 'Investigation of type i and type iii collagens of the lung in progressive systemic sclerosis', *Arthritis & Rheumatism*, 24(4), pp. 625–631. doi: 10.1002/art.1780240410.

Sharir, A., Ramniceanu, G. and Brumfeld, V. (2011) 'High resolution 3D imaging of ex-vivo biological samples by micro CT.', *Journal of visualized experiments : JoVE*. United States, (52). doi: 10.3791/2688.

Shi-wen, X. *et al.* (2006) 'CCN2 is necessary for adhesive responses to transforming growth factor-beta1 in embryonic fibroblasts.', *The Journal of biological chemistry*. United States, 281(16), pp. 10715–10726. doi: 10.1074/jbc.M511343200.

Shi-Wen, X., Leask, A. and Abraham, D. (2008) 'Regulation and function of connective tissue growth factor/CCN2 in tissue repair, scarring and fibrosis.', *Cytokine & growth factor reviews*. England, 19(2), pp. 133–144. doi: 10.1016/j.cytogfr.2008.01.002.

Sidik, K. and Smerdon2, M. J. (1990) *Bleomycin-induced DNA Damage and Repair in Human Cells Permeabilized with Lysophosphatidylcholine1*, *CANCER RESEARCH*. Available at: http://cancerres.aacrjournals.org/content/canres/50/5/1613.full.pdf (Accessed: 22 October 2018).

Sime, P. J. and O'reilly, K. M. A. (2001) 'Fibrosis of the lung and other tissues: New concepts

in pathogenesis and treatment', *Clinical Immunology*, 99(3), pp. 308–319. doi: 10.1006/clim.2001.5008.

Smith, B. L., Bauer, G. B. and Povirk, L. F. (1994) 'DNA damage induced by bleomycin, neocarzinostatin, and melphalan in a precisely positioned nucleosome. Asymmetry in protection at the periphery of nucleosome-bound DNA', *Journal of Biological Chemistry*, 269(48), pp. 30587–30594. doi: 10.1161/STROKEAHA.106.478156.

Society, A. T. (2010) 'Interstitial Lung Disease', *Breathing in America: Diseases, Progress, and Hope*, (10), pp. 99–108. doi: 10.1159/000068408.

Society, A. T. S. R. (2002) 'American Thoracic Society American Thoracic Society / European Respiratory Society International Multidisciplinary Consensus Classification of the Idiopathic Interstitial Pneumonias', *American Journal of Respiratory and Critical Care Medicine*, 166(6), pp. 518–626. doi: 10.1183/09031936.02.00492002.

Sonnylal, S. *et al.* (2010) 'Selective expression of connective tissue growth factor in fibroblasts in vivo promotes systemic tissue fibrosis', *Arthritis and Rheumatism*, 62(5), pp. 1523–1532. doi: 10.1002/art.27382.

Srinivasan, M., Sedmak, D. and Jewell, S. (2002) 'Effect of fixatives and tissue processing on the content and integrity of nucleic acids.', *The American journal of pathology*. United States, 161(6), pp. 1961–1971. doi: 10.1016/S0002-9440(10)64472-0.

Stelekati, E. and Wherry, E. J. (2012) 'Chronic Bystander Infections and Immunity to Unrelated Antigens', *Cell Host & Microbe*. Cell Press, 12(4), pp. 458–469. doi: 10.1016/J.CHOM.2012.10.001.

Stone, K. C. *et al.* (1992) 'Allometric relationships of cell numbers and size in the mammalian lung.', *American journal of respiratory cell and molecular biology*. United States, 6(2), pp. 235–243. doi: 10.1165/ajrcmb/6.2.235.

Strachan, D. P. (1989) 'Household Size', *BMJ : British Medical Journal*, 299(November), pp. 1259–1260. doi: 10.1136/bmj.299.6710.1259.

Strongman, H., Kausar, I. and Maher, T. M. (2018) 'Incidence, Prevalence, and Survival of Patients with Idiopathic Pulmonary Fibrosis in the UK', *Advances in Therapy*. Springer Healthcare, 35(5), pp. 724–736. doi: 10.1007/s12325-018-0693-1.

Suarez, C. J., Dintzis, S. M. and Frevert, C. W. (2012) 'Respiratory', *Comparative Anatomy and Histology*, pp. 121–134. doi: 10.1016/B978-0-12-381361-9.00009-3.

Swiderski, R. E. *et al.* (1998) 'Differential expression of extracellular matrix remodeling genes in a murine model of bleomycin-induced pulmonary fibrosis', *The American Journal of Pathology*, 152(3), pp. 821–828. doi: 10.1016/S0169-7218(11)02412-9.

Tanjore, H. *et al.* (2009) 'Contribution of epithelial-derived fibroblasts to bleomycin-induced lung fibrosis', *American Journal of Respiratory and Critical Care Medicine*, 180(7), pp. 657–665. doi: 10.1164/rccm.200903-0322OC.

The Jackson Laboratory (no date) *Mouse Genetics - The mouse as a model for human disease.* Available at: https://www.jax.org/personalized-medicine/why-mouse-genetics# (Accessed: 15 March 2019).

Thickett, D. R. *et al.* (2014) 'Improving care for patients with idiopathic pulmonary fibrosis (IPF) in the UK: A round table discussion', *Thorax*, 69(12), pp. 1136–1140. doi: 10.1136/thoraxjnl-2014-206284.

Thrall, R. S. *et al.* (1979) 'Bleomycin-induced pulmonary fibrosis in the rat: inhibition by indomethacin.', *The American journal of pathology*. United States, 95(1), pp. 117–130.

Tomasek, J. J. *et al.* (2005) 'Regulation of α-Smooth Muscle Actin Expression in Granulation Tissue Myofibroblasts Is Dependent on the Intronic CArG Element and the Transforming Growth Factor-β1 Control Element', *The American Journal of Pathology*. Elsevier, 166(5), pp. 1343–1351. doi: 10.1016/S0002-9440(10)62353-X.

Tomcik, M. *et al.* (2015) 'S100A4 amplifies TGF-β-induced fibroblast activation in systemic sclerosis.', *Annals of the rheumatic diseases*. BMJ Publishing Group Ltd, 74(9), pp. 1748–55. doi: 10.1136/annrheumdis-2013-204516.

Tracy, L. E., Minasian, R. A. and Caterson, E. J. (2016) 'Extracellular Matrix and Dermal Fibroblast Function in the Healing Wound', *Advances in Wound Care*, 5(3), pp. 119–136. doi: 10.1089/wound.2014.0561.

Travis, M. A. and Sheppard, D. (2014) 'TGF-beta activation and function in immunity.', *Annual review of immunology*. United States, 32, pp. 51–82. doi: 10.1146/annurev-immunol-032713-120257.

Travis, W. D. *et al.* (2013) 'An official American Thoracic Society/European Respiratory Society statement: Update of the international multidisciplinary classification of the idiopathic interstitial pneumonias', *American Journal of Respiratory and Critical Care Medicine*, 188(6), pp. 733–748. doi: 10.1164/rccm.201308-1483ST.

Tsai, C. C. *et al.* (2018) 'Essential role of connective tissue growth factor (CTGF) in transforming growth factor-β1 (TGF-β1)-induced myofibroblast transdifferentiation from Graves' orbital fibroblasts', *Scientific Reports*. Springer US, 8(1), pp. 1–10. doi: 10.1038/s41598-018-25370-3.

Tsukui, T. *et al.* (2013) 'Qualitative Rather than Quantitative Changes Are Hallmarks of Fibroblasts in Bleomycin-Induced Pulmonary Fibrosis', *The American Journal of Pathology*. doi: 10.1016/j.ajpath.2013.06.005.

Tyrrell, L., Elias, J. and Longley, J. (1995) 'Detection of specific mRNAs in routinely processed dermatopathology specimens.', *The American Journal of dermatopathology*. United States, 17(5), pp. 476–483.

Umezawa, H. *et al.* (1967) 'Studies on bleomycin.', *Cancer*. United States, 20(5), pp. 891–895.

De Val, S. *et al.* (2002) 'Identification of the key regions within the mouse Pro-α2(I) collagen gene far-upstream enhancer', *Journal of Biological Chemistry*, 277(11), pp. 9286–9292. doi: 10.1074/jbc.M111040200.

Vancheri, C. *et al.* (2010) 'Idiopathic pulmonary fibrosis: A disease with similarities and links to cancer biology', *European Respiratory Journal*, 35(3), pp. 496–504. doi: 10.1183/09031936.00077309.

Ventura, A. *et al.* (2007) 'Restoration of p53 function leads to tumour regression in vivo', *Nature*, 445(7128), pp. 661–665. doi: 10.1038/nature05541.

Voltz, J. W. *et al.* (2008) 'Male sex hormones exacerbate lung function impairment after bleomycin-induced pulmonary fibrosis.', *American journal of respiratory cell and molecular biology*. United States, 39(1), pp. 45–52. doi: 10.1165/rcmb.2007-0340OC.

Wang, C. *et al.* (2014) 'Inhibition of Wnt/ -catenin signaling promotes epithelial

differentiation of mesenchymal stem cells and repairs bleomycin-induced lung injury', *AJP: Cell Physiology*, 307(3), pp. C234–C244. doi: 10.1152/ajpcell.00366.2013.

Wang, S. and Hubmayr, R. D. (2011) 'Type I alveolar epithelial phenotype in primary culture.', *American journal of respiratory cell and molecular biology*. United States, 44(5), pp. 692–699. doi: 10.1165/rcmb.2009-0359OC.

Wang, X. *et al.* (2015) 'Blocking the Wnt/β-catenin pathway by lentivirus-mediated short hairpin RNA targeting β-catenin gene suppresses silica-induced lung fibrosis in mice', *International Journal of Environmental Research and Public Health*, 12(9), pp. 10739–10754. doi: 10.3390/ijerph120910739.

Wang, X., McLennan, S. V. and Twigg, S. M. (2011) 'CCN-2 is up-regulated by and mediates effects of matrix bound advanced glycated end-products in human renal mesangial cells', *Journal of Cell Communication and Signaling*. Springer Netherlands, 5(3), pp. 193–200. doi: 10.1007/s12079-011-0137-z.

Wang, Y. *et al.* (2015) 'Maresin 1 inhibits epithelial-to-mesenchymal transition in vitro and attenuates bleomycin induced lung fibrosis in vivo', *Shock*, 44(5), pp. 496–502. doi: 10.1097/SHK.0000000000000446.

Ward, H. E. and Nicholas, T. E. (1984) 'Alveolar type I and type II cells.', *Australian and New Zealand journal of medicine*. Australia, 14(5 Suppl 3), pp. 731–734.

Van De Water, L., Varney, S. and Tomasek, J. J. (2013) 'Mechanoregulation of the Myofibroblast in Wound Contraction, Scarring, and Fibrosis: Opportunities for New Therapeutic Intervention', *Advances in Wound Care*, 2(4), pp. 122–141. doi: 10.1089/wound.2012.0393.

Webb, J. A. and Armstrong, J. (2002) 'Chronic idiopathic pulmonary fibrosis in a West Highland white terrier.', *The Canadian veterinary journal = La revue veterinaire canadienne*. Canada, 43(9), pp. 703–705.

Weinberger, S. E., Cockrill, B. A. and Mandel, J. (2014) 'Pulmonary Anatomy and Physiology', in *Principles of Pulmonary Medicine*. doi: 10.1016/B978-1-4557-2532-8.00001-3.

Williams, K. J. *et al.* (2007) 'Equine multinodular pulmonary fibrosis: a newly recognized herpesvirus-associated fibrotic lung disease.', *Veterinary pathology*. United States, 44(6), pp. 849–862. doi: 10.1354/vp.44-6-849.

Williamson, J. D., Sadofsky, L. R. and Hart, S. P. (2015) 'The pathogenesis of bleomycin-induced lung injury in animals and its applicability to human idiopathic pulmonary fibrosis', *Experimental Lung Research*, 41(2), pp. 57–73. doi: 10.3109/01902148.2014.979516.

Wills-karp, M., Santeliz, J. and Karp, C. L. (2001) 'Revisiting the hygiene hypothesis', *Nature Reviews Immunology*, (November), pp. 69–74. doi: 10.1038/35095579.

Wolkove, N. and Baltzan, M. (2009) 'Amiodarone pulmonary toxicity.', *Canadian respiratory journal*. Egypt, 16(2), pp. 43–48. doi: 10.1155/2009/282540.

Wollin, L. *et al.* (2014) 'Antifibrotic and anti-inflammatory activity of the tyrosine kinase inhibitor nintedanib in experimental models of lung fibrosis.', *The Journal of pharmacology and experimental therapeutics*. United States, 349(2), pp. 209–220. doi: 10.1124/jpet.113.208223.

Wolters, P. J. *et al.* (2018) 'Time for a change: is idiopathic pulmonary fibrosis still idiopathic

and only fibrotic? HHS Public Access Author manuscript', *Lancet Respir Med*, 6(2), pp. 154–160. doi: 10.1016/S2213-2600(18)30007-9.

Wolters, P. J., Collard, H. R. and Jones, K. D. (2014) 'Pathogenesis of idiopathic pulmonary fibrosis.', *Annual review of pathology*, 9, pp. 157–79. doi: 10.1146/annurev-pathol-012513-104706.

Wong, M. H., Chapin, O. C. and Johnson, M. D. (2012) 'LPS-Stimulated Cytokine Production in Type I Cells Is Modulated by the Renin–Angiotensin System', *American Journal of Respiratory Cell and Molecular Biology*. American Thoracic Society, 46(5), pp. 641–650. doi: 10.1165/rcmb.2011-0289OC.

Wostmann, B. S. *et al.* (1970) 'Serum proteins and lymphoid tissues in germ-free mice fed a chemically defined, water soluble, low molecular weight diet.', *Immunology*. England, 19(3), pp. 443–448.

Wu, Q. *et al.* (2016) 'Members of the Cyr61/CTGF/NOV Protein Family: Emerging Players in Hepatic Progenitor Cell Activation and Intrahepatic Cholangiocarcinoma', *Gastroenterology Research and Practice*. doi: 10.1155/2016/2313850.

Wynn, T. A. (2008) 'Cellular and molecular mechanisms of fibrosis.', *The Journal of pathology*. England, 214(2), pp. 199–210. doi: 10.1002/path.2277.

Wynn, T. A., Chawla, A. and Pollard, J. W. (2013) 'Macrophage biology in development, homeostasis and disease.', *Nature*. England, 496(7446), pp. 445–455. doi: 10.1038/nature12034.

Xu, S. W. *et al.* (2006) 'CCN2 is necessary for adhesive responses to transforming growth factor-β1 in embryonic fibroblasts', *Journal of Biological Chemistry*, 281(16), pp. 10715–10726. doi: 10.1074/jbc.M511343200.

Xu, X. *et al.* (2018) 'Transforming growth factor-beta in stem cells and tissue homeostasis.', *Bone research*. China, 6, p. 2. doi: 10.1038/s41413-017-0005-4.

Yamamoto, K. *et al.* (2012) 'Type I alveolar epithelial cells mount innate immune responses during pneumococcal pneumonia.', *Journal of immunology (Baltimore, Md. : 1950)*. United States, 189(5), pp. 2450–2459. doi: 10.4049/jimmunol.1200634.

Yang, J. *et al.* (2014) 'Activated alveolar epithelial cells initiate fibrosis through autocrine and paracrine secretion of connective tissue growth factor', *AJP: Lung Cellular and Molecular Physiology*, 306(8), pp. L786–L796. doi: 10.1152/ajplung.00243.2013.

Yatomi, M. *et al.* (2015) '17(R)-resolvin D1 ameliorates bleomycin-induced pulmonary fibrosis in mice.', *Physiological reports*. United States, 3(12). doi: 10.14814/phy2.12628.

Yeger, H. and Perbal, B. (2007) 'The ccn family of genes: A perspective on ccn biology and therapeutic potential', *Journal of Cell Communication and Signaling*. doi: 10.1007/s12079-008-0022-6.

Yona, S. *et al.* (2013) 'Fate mapping reveals origins and dynamics of monocytes and tissue macrophages under homeostasis.', *Immunity*. United States, 38(1), pp. 79–91. doi: 10.1016/j.immuni.2012.12.001.

Yu, C.-C. *et al.* (2009) 'Thrombin-induced connective tissue growth factor expression in human lung fibroblasts requires the ASK1/JNK/AP-1 pathway.', *Journal of immunology (Baltimore, Md. : 1950)*. United States, 182(12), pp. 7916–7927. doi: 10.4049/jimmunol.0801582.

Zhang, R. *et al.* (1998) 'Identification of rCop-1, a new member of the CCN protein family, as a negative regulator for cell transformation', *Mol Cell Biol*, 18(10), pp. 6131–6141. doi: 10.1128/MCB.18.10.6131.

Zhang, Y., Kaminski, N. and Simmons, R. P. (2012) 'Biomarkers in idiopathic pulmonary fibrosis'. doi: 10.1097/MCP.0b013e328356d03c.

Zhong, Z. A. *et al.* (2015) 'Optimizing tamoxifen-inducible Cre/loxp system to reduce tamoxifen effect on bone turnover in long bones of young mice.', *Bone*. NIH Public Access, 81, pp. 614–619. doi: 10.1016/j.bone.2015.07.034.

Zhou, W. and Wang, Y. (2016) 'Candidate genes of idiopathic pulmonary fibrosis: Current evidence and research', *Application of Clinical Genetics*, 9(August 2015), pp. 5–13. doi: 10.2147/TACG.S61999.

Zhu, M. *et al.* (2008) 'Tamoxifen-inducible Cre-recombination in articular chondrocytes of adult Col2a1-CreER(T2) transgenic mice.', *Osteoarthritis and cartilage*. England, 16(1), pp. 129–130. doi: 10.1016/j.joca.2007.08.001.

Appendix A: Primer validation amplification plots

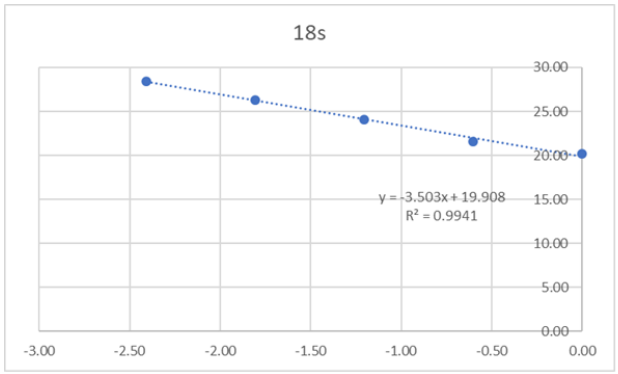

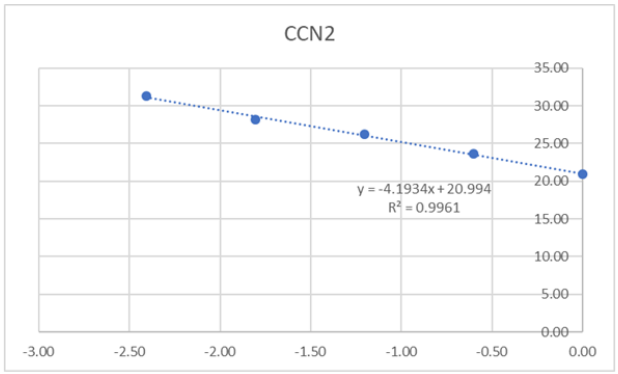

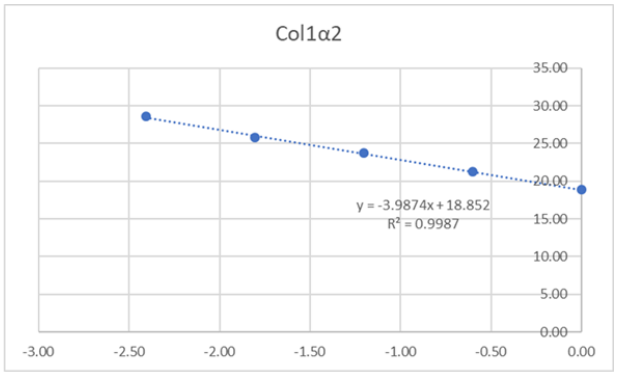

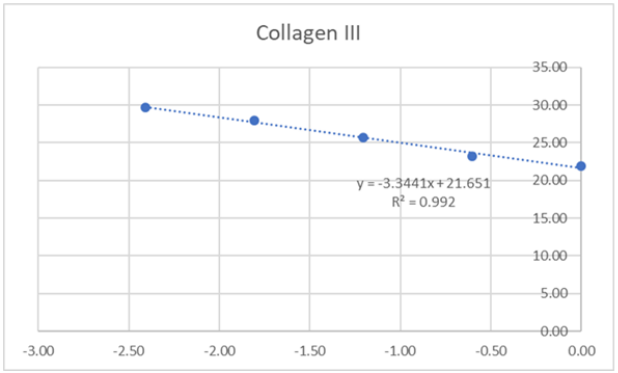

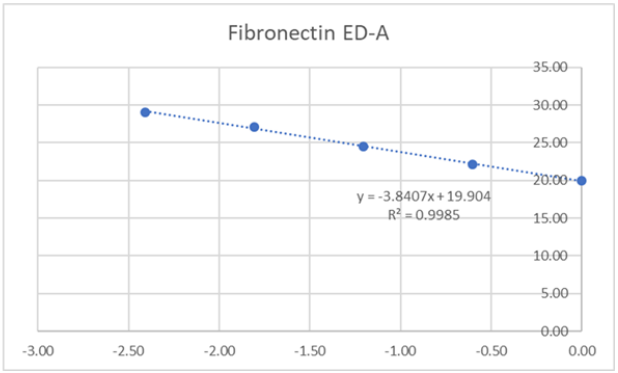

Appendix B: Primer Melt Curves

18s Melt Curve

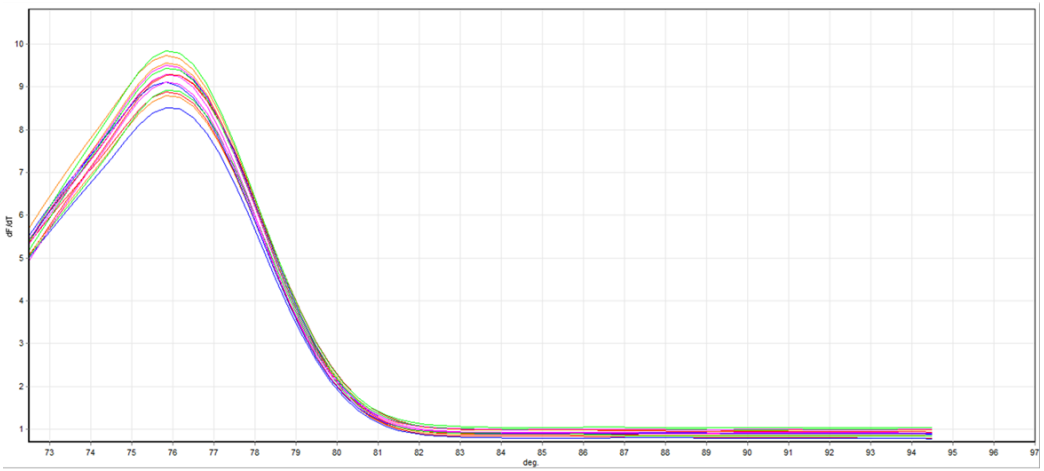

CCN2 Melt Curve

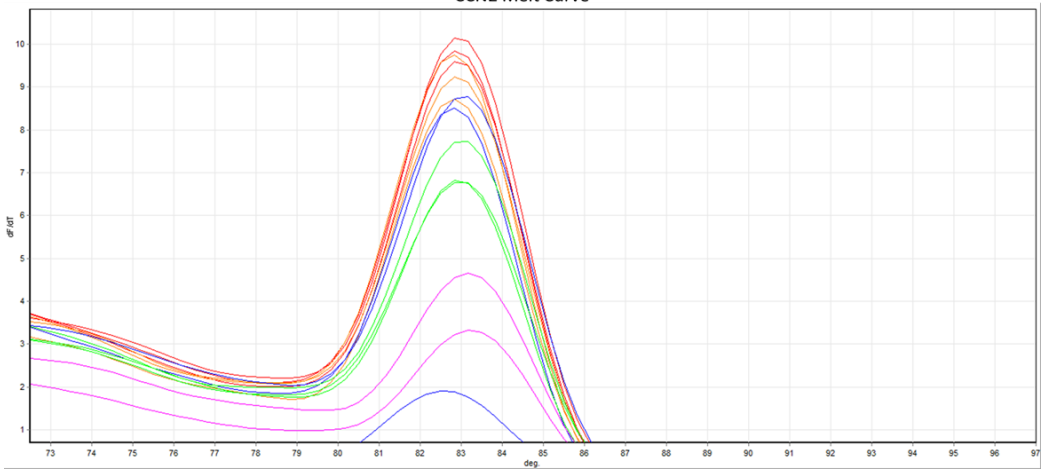

Col1a2 Melt Curve

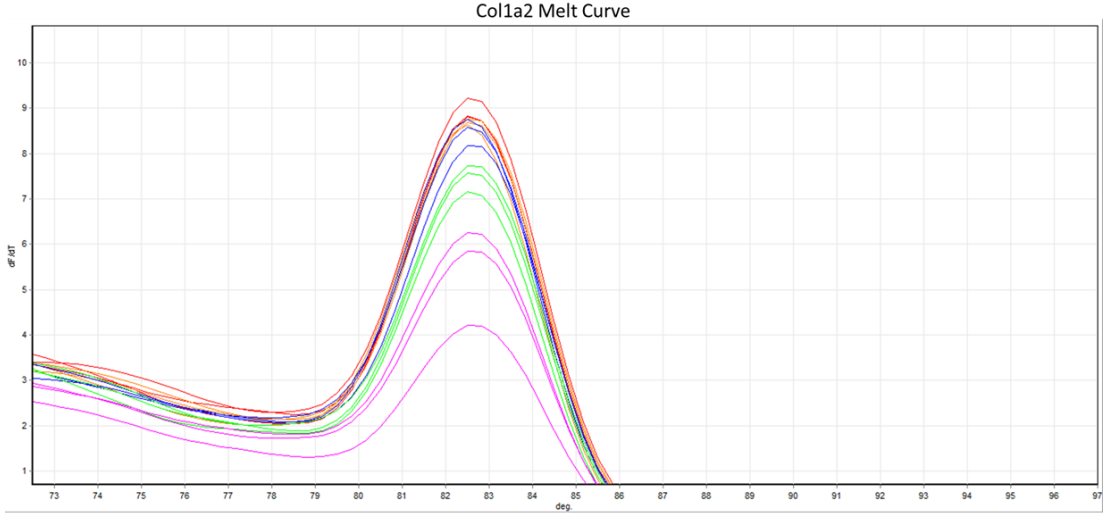

Fibronectin ED-A Melt Curve

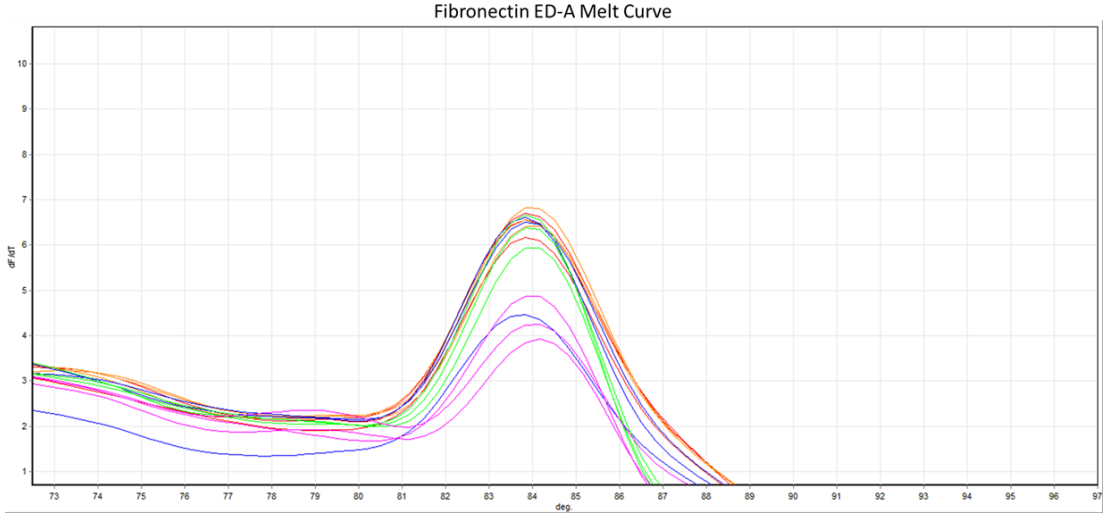

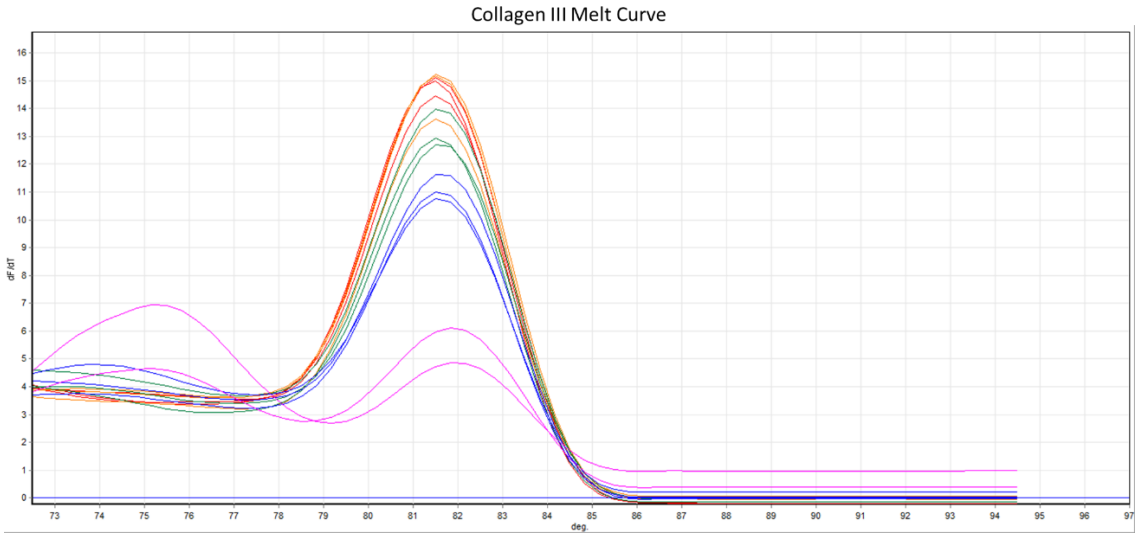
Collagen III Melt Curve
-dF/dT
deg.

Appendix 3. Lung µCT Macro Analysis

Open reconstructed images in CtAN

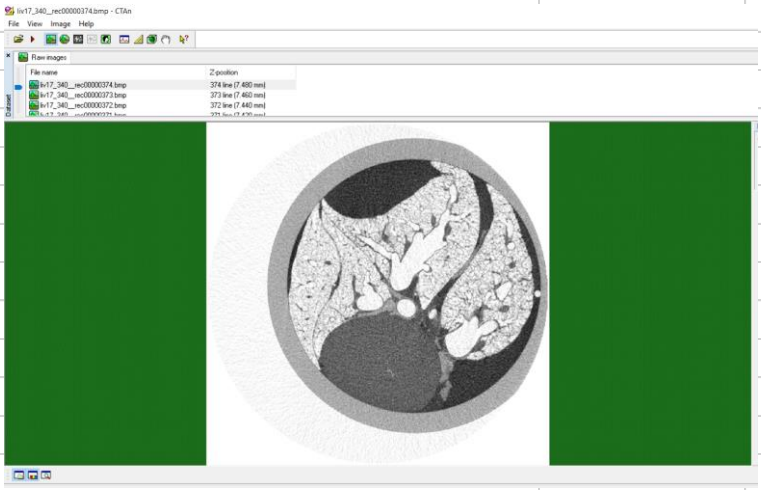

Draw region of interest

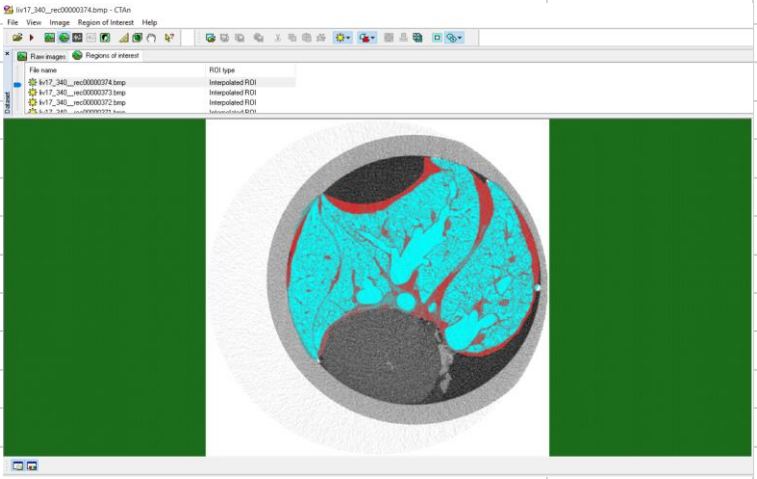

Step 1. Filtering					
Mode	Median (2D space)				
Kernel	Round				
Radius	3				

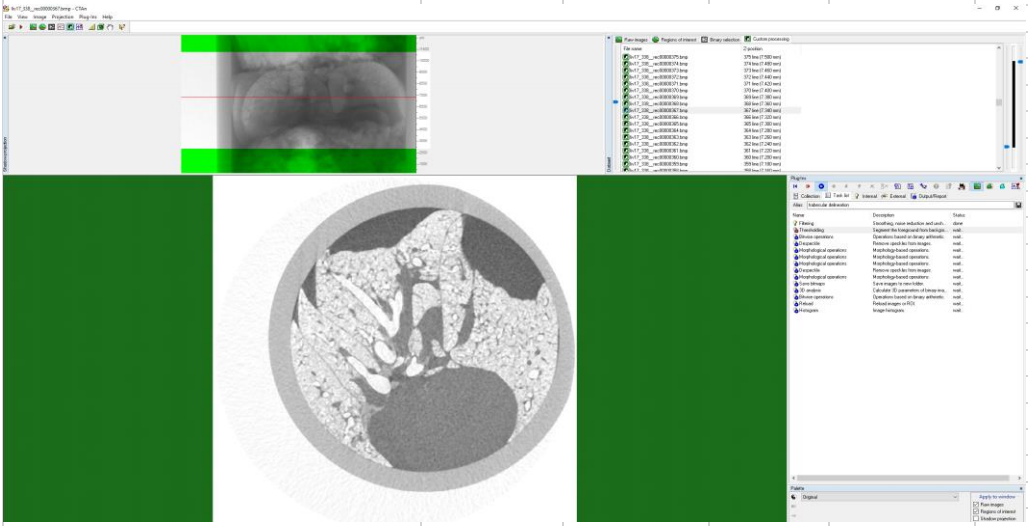

Step 2.Thresholding					
Mode	Global				
Lower grey threshold	0				
Upper grey threshold	130				

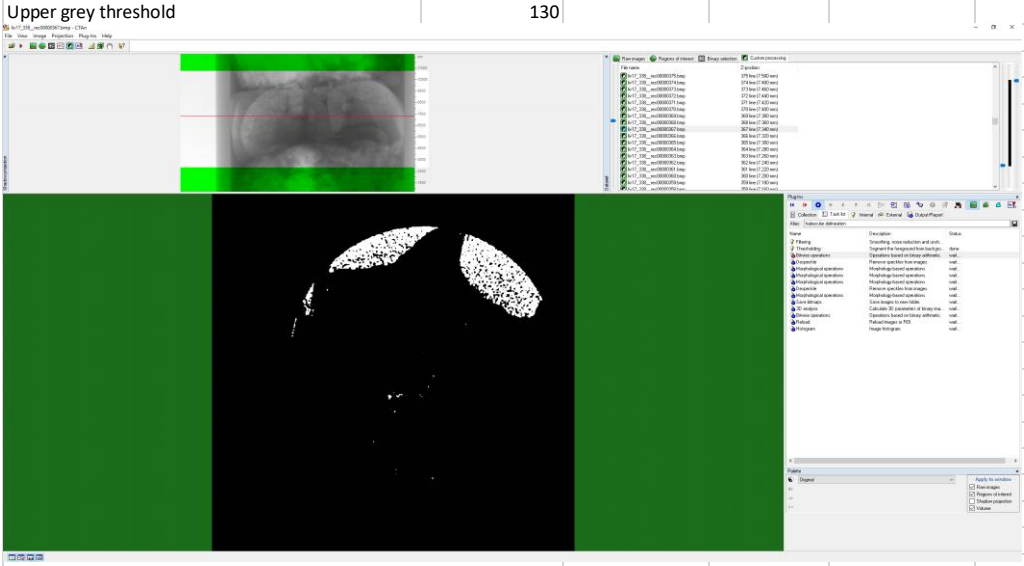

Step 3. Bitwise operations

<Image> = <Region of Interest> AND <Image>

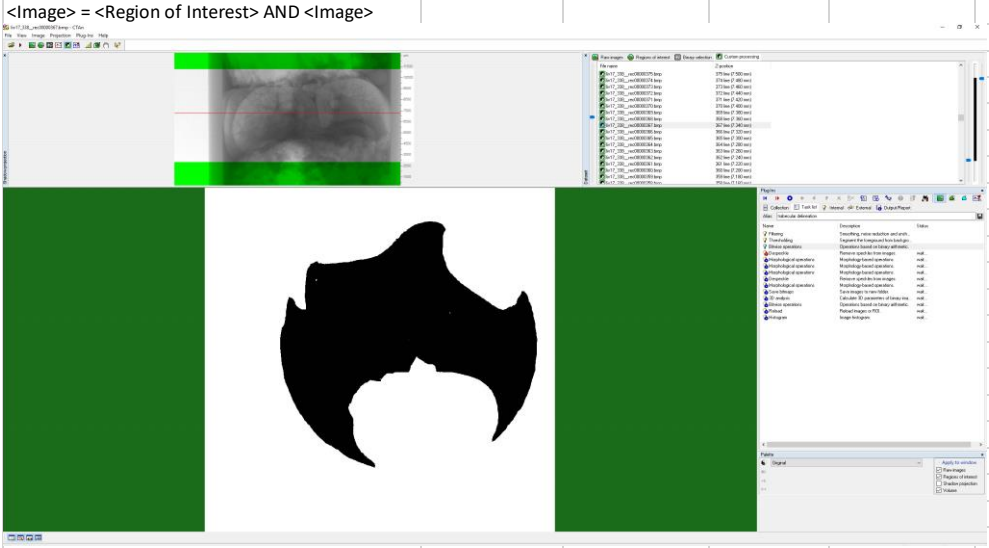

Step 4. Despeckle

Type: Sweep (3D space)

Remove: all exept the largest object

Apply to: Image

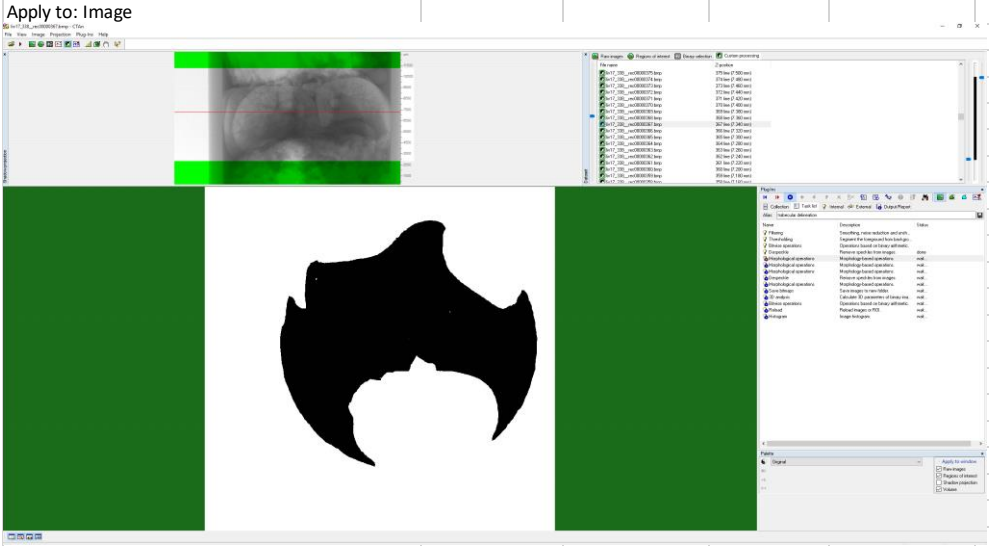

Step 5. Morphological operations

Type: Closing (2D space)

Kernel: Round

Radius: 4

Apply to: Image

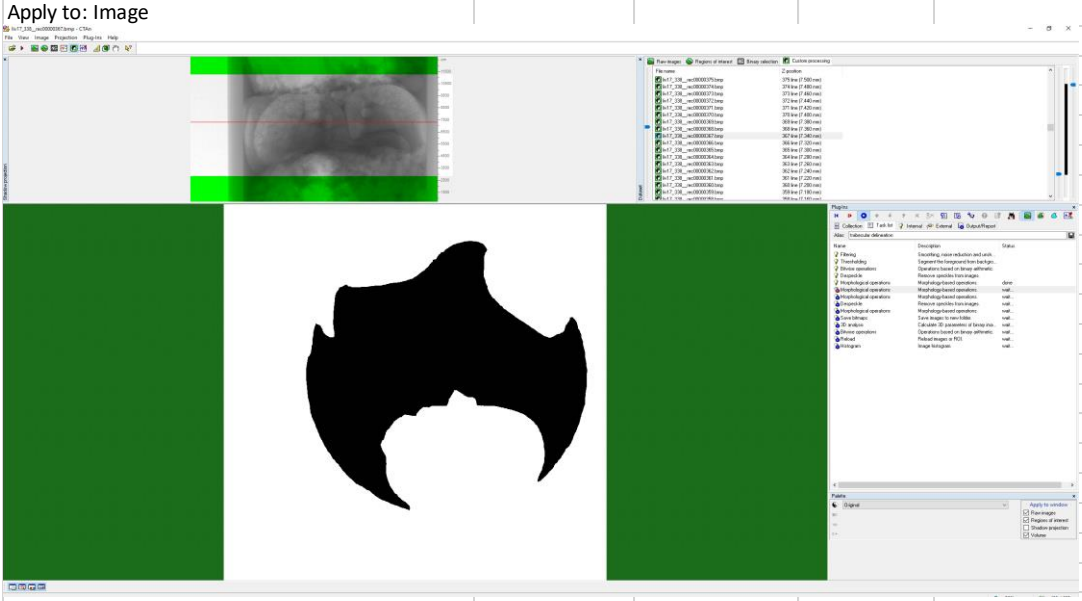

Step 6. Morphological operations

Type: Closing (3D space)

Kernel: Round

Radius: 3

Apply to: Image

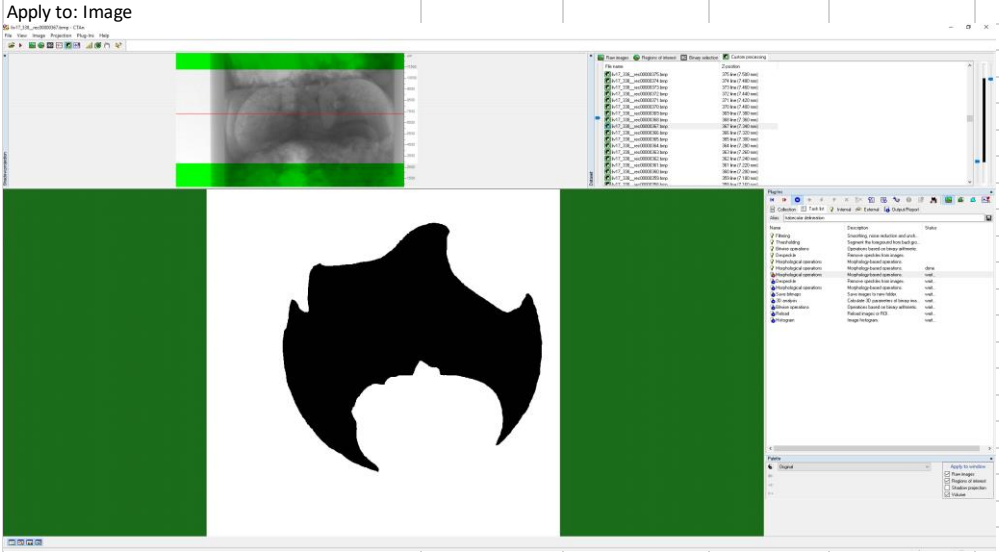

Step 7. Morphological operations

Type: Erosion (2D space)

Kernel: Round

Radius: 2

Apply to: Image

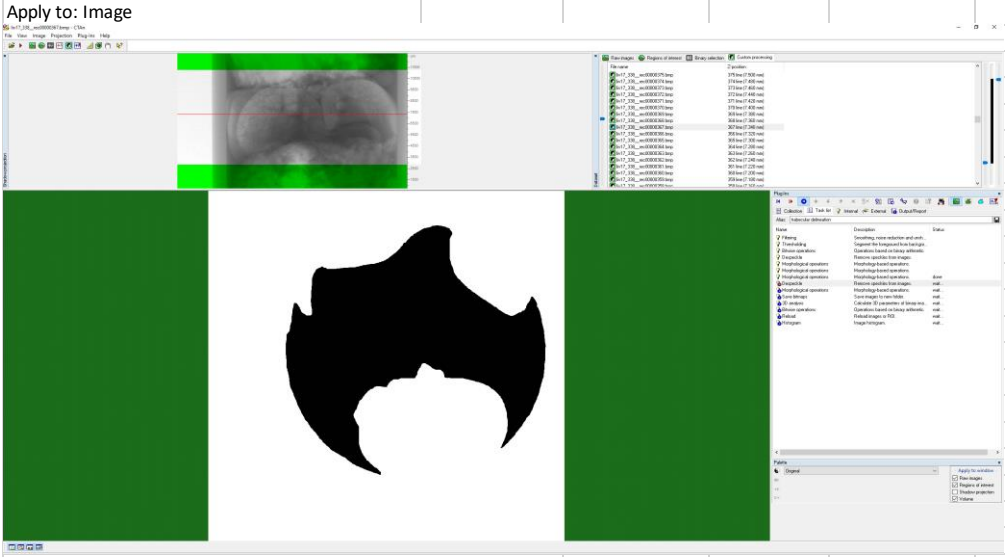

Step 8. Despeckle

Type: Remove white speckles (2D space)

Area: less than 2000 pixels

Apply to: Image

3425 speckles removed

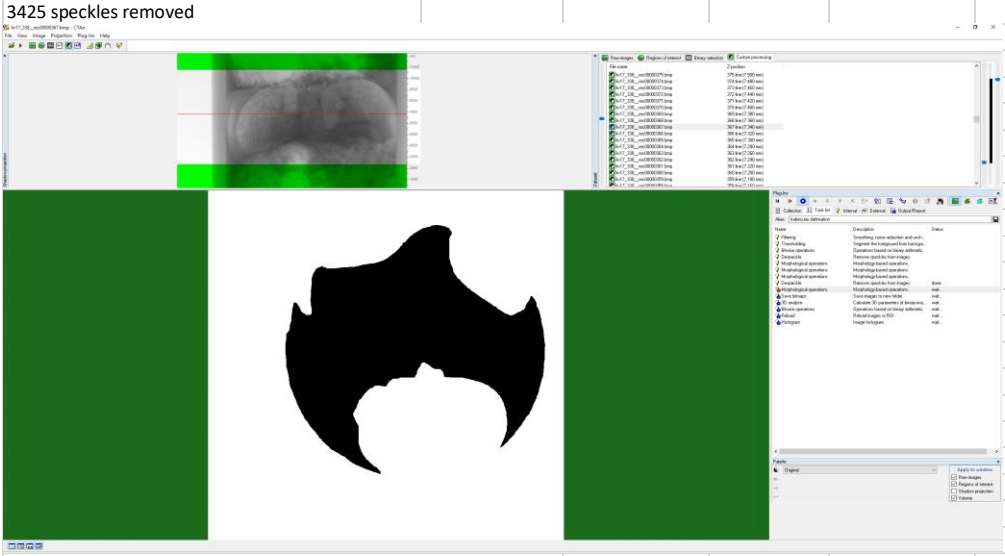

Step 9. Morphological operations

Type: Dilation (2D space)

Kernel: Round

Radius: 2

Apply to: Image

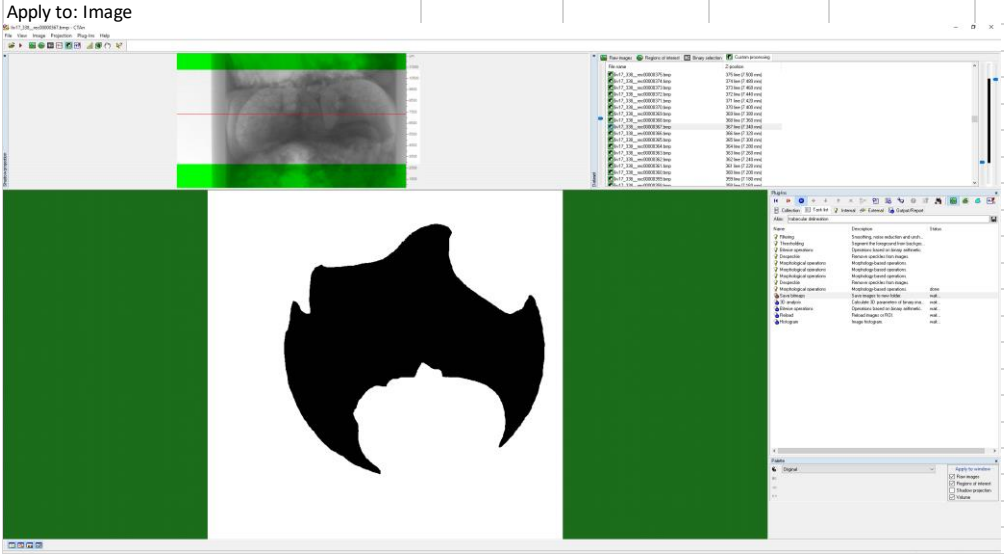

Step 10. Save bitmaps(only image):

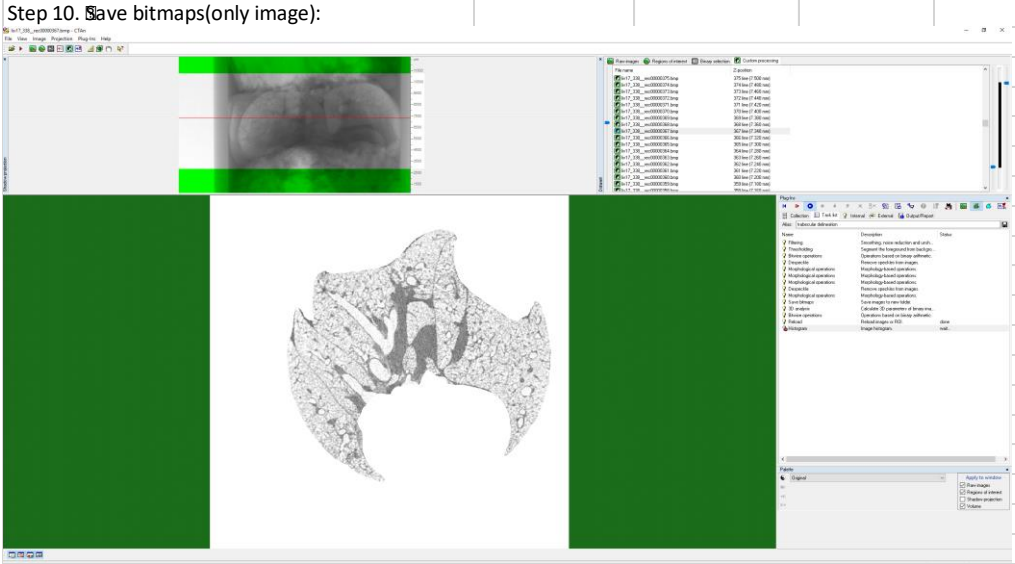

Destination folder:
V:\AMY\LIV17_340\LIV17_340_Rec\lung

File format: bmp

Number of saved files: 582

[01/09/18 16:50:09] Histogram (3D space) inside VOI

0	1	2	3	4
8792165	622836	648134	672729	697378

Mean	Standard deviation	Standard error of mean	95% confidence limit (minimum)	95% confidence limit (maximum)
48.52	41.87	0.00	48.51	48.53